

***Biochemical and Biophysical Characterisation of Heat
Shock Protein 90 and Its Domain Interactions***

A Thesis

Submitted for the Degree of

Doctor of Philosophy

by

Amir Rabu, M.Sc

Structural Biochemistry Group

The Institute of Structural and Molecular Biology

University of Edinburgh

May 2006



Abstract

Hsp90 proteins are essential and ubiquitous molecular chaperones that play important roles in folding, activation and assembly of a range of client proteins which are involved in signal transduction, cell cycle control and transcriptional regulation. Hsp90 can be divided into three domains which play vital roles in the protein function. The domains are classified as the N-terminal domain, the middle domain and the C-terminal domain. This thesis describes the study of the Hsp90 proteins from *Homo sapiens* (Hsp90 α) and *Caenorhabditis elegans*. The attempt to crystallise the C-terminal proteins is also described. The overall goal of the project was to biochemically and biophysically characterise various Hsp90 constructs and use this information to elucidate the biological role of this important family of proteins.

The C-terminal domain of human Hsp90 α . The work involved over-expression, purification and characterisation of the C-terminus of human Hsp90 α protein. The over-expression and purification led to the production of two reproducibly pure C-terminal human Hsp90 α protein constructs. The characterisation of these proteins focused on the interaction of the C-terminus with the immunophilin Cyp40 and also with ligands such as ATP and novobiocin. The characterisation utilised biophysical methods such as surface plasmon resonance, gel filtration, tryptophan fluorescence and isothermal titration calorimetry. Characterisation of the interaction with Cyp40 showed that the C-terminal region of Hsp90 binds to Cyp40 with a dissociation constant in the micromolar concentration range. In addition, the dissociation constants obtained from all the methods utilised in the study were in agreement with each other. The study of the interaction of the C-terminal domain of human Hsp90 α with ATP showed that ATP did bind to the protein, supporting the existence of second ATP binding site at the C-terminus of Hsp90. Furthermore, C-terminal human Hsp90 α also exhibits ATPase activity. The C-terminus of Hsp90 also binds to novobiocin in

the low micromolar concentration range. Further studies showed that novobiocin was able to inhibit the ATPase activity of the C-terminus suggesting the possibility that novobiocin binds at the same site as ATP. The inhibition constants estimated from the ATPase inhibition experiment show an agreement with the dissociation constants obtained from the biophysical methods.

***C. elegans* Hsp90.** The work involved the cloning, over-expression and purification of the N and C-terminus of *C. elegans* Hsp90. The cloning of genes for the N and C-termini was successful. Purification of the proteins only led to the production of one C-terminal protein but no purified N-terminal protein could be obtained. Similar characterisation studies were carried out to the C-terminus of *C. elegans* Hsp90. As for the human C-terminal protein, the *C. elegans* C-terminal protein was found to bind to Cyp40 with a dissociation constant in the micromolar concentration range. The protein also binds to ATP and novobiocin with an affinity very similar to that of the C-terminal proteins of human Hsp90 α . The C-terminus of *C. elegans* also exhibit ATPase activity but the activity was ten-fold lower than that of the C-terminal of Hsp90 human α .

The work presented in this thesis provides conclusive evidence of the existence of an ATP binding site in the C-terminal domains of the Hsp90 class of proteins. The biological relevance of this finding is also discussed.

Acknowledgements

I would like thank my supervisor, Professor Malcolm D. Walkinshaw, firstly for the opportunity to register for a PhD and also for his invaluable advice, enthusiasm and encouragement throughout the duration of the project and beyond.

I would also like to thank Dr Jacqueline Dornan and Dr Martin Wear for all their help, advice and patience in helping me with the project and thesis, and for their friendship.

I am also indebted to several people for helping me with various aspects of the projects described in this thesis. In particular, I would like to thank Dr Antony Page for all his help in *C.elegans* cloning. Also Sandra Bruce for her help with the purification of full length *C.elegans* Hsp90 and Mr Liam Worrall for his effort on protein modelling.

Thanks are also due to many people in Swann Level 3 for their friendship and support throughout good times and bad.

I would like to acknowledge Dr. Tom Ratajczak for providing the human Hsp90 clones used throughout the duration of this project. I would like to acknowledge the National University of Malaysia and the Ministry of Science, Technology and industry for sponsoring me to do my study.

My special thanks to my beloved wife, Aida for all her support and courage and to my three children, Amirah, Arief and Aisyah, thanks for always being there.

List of abbreviations

AS	ammonium sulphate
BCIP	5-bromo-4-chloro-3-indoylphosphate
bp	base pairs
CD	Circular Dichroism
cDNA	complementary DNA
ceHsp90-492	<i>C. elegans</i> Hsp90 492-702
ceHsp90	full length <i>C. elegans</i> Hsp90
Cyp3	<i>C. elegans</i> Cyclophilin 3
Cyp40	cyclophilin 40
EPIC	Edinburgh Protein Interaction Centre
FPLC	Fast performance liquid chromatography
GA	Geldanamycin
hHsp90- α 521	Hsp90 human α 521-732
hHsp90- α 596	Hsp90 human α 596-732
hHsp90- α 604	Hsp90 human α 604-732
hHsp90- α 631	Hsp90 human α 631-732
IPTG	Isopropyl β -D- thiogalactopyranoside
kDa	Kilodalton
K_i	inhibition constant
K_q	bimolecular quenching constant
LB	Luria-Bertani
MWT	Molecular weight
NBT	Nitro Blue tetrazolium
OD ₆₀₀	Optical density at 600 nm
PAGE	Polyacrylamide gel electrophoresis
PBS-T	Phosphate buffer saline with Tween 20
Pdb	Protein data bank
PFK	Phosphofructo kinase
PP5	Protein phosphatase 5
RU	response units
S200	Sephacryl 200 gel filtration column
SDS	Sodium dedecyl sulphate
SE	Standard error
TE	Tris EDTA buffer
V	Volt
v/v	volume per volume
w/v	weight per volume
α	alpha
β	beta
γ	gamma

Title	i
Abstract	ii
Declaration	iv
Acknowledgements	v
Abbreviation list	vi
Table of contents	vii
List of Figures	xiv
List of Tables	xviii

Chapter 1: Introduction

1.1. Heat shock protein 90 (Hsp90)	1-1
1.2. N-terminal domain of Hsp90	1-6
1.2.1. <i>ATP/ADP bind at the N-terminal of Hsp90</i>	1-7
1.2.2. <i>ATP hydrolysis by Hsp90</i>	1-11
1.2.2. <i>Geldanamycin (GA) binds to the N-terminal domain of Hsp90 and inhibit ATPase activity</i>	1-15
1.2.3. <i>p23 binds to N-terminal domain of Hsp90</i>	1-19
1.3. Middle domain of Hsp90	1-21
1.4. The C-terminal domain of Hsp90	1-23
1.4.1. <i>Hsp90 forms a dimer</i>	1-24
1.4.2. <i>The C-terminal domain is important for binding to client proteins</i>	1-27
1.4.3. <i>The C-terminal domain is important for interaction with Cyp40</i>	1-30
1.4.4. <i>The C-terminal domain binds to novobiocin and ATP</i>	1-33
1.4.4. <i>Crystal structure of the carboxy terminal of htpG E. coli and yeast Hsp90</i>	1-36
1.5. Function of Hsp90	1-38
References	1-42

Chapter 2: Materials and Methods

2.1. Source of chemicals and biochemicals.....	2-1
2.2. General methods used in cloning experiments	2-1
2.2.1. <i>Polymerase chain reaction (PCR)</i>	2-1
2.2.2. <i>Plasmid extraction</i>	2-2
2.2.3. <i>Digestion of DNA with restriction enzymes</i>	2-3
2.2.4. <i>DNA purification by using QIAquick gel extraction kit (Qiagen)</i>	2-3
2.2.5. <i>DNA ligation and transformation</i>	2-4
2.2.6. <i>Topo TA cloning (Invitrogen)</i>	2-5
2.2.7. <i>Test for protein expression</i>	2-5
2.2.8. <i>Western blot analysis</i>	2-6
2.3. Protein expression and purification	2-8
2.3.1. <i>Scale up of protein expression</i>	2-8
2.3.2. <i>Ni-NTA or Talon purification</i>	2-9
2.3.3. <i>Gel filtration</i>	2-9
2.3.4. <i>Anion exchange column (Mono-Q)</i>	2-10
2.4. Methods for characterizing Hsp90	2-11
2.4.1. <i>Intrinsic tryptophan fluorescence</i>	2-11
2.4.2. <i>Sensor chips preparation for Surface Plasmon Resonance (SPR)</i>	2-13
2.4.3. <i>Isothermal titration calorimetry (ITC)</i>	2-16
2.4.4. <i>Malachite green assay standard curve</i>	2-19
2.5. Methods for crystallization trials.....	2-21
2.5.1. <i>Hanging drop vapour diffusion</i>	2-21
2.5.2. <i>Crystal soaking and co-crystallisation experiments</i>	2-22
References	2-25

Chapter 3: Cloning and purification of Hsp90

3.1. Introduction	3-1
3.2. Materials and Methods	3-1
3.2.1. <i>Cloning the N and C-terminal domains of C. elegans Hsp90..</i>	3-1

3.2.1.1. Polymerase chain reaction (PCR)	3-3
3.2.1.2. Cloning strategies.....	3-6
3.2.1.2.3. Cloning into shuttle vectors (pCR®2.1-TOPO® and pENTR™/SD/D-TOPO®).....	3-6
3.2.1.2.4. Cloning into the expression vectors (Gateway system, pQE30 and pET28a).....	3-7
3.2.2. Purification of C-terminal human Hsp90 α and <i>C. elegans</i> Hsp90	3-9
3.2.2.1 .Ni-NTA/Talon affinity column	3-9
3.2.2.2. Gel filtration.....	3-9
3.2.3. Native purification of the N-terminal Hsp90 of <i>C. elegans</i> ...	3-10
3.2.4. Denatured purification and refolding of the N-terminal Hsp90 of <i>C. elegans</i>	3-11
3.2.5. Protein verification and confirmation.....	3-12
3.3. Results and discussion	3-13
3.3.1. Polymerase chain reaction of genes encoding the N and C-terminal domains of <i>C. elegans</i> Hsp90	3-13
3.3.2. Cloning of the <i>C. elegans</i> genes into shuttle vectors	3-13
3.3.3. Cloning, expression and purification of the N and C-terminal domains of <i>C. elegans</i> Hsp90.....	3-15
3.3.4. Expression and Purification of the C-terminal domain of human Hsp90	3-23
3.4. Conclusion.....	3-29
References	3-30

Chapter 4: Characterisation of the C-terminal domain of human Hsp90 α

4.1. Introduction	4-1
4.2. Materials and methods	4-3
4.2.1. Determination of the oligomeric forms of human Hsp90 α C-terminal domain	4-3

4.2.1.1. Gel filtration.....	4-3
4.2.1.2. Mass spectroscopy	4-4
4.2.2. <i>Determination of the dimerisation constant of protein</i>	4-5
4.2.3. <i>Study of the interaction of the C-terminal domain of human Hsp90 α with Cyclophilin 40 (Cyp40)</i>	4-6
4.2.3.1. Gel filtration.....	4-6
4.2.3.2. Intrinsic Tryptophan fluorescence.....	4-7
4.2.3.2.1. <i>Human Hsp90 α 521-732 (hHsp90-α521)</i>	4-7
4.2.3.2.2. <i>Human Hsp90 α 631-73(hHsp90-α631)</i>	4-7
4.2.3.3. Surface Plasmon Resonance (SPR).....	4-9
4.2.4. <i>Study of the interaction of the C-terminal domain of human Hsp90 α with small ligands</i>	4-10
4.2.4.1. Hummel-Dreyer gel filtration	4-10
4.2.4.2. Trp fluorescence.....	4-12
4.2.4.3. Malachite green ATPase assays.....	4-13
4.2.4.4. ATPase inhibition assays	4-14
4.2.4.5. Isothermal Titration Calorimetry (ITC)	4-14
4.3. Results	4-15
4.3.1. <i>Native forms of the C-terminal domains of humanHsp90 α</i> .	4-15
4.3.2. <i>Dimerisation constants of the C-terminal humanHsp90 α</i>	4-21
4.3.3. <i>Interaction of the C-terminal domain of human Hsp90 α with Cyclophilin 40 (Cyp40)</i>	4-23
4.3.3.1. C-terminal human Hsp90 α binds to the bovine Cyp40 as shown by gel filtration	4-23
4.3.3.2. The dissociation constant (Kd) of the interaction between Cyp40 and C-terminal human Hsp90 α obtained from Trp fluorescence.....	4-27
4.3.3.3. Surface Plasmon Resonance (SPR) also supports the binding of the C-terminal human Hsp90 α with bovine Cyp40	4-29
4.3.4. <i>Interaction of the C-terminal domain of human Hsp90 α with ATP and novobiocin</i>	4-32
4.3.4.1. Trp fluorescence showed that ATP bind to hHsp90- α 521 ..	4-33

4.3.4.2. Hummel-Dreyer gel filtration showed ATP binds to hHsp90- α 521 but not hHsp90- α 631.....	4-35
4.3.4.3. ATPase activity of hHsp90- α 521 detected by malachite green assay	4-36
4.3.4.4. Novobiocin binds to the C-terminal human Hsp90 α determined by Trp fluorescence and ITC.....	4-40
4.3.4.5. The inhibition of ATPase activity by novobiocin.....	4-42
4.4. Crystallization trials	4-44
4.5. Discussion.....	4-46
4.5.1. <i>The dimerisation of the C-terminal humanHsp90 α.....</i>	4-47
4.5.2. <i>Cyp40 bind to the C-terminal human Hsp90 α via MEEVD motif</i>	4-47
4.5.3. <i>The C-terminal domain consists second ATP binding site and has low ATPase activity</i>	4-50
4.5.4. <i>Novobiocin binds to the C-terminal domain and inhibits ATPase activity.....</i>	4-52
4.6. Conclusion.....	4-54
References	4-56

Chapter 5: Characterization of *C. elegans* Hsp90

5.1. Introduction.....	5-1
5.2. Material and methods.....	5-2
5.2.1. <i>Gel filtration and mass spectroscopy to confirm the identities and oligomeric properties of the <i>C.elegans</i> Hsp90 proteins.....</i>	5-2
5.2.1.1. Gel filtration.....	5-2
5.2.1.2. Mass spectroscopy	5-3
5.2.2. <i>Study of the interaction of <i>C.elegans</i> Hsp90 with bovine Cyp40 by intrinsic Trp fluorescence and Surface Plasmon Resonance (SPR).....</i>	5-3
5.2.2.1. Trp fluorescence.....	5-3
5.2.2.2. Surface plasmon resonance (SPR)	5-4

5.2.3. The study of the interaction of <i>C. elegans</i> Hsp90 with small ligands.....	5-5
5.2.3.1. Intrinsic Trp fluorescence	5-6
5.2.3.2. Malachite green ATPase activity assay.....	5-7
5.2.3.3. ATPase inhibition assays	5-8
5.2.3.4. Surface plasmon resonance (SPR)	5-9
5.3. Results	5-9
5.3.1. CeHsp90-492 forms a dimer	5-9
5.3.2. The interaction of <i>C. elegans</i> Hsp90 with bovine Cyp40.....	5-10
5.3.2.1. The dissociation constants (Kds) of the interaction between ceHsp90 and ceHsp90-492 with bovine Cyp40 determined by Trp fluorescence.....	5-11
5.3.2.2. The dissociation constants (Kds) of the interaction between bovine Cyp40 with ceHsp90-492 determined by SPR.....	5-13
5.3.3. The interaction of <i>C.elegans</i> Hsp90 with small ligands	5-15
5.3.3.1. Trp fluorescence showed GA bind weakly to ceHsp90.....	5-15
5.3.3.2. Trp fluorescence showed novobiocin bind to ceHsp90-492.....	5-18
5.3.3.3. The interaction of ATP with both of the <i>C.elegans</i> protein constructs	5-18
5.3.3.4. ATPase activities showed in both of the <i>C.elegans</i> protein constructs	5-20
5.3.3.5. The inhibition of ATPase activities of both of the <i>C .elegans</i> protein constructs	5-22
5.3.4. Crystallization trials of <i>C.elegans</i> Hsp90 proteins	5-23
5.4. Discussion.....	5-24
5.4.1. CeHsp90-492 exists as a dimer	5-24
5.4.2. <i>C. elegans</i> Hsp90 binds to Cyp40	5-25
5.4.3. <i>C. elegans</i> Hsp90 binds ATP and exhibits ATPase activity ...	5-26
5.4.4. Inhibition of the ATPase activity	5-27
5.5. Conclusion.....	5-29
References:.....	5-32

Chapter 6: General conclusions and future work

6.1. Summary	6-1
6.2. Sequence alignment of Hsp90 C-terminal domains	6-1
6.4. C-terminal domains bind to Cyp40	6-4
6.5. Sequence alignment predicted possible binding site for ATP and novobiocin	6-6
6.6. Possible mechanism for ATP binding and novobiocin inhibition.....	6-9
6.7. Future work	6-16
References	6-21

Appendix A. Crystallographic study of cyclophilin-ligand interactions.

A.1. Introduction	A-1
A.2. <i>C.elegans</i> cyclophilin 3 (Cyp3)	A-2
A.3. X-ray crystallographic ligand binding studies using Cyp3	A-3
A.4. Materials and methods.....	A-5
A.4.1. Expression, purification and crystallization of <i>C. elegans</i> Cyp3	A-5
A.4.2. Crystallization and Gly-Pro soaking experiment	A-6
A.4.3. Crystal data refinement	A-7
A.5. Results and discussion.....	A-8
A.5. Conclusion.....	A-14
References	A-16

List of figures

Chapter 1: Introduction

- Figure 1.1. Sequence alignment of the Hsp90 homologs that are utilised in the study
- Figure 1.2. Overview of interactions the Hsp90 with other chaperones and clients protein
- Figure 1.3. Cartoons of Hsp90 from different species
- Figure 1.4. The crystal structure of full length yeast Hsp90/Sba1(p23) complex and the M-C domains
- Figure 1.5. Overview of the complex structure of ATP/ADP binds to the N terminal domain
- Figure 1.6. Conformational changes of yeast Hsp90 when ATP binds to the N-terminal domain
- Figure 1.7. The suggested Hsp90 ATPase cycle
- Figure 1.8. Alternative Hsp90 ATPase cycle
- Figure 1.9. Geldanamycin- Hsp90 complex crystal structure
- Figure 1.10. The crystal structure of yeast-p23/Sba1 complex
- Figure 1.11. Middle domain structure of yeast Hsp90
- Figure 1.12. Dimerisation model of Hsp90
- Figure 1.13. The charge Y motif
- Figure 1.14. Schematic diagrams showing the composition of, and transition between intermediate and mature complexes.
- Figure 1.15. The two structures of bovine Cyclophilin 40 (Cyp40)
- Figure 1.16. Structure of the Hsp90 inhibitors
- Figure 1.17. The carboxyl-terminal structure of htpG and yeast Hsp90

Chapter 2: Materials and Methods

- Figure 2.1. Illustration of SPR reaction
- Figure 2.2. Illustration of the ITC reaction

Figure 2.3. Illustration of the set up of the hanging drop vapour diffusion technique

Chapter 3: Cloning and purification of Hsp90

Figure 3.1. The locations of primer binding sequences in *C.elegans* Hsp90 genes

Figure 3.2. Agarose gel photos of the PCR products

Figure 3.3. SDS polyacrylamide gels and a Western blot of the C-terminal *C.elegans* Hsp90 proteins

Figure 3.4. SDS polyacrylamide gel of ceHsp90-492

Figure 3.5. Purification of ceHsp90-6 under native and denatured conditions

Figure 3.6. Sds polyacrylamide gel and Western blot of the expression of the C-terminal domain of human Hsp90 α

Figure 3.7. Amino acid sequences of human Hsp90 α show the location of protein constructs

Figure 3.8. SDS polyacrylamide gel of the C-terminal domain of human Hsp90 α after purification

Chapter 4: Characterisation of the C-terminal domain of human Hsp90 alpha

Figure 4.1. A cartoon representation of the C-terminal domains of the human Hsp90 α constructs used in this study.

Figure 4.2. Calibration curve of Superdex 200 plotted based on the K_{av} of the standard proteins

Figure 4.3. Chromatogram of the proteins eluted from Superdex 200 (Amersham Biosciences) gel filtration column

Figure 4.4. HHsp90- α 631 dimer formation

Figure 4.5. Gel filtration studies of complex formation using hHsp90- α 631 and bovine Cyp40

Figure 4.6. Gel filtration studies of the formation of complex between hHsp90- α 521 and bovine Cyp40

- Figure 4.7. Graphs showing Trp fluorescence measurements of the interaction between the C-terminal domains of human Hsp90 α with bovine Cyp40
- Figure 4.8. Generation of an NTA-hHsp90- α 521 sensor surface
- Figure 4.9. Binding of Cyp40 to Ni²⁺-NTA immobilized hHsp90- α 521
- Figure 4.10. Intrinsic Trp fluorescence of hHsp90- α 521 titrated with an increasing concentration of ATP
- Figure 4.11. Hummel- dryer experiment of hHsp90- α 521 and ATP
- Figure 4.12. ATPase activity of C-terminal human Hsp90 α using the malachite green assay system
- Figure 4.13. Study of the interactions of hHsp90- α 521 and N-acetyl tryptophan with novobiocin
- Figure 4.14. Inhibition of ATPase activity by novobiocin using the Malachite green assay
- Figure 4.15. Crystals of hHsp90- α 521

Chapter 5: Characterization of *C. elegans* Hsp90

- Figure 5.1. Chromatogram of the gel filtration experiment of cehp90 492 applied to a Superdex 200 column (Amersham)
- Figure 5.2. Interactions of *C. elegans* Hsp90 with bovine Cyp40
- Figure 5.3. SPR of the interaction between ceHsp90 492 with Cyp40
- Figure 5.4. Trp fluorescence experiment of GA binding to full length *C. elegans* Hsp90
- Figure 5.5. Graph of the Trp fluorescence observed upon binding between CeHsp90 492 and novobiocin
- Figure 5.6. Graph of the Trp fluorescence observed upon binding of CeHsp90 with ATP
- Figure 5.7. The ATPase activity of *C. elegans* protein and its inhibition of by novobiocin and geldanamycin
- Figure 5.8. ATPase activity and inhibition of ceHsp90 492-702

Chapter 6: General conclusions and future work

- Figure 6.1. The sequence alignment of C-terminal human Hsp90 α (hHsp90- α 521), yeast hsp82, *daf21*(*C. elegans*) and htpG
- Figure 6.2. The secondary structure prediction for the C-terminal human Hsp90 α and *C. elegans-daf21*
- Figure 6.3. Illustration of the binding of Cyp40 to the Hsp90
- Figure 6.5. Sequence alignments of yeast, *daf21*, human α and *htpG* C-terminal Hsp90 to show the motifs involved in ATP binding and hydrolysis
- Figure 6.7. Novobiocin binds to the C-terminal human Hsp90 α model structure
- Figure 6.8. Two molecules of ATP bind to the C-terminal binding pocket of human Hsp90 α
- Figure 6.9. Illustration of the mechanism of ATP binding to the C-terminal of Hsp90

Appendix A. Crystallographic study of cyclophilin-ligand interactions

- Figure A.1. Cyclophilin 3 crystal structure
- Figure A.2. The Xaa-Pro dipeptide utilised in the study
- Figure A.3. Refined occupancy of different crystal soaked in the series of Gly-Pro concentrations
- Figure A.4. Two density maps of Cyp3 soaked with Gly-Pro
- Figure A.5. Superposition of Xaa-Pro dipeptide:Cyp3 structures

List of tables

Chapter 2: Materials and Methods

Table 2.1. Phosphate dilution series used to produce the standard curve for phosphate used in the malachite green ATPase assays

Chapter 3: Cloning and purification of Hsp90

Table 3.1. List of the genes and their sizes that were cloned to obtain the target proteins

Table 3.2. List of the primers used in the cloning experiments

Table 3.3. Summary of the cloning and expression of C-terminal *C. elegans* Hsp90

Table 3.4. Lists of the constructs of the C-terminal of human Hsp90 α

Chapter 4: Characterisation of the C-terminal domain of human Hsp90alpha

Table 4.1. Proteins standards used to calibrate the Superdex 200 gel filtration column

Table 4.2. Lists of the information obtained by running 100 μ M of each proteins through Superdex 200

Table 4.3. List of results obtained from all the human Hsp90 α experiments that were carried out in Chapter 4

Chapter 5: Characterization of *C. elegans* Hsp90

Table 5.1. List of the results obtained from all the experiments carried out to the *C. elegans* Hsp90 in chapter 4

Chapter 6: General conclusions and future work

Table 6.1. Function of conserved motifs in the nucleotide binding domain of ABC transporter

Table 6.2. List of the results obtained from the experiments that were carried out throughout the thesis.

Appendix A. Crystallographic study of cyclophilin-ligand interactions

Table A.1. Crystallographic statistics of the four Cyp3 structures

Table A.2. A summary of the K_{dc} and the K_{ds} values of the the Xaa-Pro interaction with Cyp3

Chapter 1: Introduction

1.1. Heat shock protein 90 (Hsp90)

The 90-kDa heat shock protein (Hsp90) is a ubiquitously distributed molecular chaperone and is an essential protein in eukaryotic cells [10]. The protein exists in most of the compartments of mammalian cells. For example, human Hsp90 α is present in the cytosol [38]; the 94-kDa glucose regulated protein (GRP94) is expressed in the lumen of the endoplasmic reticulum [75] and TRAP1/Hsp75 is expressed in mitochondria [31]. Hsp90 homologues are also found in several species such as the high temperature regulated protein (htpG) in *E. coli* [9, 36] and *daf21* in *C. elegans* [24]. Hsp90 is involved with a variety of proteins however a primary function is as a molecular chaperone.

As mentioned, Hsp90 is present in various species, however the core sequences of all the molecules are highly conserved. A multiple sequence alignment of Hsp90 human alpha and beta, yeast and *daf21* which will be frequently referred to in this thesis showed 60 to 70% sequence identity. Only htpG gives a lower value of 50% identity as would be expected because htpG lacks several of the very highly conserved C-terminal sequences as well as showing differences in the middle domain (Figure 1.1).

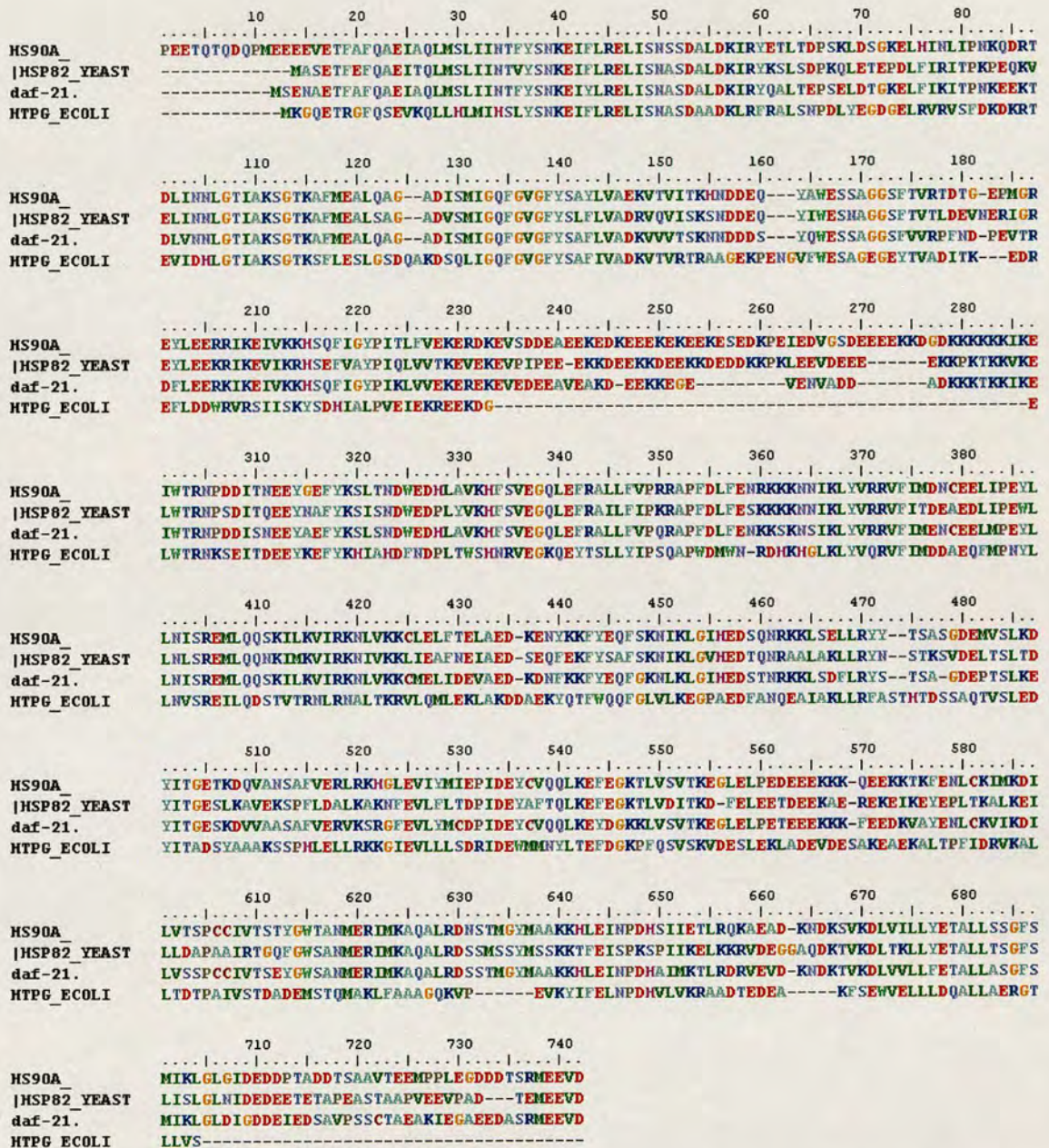


Figure 1.1. Sequence alignment of the Hsp90 homologs that are utilised in the study. The proteins were very similar sharing almost 70% identity. HtpG is the most divergent, lacking 100 amino acids very well conserved in other molecules including the MEEVD from the C-terminus. The alignment was carried by using ClustalW.

The interactions between Hsp90 and a number of other proteins have been extensively investigated. These partner proteins have been classified as co-chaperones as they function together with the Hsp90 and influence its interactions with client proteins [13]. The best characterised examples of co-chaperones are Hsp70 [16, 61, cdc37 {Abbas-Terki, 2002 #108, 63, 74, 79}] and TPR containing proteins such as Cyp40, FKBP51, Hop, FKBP52 [16, 18, 20, 27]. By binding to the co-chaperone, Hsp90 is able to bind to the client proteins promoting amongst other functions refolding and dissociation [93]. Examples of client proteins include many kinases such as eIF-2alpha [26], v-Src [37, 45], Akt [13] and transcription factors including p53 [60, 62].

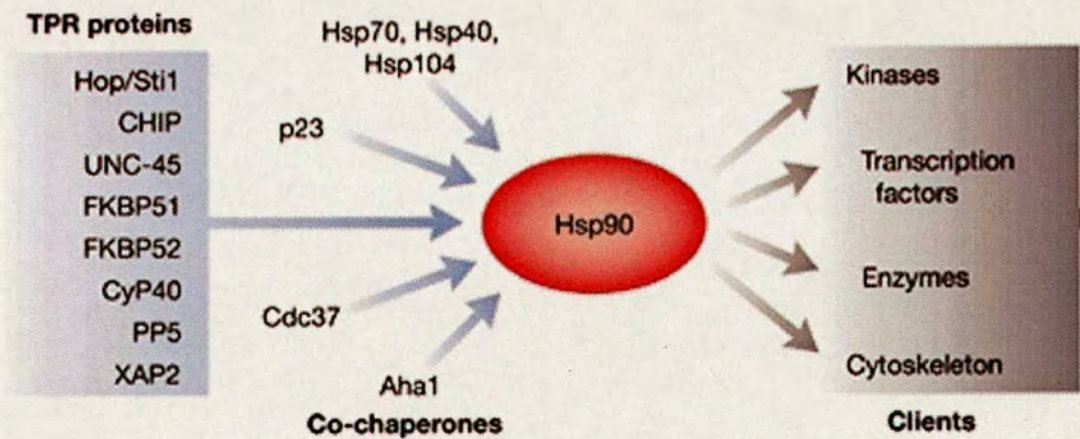


Figure 1.2. Overview of interactions the Hsp90 with other chaperones and clients protein. The cartoon is modified from that of Caplan *et. al.* [13].

Structurally, Hsp90 consists of three domains. Each of the domains are vital to Hsp90 to enable the binding seen with partner proteins and also to allow them to carry out specific functions. These domains are the N-, middle and the C-terminal (Figure 1.3) [12, 84]. The N and C-termini of Hsp90 are well conserved. The middle domain is a highly charged region that differs between species (Figure 1.3). The middle domain is largely missing in prokaryotes such as the *E. coli* htpG [12]. Full length Hsp90 is elongated in shape and forms a dimer via its C-terminal domain [81, 84, 87, 105].

Recently, the crystal structure of the full length yeast Hsp90 was solved [3]. The solved crystal structure is a complex of the full length yeast Hsp90 with an ATP analogue and the co chaperone p23/Sba1 (Figure 1.4). The crystal structure containing just the middle and the C-terminal protein were also solved (Figure 1.4). The crystal structure of the complexes (termed 'closed' structure) reveals more information on the structure and function of Hsp90 in binding to ATP and co-chaperone proteins p23/Sba1.

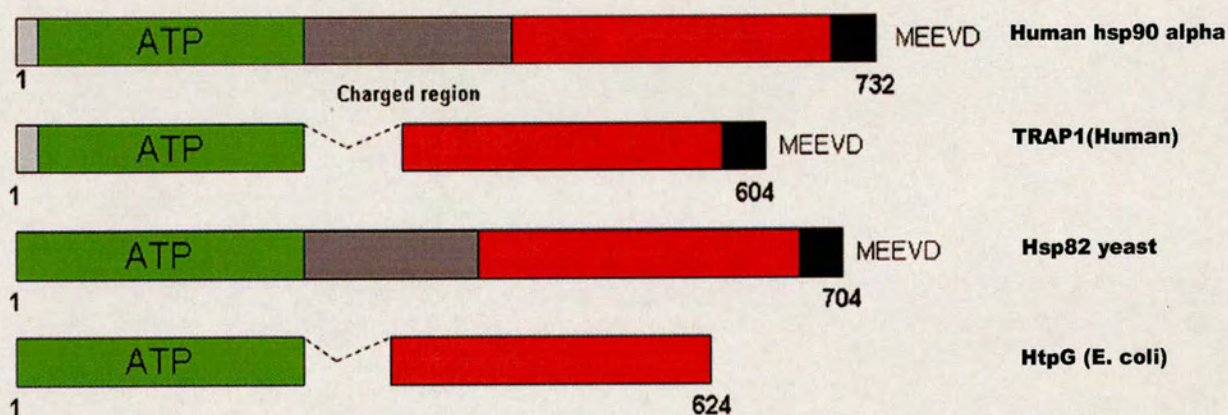


Figure 1.3. Cartoons of Hsp90 from different species. The charged region is almost missing in some eukaryotes such as TRAP 1 and prokaryotes such as htpG. The N-terminal (Green) consists of the ATP binding site and is well conserved between species. The C-terminal domain consists of MEEVD motif (Black) which also well conserved except in htpG.

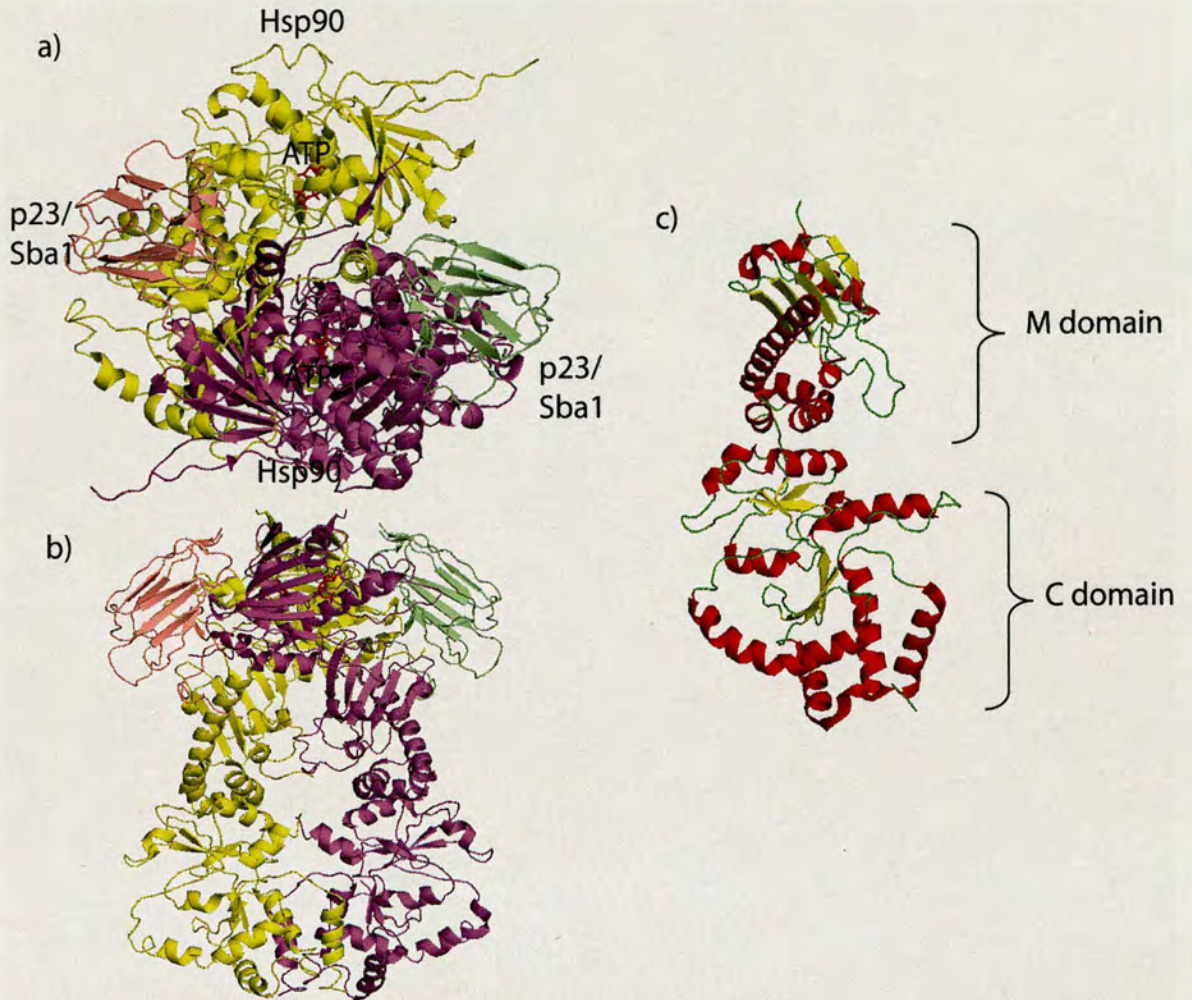


Figure 1.4. The crystal structure of full length yeast Hsp90/Sba1(p23) complex and the M-C domains. a) Top view of the crystal structure of the Hsp90-p23/Sba1-ATP complex. b) Side view of the same complex crystal structure. c) The crystal structure of the M-C domain of yeast Hsp90. The figures were generated with PyMol by using PDB files Id 2CGE and 2CG9.

1.2. N-terminal domain of Hsp90

The N-terminal roughly consists of amino acids 1-220. The N-terminal domains of Hsp90 are well conserved among species. The N-terminal domains of Hsp90 human

α , yeast and *C. elegans* are 60-70% identical. However, the N-terminal domain of htpG is only 40% identical to other Hsp90 molecules. The N-terminal domain contains a binding site for ATP/ADP [40, 80, 84]. Published studies of the ATP binding site in the N-terminus of Hsp90 have improved our understanding of Hsp90. Details of the molecular interactions are also now available with the structure determinations of the full length yeast Hsp90 and the N-terminal domain on its own [12, 81-84, 87, 88 {Ali, 2006 #1042, 90, 104}. Besides ATP, Hsp90 binds specifically to geldanamycin (GA) [91, 98] and radicicol [91]. The N-terminal structure was also solved by x-ray crystallography, as a complex between geldanamycin and the N-terminus of yeast Hsp90 [81, 91] and human Hsp90 [98]. The N-terminal domain also binds to p23/Sba1, but p23/Sba1 only binds to ATP bound Hsp90.

1.2.1. ATP/ADP bind at the N-terminal of Hsp90

The N-terminal domain of Hsp90 contains the site for binding to ATP. The site was confirmed from the crystal structure of yeast Hsp90 as well as biochemical studies. [34, 71, 83, 90]. In the crystal structure (Figure 1.5), the binding site is shown to lie in a deep pocket on the helical face of the N-terminal domain. The binding pocket is made up of helices from 28–50 and from 85–94 on two sides. The other two sides of the pocket are made by the end of the helix and loop from 117–124 and the loop from 81–85. The base of the pocket is made up from residues Ile-77, Asp-79, Val-136, Ser-138, Thr-171, and Ile-173, whose side chains project up from the buried face of the β sheet. The adenine base of ATP/ADP penetrates the base of the pocket and makes the only direct hydrogen bond to Asp-79. The adenine base also makes other hydrogen bonds but

indirectly via water molecules to Leu-34, Asn-37, Asp-79, Gly-83, and Thr-171. The ribose of an ADP is also indirectly hydrogen bonded to the side chain of Asn-92, through a water molecule [80].

In the recent structure, the γ -phosphate is located in a glycine-rich loop at the C-terminal hinge of the lid and forms a hydrogen bond with the peptide backbone of Gln 119, Gly 121, Val 122 and Gly 123 (Figure 1.6 b). The β -phosphate hydrogen bonds with the peptides of Phe 124, and Gly 100 from the N-terminal hinge [3]. With an ATP analogue bound to the N-terminal domain, the small middle domain (residues 445-524) was brought forward to 10 Å closer. The large middle domain (262-444) was brought closer about 20 Å together. As a result, the gap remaining between the middle domain is too small to accommodate a folded client protein (Figure 1.6a).

Based on Isothermal Titration Calorimetry (ITC) studies, ATP and ADP bind to the N-terminal of Hsp90 with a dissociation constant of 132 ± 47 and 29 ± 3 μM , respectively, with binding stoichiometries that have been shown to be close to 1 nucleotide per N-domain monomer [80]. ITC was also carried out using Hsp90 human α and the K_d was 240 ± 14 μM [McLaughlin, 2004 #6] Both of the experiments were carried out at 25°C. However, human Hsp90 α was shown to bind more strongly to ADP at 25°C with a K_d of 7.4 ± 1.1 μM . The K_d was decreased to 41 ± 6 μM when the temperature was increased to 37°C [52].

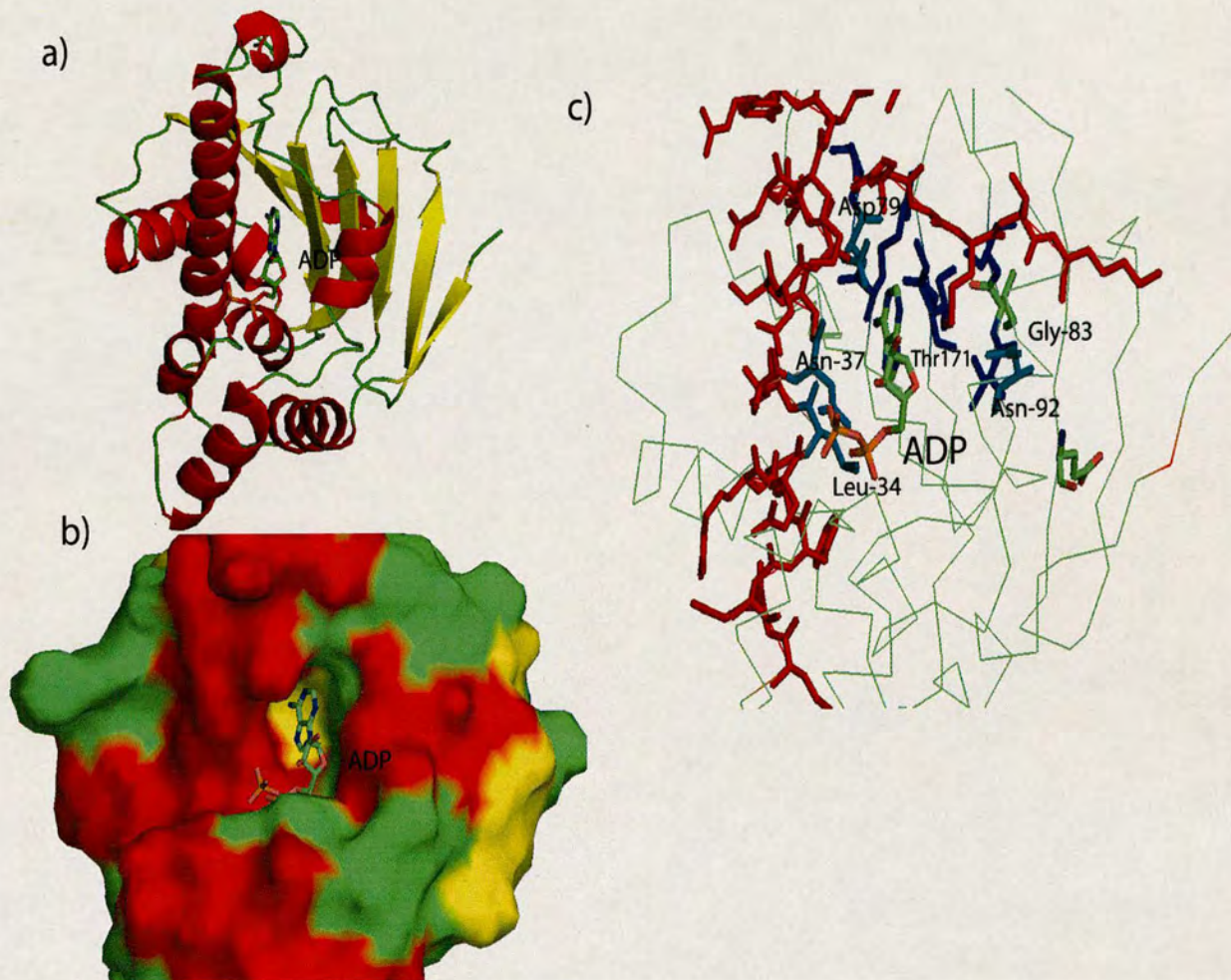


Figure 1.5. Overview of the complex structure of ATP/ADP bound to the N terminal domain. a) and b) are the same pictures show ADP bound to the molecule except b) shows ADP docking on to the surface of the N-terminal. c) ADP orientation on the binding pocket. Red coloured residues show the sites of the binding pocket. The blue coloured residues indicate the base of the pocket. The labelled light blue coloured residues show the amino acids that are involved in the interaction with ADP. The picture was modified from PDB file id 1AM1 by using PyMol.

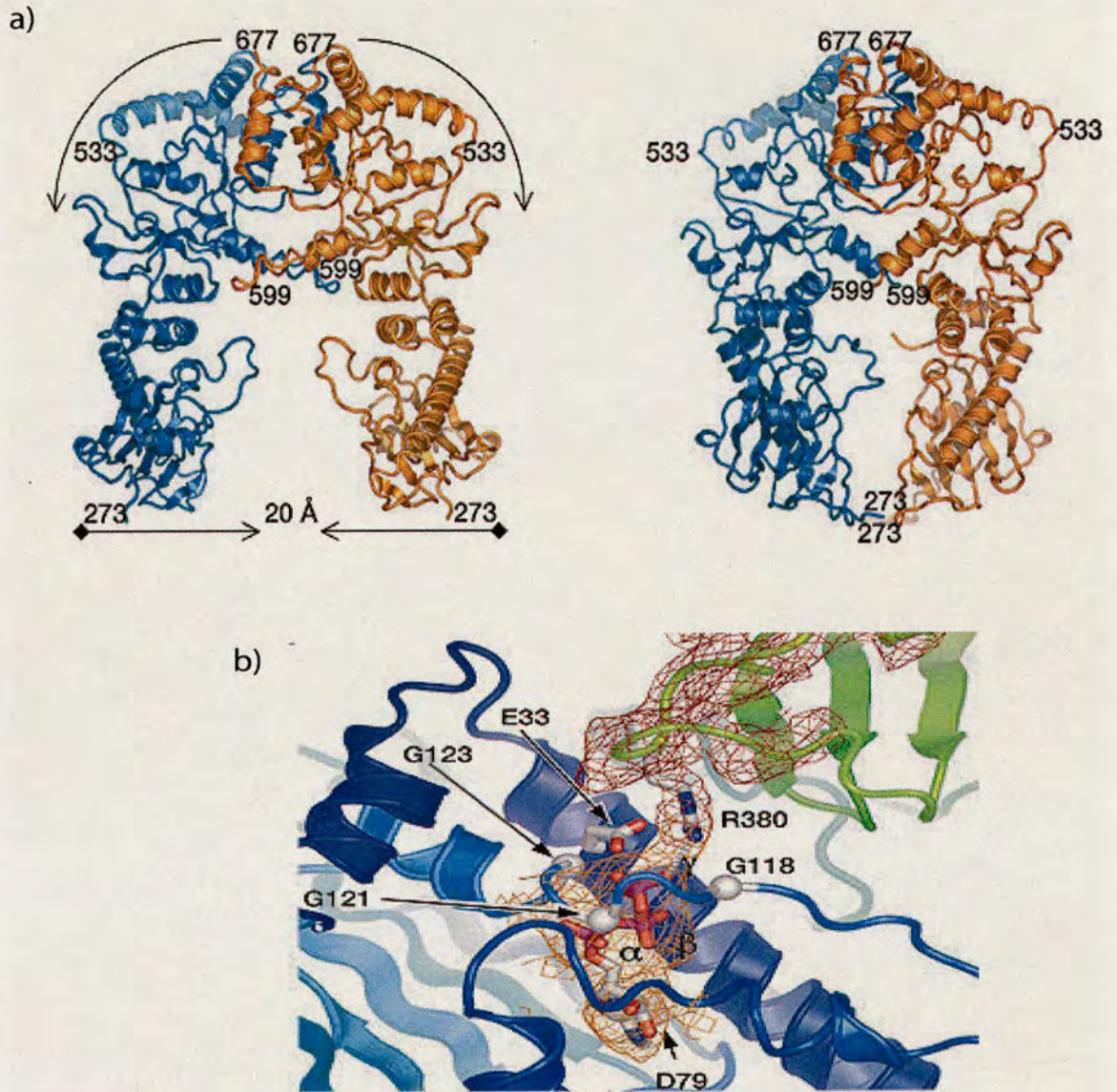


Figure 1.6. Conformational changes of yeast Hsp90 when ATP binds to the N-terminal domain. a) The conformational changes of the M-C domains when ATP binds to the N-terminal. The binding of ATP brings the large middle domain 20Å closer. b) The position of AMP-PNP when cradled into the glycine rich loop. The γ -phosphate of AMP-PNP is orientated for attack by water activated by Glu-33. Arg-380 polarizes the γ - β phosphodiester bond and neutralises the transition state. The figures were adapted from Ali *et. al.* [3].

1.2.2. ATP hydrolysis by Hsp90

ATP not only binds to Hsp90 but is also hydrolysed by the protein [2, 49, 52, 96]. The rate of ATP hydrolysis differs between species. Yeast Hsp90 hydrolysed ATP with a K_{cat} of 0.47 min^{-1} [52, 71, 83] which is the fastest published ATPase rate of any Hsp90 species. Human Hsp90 has a very weak ATPase activity which is 0.092 min^{-1} [52]. The suggested mechanism of the ATPase cycle is illustrated on figure 1.7 which was modified from [86]. In the ATPase cycle, Hsp90 is presumed to be a dimer. When ATP binds to the N terminal, the Hsp90 molecule undergoes a structural transition in which the ATP becomes committed to hydrolysis. The conformation of Hsp90 changes and traps the ATP molecule at the nucleotide binding cleft of the N-terminus [104]. It had been reported that Hsp90 becomes more hydrophobic in the presence of ATP [99]. Under these conditions, the N-terminal domain of the dimer, (which usually points outward), closes up and lysine 342 of the Hsp90 forms an additional protein/nucleotide interaction that is required for maximum turnover. As the nucleotide pocket closes, ATP is hydrolyzed. The ATPase cycle of Hsp90 is completed by the release of ADP.

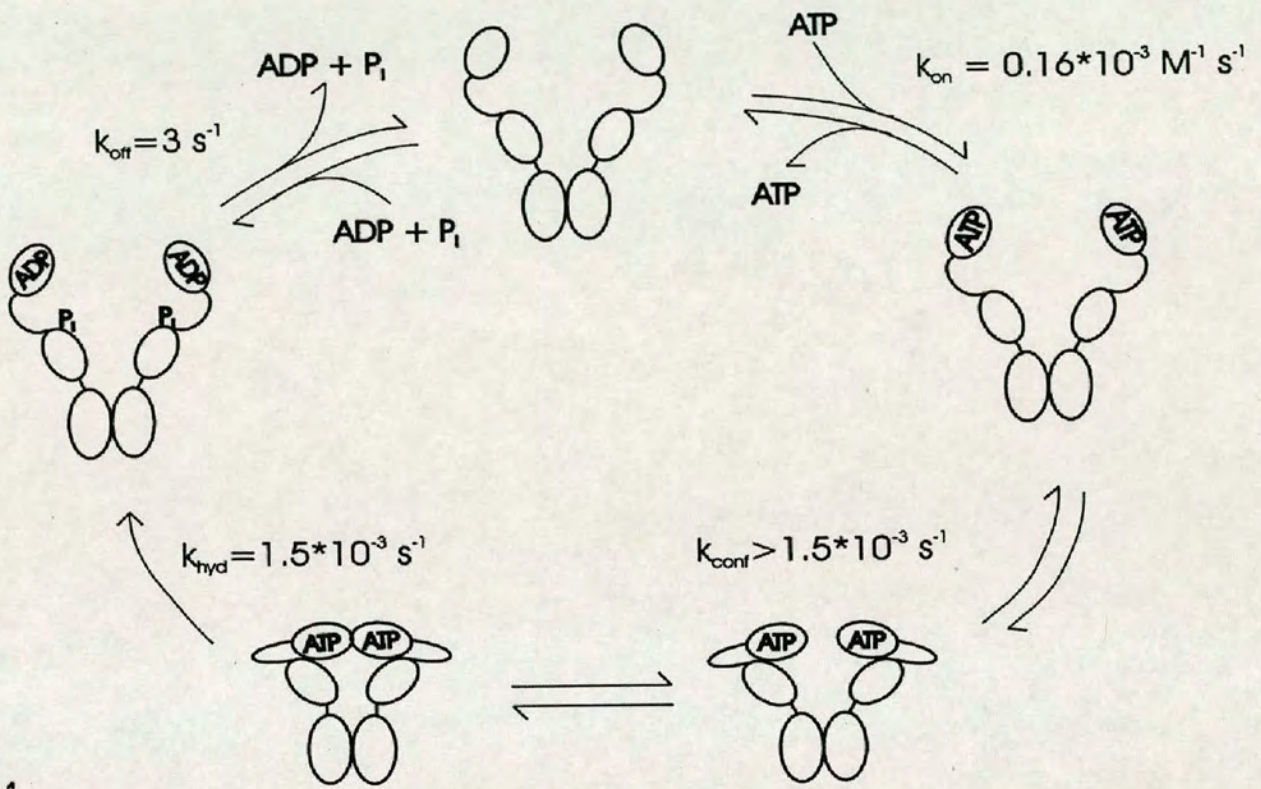


Figure 1.7. The suggested Hsp90 ATPase cycle. The cycle involves two conformational changes that lead to ATP being trapped. ATP is hydrolysed and finally ADP is released. The kinetic data was obtained from [104]. $k_{\text{on/off}}$ refer to the rate of ATP binding and ADP dissociating from the molecule of Hsp90. k_{conf} indicates the rate of conformational changes of Hsp90 molecule to N-terminal dimerisation. k_{hyd} represents the ATP hydrolysis rates. The illustration was modified from [86].

Besides the above model of ATPase cycle, McLaughlin *et. al*, [52] have proposed an alternative ATPase cycle based on their studies (Figure 1.8). In their model, ATP binds rapidly to Hsp90 under diffusion control (A to B). ATP induces a conformational change possibly involving the “ATP-lid” in the N-terminal domain and /or contact between the N and M domain (B to C). At this stage, the affinity for client proteins as well as co-chaperone p23 is very high. The ATP is then hydrolysed possibly involving the rearrangement of a catalytic loop in the M domain. The ADP bound state D has a lower affinity for both the client and p23. In this model, the dimerisation of the N-terminal domain when bound to ATP is not necessary, however the dimerisation of the C-terminal is important to increase the binding as well as the hydrolysis [51, 52].

ATPase activity in yeast Hsp90 is vital to the *in vivo* function [69, 71]. The deletion of both Hsp90 proteins in *Saccharomyces cerevisiae* (hsp82 and hsc82 which are 97% identical) also results in cell death [10]. The mutations of Glu-33 (E33) or Asp-79 (D79) of yeast Hsp90 which is involved in the binding and hydrolysis of ATP, makes the protein unable to bind to p23. This suggests that ATP binding is important for the interaction of Hsp90 to p23 [69, 99{Ali, 2006 #1042}. In contrast, Sti1 binds to Hsp90 independent of ATP and inhibits the ATP binding and hydrolysis [82], thus also inhibiting any interaction with proteins that may be dependent on ATP binding.

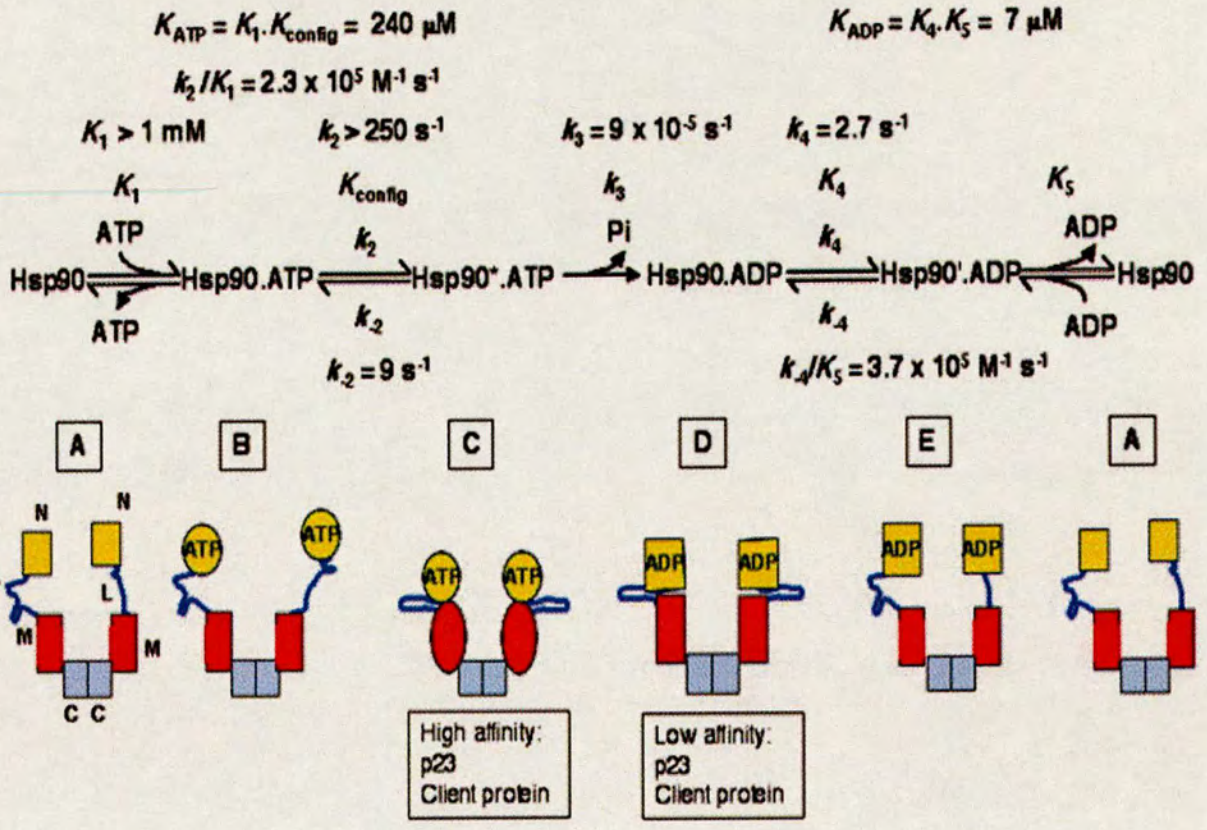


Figure 1.8. Alternative Hsp90 ATPase cycle [52]. The study was based on human Hsp90 α Hsp90 molecule in dimer formation binds to ATP under control of rapid diffusion. The ATP is hydrolysed after the 'lid' formation between N and the middle domain. During the 'lid' formation, Hsp90 has high affinity to p23 and client proteins. The conformation was restored after the release of ADP.

1.2.2. Geldanamycin (GA) binds to the N-terminal domain of Hsp90 and inhibit ATPase activity

Besides binding to ATP at the N-terminal domain, GA has also been shown to bind at the same site. The binding of GA was observed from the crystal structure of the complex that was obtained by co-crystallization [98]. GA, a benzoquinone ansamycin antibiotic and natural product of *Streptomyces geldanus*, binds with high affinity to ATP-binding sites of Hsp90 (Figure 1.16)[25]. The crystal of the human Hsp90 was obtained from the amino terminal that corresponded to the geldanamycin binding domain (Hsp90-GBP). The protein consists of amino acids 9 to 236 of the human Hsp90 human. The protein crystallized to give two distinct forms which show different local conformations. The two apo forms of the Hsp90-GBP diffracted to 1.65 Å and 2.2 Å respectively while the structure of the geldanamycin complex diffracted at 1.95 Å [98]. The structure consists of nine α helices and eight anti-parallel β -sheets that form the α + β sandwiches (Figure 1.9). Four of the helices (H1, H2, H4 and H9) pack flatly onto the β sheet and their axes are parallel to the β strands. However, another helix (H7) packs steeper or almost perpendicular to the β sheet. There is also a second layer of helices (H5 and H6) that pack onto the first layer. In addition, two other helices H3 and H8 were packed at the periphery of the sandwich. At the centre of the domain, the helical face of the sandwich has a wide opening which extends into the hydrophobic core of the structure and forms a pocket about 15 Å deep. The pocket has a β sheet as its base and its walls are made by three helices and a loop [98]. In the crystal complex, the tip of the GA molecule has a ring that consists of carbamate C23 methoxy, and C25 and C26

methyl group substituents, which binds near the bottom of the Hsp90 pocket and form a large number of van der Waals contacts.

The N-terminal structure of yeast also exhibits a similar arrangement in its tertiary structure. It consists of an eight- stranded highly twisted β -sheet covered on one face by α helices. Even though, this is extremely similar, the quaternary structure of the yeast N-terminal is different. The yeast N-terminal domain crystallised as a dimer while the human N-terminal crystallised as a monomer. The dimer forms of the crystal provides a better mimic for Hsp90 in nature. In the structure of the yeast N-terminal domain observed from the crystal, the C-terminal of the β sheets of each monomer are antiparallel with each other and form a continuous hydrogen bonded sheet within the 16 β sheets of the dimer [80]. The dimer sheet folds back to form a cylindrical channel between the two monomers. The channel can accommodate around 8 to 10 residues of polypeptide chain in an extended conformation. This arrangement and shape, suggests that it may function as a molecular clamp (Figure 1.9).

Geldanamycin binds to the full length dimeric Hsp90 with a K_d of 1.2 μM with a stoichiometry of one molecule GA to one monomer of Hsp90 [91]. The dissociation constant was determined by ITC [91]. Radicol is also shown to bind to the N-terminal domain of Hsp90 [1, 92, 95]. The binding was shown to be tighter than GA with a K_d of 19 nM [91]. Both of the inhibitors above were shown to be specific inhibitors of the ATPase activity of Hsp90. They are thought to bind to the ATP site and prevent ATP

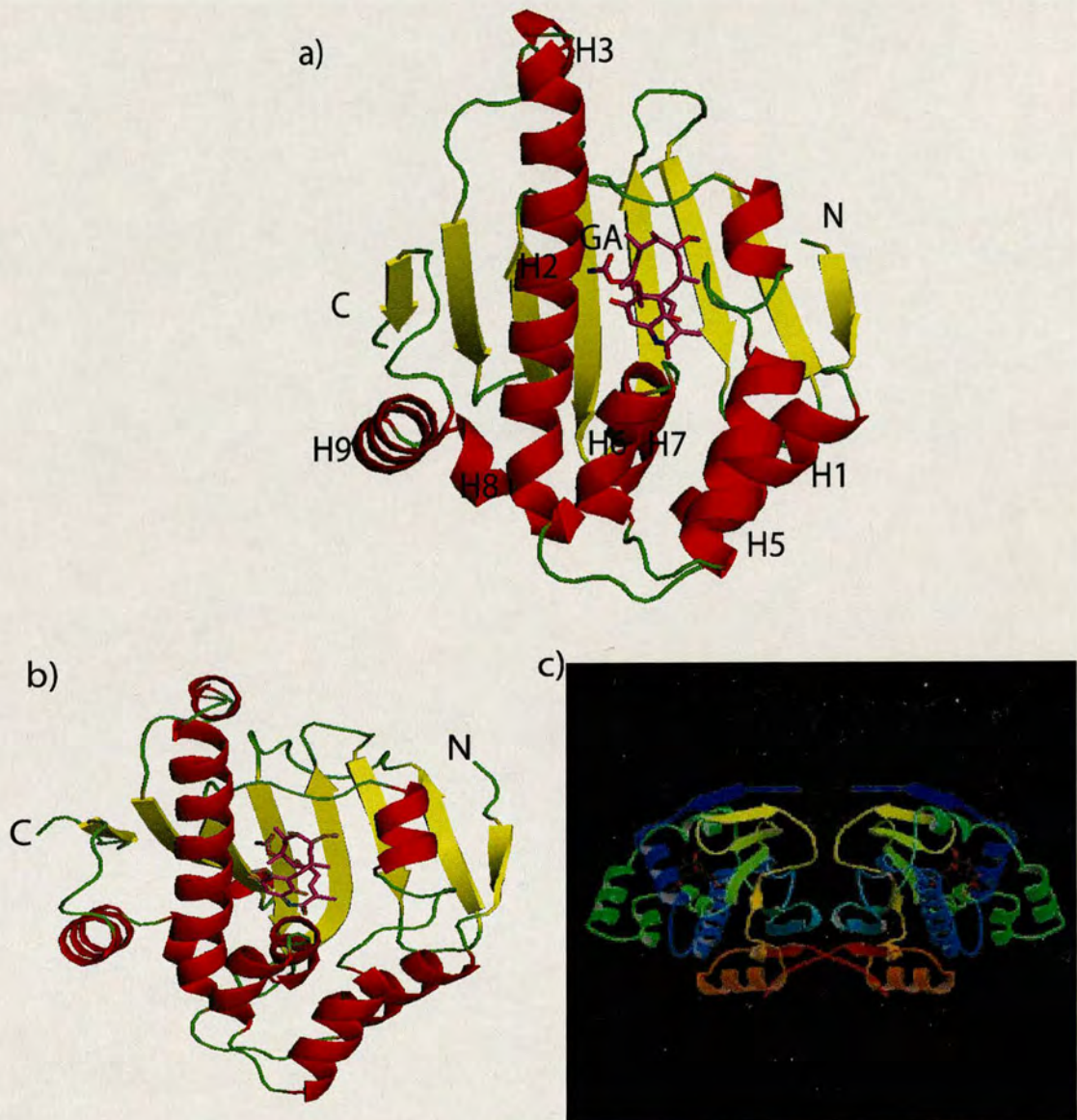


Figure 1.9. Geldanamycin- Hsp90 complex crystal structure. a) N-terminal domain of Hsp90 human-GA complex structure .The helices are labelled. The structure was extremely similar with b) which is the structure of the yeast Hsp90-GA complex. However, the quaternary structure of the yeast Hsp90-GA complex, c), was different because the N-terminal of the yeast Hsp90 crystallised as a dimer, where the C-terminal of the domain form continuous hydrogen bond. The dimer forms a cylindrical channel which can accommodate a peptide binding between them.

from binding to the Hsp90 [80, 91], thus resulting in the inhibition of p23 binding [34, 70, 77].

GA was shown to be resistant to the homolog of Hsp90 in *C.elegans* (*daf-21*). In the studies [24], the soil-dwelling nematode *Caenorhabditis elegans* was exposed to GA under a series of conditions designed to optimize the drug uptake. However, exposure of worms to GA produced no discernable phenotypes. In agreement, solid phase-immobilized GA failed to bind worm Hsp90 from worm protein extracts. Further study was carried out by expressing plasmid constructs encoding either unmodified chick and worm protein or chimeric proteins by using transcription-translation reactions in reticulocyte lysate. The chimeric proteins consist of either chick N-terminus fused to worm C-terminus (c/w) or worm N-terminus fused to chick C-terminus (w/c). GA affinity precipitation was carried out with these proteins. The c/w chimeric protein was able to bind to GA beads as the unmodified chick Hsp90. Similarly, the w/c chimeric protein was unable to bind to GA beads as the unmodified worm Hsp90. This, suggests that the inability of worm Hsp90 to bind GA was unlikely to be a result of intramolecular interference by the worm's C-terminal domain [25]. These chimeric proteins produce were also still able to bind to adenosine triphosphate. Heterologous expression of worm Hsp90 in tumor cells, however, were still susceptible to GA.

1.2.3. p23 binds to N-terminal domain of Hsp90

As mentioned before, the N-terminal domain consists of the site for binding and hydrolysis of ATP. The regulation of the Hsp90 ATPase cycle was assisted by p23 or its yeast homolog Sba1 and several other proteins [3, 53, 77{Chen, 1998 #18}. p23 was shown to have a preference to bind to the ATP bound form of Hsp90 [41, 43, 89, 101] and the binding of p23 reduces the rate of ATPase activity. Therefore, more time is available for the client proteins to bind to Hsp90, thus allowing Hsp90 to carry out its structural functions. However, there is evidence that p23 can bind to the ATP free form of Hsp90 but less tightly than with ATP bound form of Hsp90 [53, 89]. p23 binds to Hsp90 with the stoichiometry of one dimer Hsp90 to two p23 [53{Ali, 2006 #1042, 89]. In the complex crystal structure of yeast Hsp90, p23 and ATP analogue (Figure 1.10), the p23 /Sba1 is symmetrically attached on each site of the Hsp90 monomer. The N-domain connects to the middle segment by antiparallel β strands involving residues 206-213 and 262-269. The monomers of Hsp90 have a parallel arrangement with the N-terminal domains at one end of the dimer and the C-terminal domains at the other. This is achieved when the Hsp90 molecule makes a left handed twist. As a result of the twist, the amphiphatic loop (residues 329-339) projects from the inner surface of the large domain towards its equivalent in the other monomer (Figure 1.10) [3].

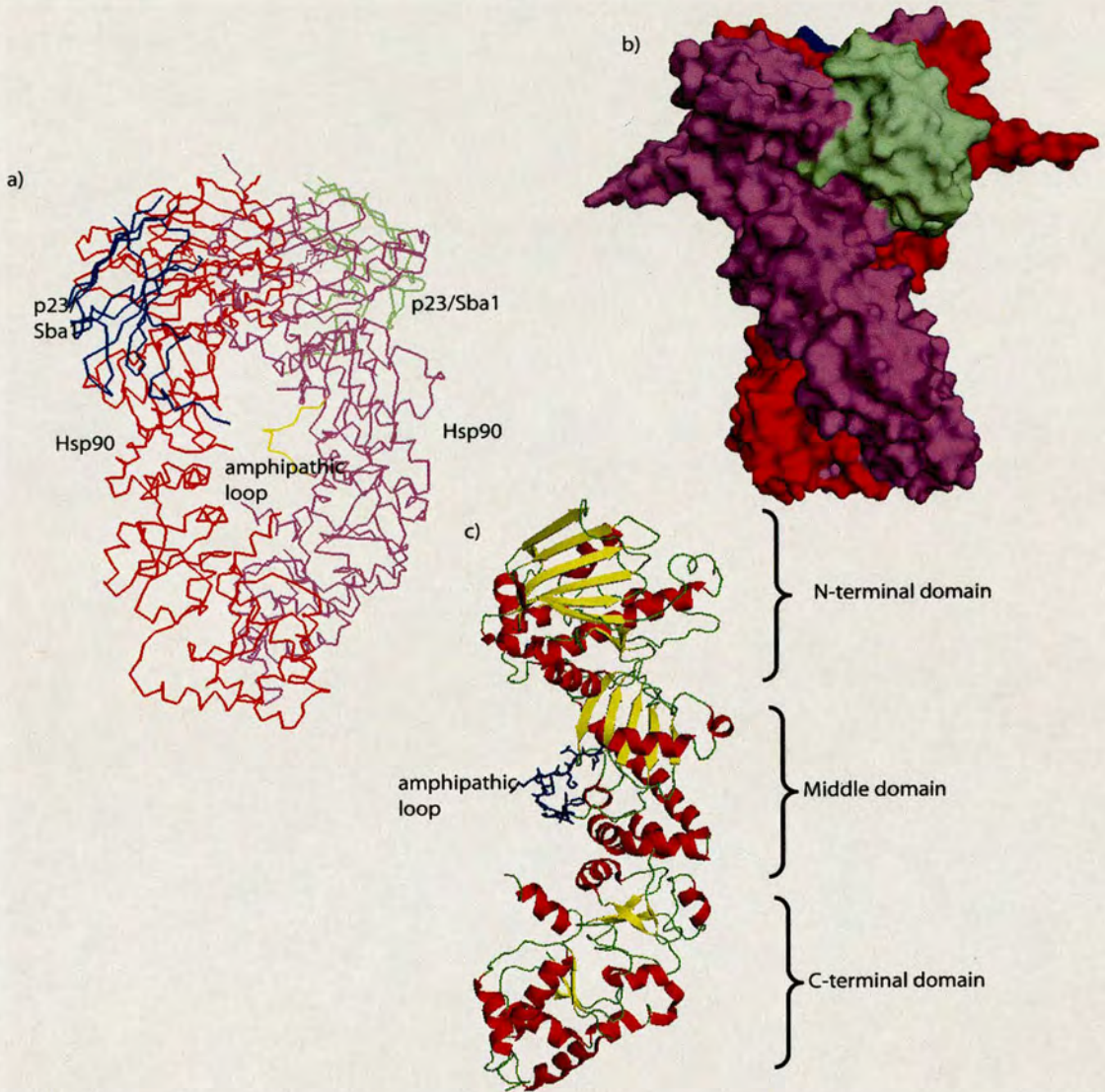


Figure 1.10. The crystal structure of yeast-p23/Sba1 complex. a) Backbone tracing of the complex. Hsp90; purple and red. p23/Sba1; blue and green. The yellow colour indicates the location of amphipathic loop. b) Molecular surface representations of the complex but 90° twisted along the dimer vertical axis. The colour codes are the same as a). c) Orthogonal view of the Hsp90 monomer showing the N to C-terminal domains. Amphipathic loop was represented by blue colour.

1.3. Middle domain of Hsp90

The middle domain of Hsp90 is a highly charged region. The middle region varies between species and is not well conserved. The region is almost missing in prokaryotic cells [12]. The region is involved in the association of Hsp90 with steroid receptor [23]. It binds to Aha1 [45] and is also involved in the binding of ASK1 or Akt. Furthermore, the domain holds both of the proteins in close proximity thus initiating the formation of complexes between Akt and ASK1 [110]. As mentioned before, the middle domain binds to Aha1 as well as its homolog Hch1. However, Hch1 was only found in *Candida albicans* and was not conserved between species [45, 55] The binding of Hsp90 with these proteins increases the rate of ATPase activity up to 12-fold [50]. Aha1 was shown to be stage independent when binding to Hsp90 and does not interfere with the binding of co-chaperones. In the presence of Aha1, p23 can still inhibit the hydrolysis of ATP [50, 72].

The middle domain of yeast Hsp90 and *E.coli* Hsp90 (htpG) were crystallised and the structures have also been solved [3, 40, 54]. In the yeast Hsp90 middle domain, it can be divided into three regions that form α - β - α sandwich (Figure 1.11). The sandwich consists of a five stranded β sheet, a three turn α helix and irregular loops on the convex surface and a six turn α helix nestling in the concavity of the opposite face [3, 54]. Three features were identified in the middle domain that play vital roles in catalysing ATP hydrolysis. A catalytic loop (Gln 335-Ile388) was identified to help the ATPase hydrolysis by sensing the γ -phosphate of ATP when it is bound to the N-terminal. This

event will then activate the attacking water molecule in the ATPase hydrolysis reaction. There is also a hydrophobic surface patch centred on Phe 349 which is near the tip of the loop formed by residues 342-352. This hydrophobic patch is suggested to be involved in the interdomain communication and positioning of the catalytic groups from the N-domain and middle segments. Another hydrophobic patch which is exposed and consists of Trp 300, and Phe 329, Leu 331 and Phe 332 formed one side and the tip of a conformationally flexible loop, have been identified which could be involved in protein-protein interactions [54.. The flexible loop was cantilevered out from the body of the main structure. This solvent-exposed loop has an unusual sequence (327-A P F D L F E S K K K K N N-340) generating an amphipathic structure, with one hydrophobic side and one positively charged side {Meyer, 2003 #368, 56}. The amphipathic loop was observed to project from the inner face of the large domain towards its equivalent in the other monomer when bound to p23 (Figure 1.10 c). The middle domain is also shown to stabilise the closed formation of Hsp90 when it binds to ATP by coming closer to each other but without making any direct inter domain contacts [3].

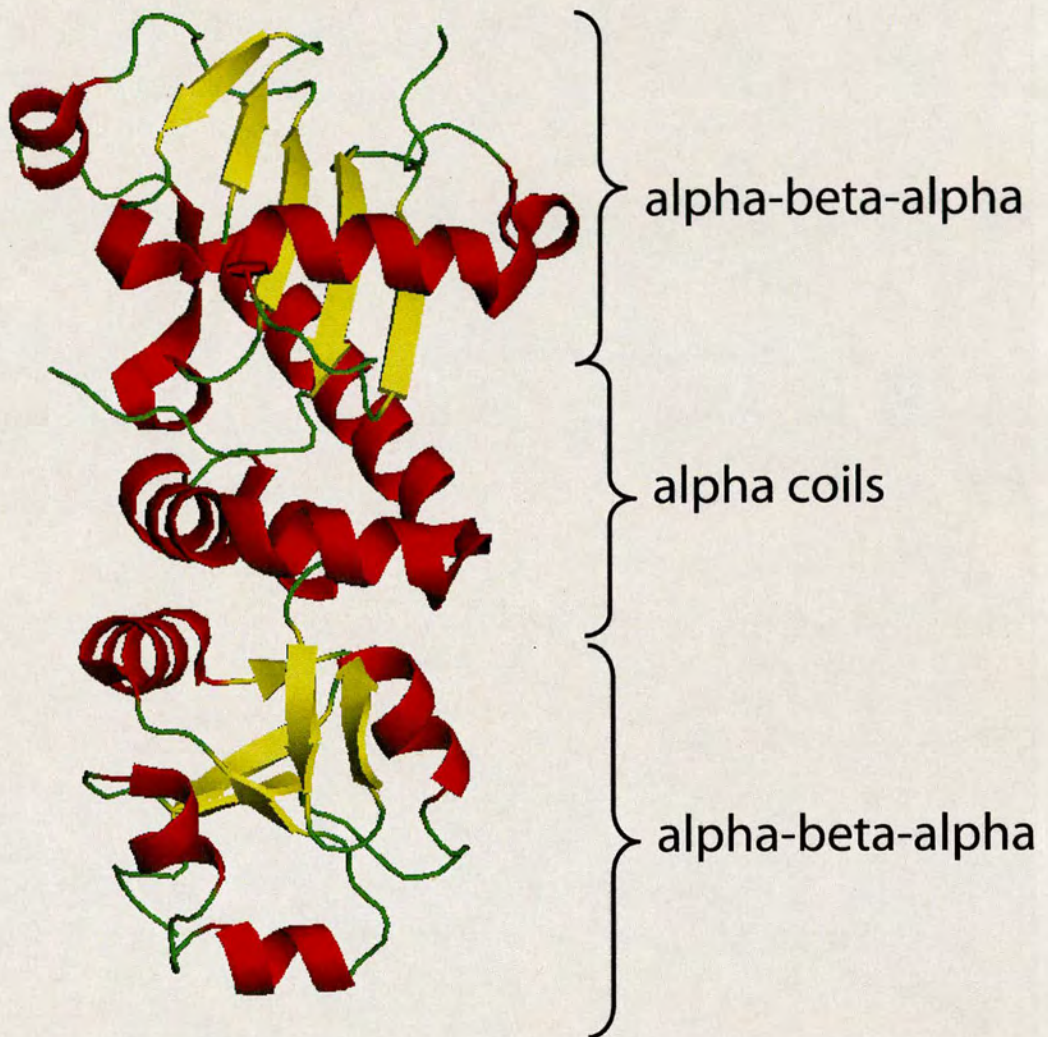


Figure 1.11. Middle domain structure of yeast Hsp90. The structure consists of sandwiches of $\alpha\beta\alpha$. The PDB id of is 1HK7. The picture was modified by using PyMol.

1.4. The C-terminal domain of Hsp90

The C-terminal domain of Hsp90 also plays a number of vital roles in the function of Hsp90. This domain has been shown to bind client proteins such as the TPR

containing proteins [11, 21, 39, 85] and immunophilins [20, 27, 105] as well as inhibitor such as novobiocin and coumarin [44, 109].

1.4.1. Hsp90 forms a dimer

Hsp90 exists in solution as a homodimer. Dimerization occurs through the C-terminal domain of Hsp90 [57, 87, 90, 103]. The dimerisation of Hsp90 is important for the function of the protein. Studies on Hsp90 human α and β revealed that the C-terminal domain contains the site for dimer formation, deletion of this region of the protein resulted in the loss of dimer formation. Hsp90 human α requires at least 50 residues of the C-terminal domain to enable dimer formation [57]. A C-terminal construct of Hsp90 human α containing residues 542-732 was sufficient to form a dimer [67]. The dimerisation constants of wild type Hsp90 was shown to be around 60 nM as determined by gel filtration studies [87]. A model of the mechanism of dimerisation was proposed which suggested that the dimer formed in an antiparallel fashion [66, 68]. The study was carried out using limited proteolysis of the protein coupled with two dimensional page. From this study, the protein could be delineated into three domains designated A,B and C. The C domains bind to each other in anti parallel fashion to form the dimer. Further studies were carried out on htpG and revealed similar domain structure, however domain B consists of two sub-domains designated BI and BII [68]. This extended model showed that 16 residues of BII were also involved in the dimerisation of Hsp90.

In the carboxy terminal structure of htpG, the dimerisation domain was identified to be located on the two helices at the end of the proteins (Figure 1.12). The two helices

(H4 and H5) were formed by the residues 587 to 624 of htpG. The two helices interact with their equivalent counterparts from the second monomer and formed a four helix bundle [36]. The same observation was made with the yeast Hsp90 structure. In addition, a helix strand segment (residues 587-610) projects from the core of the C domain towards the N-terminal end of the dimer and is involved in the dimer interaction (Figure 1.12). The helix strand segment become disordered when ATP binds to the Hsp90 [3]. Dimerisation through the C-terminus of Hsp90 was vital for effective hydrolysis of ATP. In the absence of the dimeric form of the protein, the rate of ATP turnover of Hsp90 was reduced [52, 87, 103].

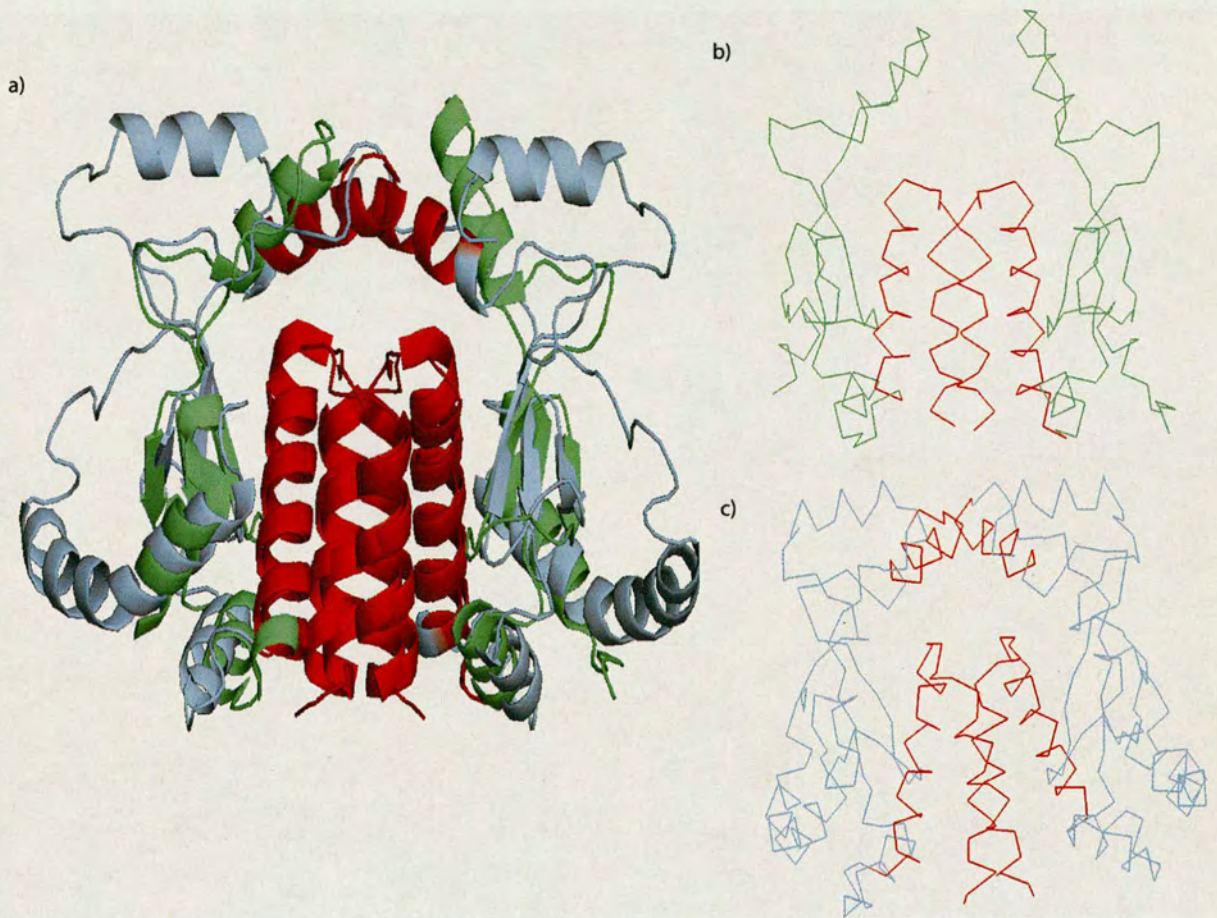


Figure 1.12. Dimerisation model of Hsp90. a) Overlay of the C-terminal structures of htpG (green colour) and yeast Hsp90 (light blue). The dimerisation motif was labelled with red colour. b) and c) ribbon view of the dimer formation in htpG (b) and yeast Hsp90 (c). The dimerisation motif of yeast Hsp90 also involved extra residues in yeast Hsp90. The residues can be seen in red in c).

1.4.2. The C-terminal domain is important for binding to client proteins

Hsp90 binds to several client proteins especially those that contain a TPR domain [82] such as Hsp90 Organiser Protein (Hop), Cyp40 [15], FKBP 52 [20] and many others through its C-terminal domain. TPR domains contain between one and 16 tandem repeats of the basic 34 residue motif. Most commonly, three tandem TPRs are found, suggesting that this is the usual length of a functional TPR domain and that longer sequences of repeats contain several such functional units [21]. The C-terminus of Hsp90 ends with the following residues MEEVD. This sequence of residues at the end of the protein is generally well conserved between species. However, htpG the *E. coli* homolog of Hsp90 lacks this C-terminal motif. The MEEVD motif of Hsp90 has been shown to interact with the TPR containing proteins via one of the TPR domains [21, 82, 107]. Hop consist of three TPR domains, one of which binds to the C-terminal of Hsp70 and another one binds to the C-terminal of Hsp90 [19]. Protein phosphatase 5 (PP5) is a serine/threonine protein phosphatase consists of TPR domain N-terminal to its phosphatase domain. PP5 is involved in signalling pathways that control cellular responses to stress, glucocorticoids and DNA damage [106]. PP5 also binds to Hsp90 through its N-terminal TPR domain [17]. Even though the TPR domain proteins bind to Hsp90 using the same motif, they have distinctive Hsp90 binding properties. The Hsp90/steroid receptor complexes are amongst the best characterised interactions, the sequential nature of the interaction has been studied in some detail [20]. The different proteins have distinctive properties was shown in the study of interactions between

FKBP 51 and 52 to Hsp90. Both of the proteins consists of a core TPR domain necessary to bind Hsp90 but not sufficient to result in 'full' binding. This study proposed that in addition to the TPR domain, a conserved region called the charged Y region, located downstream of the core TPR domain contributed to the distinctive binding seen with different TPR binding proteins. The conserved region can also be observed in other Hsp90-TPR binding proteins (Figure 1.13). The charged Y motif consists of 11-amino acids motif, was identified with the consensus organization $-+--+X\$YXXMF$, where $-$ represents Glu or Asp, $+$ represents Lys or Arg, $\$$ represents a hydrophobic amino acid, and X represents any amino acid [20]. The binding of both the core TPR domain and the charge Y motif was observed to give a higher binding affinity of FKBP 51 when compared to FKBP 52. Therefore the difference in the binding to Hsp90 might be caused by the involvement of the charge Y region.

	$-+--+ \$Y MF -$
BOVIN cyp40	AELLKVKQKIKAKQDKKAAAYAKMFA -----
CHIP	QEQILIPNLAMKEVIDAFISENGWVEDY -----
AIP	RELRALEARIRQKDEEDKARFRGIFSH -----
FKBP 52	TQLAVCQQRIRRQLAREKKLYANMFERLAEENKAKAEASSI
FKBP 51	LQISMCQKKAKEHNERDRRIYANMFKKFAEQDAKEEANKAMI

Figure 1.13. The charge Y motif. Sequence alignment of several TPR containing proteins shows the existence of the charge Y motif. The consensus sequence of the Charge Y motif is depicted above the sequences alignment.

The binding of the client proteins to the C-terminal also involved the cooperation of other Hsp90 domains. Further studies on the interaction of Sti1 with Hsp90 showed that Sti1 exist as a dimer and can bind to both of the TPR sites in the Hsp90 dimer [82]. Sti1 is the yeast homolog of Hop [102]. The binding of Sti1 inhibited the ATPase activity of Hsp90. The ATPase activity was restored when Sti1 is replaced with Cpr6 or the TPR domain of PP5. Cpr6 is the yeast homolog of Cyp40 [28, 30]. From this finding [82], it was proposed that in the intermediate stage of the interaction of Hsp90 with client proteins, Sti1/Hop will bind to the Hsp90 dimer and inhibit the binding of f ATP. In the maturation stage of the interaction, Sti1/Hop was replaced by other immunophilins that subsequently allowed the binding of ATP and p23 at the N-terminus. ATP hydrolysis occurs and promotes the release of p23 and the client proteins. Sti1 binds to Hsp90 and triggers the release of ADP. The proposed mechanism was illustrated in figure 1.14 and suggests that the binding of TPR client proteins act as regulators for the ATP binding and consequently hydrolysis. Thus, it also suggests that cooperation between the N and C terminal domains of is required in the interaction with co-chaperone. Hsp90 binds to the TPR domains with a various binding affinity. Hsp90 bind to Cpr6 with a Kd of $0.24 \pm 0.005 \mu\text{M}$. In addition, Hsp90 binds to Sti1 with a Kd of $0.33 \pm 0.03 \mu\text{M}$, these interactions were determined by using ITC [82].

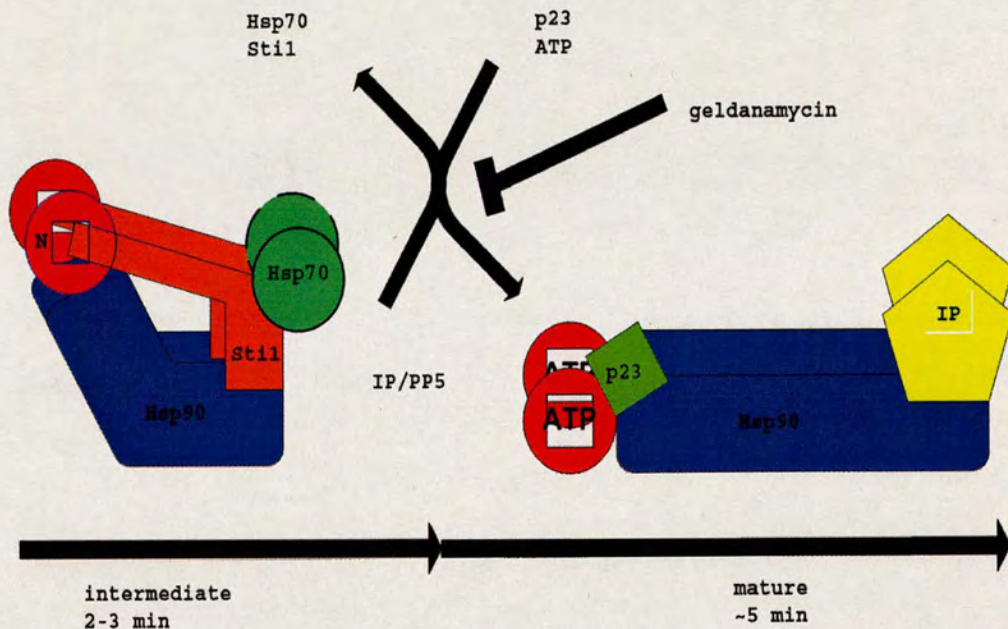


Figure 1.14. Schematic diagrams showing the composition of, and transition between intermediate and mature complexes. The diagram was modified from, and based on the study of [82]. In the intermediate state, St11/ hsp70 complex binds to the C-terminal and makes contact with the N-terminal, thus inhibiting ATP binding. In the mature stage, immunophilins/PP5 replaces the St11 complexes and permits the binding of ATP and p23 at the N-terminal. ATP was then hydrolysed to release the immunophilins/PP5 as well as other client proteins [82].

1.4.3. The C-terminal domain is important for interaction with Cyp40

The majority of the studies described in this thesis involve the binding of Hsp90 to the immunophilins Cyp40. Cyp40 is the members of large immunophilin family together along side with FKBP52 and FKBP 51. Cyp40 has three TPR domains which

are involved in the binding to Hsp90 [100]. The substitution of the EEVD motif to AAVD motif reduced the binding affinity of Hsp90 to other TPR proteins but disrupted the binding of Cyp40 and Hop to Hsp90 [14, 18]. The deletion of 24 amino acids from residues 700 to 724 of human Hsp90 β also abolished the interaction between these two proteins. Even though the MEEVD motif is important to the binding with Cyp40, a study of a number of Hsp90 mutants showed that 124 residues outwith the COOH terminal domain of Hsp90 contain the recognition site for Cyp40 and could be shown to stabilise the interaction [14].

Two different crystal structures of Cyp40 have been solved [100], in both monoclinic and tetragonal forms. The TPR domain of the monoclinic crystal structure of Cyp40 comprises of seven helices labelled P, Q, R, S, T, U, and V. The helices form a helix turn helix pattern (Figure 1.15). In the tetragonal crystal, only helix P and Q are retained, the second helix R and S helices were found to spring out and form one elongated helix (the other helices were not visible in the electron density) (Figure 1.15). Therefore, the tetragonal form of the crystal is regarded as a trapped intermediate in the folding pathway of the helix domain. The structure was used to model the interaction of Cyp40 with the Hsp90 C-terminal MEEVD sequence. The model showed the requirement of the MEEVD to run in opposite direction from the direction found in the Hop-peptide complex [94]. Both models however suggest that the binding groove of the TPR domains is the likely peptide binding site [100].

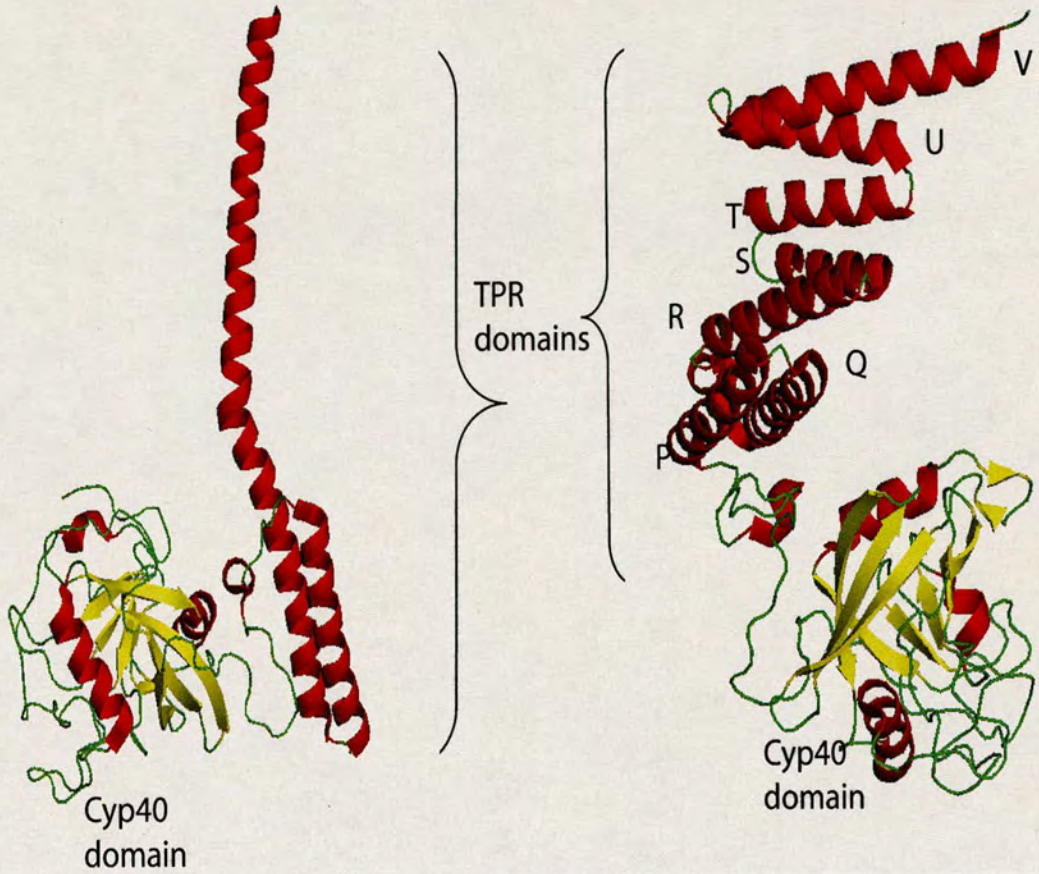


Figure 1.15. The two structures of bovine Cyclophilin 40 (Cyp40). a) Tetragonal form of cyp40 structure. The TPR domain helices were disordered. Helix R and S sprung together to be just one elongated helix. The other helices were not visible in the density map. b) Monoclinic form of cyp40 structure. Seven helices of the TPR domain were labelled from P to V. The structures were taken from PDB files id 1IHG and 1IIP respectively.

1.4.4. The C-terminal domain binds to novobiocin and ATP

Heat shock protein 90 (Hsp90) is a molecular chaperone whose association is required for stability and function of multiple mutated, chimeric, and over-expressed signalling proteins that promote cancer cell growth and/or survival. Therefore, it is the ideal target for anti-tumor drugs [33, 58, 64, 65]. Drugs such as geldanamycin, radicicol and 17-AAG are known to bind at the N-terminus of Hsp90 [1, 25, 29, 46, 59, 76, 92, 93, 111]. There is also evidence of the binding of novobiocin to Hsp90 [4, 44, 47, 48]. The binding was observed to inhibit the autophosphorylation of Hsp90 [44]. Plant Hsp90 and rat Hsp90 were shown to autophosphorylate or phosphorylate other protein substrates *in vitro* but only in the presence of Mn^{2+} or Ca^{2+} . Thus, suggesting the existence of Hsp90-associated kinase activity in the presence of specific divalent cations [44]. This Hsp90-associated kinase activity may be essential for proper functioning of Hsp90 in both protein folding processes and signal transduction pathways [44]. The binding of novobiocin was observed to occur at a different site from the geldanamycin/radicicol-binding site. Furthermore, novobiocin is able to interfere with chaperone function of Hsp90 and to deplete tumor cells. Thus, in SKBR3 breast cancer cells, a 16-hour exposure to novobiocin reduced p185^{erbB2}, mutated p53, and Raf-1 protein levels in a dose-dependent fashion [48].

Further study of the binding between novobiocin and Hsp90 revealed that the binding site is in the C-terminal of Hsp90 [47]. In this study, several mutants of consisting C-terminal Hsp90 chicken were made and tested against the binding to

novobiocin. The deletion of amino acid 657-677 markedly reduced the binding of novobiocin suggesting that novobiocin bind to these sites. A peptide of sequence

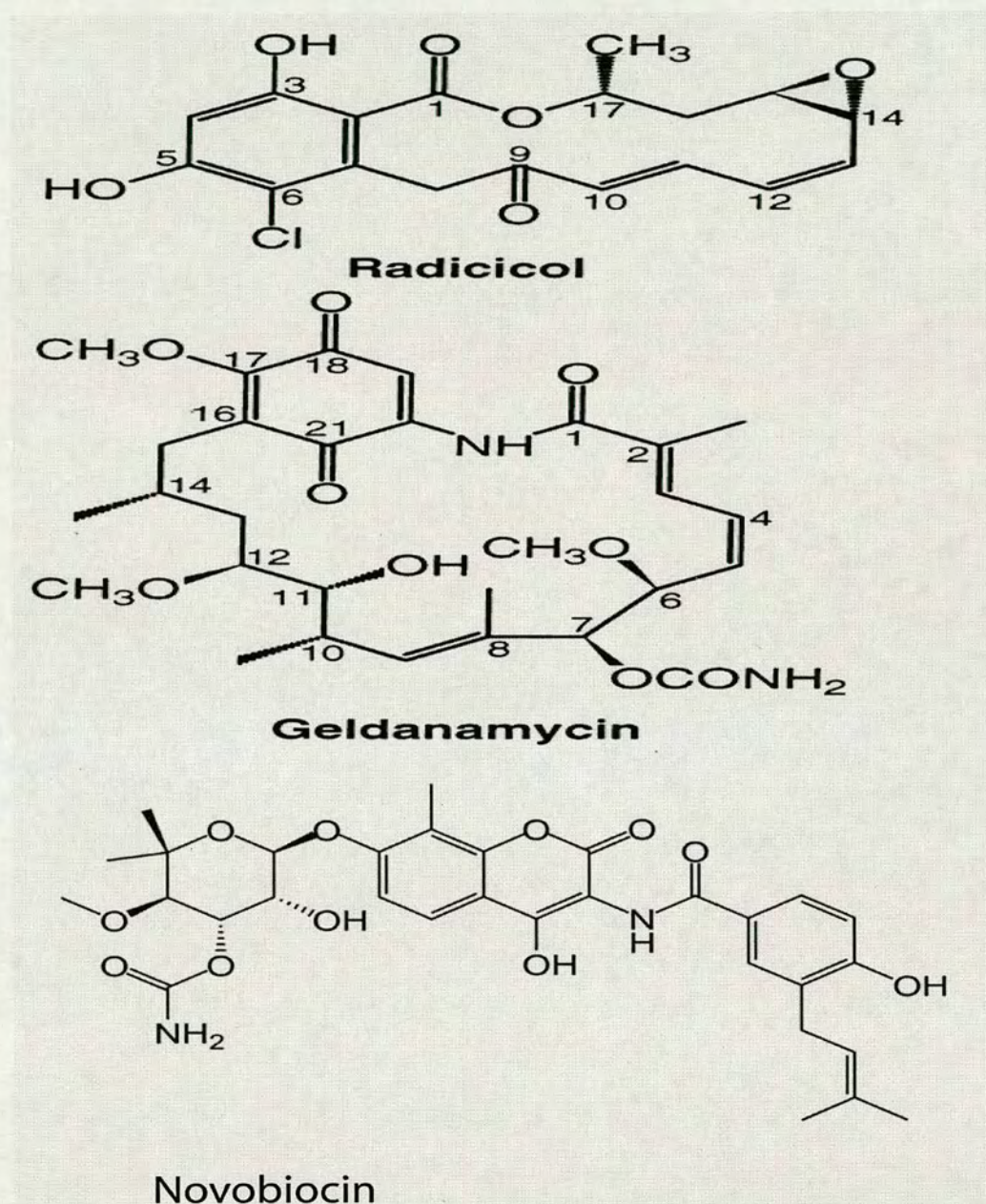


Figure 1.16. Structure of the Hsp90 inhibitors. Radicicol and geldanamycin were known to bind to the N-terminal of Hsp90. Novobiocin was observed to bind to the C-terminal of Hsp90.

YETALLSSGFSLED, corresponding to amino acids 663-676 of Hsp90 was synthesized and showed to be able to compete with the C-terminal chicken Hsp90 mutants from binding to the immobilized novobiocin.[47].

The binding of novobiocin inhibits Hsp90-dependent maturation of newly synthesized client target such as the maturation and activation of the Hsp90/Cdc37-dependent kinase HRI. Furthermore, the binding of novobiocin was observed to decrease the interaction of Hsp90 to TPR client proteins [109]. In additions, the binding of novobiocin also protects the C-terminal from trypsin cleavage which suggested that the conformation of the protein was changed on binding [109]. Recently, it is has been shown that novobiocin in concentrations up to 1 mM can interfere with the dimerisation of C-terminal Hsp90. However, up to 10 mM of novobiocin was needed to completely inhibit the binding of immunophilins to the protein, provided that novobiocin was incubated with Hsp90 prior to addition of the immunophilins [4]. This finding suggests that the disruption of the dimerisation may be part of the reason for reduction in chaperones binding.

As mentioned before, the binding of the C-terminal mutants of chicken Hsp90 to novobiocin sepharose were inhibited when the proteins were incubated with ATP before running them on to the column. The same result was obtained when the proteins were incubated with novobiocin before running the complex on ATP Sepharose which suggested novobiocin can inhibit the binding of ATP [47]. The ATP binding site was observed by Garnier *et. al*, (2002) using ITC and circular dichroism (CD) [32]. However, the binding of C-terminal of chicken Hsp90 with ITC can only be analysed in the present of Mg^{2+} . Mg^{2+} was shown to promote the oligomerization of Hsp90 but in

the presence of ATP, Mg^{2+} inhibits the oligomerization process. When GA is applied, the oligomerization induced by Mg^{2+} is retained suggesting that the effects are not caused by the binding of GA/ATP to the N-terminal. A likely explanation is that, the effects are caused by the binding of ATP to the other ATP sites in the C-terminal domain [32]. The C-terminal Hsp90 ATP binding site can also bind to other nucleotide such as GTP and UTP but not NAD. Furthermore, the site is said to be hidden and can only be accessed if the N-terminal binding site was occupied [97].

Based on the study of the C-terminal Hsp90 domain, it was shown that the C-terminal site probably plays a vital role in the function of Hsp90 but the true mechanism and function still remains unclear. There are two structures of the C-terminal domain now available, C-terminal of *E. coli* htpG [36] which is just 50% identical to other Hsp90 and more recently, the structure of the full length yeast Hsp90 [3]. The C-terminal domain of yeast structure was not very much different from htpG. However, the structure of the extreme end of the yeast Hsp90 containing the MEEVD motif was still unsolved. In the crystal structure, these amino acids were disordered.

1.4.4. Crystal structure of the carboxy terminal of htpG *E. coli* and yeast Hsp90

The crystal structure of htpG consists of five helices and three β sheets (Figure 1.17). The carboxy terminal starts with a short α helix (H1) that leads to three anti-parallel β sheets (a, b and c). A second helix (H2) was located between strands b and c.

The β - sheet is followed by helices H3, H4 and H5. In the crystal structure, H4 and H5 interact with their equivalent counterparts from a second molecule around 2-fold symmetry axes to form a dimer via the four helix bundle [36].

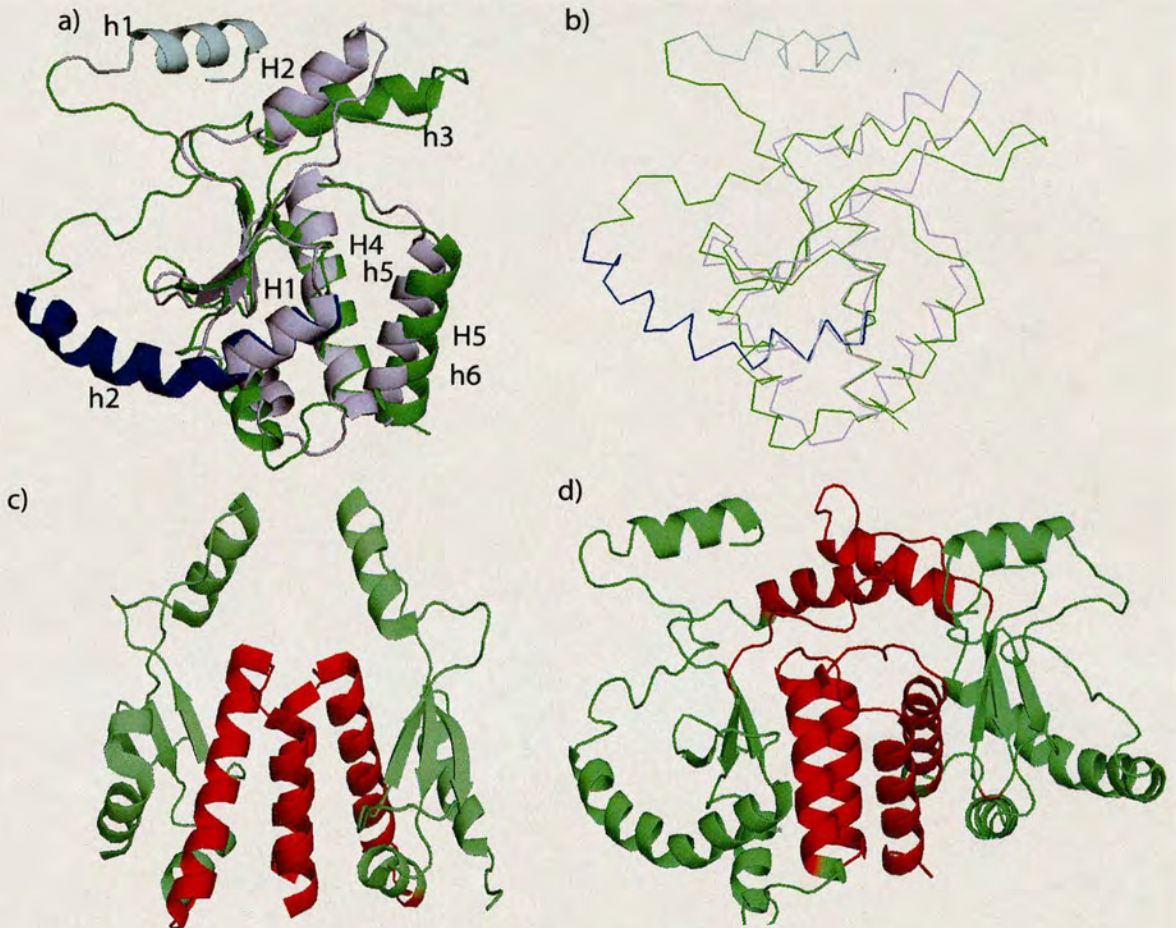


Figure 1.17. The carboxyl-terminal structure of htpG and yeast Hsp90. a) Monomeric structure of htpG carboxyl terminal (light purple) overlaid with the yeast Hsp90 C-terminal (green). The helices of C-terminal of htpG were labelled with capital letters and the helices for C-terminal Hsp90 were labelled with small letters. The blue colour helix (h2) was longer than H1. The light blue helix h1) indicates the extra helix in the yeast Hsp90 C-terminal structure. b) The same pictures as a) but in ribbon view. c) and d) The dimeric structure of htpG and yeast Hsp90 C-terminal domains. The red colour indicates the dimerisation motifs.

The C-terminal of yeast Hsp90 consists of six helices and three β sheets (Figure 1.17). The yeast structure consists of one extra helix (h1) (before H1 of htpG) that contributes extra residues to the C-terminal domain (not present in htpG). Furthermore, helix 2 (h2) of the yeast structure which corresponds to H1 in htpG was longer. In addition, residues 587-610 (h3) of the yeast C-terminal are also involved in the dimer interaction. Even though H2 in htpG correspond to h3 in yeast Hsp90, it is not involved in the dimerisation motif of htpG [36].

1.5. Function of Hsp90

The Hsp90 orthologues are essential and ubiquitous molecular chaperones that play important roles in folding, activation and assembly of a range of client proteins which are involved in signal transduction, cell cycle control or transcriptional regulation [73, 78]. Hsp90 was observed to help the folding of citrate synthase [42]. Denatured citrate synthase in the absence of added chaperones aggregates when diluted into renaturation buffer. In the presence of Hsp90, aggregation is significantly suppressed, suggesting that Hsp90 binds to these aggregation sensitive folding intermediates and leads them to follow the correct folding pathway, thus allowing a higher number of molecules to reach the active, native state. Hsp90 influences the folding and activity of a number of different non-native proteins, suggesting that Hsp90 functions *in vivo* as a molecular chaperone [42].

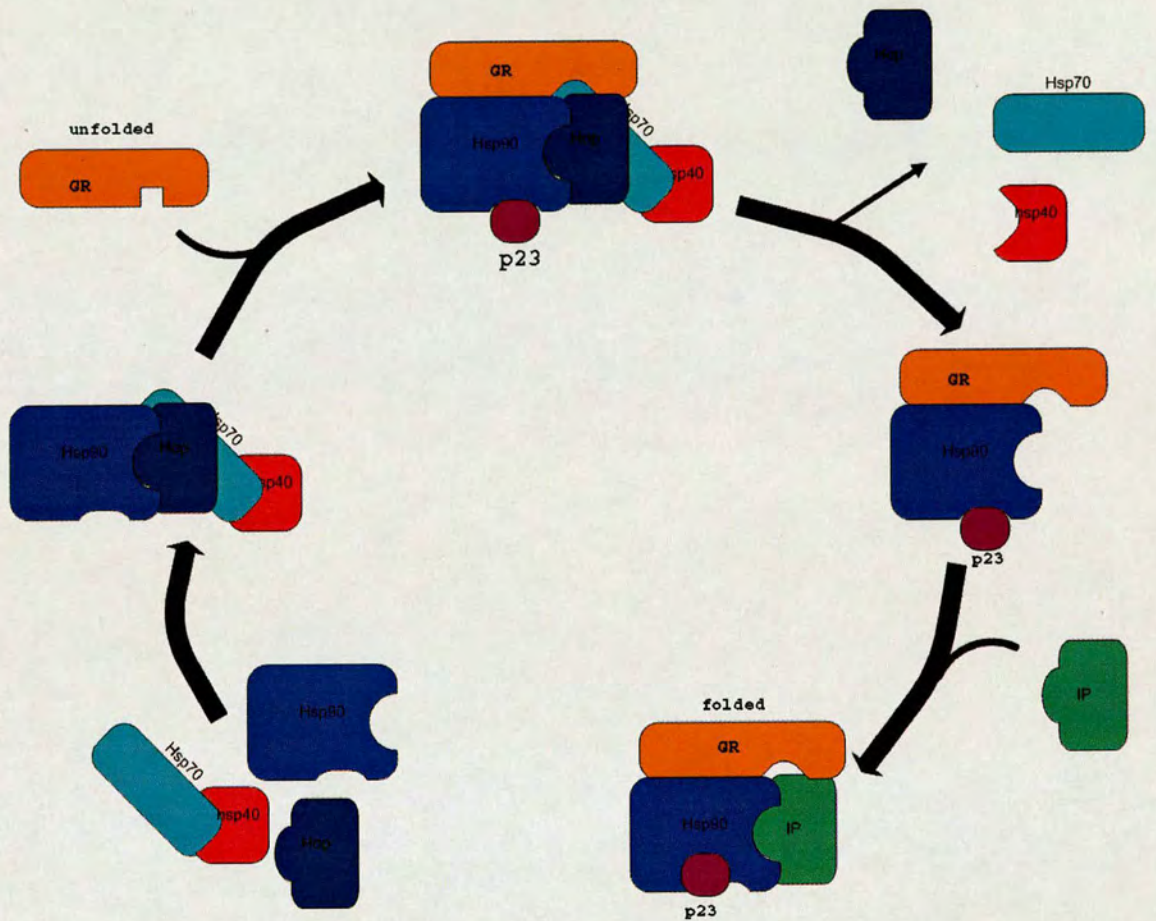


Figure 1.18. Mechanism of Hsp90 in steroid receptor cycle. The Hsp90/Hsp70-based chaperone machine or foldosome, converts the glucocorticoid receptor (GR) from unfolded conformations to a folded conformation that will be accessible to bind with steroid hormone. Hop binds to Hsp90 and hsp70 through the TPR domain to form the foldosome. In the presence of ATP, Hsp90 is converted to ATP bound conformation which permits the binding of unfolded GR. p23 also binds to Hsp90 and the hsp70 complex was released. As the TPR binding site is empty, immunophilins (IP) can bind to it. During the final stage, the GR is already folded and ready to be released to bind to the steroid hormone.

Hsp90 is also involved in the signalling pathway inside the cell. The best characterized example is that of the steroid hormone receptor [22, 108]. In this pathway, monomeric glucocorticoid receptor binds to Hsp90 via a Hsp90/Hop dependent mechanism or foldosome. The mechanism up to the binding of glucocorticoid receptor was illustrated in Figure 1.18. In this scheme, the glucocorticoid receptors attain their hormone binding conformation after binding Hsp90. When the folded monomeric receptor is released, it either binds the appropriate steroid hormone resulting in dimerisation and activation, or remains unstable and is recognized again by the chaperone machinery [22, 78].

Hsp90 is also involved in stabilizing the catalytic domains of kinases such as v-src before assembly of the kinases into the final signalling complex. Similarly, Hsp90 stabilizes kinases such as the integrin link kinase (ILK). ILK has been shown to induce the phosphorylation of Akt and GSK-3 β that leads to cell survival and proliferation. It also phosphorylates transcriptional factor α NAC and promotes the invasion by upregulating matrix metalloproteinase 9 expression through AP-1 activation [5]. Therefore, ILK indirectly involves the participation of Hsp90 in the pathway. By inhibiting Hsp90, ILK expression was suppressed [5] and because ILK overexpression and hyperactivity is involved in tumor development [6-8, 35, it will be an excellent target in cancer treatment. Hsp90 is also involved in other kinase cycles that can lead to the control of cancer. This makes Hsp90 an interesting target for the development of novel anti cancer drugs {Arlander, 2003 #408}.

Therefore, the thesis described the work carried out to Hsp90 proteins and the aims were:

- To characterise the interactions of the C-terminal and full length Hsp90 with TPR containing proteins including Cyp40 by biochemical and biophysical methods.
- To characterise the interactions of C-terminal and full length Hsp90 with small ligands such as novobiocin, ATP and geldanamycin by biochemical and biophysical methods.

References

1. Akimoto, T., Nonaka, T., Harashima, K., Sakurai, H., Ishikawa, H., Mitsuhashi, N. (2004) Radicol potentiates heat-induced cell killing in a human oesophageal cancer cell line: the Hsp90 chaperone complex as a new molecular target for enhancement of thermosensitivity. *Int J Radiat Biol* 80: 483-92
2. Alekseev, M. O, Widgren, E. E, Richardson, T. R, O'Rand, G. M (2005) Association of NASP with HSP90 in mouse spermatogenic cells: stimulation of ATPase activity and transport of linker histones into nuclei. *J Biol Chem* 280: 2904-11
3. Ali, M. M, Roe, M. S, Vaughan, K. C, Meyer, P., Panaretou, B., Piper, W. P, Prodromou, C., Pearl, H. L (2006) Crystal structure of an Hsp90-nucleotide-p23/Sba1 closed chaperone complex. *Nature* 440: 1013-7
4. Allan, K. R, Mok, D., Ward, K. B, Ratajczak, T. (2006) The carboxy-terminal domain Of Hsp90: Modulation of chaperone function and cochaperone interaction by novobiocin. Evidence that coumarin antibiotics disrupt Hsp90 dimerization. *J Biol Chem*
5. Aoyagi, Y., Fujita, N., Tsuruo, T. (2005) Stabilization of integrin-linked kinase by binding to Hsp90. *Biochem Biophys Res Commun* 331: 1061-8
6. Arlander, J. S, Felts, J. S, Wagner, M. J, Stensgard, B., Toft, O. D, Karnitz, M. L (2006) Chaperoning checkpoint kinase 1 (Chk1), an Hsp90 client, with purified chaperones. *J Biol Chem* 281: 2989-98
7. Bagatell, R., Whitesell, L. (2004) Altered Hsp90 function in cancer: a unique therapeutic opportunity. *Mol Cancer Ther* 3: 1021-30
8. Bagatell, R., Beliakoff, J., David, L. C, Marron, T. M, Whitesell, L. (2005) Hsp90 inhibitors deplete key anti-apoptotic proteins in pediatric solid tumor cells and demonstrate synergistic anticancer activity with cisplatin. *Int J Cancer* 113: 179-88
9. Bardwell, C. J, Craig, A. E (1987) Eukaryotic Mr 83,000 heat shock protein has a homologue in *Escherichia coli*. *Proc Natl Acad Sci U S A* 84: 5177-81
10. Borkovich, A. K, Farrelly, W. F, Finkelstein, B. D, Taulien, J., Lindquist, S. (1989) hsp82 is an essential protein that is required in higher concentrations for growth of cells at higher temperatures. *Mol Cell Biol* 9: 3919-30
11. Brinker, A., Scheufler, C., Mulbe VD, F., Fleckenstein, B., Herrmann, C., Jung, G., Moarefi, I., Hartl, U. F (2002) Ligand discrimination by TPR domains. Relevance and selectivity of EEVD-recognition in Hsp70 x Hop x Hsp90 complexes. *J Biol Chem* 277: 19265-75
12. Buchner, J. (1999) Hsp90 & Co. - a holding for folding. *Trends Biochem Sci* 24: 136-41
13. Caplan, J. A, Jackson, S., Smith, D. (2003) Hsp90 reaches new heights. Conference on the Hsp90 chaperone machine. *EMBO Rep* 4: 126-30
14. Carrello, A., Ingley, E., Minchin, F. R, Tsai, S., Ratajczak, T. (1999) The common tetratricopeptide repeat acceptor site for steroid receptor-associated immunophilins and hop is located in the dimerization domain of Hsp90. *J Biol Chem* 274: 2682-9
15. Carrello, A., Allan, K. R, Morgan, L. S, Owen, A. B, Mok, D., Ward, K. B, Minchin, F. R, Toft, O. D, Ratajczak, T. (2004) Interaction of the Hsp90 cochaperone cyclophilin 40 with Hsc70. *Cell Stress Chaperones* 9: 167-81
16. Carrigan, E. P, Sikkink, A. L, Smith, F. D, Ramirez-Alvarado, M. (2006) Domain:domain interactions within Hop, the Hsp70/Hsp90 organizing protein, are required for protein stability and structure. *Protein Sci* 15: 522-32
17. Chen, M.X, Mcpartlin, A.E, Brown, L., Chen, Y.H., Barker, Cohen HMa, P.T.W (1994) A novel human protein serine/threonine phosphatase, which possesses 4 tetratricopeptide repeat motifs and localizes to the nucleus. *EMBO J.* 13: 4278-4290
18. Chen, S., Sullivan, P. W, Toft, O. D, Smith, F. D (1998) Differential interactions of p23 and the TPR-containing proteins Hop, Cyp40, FKBP52 and FKBP51 with Hsp90 mutants. *Cell Stress Chaperones* 3: 118-29
19. Chen, S.Y., Smith a, D.F, (1998) Hop as an adaptor in the heat shock protein 70 (Hsp70) and Hsp90 chaperone machinery. *J. Biol. Chem.* 273: 35194-35200

20. Cheung-Flynn, J., Roberts, J. P, Riggs, L. D, Smith, F. D (2003) C-terminal sequences outside the tetratricopeptide repeat domain of FKBP51 and FKBP52 cause differential binding to Hsp90. *J Biol Chem* 278: 17388-94
21. Cliff, J. M, Williams, A. M, Brooke-Smith, J., Barford, D., Ladbury, E. J (2005) Molecular recognition via coupled folding and binding in a TPR domain. *J Mol Biol* 346: 717-32
22. Csermely, P., Schnaider, T., Soti, C., Prohaszka, Z., Nardai, G. (1998) The 90-kDa molecular chaperone family: structure, function, and clinical applications. A comprehensive review. *Pharmacol Ther* 79: 129-68
23. Dao-Phan, P. H, Formstecher, P., Lefebvre, P. (1997) Disruption of the glucocorticoid receptor assembly with heat shock protein 90 by a peptidic antiglucocorticoid. *Mol Endocrinol* 11: 962-72
24. David, L. C, Smith, E. H, Raynes, A. D, Pulcini, J. E, Whitesell, L. (2003) Expression of a unique drug-resistant Hsp90 ortholog by the nematode *Caenorhabditis elegans*. *Cell Stress Chaperones* 8: 93-104
25. Dey, A., Cederbaum, I. A (2006) Geldanamycin, an inhibitor of Hsp90, potentiates cytochrome P4502E1 mediated toxicity in HepG2 cells. *J Pharmacol Exp Ther*
26. Donze, O., Abbas-Terki, T., Picard, D. (2001) The Hsp90 chaperone complex is both a facilitator and a repressor of the dsRNA-dependent kinase PKR. *Embo J* 20: 3771-80
27. Dorman, J., Taylor, P., Walkinshaw, D. M (2003) Structures of immunophilins and their ligand complexes. *Curr Top Med Chem* 3: 1392-409
28. Duina, A. A, Chang, C. H, Marsh, A. J, Lindquist, S., Gaber, F. R (1996) A cyclophilin function in Hsp90-dependent signal transduction. *Science* 274: 1713-5
29. Dymock, W. B, Barril, X., Brough, A. P, Cansfield, E. J, Massey, A., McDonald, E., Hubbard, E. R, Surgenor, A., Roughley, D. S, Webb, P., Workman, P., Wright, L., Drysdale, J. M (2005) Novel, potent small-molecule inhibitors of the molecular chaperone Hsp90 discovered through structure-based design. *J Med Chem* 48: 4212-5
30. Fang, Y., Fliss, E. A, Rao, J., Caplan, J. A (1998) SBA1 encodes a yeast hsp90 cochaperone that is homologous to vertebrate p23 proteins. *Mol Cell Biol* 18: 3727-34
31. Felts, J. S, Owen, A. B, Nguyen, P., Trepel, J., Donner, B. D, Toft, O. D (2000) The hsp90-related protein TRAP1 is a mitochondrial protein with distinct functional properties. *J Biol Chem* 275: 3305-12
32. Gamier, C., Lafitte, D., Tsvetkov, O. P, Barbier, P., Leclerc-Devin, J., Millot, M. J, Briand, C., Makarov, A. A, Catelli, G. M, Peyrot, V. (2002) Binding of ATP to heat shock protein 90: evidence for an ATP-binding site in the C-terminal domain. *J Biol Chem* 277: 12208-14
33. Goetz, P. M, Toft, O. D, Ames, M. M, Erlichman, C. (2003) The Hsp90 chaperone complex as a novel target for cancer therapy. *Ann Oncol* 14: 1169-76
34. Grenert, P. J, Sullivan, P. W, Fadden, P., Haystead, A. T, Clark, J., Mimnaugh, E., Krutzsch, H., Ochel, J. H, Schulte, W. T, Sausville, E., Neckers, M. L, Toft, O. D (1997) The amino-terminal domain of heat shock protein 90 (hsp90) that binds geldanamycin is an ATP/ADP switch domain that regulates hsp90 conformation. *J Biol Chem* 272: 23843-50
35. Hannigan, G., Troussard, Dedhar A A, S (2005) Integrine-linked kinase: a cancer therapeutic target unique among its ILK. *Nat. Rev. Cancer* 5: 51-63
36. Harris, F. S, Shiau, K. A, Agard, A. D (2004) The crystal structure of the carboxy-terminal dimerization domain of htpG, the *Escherichia coli* Hsp90, reveals a potential substrate binding site. *Structure* 12: 1087-97
37. Harst, A., Lin, H., Obermann, M. W (2005) Aha1 competes with Hop, p50 and p23 for binding to the molecular chaperone Hsp90 and contributes to kinase and hormone receptor activation. *Biochem J* 387: 789-96
38. Hickey, E., Brandon, E. S, Smale, G., Lloyd, D., Weber, A. L (1989) Sequence and regulation of a gene encoding a human 89-kilodalton heat shock protein. *Mol Cell Biol* 9: 2615-26
39. Hoffmann, K., Handschumacher, E. R (1995) Cyclophilin-40: evidence for a dimeric complex with hsp90. *Biochem J* 307 (Pt 1): 5-8
40. Huai, Q., Wang, H., Liu, Y., Kim, Y. H, Toft, D., Ke, H. (2005) Structures of the N-terminal and middle domains of *E. coli* Hsp90 and conformation changes upon ADP binding. *Structure* 13: 579-90

41. Jackson, E. S, Queitsch, C., Toft, D. (2004) Hsp90: from structure to phenotype. *Nat Struct Mol Biol* 11: 1152-5
42. Jakob, U. (1996) HSP90--news from the front. *Front Biosci* 1: d309-17
43. Johnson, L. J, Toft, O. D (1995) Binding of p23 and hsp90 during assembly with the progesterone receptor. *Mol Endocrinol* 9: 670-8
44. Langer, T., Schlatter, H., Fasold, H. (2002) Evidence that the novobiocin-sensitive ATP-binding site of the heat shock protein 90 (hsp90) is necessary for its autophosphorylation. *Cell Biol Int* 26: 653-7
45. Lotz, P. G, Lin, H., Harst, A., Obermann, M. W (2003) Aha1 binds to the middle domain of Hsp90, contributes to client protein activation, and stimulates the ATPase activity of the molecular chaperone. *J Biol Chem* 278: 17228-35
46. Machida, H., Matsumoto, Y., Shirai, M., Kubota, N. (2003) Geldanamycin, an inhibitor of Hsp90, sensitizes human tumour cells to radiation. *Int J Radiat Biol* 79: 973-80
47. Marcu, G. M, Chadli, A., Bouhouche, I., Catelli, M., Neckers, M. L (2000) The heat shock protein 90 antagonist novobiocin interacts with a previously unrecognized ATP-binding domain in the carboxyl terminus of the chaperone. *J Biol Chem* 275: 37181-6
48. Marcu, G. M, Schulte, W. T, Neckers, L. (2000) Novobiocin and related coumarins and depletion of heat shock protein 90-dependent signaling proteins. *J Natl Cancer Inst* 92: 242-8
49. Martinez-Ruiz, A., Villanueva, L., Orduna Gd, C., Lopez-Ferrer, D., Higuera, A. M, Tarin, C., Rodriguez-Crespo, I., Vazquez, J., Lamas, S. (2005) S-nitrosylation of Hsp90 promotes the inhibition of its ATPase and endothelial nitric oxide synthase regulatory activities. *Proc Natl Acad Sci U S A* 102: 8525-30
50. Mayer, P. M, Nikolay, R., Bukau, B. (2002) Aha, another regulator for hsp90 chaperones. *Mol Cell* 10: 1255-6
51. McLaughlin, H. S, Smith, W. H, Jackson, E. S (2002) Stimulation of the weak ATPase activity of human hsp90 by a client protein. *J Mol Biol* 315: 787-98
52. McLaughlin, H. S, Ventouras, A. L, Lobbezoo, B., Jackson, E. S (2004) Independent ATPase activity of Hsp90 subunits creates a flexible assembly platform. *J Mol Biol* 344: 813-26
53. McLaughlin, H. S, Sobott, F., Yao, P. Z, Zhang, W., Nielsen, R. P, Grossmann, G. J, Laue, D. E, Robinson, V. C, Jackson, E. S (2006) The co-chaperone p23 arrests the Hsp90 ATPase cycle to trap client proteins. *J Mol Biol* 356: 746-58
54. Meyer, P., Prodromou, C., Hu, B., Vaughan, C., Roe, M. S, Panaretou, B., Piper, W. P, Pearl, H. L (2003) Structural and functional analysis of the middle segment of hsp90: implications for ATP hydrolysis and client protein and cochaperone interactions. *Mol Cell* 11: 647-58
55. Meyer, P., Prodromou, C., Liao, C., Hu, B., Roe, M. S, Vaughan, K. C, Vlastic, I., Panaretou, B., Piper, W. P, Pearl, H. L (2004) Structural basis for recruitment of the ATPase activator Aha1 to the Hsp90 chaperone machinery. *Embo J* 23: 1402-10
56. Meyer, P., Prodromou, C., Liao, C., Hu, B., Roe, M. S., Vaughan, K. C, Vlastic, I., Panaretou, B., Piper, W. P, Pearl, H. L (2004) Structural basis for recruitment of the ATPase activator Aha1 to the Hsp90 chaperone machinery. *Embo J* 23: 511-9
57. Minami, Y., Kimura, Y., Kawasaki, H., Suzuki, K., Yahara, I. (1994) The carboxy-terminal region of mammalian HSP90 is required for its dimerization and function in vivo. *Mol Cell Biol* 14: 1459-64
58. Miyata, Y. (2003) [Molecular chaperone HSP90 as a novel target for cancer chemotherapy]. *Nippon Yakurigaku Zasshi* 121: 33-42
59. Miyata, Y. (2005) Hsp90 inhibitor geldanamycin and its derivatives as novel cancer chemotherapeutic agents. *Curr Pharm Des* 11: 1131-8
60. Muller, P., Ceskova, P., Vojtesek, B. (2005) Hsp90 is essential for restoring cellular functions of temperature-sensitive p53 mutant protein but not for stabilization and activation of wild-type p53: implications for cancer therapy. *J Biol Chem* 280: 6682-91
61. Murphy, J. P, Kanelakis, C. K, Galigniana, D. M, Morishima, Y., Pratt, B. W (2001) Stoichiometry, abundance, and functional significance of the hsp90/hsp70-based multiprotein chaperone machinery in reticulocyte lysate. *J Biol Chem* 276: 30092-8

62. Murphy, J. P, Galigniana, D. M, Morishima, Y., Harrell, M. J, Kwok, P. R, Ljungman, M., Pratt, B. W (2004) Pifithrin-alpha inhibits p53 signaling after interaction of the tumor suppressor protein with hsp90 and its nuclear translocation. *J Biol Chem* 279: 30195-201
63. Nardo D, D., Masendycz, P., Ho, S., Cross, M., Fleetwood, J. A, Reynolds, C. E, Hamilton, A. J, Scholz, M. G (2005) A central role for the Hsp90.Cdc37 molecular chaperone module in interleukin-1 receptor-associated-kinase-dependent signaling by toll-like receptors. *J Biol Chem* 280: 9813-22
64. Neckers, L. (2002) Hsp90 inhibitors as novel cancer chemotherapeutic agents. *Trends Mol Med* 8: S55-61
65. Neckers, L. (2003) Development of small molecule Hsp90 inhibitors: utilizing both forward and reverse chemical genomics for drug identification. *Curr Med Chem* 10: 733-9
66. Nemoto, T., Ohara-Nemoto, Y., Ota, M., Takagi, Yokoyama T, K., (1995) Mechanism of dimer formation of the 90-kDa heat-shock protein. *Eur. J. Biochem.* 233: 1-8
67. Nemoto, T., Sato a, N. (1998) Oligomeric forms of the 90-kDa heat shock protein. *Biochem. J* 330: 989-995
68. Nemoto, K. T, Ono, T., Kobayakawa, T., Tanaka, E., Baba, T. T, Tanaka, K., Takagi, T., Gotoh, T. (2001) Domain-domain interactions of HtpG, an Escherichia coli homologue of eukaryotic HSP90 molecular chaperone. *Eur J Biochem* 268: 5258-69
69. Obermann, M. W, Sondermann, H., Russo, A. A, Pavletich, P. N, Hartl, U. F (1998) In vivo function of Hsp90 is dependent on ATP binding and ATP hydrolysis. *J Cell Biol* 143: 901-10
70. Owens-Grillo, K. J, Stancato, F. L, Hoffmann, K., Pratt, B. W, Krishna, P. (1996) Binding of immunophilins to the 90 kDa heat shock protein (hsp90) via a tetratricopeptide repeat domain is a conserved protein interaction in plants. *Biochemistry* 35: 15249-55
71. Panaretou, B., Prodromou, C., Roe, M. S, O'Brien, R., Ladbury, E. J, Piper, W. P, Pearl, H. L (1998) ATP binding and hydrolysis are essential to the function of the Hsp90 molecular chaperone in vivo. *Embo J* 17: 4829-36
72. Panaretou, B., Siligardi, G., Meyer, P., Maloney, A., Sullivan, K. J, Singh, S., Millson, H. S, Clarke, A. P, Naaby-Hansen, S., Stein, R., Cramer, R., Mollapour, M., Workman, P., Piper, W. P, Pearl, H. L, Prodromou, C. (2002) Activation of the ATPase activity of hsp90 by the stress-regulated cochaperone aha1. *Mol Cell* 10: 1307-18
73. Pearl, H. L, Prodromou, C. (2000) Structure and in vivo function of Hsp90. *Curr Opin Struct Biol* 10: 46-51
74. Pearl, H. L (2005) Hsp90 and Cdc37 -- a chaperone cancer conspiracy. *Curr Opin Genet Dev* 15: 55-61
75. Pelham, R. H (1986) Speculations on the functions of the major heat shock and glucose-regulated proteins. *Cell* 46: 959-61
76. Pelicano, H., Carew, S. J, McQueen, J. T, Andreeff, M., Plunkett, W., Keating, J. M, Huang, P. (2006) Targeting Hsp90 by 17-AAG in leukemia cells: mechanisms for synergistic and antagonistic drug combinations with arsenic trioxide and Ara-C. *Leukemia*
77. Picard, D. (2006) Intracellular dynamics of the Hsp90 co-chaperone p23 is dictated by Hsp90. *Exp Cell Res* 312: 198-204
78. Pratt, B. W (1998) The hsp90-based chaperone system: involvement in signal transduction from a variety of hormone and growth factor receptors. *Proc Soc Exp Biol Med* 217: 420-34
79. Prince, T., Matts, L. R (2005) Exposure of protein kinase motifs that trigger binding of Hsp90 and Cdc37. *Biochem Biophys Res Commun* 338: 1447-54
80. Prodromou, C., Roe, M. S, O'Brien, R., Ladbury, E. J, Piper, W. P, Pearl, H. L (1997) Identification and structural characterization of the ATP/ADP-binding site in the Hsp90 molecular chaperone. *Cell* 90: 65-75
81. Prodromou, C., Roe, M. S, Piper, W. P, Pearl, H. L (1997) A molecular clamp in the crystal structure of the N-terminal domain of the yeast Hsp90 chaperone. *Nat Struct Biol* 4: 477-82
82. Prodromou, C., Siligardi, G., O'Brien, R., Woolfson, N. D, Regan, L., Panaretou, B., Ladbury, E. J, Piper, W. P, Pearl, H. L (1999) Regulation of Hsp90 ATPase activity by tetratricopeptide repeat (TPR)-domain co-chaperones. *Embo J* 18: 754-62

83. Prodromou, C., Panaretou, B., Chohan, S., Siligardi, G., O'Brien, R., Ladbury, E. J, Roe, M. S, Piper, W. P, Pearl, H. L (2000) The ATPase cycle of Hsp90 drives a molecular 'clamp' via transient dimerization of the N-terminal domains. *Embo J* 19: 4383-92
84. Prodromou, C., Pearl, H. L (2003) Structure and functional relationships of Hsp90. *Curr Cancer Drug Targets* 3: 301-23
85. Ratajczak, T., Carrello, A. (1996) Cyclophilin 40 (CyP-40), mapping of its hsp90 binding domain and evidence that FKBP52 competes with CyP-40 for hsp90 binding. *J Biol Chem* 271: 2961-5
86. Richter, K., Buchner, J. (2001) Hsp90: chaperoning signal transduction. *J Cell Physiol* 188: 281-90
87. Richter, K., Muschler, P., Hainzl, O., Buchner, J. (2001) Coordinated ATP hydrolysis by the Hsp90 dimer. *J Biol Chem* 276: 33689-96
88. Richter, K., Muschler, P., Hainzl, O., Reinstein, J., Buchner, J. (2003) Sti1 is a non-competitive inhibitor of the Hsp90 ATPase. Binding prevents the N-terminal dimerization reaction during the atpase cycle. *J Biol Chem* 278: 10328-33
89. Richter, K., Walter, S., Buchner, J. (2004) The Co-chaperone Sba1 connects the ATPase reaction of Hsp90 to the progression of the chaperone cycle. *J Mol Biol* 342: 1403-13
90. Richter, K., Moser, S., Hagn, F., Friedrich, R., Hainzl, O., Heller, M., Schlee, S., Kessler, H., Reinstein, J., Buchner, J. (2006) Intrinsic inhibition of the Hsp90 ATPase activity. *J Biol Chem*
91. Roe, M. S, Prodromou, C., O'Brien, R., Ladbury, E. J, Piper, W. P, Pearl, H. L (1999) Structural basis for inhibition of the Hsp90 molecular chaperone by the antitumor antibiotics radicicol and geldanamycin. *J Med Chem* 42: 260-6
92. Rowlands, G. M, Newbatt, M. Y, Prodromou, C., Pearl, H. L, Workman, P., Aherne, W. (2004) High-throughput screening assay for inhibitors of heat-shock protein 90 ATPase activity. *Anal Biochem* 327: 176-83
93. Scheibel, T., Buchner, J. (1998) The Hsp90 complex--a super-chaperone machine as a novel drug target. *Biochem Pharmacol* 56: 675-82
94. Scheufler, C., Brinker, A., Bourenkov, G., Pegoraro, S., Moroder, L., Bartunik, H., Hartl, U. F, Moarefi, I. (2000) Structure of TPR domain-peptide complexes: critical elements in the assembly of the Hsp70-Hsp90 multichaperone machine. *Cell* 101: 199-210
95. Schulte, W. T, Akinaga, S., Soga, S., Sullivan, W., Stensgard, B., Toft, D., Neckers, M. L (1998) Antibiotic radicicol binds to the N-terminal domain of Hsp90 and shares important biologic activities with geldanamycin. *Cell Stress Chaperones* 3: 100-8
96. Siligardi, G., Hu, B., Panaretou, B., Piper, W. P, Pearl, H. L, Prodromou, C. (2004) Co-chaperone regulation of conformational switching in the Hsp90 ATPase cycle. *J Biol Chem* 279: 51989-98
97. Soti, C., Vermes, A., Haystead, A. T, Csermely, P. (2003) Comparative analysis of the ATP-binding sites of Hsp90 by nucleotide affinity cleavage: a distinct nucleotide specificity of the C-terminal ATP-binding site. *Eur J Biochem* 270: 2421-8
98. Stebbins, E. C, Russo, A. A, Schneider, C., Rosen, N., Hartl, U. F, Pavletich, P. N (1997) Crystal structure of an Hsp90-geldanamycin complex: targeting of a protein chaperone by an antitumor agent. *Cell* 89: 239-50
99. Sullivan, W., Stensgard, B., Caucutt, G., Bartha, B., McMahon, N., Alnemri, S. E, Litwack, G., Toft, D. (1997) Nucleotides and two functional states of hsp90. *J Biol Chem* 272: 8007-12
100. Taylor, P., Dorman, J., Carrello, A., Minchin, F. R, Ratajczak, T., Walkinshaw, D. M (2001) Two structures of cyclophilin 40: folding and fidelity in the TPR domains. *Structure* 9: 431-8
101. Toft, D. (1998) Recent Advances in the Study of hsp90 Structure and Mechanism of Action. *Trends in Endocrinology and Metabolism*, Issue 6, 9: 238-243
102. Wegele, H., Haslbeck, M., Reinstein, J., Buchner, J. (2003) Sti1 is a novel activator of the Ssa proteins. *J Biol Chem* 278: 25970-6
103. Wegele, H., Muschler, P., Bunck, M., Reinstein, J., Buchner, J. (2003) Dissection of the contribution of individual domains to the ATPase mechanism of Hsp90. *J Biol Chem* 278: 39303-10

104. Weikl, T., Muschler, P., Richter, K., Veit, T., Reinstein, J., Buchner, J. (2000) C-terminal regions of Hsp90 are important for trapping the nucleotide during the ATPase cycle. *J Mol Biol* 303: 583-92
105. Yamada, S., Ono, T., Mizuno, A., Nemoto, K. T (2003) A hydrophobic segment within the C-terminal domain is essential for both client-binding and dimer formation of the HSP90-family molecular chaperone. *Eur J Biochem* 270: 146-54
106. Yang, J., Roe, M. S, Cliff, J. M, Williams, A. M, Ladbury, E. J, Cohen, T. P, Barford, D. (2005) Molecular basis for TPR domain-mediated regulation of protein phosphatase 5. *Embo J* 24: 1-10
107. Young, C. J, Obermann, M. W, Hartl, U. F (1998) Specific binding of tetratricopeptide repeat proteins to the C-terminal 12-kDa domain of hsp90. *J Biol Chem* 273: 18007-10
108. Young, C. J, Moarefi, I., Hartl, U. F (2001) Hsp90: a specialized but essential protein-folding tool. *J Cell Biol* 154: 267-73
109. Yun, G. B, Huang, W., Leach, N., Hartson, D. S, Matts, L. R (2004) Novobiocin induces a distinct conformation of Hsp90 and alters Hsp90-cochaperone-client interactions. *Biochemistry* 43: 8217-29
110. Zhang, R., Luo, D., Miao, R., Bai, L., Ge, Q., Sessa, C. W, Min, W. (2005) Hsp90-Akt phosphorylates ASK1 and inhibits ASK1-mediated apoptosis. *Oncogene* 24: 3954-63
111. Zsebik, B., Citri, A., Isola, J., Yarden, Y., Szollosi, J., Vereb, G. (2006) Hsp90 inhibitor 17-AAG reduces ErbB2 levels and inhibits proliferation of the trastuzumab resistant breast tumor cell line JIMT-1. *Immunol Lett* 104: 146-55

Chapter 2: Materials and Methods

In Chapter 2 the general materials and methods used throughout the study are outlined. The general methods include any well established technique or protocol widely used such as those utilised in cloning, protein purification and biochemical assays. This chapter also covers the use of commercial kits for a number of methods/techniques, in general the protocols as outlined by the manufacturer of the kits were followed. More details of a particular technique or when a standard protocol was modified in specific experiments are described in the relevant chapters.

2.1. Source of chemicals and biochemicals

The chemicals were of analytical or laboratory reagent grade. Specialized chemicals and biochemical components and their sources are listed in the appropriate section of the protocols.

2.2. General methods used in cloning experiments

2.2.1. Polymerase chain reaction (PCR)

The PCR was utilised to obtain the gene of interest for cloning. The template for the reaction was *C. elegans* Hsp90 DNA cloned in pQE30 plasmid by Dr. Antony Page. 0.5 μ l of plasmid was used in the PCR reaction. PCR was carried out in a reaction mixture containing 200 μ M of dNTPs, 1 X reaction buffer [200 mM Tris-

HCl (pH 8.8 at 25°C), 100 mM KCl, 100 mM (NH₄)₂SO₄, 20 mM MgSO₄, 1% Triton X-100 and 1 mg/ml nuclease-free BSA], 0.5 μM forward primers, 0.5 μM of the reverse primer and 5U of Pfu DNA polymerase (Stratagene). The mixture was made up to the desire volume using sterile distilled H₂O. The reaction was then carried out in the thermal cycler (Biometra) under the following conditions {95°C 2 min, (95°C 1 min, 55°C 1 min, 72°C 1 min) for 30 cycles, 72°C for 10 min}. At the completion of the reaction, the PCR products were analysed on 1.0% (w/v) agarose gel using Tris-Acetate-EDTA (TAE; 90 mM Tris, 90 mM Acetic acid and 2 mM EDTA). The agarose gel was stained with ethidium bromide (0.5 μg/ml) and observed over ultra violet light (260 nm).

For screening purposes, Taq polymerase (Roche) was used instead of Pfu DNA polymerase (Stratagene). The DNA template used was a single colony from the transformation plate. Furthermore, the PCR was carried out under following conditions {95°C 10 min, (95°C 1 min, 55°C 1 min, 72°C 1 min) for 30 cycles, 72°C for 10 min}.

2.2.2. Plasmid extraction

Plasmid extraction was carried out using the Qiaprep Miniprep kit (Qiagen), following the manufacturer's protocol [17]. Basically, the DNA plasmid extraction was carried out in microcentrifuge tube. 10 ml of bacterial culture was spun down in a 50 ml Falcon (10 min at 3000 rpm) and the pellet resuspend in 250 μl of buffer P1 (50 mM TrisCl, 10 mM EDTA, pH 8.0; 100 μg/ml RNase A). The re-suspended pellet was transferred into a microcentrifuge tube. 250 μl buffer P2 (200 mM NaOH,

1% SDS (w/v)) was added to the mixture which was then thoroughly mixed by inverting the tube 4-6 times. 350 μ l of buffer P3 (3.0 M potassium acetate, pH5.5) was added and immediately mixed as above. The sample was spun down at 13,000 rpm for 10 min in a table top centrifuge. The supernatant was harvested and applied to a Qiaprep spin column. The column was spun down for 60s at 13000 rpm, the flow through discarded. The column was then washed with 750 μ l of buffer PE by spinning it for 60s. The flow through was discarded and the column was spun down to remove residual PE buffer from the column which column was then placed into a 1.5 ml microcentrifuge tube. The plasmid was eluted by adding sterile distilled H₂O to the center of the column followed by spinning at 13000 rpm for 60s.

2.2.3. Digestion of DNA with restriction enzymes

Digestion of DNA was achieved using appropriate restriction enzymes in a total volume of 50 μ l containing an appropriate buffer (1X), 2 μ g acetylated BSA, 10U of each of the restriction enzymes (NEB) and 200 ng DNA. The mixtures were incubated at 37°C for 4-8 hrs and analysed immediately on a DNA agarose gel. The band of interest was excised and purified.

2.2.4. DNA purification by using QIAquick gel extraction kit

(Qiagen)

The DNA purification was carried out following the manufacturer protocol [15]. Basically, the digested product was run out on a DNA agarose gel. The band of interest was then excised with a clean, sharp scalpel. The excised gel piece was

weighed and 3 volumes of buffer QG added to 1 volume of gel (100mg~ 100 μ l). The sample was incubated at 50°C for 10 min with vortexing every 2 min. After the gel piece had completely dissolved, 1 volume of isopropanol was added followed by mixing. The sample was then applied to a QIAquick column and centrifuged for 60s at 13000 rpm. The column was washed using 750 μ l of buffer PE followed by another 60s centrifugation step. The flow through was discarded and the sample centrifuged for another 60s. After that, the column was placed into 1.5 ml microcentrifuge tube. The DNA was eluted by adding 50 μ l of water to the centre of the column followed by centrifugation at 13000 rpm for 60s.

2.2.5. DNA ligation and transformation

The ligation step was carried out to ligate the genes of interest into the expression vector after the DNA had been purified using the gel extraction kit [15]. Ligation was carried out using a Rapid DNA ligation kit (Roche). Basically, 50 μ g of vector and 150 ng of insert were mixed together in a microcentrifuge tube. 1x T4 DNA ligation buffer and 5U of the T4 DNA ligase were added to the mixture. The ligation mixture was incubated at room temperature for 1 hr. After incubation, the ligation mixture was immediately used to transform appropriate competent cells.

Transformation was carried out using standard methods described elsewhere in the literature [16]. The transformation method described here was also used throughout the study to transform any plasmid into an appropriate competent cell and does not only refer to the method used in the ligation mixture. 3-5 μ l of plasmid DNA was added to 50 μ l of competent cells and the mixture incubated on ice for 30 min. After the incubation, the mixture was heat shocked at 42°C for 45s, followed by

a 2 min incubation on ice. After the incubation period, 300 μ l of LB/SOC was added and the mixture incubated for 1 hr at 37°C with shaking. 80 μ l of the culture was spread onto an LB plate containing the appropriate antibiotics.

2.2.6. *Topo TA cloning (Invitrogen)*

This particular cloning technique was used to clone PCR products into either a pEntr or a pCR2.1 shuttle vector before the genes of interest were transferred to the final expression vector either pDest, pQe30 or pET. The kit used for these cloning experiments was supplied by Invitrogen, the manufacturer's protocol was followed. Basically, 4 μ l of fresh PCR product was mixed with 1 μ l of vector. 1 μ l of the salt solution (200 mM NaCl, 10 mM MgCl₂) was added to the mixture, which was then incubated for 30 min at room temperature. After incubation, 3 μ l of the mixture was used to transform 50 μ l Top 10 competent cells (Invitrogen). Transformation was carried out as described earlier in this chapter (Section 2.2.5). The transformation mixture was spread onto LB plate containing 50 μ g ampicillin, the plate was then incubated overnight at 37°C. Transformants that appeared on the plate were screened by PCR, plasmids from colonies of interest were extracted and sent for DNA sequencing.

2.2.7. *Test for protein expression*

Before the protein was expressed in large volume, pilot test expression was carried out to determine the optimal conditions for production of each of the proteins. The plasmid containing the gene of interest was transformed to appropriate expression

cells following transformation steps in section 2.2.5. One transformant was picked and inoculated into 10 ml of broth with appropriate antibiotic and incubated at 37°C overnight with shaking. The next day, 10 ml of new LB broth containing appropriate antibiotic was inoculated with 100 µl of overnight culture. The culture was then grown in a shaking w incubator at 37 °C, shake at 200 rpm. OD₆₀₀ of the culture was measured every hour by taking a 1ml sample and measured with spectrophotometer. The culture was induced when the OD₆₀₀ reached 0.6 by the addition of IPTG to a final concentration of 1 mM. The culture was incubated for a further 5 hrs with a sample for SDS PAGE analysis being taken every hour. All the samples were spun down, the supernatant discarded, 50 µl of SDS loading buffer was added to each sample and the cell pellet resuspended and boiled for 10 min. The samples were then analysed on an SDS polyacrylamide gel. Based on the results of the test expression, the optimal conditions such as the length of time to get reasonable protein was determined and were used for larger scale protein production. The optimization was carried out as a standard for all the proteins and if the protein productions were not satisfied under this condition, further optimisation was carried out. The further optimisation of the protein production was mentioned to for the relevant protein in Chapter 3.

2.2.8. Western blot analysis

The cell extracts or purified protein was run on a 13-15% SDS polyacrylamide gel using standard conditions as outlined earlier. The protein was transferred onto a nitrocellulose membrane using a semidry transfer unit (BioRad). Briefly, a sheet of thick filter paper was saturated with transfer buffer (25 mM Tris-

HCl, 190 mM glycine, 20% (v/v) methanol) and placed on the anode (lower electrode), followed by pre-soaked nitrocellulose membrane, the gel and finally another sheet of buffer saturated filter paper. The cathode was placed carefully on top of the "blotting sandwich", the transfer was carried out for 1 hr at a constant voltage of 15 V.

After transfer, the nitrocellulose membrane was blocked with a 10% (w/v) solution of skimmed milk in PBS-T (PBS containing 0.002% Tween 20) for 1 hour. Skimmed milk was used for blocking to prevent the unspecific binding of the primary and secondary antibody to the membrane. The blocking solution was discarded and the membrane washed with 10ml PBS-T. Anti-Hsp90 antibodies (Stressgen) or anti-His antibodies (Qiagen) were diluted (1:1000) in PBS-T and incubated with the blocked membrane. After 1 hr incubation with the primary antibody, the antibody solution was discarded and the blot washed. A secondary alkaline phosphatase conjugated antibody at a dilution of 1:3000 in PBST was added and incubated. The nitrocellulose membrane was washed after every step at least three times with 20 ml of PBS-T. Finally, substrate containing 0.05 mg/ml of NBT (Nitro Blue tetrazolium) and 0.1 mg/ml BCIP (5-bromo-4-chloro-3-indoylphosphate) (Promega) in alkaline phosphatase buffer (50 mM Tris , 3 mM $MgCl_2$, pH 9.8) was added to the membrane which was incubated until the colour from the reaction developed.

2.3. Protein expression and purification

2.3.1. Scale up of protein expression

Cultures of *E. coli* cells harbouring the recombinants plasmids were grown overnight in 100 ml LB broth containing an appropriate antibiotic. On the next day, the overnight culture was spun down at 3000 rpm for 10 min, the supernatant discarded and the pellet resuspended in 40 ml of fresh LB with antibiotic. 10 ml of the resuspended overnight culture was used to inoculate 1L of LB broth containing an appropriate antibiotic followed by shaking incubation at 37°C until the OD₆₀₀ reached 0.6. Normally 4L of LB was used in each of the scale up experiments. The cultures were induced by adding IPTG (isopropyl-β-D-thiogalactopyranoside) to a final concentration of 1 mM and incubated for an additional 5hrs. Cells were pelleted by centrifugation at 8000 rpm for 15 min in a Beckman JLA9100 rotor. The pellet was resuspended in lysis buffer (50 mM NaH₂PO₄, 300 mM NaCl, 5mM Imidazole, 20 mM β-mercaptoethanol; pH 8.0) containing 1 mg/ml lysozyme (Sigma). The resulting cell lysate was incubated with the lysozyme for 30 minutes before it was sonicated (5 times at 30s bursts). After sonication, the cells lysate was spun down at 22000 rpm in Beckman JA 25.50 for 1 hr. The pellet was discarded and the supernatant filtered with 0.45 μm syringe filter. At this point the supernatant could be frozen at -20°C if required.

2.3.2. Ni-NTA or Talon purification

The purifications were carried out using an AKTA Prime system (Amersham Pharmacia). Ni-NTA or Talon resin was packed into an appropriate column following the manufacturer's protocol. The column containing (either Ni-NTA (Qiagen) or Talon (BD Biosciences) resin was equilibrated with 5 volumes of buffer A (50 mM NaH₂PO₄, 300 mM NaCl, 5 mM Imidazole; pH 8.0) or until a stable baseline was reached. The flow rate of the machine was 1ml/min. Filtered cell lysate was applied to the column which was then washed with buffer A until the baseline was reached. The column was then washed with 10 % buffer B (50 mM NaH₂PO₄, 300 mM NaCl , 250 mM Imidazole; pH 8.0). This step was used to wash off the proteins bound non-specifically to the resin. A slow gradient elution from 10 to 100% buffer B was carried out over 10 column volumes. 10 or 5 ml fractions were collected at this stage. The column was then washed with 3 column volumes of 100% buffer B. Finally, the column was re-equilibrated with 5 column volumes of Buffer A. The fractions from the elution were analysed on an SDS polyacrylamide gel to visualise the proteins.

2.3.3. Gel filtration

Gel filtration was used as a polishing step in the purification and also to analyse proteins and protein complexes. The columns used were Sephacryl 200 and Superdex 200 or 75 (Amersham). The purification was carried out using an AKTA FPLC system (Amersham). The column was equilibrated with one column volume of appropriate buffer until a stable baseline was reached. The flow rate for the experiments was 0.5 ml/min. The filtered solution containing the target protein was

concentrated to an appropriate volume and loaded onto the column. The volume of sample loaded was dependent on the manufacturer's suggestion for each specific column, however as a general guideline no more than 1 % (v/v) of the column volume should be applied to maximise resolution of the desired protein(s). The elution was carried with one column volume of buffer and 0.5 or 1 ml fractions were collected over the elution period. The fractions were then analysed on a 12-15% SDS polyacrylamide gel.

2.3.4. Anion exchange column (Mono-Q)

This column was used to increase the purity of the C-terminal domain of human Hsp90 α during a trial purification. 10 ml of 30 Q resin was packed into an XK16 (Amersham) column according to manufacturer's protocol. The purification was carried out using an AKTA Prime system. The column was equilibrated with 5 column volumes of buffer A (50 mM Tris; pH 7.5) at a flow rate of 1 ml/min. The sample after dialysis overnight in buffer A, was loaded onto the column which was washed with buffer A until baseline was reached. The protein was eluted using buffer B (Buffer A + 0.5M NaCl). A gradient over 10 column volumes from 0 to 50 % buffer B was used, 10 ml fractions were collected over the gradient. The gradient was then increased from 51 to 100 % over another 5 column volumes and 10 ml fractions collected. Another 5 column volumes of 100% were carried to clean the column. The column was re-equilibrated with buffer A for 3 column volumes and kept for further use.

2.4. Methods for characterizing Hsp90

2.4.1. *Intrinsic tryptophan fluorescence*

The experiments were carried out using Flouromax-3 (Jobin Yvon, Hariba). The experiment was carried out by using either a 200 μl or a 3 ml cuvette having path lengths of 0.1 and 0.5 cm respectively. The 3 ml cuvette was used in the experiment where ligands were titrated into a protein solution. The rationale behind carrying out the experiments in this way is as follows: ligands can be prepared at very high concentrations and can therefore be titrated into the protein. The protein samples are not amenable to being maintained at such high concentrations, a further potential problem of conducting the experiments in this way would be the very large amount of protein required. Furthermore, the total volume added during the titration ideally must not be more than 4% of the initial volume. Adhering to this goal makes the resulting dilution factor negligible and minimizes change in the initial concentration of the protein. Therefore, in the protein-protein interactions studied using fluorescence or when the availability of one component was limiting, the samples were prepared separately in a total volume of 200 μl and the 200 μl cuvette was used to measure the emission.

Preliminary experiments were carried out using the 200 μl cuvette. The aim of the experiment was to determine if an interaction occurred between the proteins/ligands by carrying out an emission scan using the data acquisition program on the fluorimeter machine. Briefly, 1 μM protein was excited at 295 nm and the emission was scanned at a range of wavelengths between 310 to 460 nm. The scan was repeated with the complex mixture and also with a 50 μM solution of the other

proteins or ligands. The profiles from the emission scans were compared to determine if either quench or enhancement was observed in the complex when compared to both of the components alone. The scan was also monitored for the existence of blue or red shift of the emission profile. Based on this the emission wavelength of the peak during the complex scan was taken and used later for further experiments.

The experiment was repeated using a time based acquisition program supplied with the machine. The temperature of the machine was adjusted to an appropriate temperature for the experiment, usually 25⁰C which is the RT. The excitation wavelength was set at 295 nm but the emission wavelength was based upon data from the emission scan and in the experiments was either 350 or 355 nm. The emission was measured for 60s. The measurements were then averaged and corrected against inner filter effects, background fluorescence and also dilution factor. In the experiments, the slits were usually set at 2.5 mm for excitation and 2.5 mm or 5.0 mm for emission. There are two slits in the machine that control excitation and emission. The wider the slits, the more light during excitation or emission was permitted to reach the sample or release from the sample. The slits can not be too wide as error of measurements can occur. Therefore, the slits were dependent on the initial emission of the sample and were used for all of the experiments. In the titration experiments, 1 μ M protein in 3 ml buffer solution was titrated into the ligands under test using a Hamilton syringe. The solutions were mixed gently and left for 5 min before the measurement was taken. In the other experiment, a separate reaction was prepared in a total volume of 200 μ l in a micro-centrifuge tube. The mixture was then incubated for the desired time before the measurement was taken.

The data was treated for correction of inner filter effects as well as background but not for the effect of the dilution factor. The details of the specific experiments utilising Trp fluorescence are more fully described in a later chapter (Chapter 4, section 4.2.3.2).

2.4.2. Sensor chips preparation for Surface Plasmon Resonance (SPR)

SPR is an evanescent wave biosensor technology that monitors the interaction of two or more molecules in real-time. The technique detects the change in refractive index of a sensor surface. For example, when ITC was used to study the interaction of two proteins, which are A and B. Protein B was immobilised on the surface of a sensor chip whereas potential binding partner A was carried in a flow of buffer solution through a miniature flow cell (Figure 2.1). In the event of binding of the protein A and B, the changes in the refractive index of the sensor chip was captured by the detector. The refractive index changes over time were recorded on the sensorgram (Figure 2.1). Then, the sensorgrams can be analysed to give the binding strength and also kinetic of the interaction.

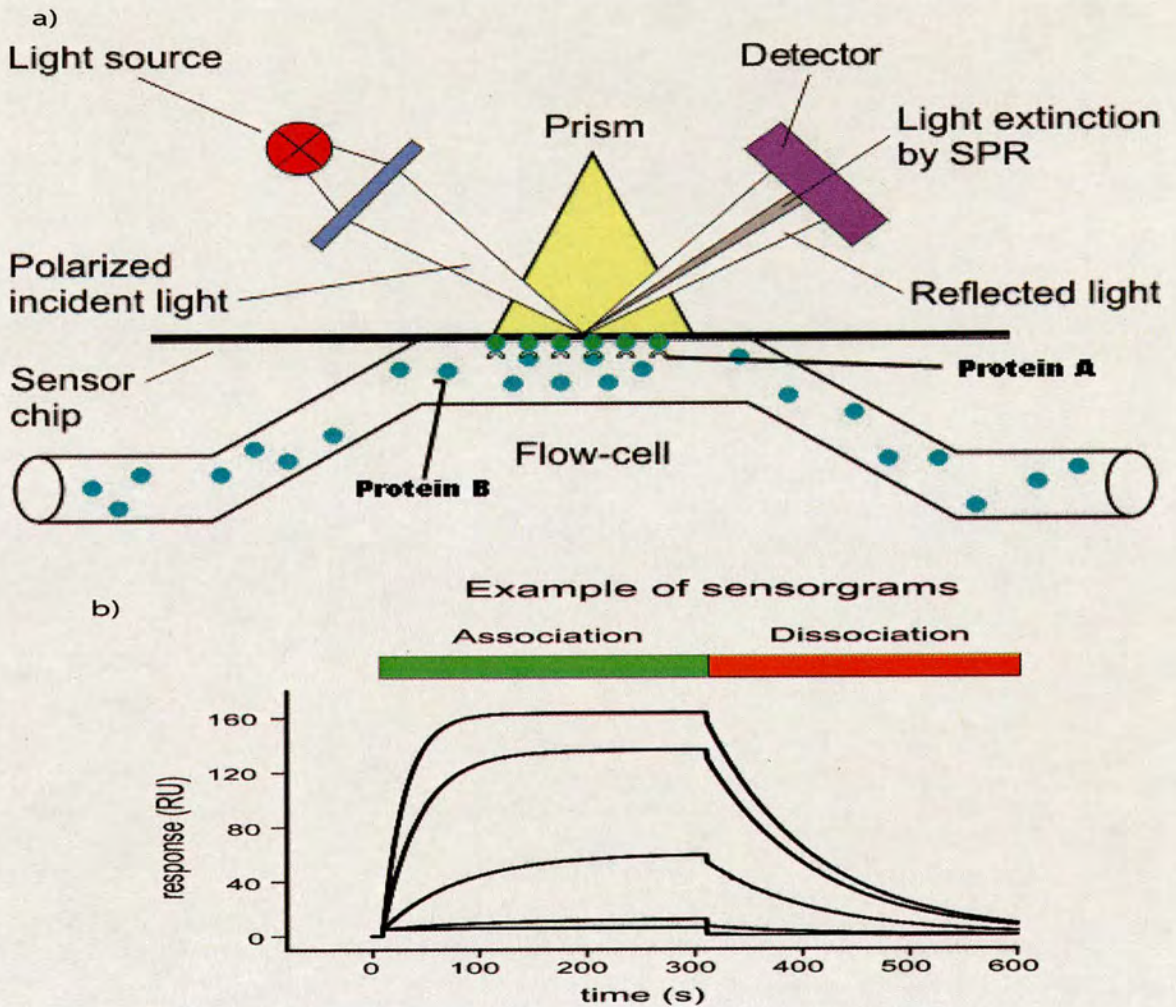


Figure 2.1. Illustration of SPR reaction. a) Protein A was immobilised onto a sensor chip. The chip was selected dependent on the type of coupling suitable to the protein. In this experiment, hHsp90- α 521 was coupled to the NTA chip via the histidine tag on the protein. On the other hand, the ceHsp90-492 was coupled to the CM5 chip via primary amine. In the experiment, the potential binding partner such as Cyp40 was passed over the surface. If the interaction occurs, the density of the surface was changed and when polarized light shines on it, the refractive index will also changes. The changes of refractive index over time were interpreted into sensorgrams b). The sensorgram can be analysed to give strength of binding and also kinetics of the interaction. The picture was taken and modified from [1].

The experiments were carried out using a Biacore 3000/T1000 instrument (Biacore). The experiments were designed to investigate the binding of Hsp90 protein to the immunophilin Cyp40. In order to carry out the experiment; two types of sensor chip were prepared. The hHsp90- α 521 was coupled via its histidine tag to the Ni-NTA chip, whereas the ceHsp90-492 was coupled covalently to CM5 chip. For coupling via the His-tag, the NTA sensor was preloaded with Ni^{2+} according to Biacore protocols. Briefly, the NTA sensor was charged with NiCl_2 by running 5 ml of 500 μM NiCl_2 in Hepes-buffered saline (HBS) (10 mM Hepes 0.15 M NaCl, 0.005% surfactant P20, pH 7.4) over the surface of an the chip at a flow rate of 20 $\mu\text{l}/\text{min}$. Loading the chip with nickel in this way should give a baseline rise of only 40 RU [14], The chip was washed with the same buffer to discharge unbound Ni^{2+} . The His-tagged protein (100 to 500 nm) in Running buffer (10 mM HEPES, pH 7.4; 150 mM NaCl; 0.005% surfactant P20) was passed over the sensor surface for 60s at a flow rate of 5 $\mu\text{l min}^{-1}$. The change in response unit seen for each of the runs was monitored to obtain the optimal conditions producing a saturation response. The optimal conditions determined were then used to bind the His-tagged protein to the Ni- NTA sensor chip. The chip was washed with running buffer to clear the unbound protein [14, 23]. The NTA sensor chip with protein bound was now ready to be used in the binding experiments with Cyp40. This step was regenerated between each injection of a new concentration of the partner protein. The experiments were each repeated three times. The data was analysed using software supplied by Biacore. Specific details of the experiments are described in greater details in chapter 4, section 4.2.3.3. as well as the results.

The ceHsp90-492 was coupled to the CM5 chip via the protein primary amine. In order to do this, the surface was first activated by running 1:1 mixture of 0.4 M 1-ethyl-3-(3-dimethylaminopropyl)-carbodiimide (EDC) and 0.1 M N-hydroxysuccinimide (NHS) in water at 5 $\mu\text{l min}^{-1}$ for 3 min. After the surface activation, 200 nM of ceHsp90-492 was passed over the surface to start the coupling reaction. The coupling process was carried at 5 $\mu\text{l min}^{-1}$ for 10 min until the response deposited reach 6000 RU. The sensor was then washed with 1 M ethanolamine, pH 8.5 to deactivate the excess carboxyl group on the sensor surface. The chip was now ready to be used in the interaction with Cyp40. The details of the SPR experiment of ceHsp90-492 are described in Chapter 5.

2.4.3. Isothermal titration calorimetry (ITC)

ITC is known to be a useful technique in the study of protein and small inhibitor interactions [7, 9, 18]. The study used a VP-ITC machine (Microcal, U.K). In principal, the machine contains two cells, known as the reference and sample cells. The reference cell contains just the buffer used throughout the experiment. The sample cell is filled with a protein (B) whereas the ligand (A) is taken up in the syringe supplied with the ITC machine. The sample and the reference cells are kept within the same temperature between them. The ligand A is injected into the sample cell and is free to interact with protein B. After each injection, the heat released or absorbed in the sample cell was measured by comparison to the reference cell (Figure 2.2) [2, 11]. The heat released or absorbed gives several peaks which then converted over time to give apparent heat change. If the molar ratio of A to protein B was low at the beginning of titration, all of A will bind to the protein and the peak

areas are similar. As the molar ratio increase, protein B becomes saturated and the heat changes gradually decreased. The small heat change still occurring at the end of the titration was caused by the dilution of A and other non-specific effects [10].

The experiment was started by thoroughly cleaning the reference, sample cells and the syringe with sterile distilled water and then with buffer (100 mM Tris; pH 7.5, 50 mM NaCl). The ligand, buffer and the protein solutions were then degassed. 1.4 ml of degassed buffer was placed inside the reference cell. The sample cell was usually filled with protein, but the ligand used in this experiments precipitated at high concentration. Therefore, it was used in the sample cell in low concentration and titrated with the protein. Ligand (50 -100 μM) in a total volume of 1.4 ml was placed inside the sample cell. The syringe was filled with protein (300 – 500 μM) to a final volume of 280 μl . The temperature of the experiment was set to either 18 or 30 $^{\circ}\text{C}$. The sample was stirred at 300 rpm. The protein was titrated in to the fixed ligand solution. The titration was carried out by setting the program on the machine. The initial volume injection was 5 μl . Subsequent injection volumes were either held at 5 μl or increased to 10 μl , dependent upon the signal of the heat different between injections. The number of injections per experiment was either 50 or 25 and was dependent upon the volume used per injection as the total volume that can be taken up by the syringe is 280 μl . Following careful setup of the experiment, the data aquisition program was started and the data obtained were analyzed using the analysis package supplied with the Origin software. More details of the experiment are given in chapter 4, section 4.2.4.5.

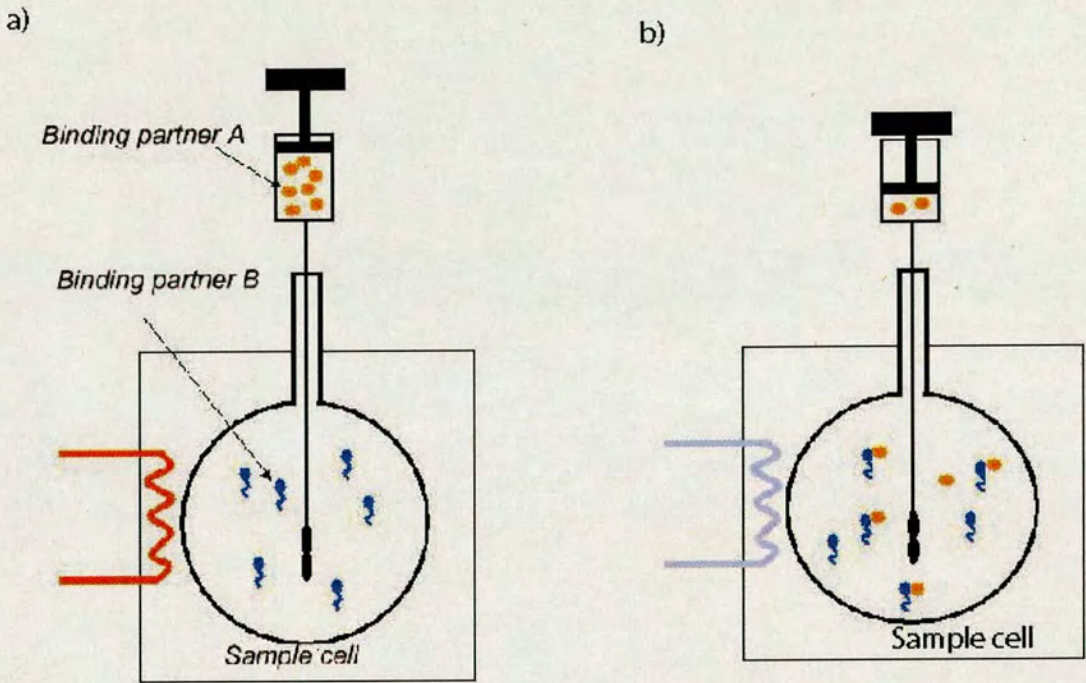


Figure 2.2. Illustration of the ITC reaction. a) Sample cells were filled with binding partner B (usually a protein). In the experiments described in this thesis, binding partner B was ligand. Binding partner A was usually a ligand but in that experiment carried out it was filled with protein. b) When binding partner A was injected into the cell, an interaction occurred. If the interaction is exothermic, less energy is needed to be supplied to the sample cell when compared to the reference cell to re-equilibrate the temperatures. If the interaction is endothermic more energy needed to return the temperature of the sample cell to that of the reference cell. The difference in the amount of energy required to re-establish an equilibrium temperature between the two cells was monitored and interpreted to analyse the interactions.

2.4.4. Malachite green assay standard curve

Malachite green was used to study the ATPase activity of the C-terminal Hsp90 in this thesis. The assay was straight forward. The malachite green solution was obtained from Upstate, UK. The solution contains (0.0812%, (w/v)) malachite green dye, polyvinyl alcohol (2.32%, (w/v)); dissolves with difficulty and requires heating), ammonium molybdate (5.72%, (w/v), in 6 M HCl), and water, mixed in the ratio 2:1:1:2 [19]. During ATPase activity, phosphate was released and bound to molybdate ion to form phosphomolybdate. The compound was then reacted with the malachite green dye and formed a green colour that can be measured at 620 nm. The malachite green solution also functions to stop the ATPase activity because it contains a high concentration of HCl (6M) in the solution. 34% sodium citrate was added to the mixture after adding malachite green solution to stabilise the signal and reduce background due to unspecific phosphate release from the reaction [19].

The standard curve for this assay utilises phosphate and was obtained by following the manufacturer's protocol (Upstate, UK). Briefly, 10 μ l of 1% Tween 20 solution (Sigma) was mixed with 1ml of malachite green solution. The malachite green solution containing the Tween 20 was used in one experiment. A 1 mM stock of KH_2PO_4 was made and diluted to 0.1 mM prior to use. The 0.1 mM phosphate solution was further diluted as listed in Table 2.1.

Volume of diluted stock (0.1 mM)	Volume of distilled water or diluent	Phosphate concentration per 100 μ l
50	200	2000 pmoles
45	205	1800
35	215	1400
30	220	1200
25	225	1000
15	235	600
10	240	400
5	245	200
0	250	0

Table 2.1. Phosphate dilution series used to produce the standard curve for phosphate used in the malachite green ATPase assays. The total volume of each of the reactions was 250 μ l. The dilutions were then used to carry out the malachite green assay as described below.

100 μ l of each of the dilution series was aliquoted into individual microcentrifuge tubes. 320 μ l of malachite green solution containing 1% Tween was added to each tube followed by gentle mixing. 50 μ l of a 34% sodium citrate solution in water was added immediately and mixed thoroughly. The reactions were left for 15 min. After 15 min, the absorbance at 620 nm was taken. From the absorbance, a standard curve was plotted and used to measure the amount of phosphate released in ATPase assay.

2.5. Methods for crystallization trials

2.5.1. Hanging drop vapour diffusion

All the purified proteins were subjected to crystallization trials. The trials were carried out using the hanging drops vapour diffusion method. This method is most widely used for crystallization trials due to its relative ease of use and simplicity [3, 4, 6]. The method utilises 24-well Linbro plates (Molecular Dimension Limited). The lip surrounding each of the wells was greased using soft paraffin wax. The Siliconized glass cover slips (Molecular dimension limited) were thoroughly cleaned by wiping them with a soft lens tissue to remove any fibres or dust. The wells were filled with 1ml of each of the required reservoir solutions containing a variety of precipitants. 2 μ l of protein was pipetted into the center of the siliconised cover slip. Then, 2 μ l of each of the well solutions was added to the appropriate protein drop. The cover slip was inverted immediately but carefully and placed onto the rim of the appropriate well of the Linbro plate (Figure 2.3). The coverslip was then gently pressed down into the paraffin wax, making a seal between the coverslip and the plate beneath. The above steps were repeated for all wells.

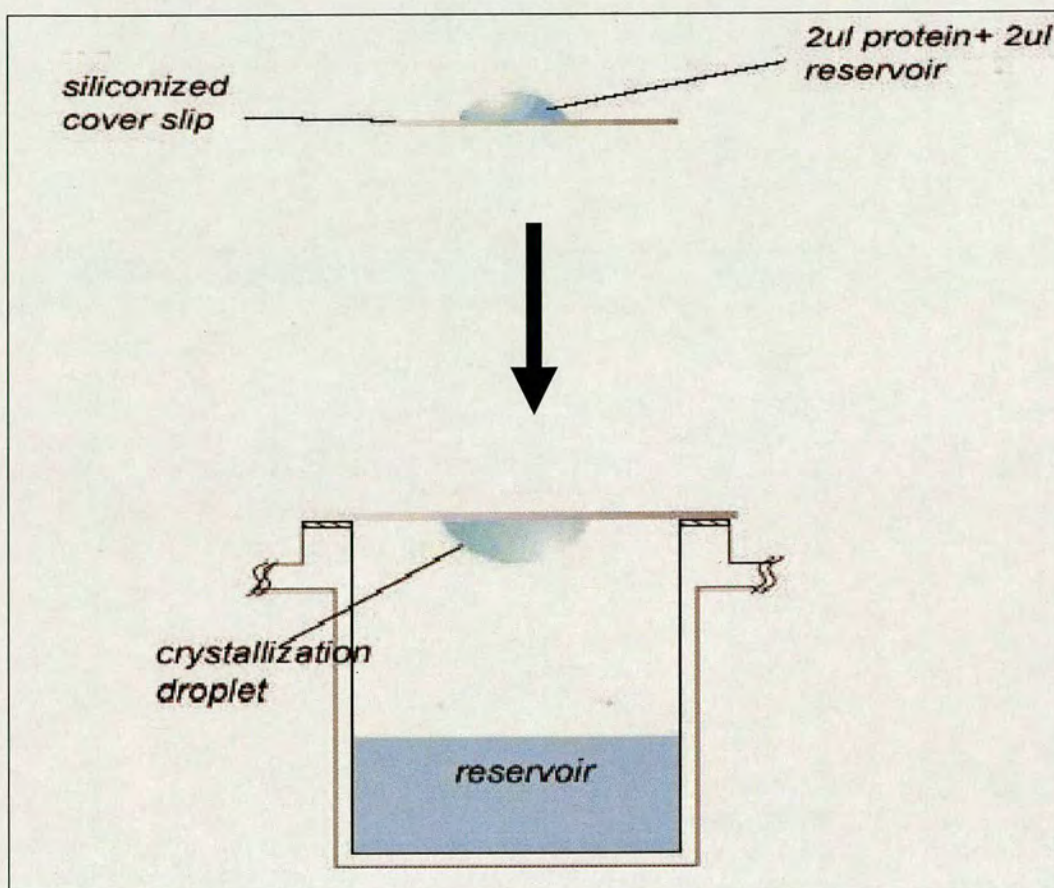


Figure 2.3. Illustration of the set up of the hanging drop vapour diffusion technique. The drop containing 2 μ l of protein solution and 2 μ l of reservoir solution was placed in the center of a siliconised cover slip. The cover slip was then inverted and placed on top of the grease at the mouth of the well.

2.5.2. Crystal soaking and co-crystallisation experiments

Crystal soaking experiments were a useful tool for the project described in Appendix A. Crystal soaking can be used to study the interaction of protein with a ligand or inhibitor [13, 20 21, 22]. Crystals were grown following standard methods as outlined above. A plate was set up using conditions very similar to those that

produce native crystals. Separate reservoirs containing a range of concentrations of ligands were made. 2 μ l of each of the reservoir solutions containing the ligands were placed in the center of a cover slip (one per ligand concentration). One or more native crystal was picked and put into the droplet containing ligand. The steps were repeated for all other concentrations of the ligands. In the experiment (appendix A), Cyp3 crystals were soaked in an increasing concentration of 1.5 to 120 mM of dipeptide Gly-Pro. The crystal was soaked for 20, 60 and 120 minutes for each of the dipeptide concentrations. The crystals were then flash frozen and stored in liquid nitrogen before X-ray data was collected using either the home source or station 14.1 at the SRS, Daresbury.

Besides crystal soaking, co-crystallization can also be utilised to study the interaction of protein with ligands [5, 8, 12, 20, 24]. This technique can also be helpful in obtaining crystals from a “new” previously structurally uncharacterised protein by utilising a protein partner which has already been crystallised. Therefore, co-crystallization experiments were used for the C-terminal domain of Hsp90. The partner proteins/ligands used with the Hsp90 constructs were Cyp40, ATP and novobiocin. Basically, the protein(s) were incubated together before the complex mixture was placed onto the cover slip. The protein mixture was set up and incubated at RT or 4⁰C for 30 min. The mixture was mixed with the ratio of 1 concentration of protein to 10 times of the ligand dissociation constant (K_d) plus the protein concentration. The mixture was set up based on the assumption that the occupancy of a binding site is independent of the protein concentration and only determined by the actual concentration of the ligand. For example, 300 μ M (10mg/ml) of hHsp90- α 521 was used to in the co-crystallisation. In order to get the occupancy of hHsp90- α 521

near saturation, 10 times the K_d of the interaction ($K_d \sim 70 \mu\text{M}$) was needed in the co-crystallisation. Therefore the concentration of ligand needed was 1mM ($10 * K_d + [\text{protein}] = 10 (70) + 300 = 1\text{mM}$). The mixture was then used to set up crystallisation trials with various precipitant and commercial screening kits.

References

1. (IBI IFBIP (2003) Protein-Protein Interactions :Surface Plasmon Resonance Spectroscopy (SPR). In: (IBI-1) CSP (ed) http://www.fz-juelich.de/ibi/ibi-1/protein-protein_interaction
2. Ababou, A., Ladbury, E. J (2006) Survey of the year 2004: literature on applications of isothermal titration calorimetry. *J Mol Recognit* 19: 79-89
3. Adachi, N., Natsume, R., Senda, M., Muto, S., Senda, T., Horikoshi, M. (2004) Purification, crystallization and preliminary X-ray analysis of Methanococcus jannaschii TATA box-binding protein (TBP). *Acta Crystallogr D Biol Crystallogr* 60: 2328-31
4. Bogaerts, I., Verboven, C., Rabijns, A., Waelkens, E., Baelen V, H., Ranter D, C. (2001) Purification, crystallization and preliminary X-ray investigation of the complex of human vitamin D binding protein and rabbit muscle actin. *Acta Crystallogr D Biol Crystallogr* 57: 740-2
5. Chooback, L., West, H. A (2003) Co-crystallization of the yeast phosphorelay protein YPD1 with the SLN1 response-regulator domain and preliminary X-ray diffraction analysis. *Acta Crystallogr D Biol Crystallogr* 59: 927-9
6. Dornan, J., Page, P. A, Taylor, P., Wu, S., Winter, D. A, Husi, H., Walkinshaw, D. M (1999) Biochemical and structural characterization of a divergent loop cyclophilin from *Caenorhabditis elegans*. *J Biol Chem* 274: 34877-83
7. E B, KD C, M H, PL S, AM R, BV P, R OB, JE L, M. S (1999) Structure of the PH domain from Bruton's tyrosine kinase in complex with inositol 1,3,4,5-tetrakisphosphate. *Structure* 7: 449-460
8. Harris, S. M, Bock, H. J, Choi, G., Cialdella, S. J, Curry, A. K, Deibel, R. M, Jr., Jacobsen, J. E, Marshall, P. V, Murray, W. R, Jr., Vosters, F. A, Wolfe, L. C, Yem, W. A, Baldwin, T. E (2002) Co-crystallization of *Staphylococcus aureus* peptide deformylase (PDF) with potent inhibitors. *Acta Crystallogr D Biol Crystallogr* 58: 2153-6
9. I C, VA V, TR M, BA S, RJ. L (1999) Interaction of heparin with annexin V. *FEBS Lett.* 446: 327-330.
10. Jelesarov, I., Bosshard, R. H (1999) Isothermal titration calorimetry and differential scanning calorimetry as complementary tools to investigate the energetics of biomolecular recognition. *JOURNAL OF MOLECULAR RECOGNITION* 12: 3-18
11. Ladbury, E. J (1995) Counting the calories to stay in the groove. *Structure* 15 635-639
12. Mazza, C., Segref, A., Mattaj, W. I, Cusack, S. (2002) Co-crystallization of the human nuclear cap-binding complex with a m7GpppG cap analogue using protein engineering. *Acta Crystallogr D Biol Crystallogr* 58: 2194-7
13. Nagem, A. R, Ambrosio, L. A, Rojas, L. A, Navarro, V. M, Golubev, M. A, Garratt, C. R, Polikarpov, I. (2005) Getting the most out of X-ray home sources. *Acta Crystallogr D Biol Crystallogr* 61: 1022-30
14. Nieba, L., Nieba-Axmann, SE., Persson, A., la"inen Hm, M., Edebratt, F., Hansson, A., Lidholm, J., Magnusson, K., Karlsson, F. A, P, A. (1997) BIACORE Analysis of Histidine-Tagged Proteins Using a Chelating NTA Sensor Chip. *ANALYTICAL BIOCHEMISTRY* 252: 217-228
15. Qiagen (2002) QIAquick Gel Extraction Kit Protocol. In: Qiagen (ed) QIAquick® Spin Handbook, pp 23-24
16. Qiagen (2003) The QIAexpressionist, 5th edn. Qiagen
17. Qiagen (2005) Protocol: Plasmid DNA Purification Using the QIAprep Spin Miniprep Kit and a Microcentrifuge. In: Qiagen (ed) QIAprep® Miniprep Handbook pp 22-23
18. R B, GT R, TJ W, GR. C (1999) Affinity modulation of small-molecule ligands by borrowing endogenous protein surfaces. *Proc.Natl.Acad.Sci.U.S.A.* 96: 1953-1958
19. Rowlands, G. M, Newbatt, M. Y, Prodromou, C., Pearl, H. L, Workman, P., Aherne, W. (2004) High-throughput screening assay for inhibitors of heat-shock protein 90 ATPase activity. *Anal Biochem* 327: 176-83
20. Schlichting, I. (2005) X-ray crystallography of protein-ligand interactions. *Methods Mol Biol* 305: 155-66

21. Sy W, S., S., Dornan, J., Kontopidis, G., Taylor, P., Walkinshaw, D. M (2001) The First Direct Determination of a Ligand Binding Constant in Protein Crystals. *Angew Chem Int Ed Engl* 40: 582-586
22. Tsai, L. M, Liaw, H. S, Chang, C. N (2004) The crystal structure of Yml at 1.31 Å resolution. *J Struct Biol* 148: 290-6
23. Wear, A. M, Patterson, A., Malone, K., Dunsmore, C., Turner, J. N, Walkinshaw, D. M (2005) A surface plasmon resonance-based assay for small molecule inhibitors of human cyclophilin A. *Anal Biochem* 345: 214-26
24. Zhou, Z., Gong, W. (2004) Co-crystallization of *Leptospira interrogans* peptide deformylase with a potent inhibitor and molecular-replacement schemes with eight subunits in an asymmetric unit. *Acta Crystallogr D Biol Crystallogr* 60: 137-9

Chapter 3: Cloning and purification of Hsp90

3.1. Introduction

Chapter 3 describes the cloning and purification of both the N and C-terminal domains of *C. elegans* Hsp90. Clones for human Hsp90 α were supplied by Thomas Rataczak from Department of Pharmacology, University of Western Australia. The individual protein purification protocol developed for each of the target proteins are also outlined in this chapter.

3.2. Materials and Methods

3.2.1. Cloning the N and C-terminal domains of *C. elegans* Hsp90

The C-terminal domain of *C. elegans* can be used as a comparison with the C-terminal of human Hsp90. Cloning was carried out with the help of Dr. Antony Page from Wellcome Centre for Molecular Parasitology, The Anderson College, University of Glasgow. The cloning experiments were carried out in his lab as well in-house. Cloning of the C-terminal domain of *C. elegans* Hsp90 was carried out to enable the production of an analogous region of the protein from a different species, allowing parallel characterization and crystallization trials with those of the C-

terminal domain of Hsp90 human. Basically, the regions to be cloned were selected by sequence analysis and secondary structure prediction to be as directly comparable

Gene name	DNA fragment length (bp)	Protein name	Protein size (kDa)
C1F	386	<i>C. elegans</i> <i>Hsp90</i> 575-702 (ceHsp90-575)	12.5
C2F	545	<i>C. elegans</i> <i>Hsp90</i> 525-702 (ceHsp90-525)	17.5
C3F	635	<i>C. elegans</i> <i>Hsp90</i> 492-702 (ceHsp90-492)	21
N-terminal	660	<i>C. elegans</i> <i>Hsp90</i> 6-219 (ceHsp90-6)	24

Table 3.1. List of the genes and their sizes that were cloned to obtain the target proteins. The target protein was as named based on where the protein fragments started and ended. The calculated sizes of the proteins without any linker are shown.

as possible to the cloned peptide sequences available for human Hsp90. Cloning experiments produced a number of target proteins as listed in Table 3.1.

The N-terminal domain of *C. elegans* Hsp90 (ceHsp90-6) was cloned in order to investigate reports that, despite high sequence identity with human Hsp90, the *C. elegans* Hsp90 is resistant to the ansamycin antibiotic geldanamycin. A clone of full length *C. elegans* Hsp90 was available, however the resultant protein was not very stable and to date despite extensive efforts no crystals have as yet been obtained. It was hoped that the N-terminus alone would produce more stable protein and therefore be more amenable to experiments investigating the characteristics of the *C. elegans* Hsp90 interaction with ligands such as ATP and geldanamycin.

3.2.1.1. Polymerase chain reaction (PCR)

The PCRs were carried out as described in Chapter 2 (Section 2.2.1). The primers used for the reactions were listed in Table 3.2 and the regions where the

Primer	Primer type	Vector for cloning	Primer sequences
Hsp90bamc1f	Forward	pQE-30(Qiagen)	5'-cgggat cgggatggtccgctaa catggagcgc-3'
Hsp90bamc2f			5'-cgggatccaccgaggaggagaa gaagaaga-3'
Hsp90bamc3f			5'-cgggatcctgacccaa ttgatgagtactgc-3'
Hsp90pstr	Reverse		5'-gcctgcagttagtcgacctctc catgcg-3'
GWC1F forward	Forward	pEntr TOPO- gateway pDest17-Gateway	5'-caccggatggtccgctaactg-3'
GWC2F forward			5'-caccgaggagaagaagaagttc-3'
GWC3F forward			5'-cacctgcgacccaattgatgagtac-3'
Hsp90pstr	Reverse		5'-gcctgcagttagtcgacctctc catgcg-3'
Hsp90C3fNdeI	Forward	pET 28a	5'-gaagtcctccatattgtcgac ccaattgatgag-3'
Hsp90BamHI	Reverse		5'-ggcttaaggatccttagtcgacctctc catgcg -3'
NtermF6NdeI	Forward		5'-atgtccgagcatatggaaccttcgca-3'
Nterm219BamHI	Reverse		5'-gacagcctcggatccttaaa cctccttctc-3'

Table 3.2. List of the primers used in the cloning experiments. The primers were designed to produce the same region, however, there are sequence differences because the cloning sites for each of the vectors were varied.



Figure 3.1. The locations of primer binding sequences in *C. elegans* Hsp90 genes. Forward arrows indicate the start of the four protein constructs. The backward arrows show the location of reverse primer binding sequences. The red highlighted sequences indicate the restriction sites in each primer. The blue highlighted sequences show the common sequences in the forward primer for every region.

primers bound was shown in figure 3.1. The primers were slightly different, being dependent upon the cloning vector.

The PCR products obtained from all the reactions were confirmed by running them on 1% agarose gels containing ethidium bromide followed by visualization using UV light.

3.2.1.2. Cloning strategies

3.2.1.2.3. Cloning into shuttle vectors (pCR®2.1-TOPO® and pENTR™/SD/D-TOPO®)

After all the gene products had been sequenced to confirm they contained the correct DNA, they were cloned into either the pCR®2.1-TOPO® vector or the pENTR™/SD/D-TOPO® vector. However, the PCR products were first concentrated and cleaned up by using PCR cleaning kit (Qiagen). Then, 4 µl of the PCR products were added to the mixture containing salt solutions (1.2 M NaCl, 0.06 MgCl₂) and pCR®2.1-TOPO®. The mixture was incubated for 5 min at RT. 3 µl of the mixture was used to transform DH5α competent cells. The transformation protocol followed was as described in Chapter 2. The transformation mixtures were spread onto LB plates containing 50 µg/ml of both ampicillin and kanamycin followed by overnight incubation at 37⁰C. The transformants were then screened directly by PCR using the method of direct colony PCR. The positive transformants were grown up overnight in 10 ml LB broth containing 50 µg of ampicillin. On the next day, plasmid extraction was carried out from the overnight culture. These plasmids were used for cloning into the desired expression vector.

3.2.1.2.4. Cloning into the expression vectors (Gateway system, pQE30 and pET28a)

The next steps of the cloning experiments were largely vector dependant. In the Gateway cloning system, the genes of interest previously cloned into the pENTR™/SD/D-TOPO® vector can be transferred into an expression vector without having to digest the genes out from the pENTR™/SD/D-TOPO® vector. After the PCR products had been shown to be correctly cloned into the pENTR™/SD/D-TOPO® vector, the genes were transferred to pDest 17 (His-Tag containing vector) or pDest15 (GST-Tag containing vector) by the LR recombination reaction. The LR recombination reaction was performed as followed: A mixture of 4 μ l of pENTR™/SD/D-TOPO® containing the gene of interest, 1 μ l of pDest17/15 were mixed and made up to a volume of 8 μ l with TE buffer. 2 μ l of LR Clonase II Enzyme was added up to the reaction. The LR clonase reaction was incubated at 25⁰C for an hour. Then, 1 μ l of Proteinase K was added and the reaction was incubated at 37⁰C for 10 min. Finally, the mixture of reaction was transformed into the DH5 α competent cells. The transformation mixture was spread onto LB agar plates containing 50 μ g/ml of kanamycin.

Transformants appearing on the plate were screened by direct colony PCR. Positive transformants were used to inoculate a 10 ml culture of LB broth, followed by growth of the culture overnight at 37⁰C, The plasmid was extracted from the overnight culture and transformed into the expression host BL21 A1 cells. The plasmids were also sent for sequencing. Several transformants on the plate were picked and a pilot test expression (as outlined in Chapter 2) was carried out.

In order to clone the genes of interest into the pET 28a (Novagen) and pQE30 (Qiagen) vectors, a different approach compared to that for the Gateway system was taken. Digestion of the TOPO vector was used during the cloning procedures for Pet28a and pQE30. The TOPO plasmids that contain the genes and the vectors were digested using the same restriction sites used to clone the genes. The vector was treated with Antarctic phosphatase (NEB) to prevent self-ligation. Both the digested vector and the TOPO plasmid were run on DNA gels. Bands corresponding to the digested vectors and the gene fragments were excised and recovered using a gel extraction kit (Qiagen). The purified vector and the gene fragments were ligated using a Rapid DNA ligation kit (Roche), the ligation mixture was transformed into DH5 α competent cells. The transformation mixture was spread on LB agar containing antibiotics as appropriate to the vector used.

Direct colony PCR was used to screen for positive transformants. The colony that gave positive results from the PCR screen was grown overnight in 10 ml LB broth containing the appropriate antibiotic. The plasmid was extracted as before. The plasmid was then transformed into appropriate competent cells for large scale protein expression. Various competent cells were used to in attempts to maximise protein expression. The plasmid was also sent to School of Biological Sciences (Edinburgh University) Sequencing Service (SBSSS) for DNA sequencing.

3.2.2. Purification of C-terminal human Hsp90 α and *C. elegans*

Hsp90

In order to purify the proteins, the bacterial cells containing the recombinant plasmid were grown up in a large volume of LB and prepared for purification as described in Chapter 2. The lysate was filtered with 0.45 μ M syringe filter.

3.2.2.1 .Ni-NTA/Talon affinity column

The column was equilibrated with Buffer A (50 mM NaHPO₄, 300 mM Tris, 5 mM Imidazole, pH 8.0). After a stable baseline was observed, the filtered lysate was loaded and the column washed with Buffer A until the absorbance at 280 nm returned to baseline. The column was then washed with 50 mM imidazole to remove contaminating proteins. After the baseline was reached, a gradient of buffer B (50 mM NaHPO₄, 300 mM Tris, 250 mM imidazole, pH 8.0) was applied to the column (from 50 mM to 250 mM Imidazole over 5 column volumes). 5 ml fractions were collected over the gradient. The fractions were analysed on 12% SDS polyacrylamide gel to confirm a protein of the correct size had been purified.

3.2.2.2. Gel filtration

Gel filtration was used as the second purification step using an S200 (Amersham) column. The column was equilibrated with 1 column volume of buffer (50mM Tris, 100 mM NaCl, pH 7.7 1 mM DTT). The sample (1 ml after concentration), was loaded onto the column followed by elution using one column volume of buffer (50mM Tris, 100 mM NaCl, pH 7.7 1 mM DTT). 1 ml fractions

were collected throughout the experiment. The fractions were run on SDS polyacrylamide gels. The fractions corresponding to the peak of the protein of interest were pooled.

3.2.3. Native purification of the N-terminal Hsp90 of *C. elegans*

CeHsp90-6 was purified using ion exchange and gel filtration. The first step of the purification utilises anion exchange chromatography. A 10 ml column of Q Sepharose resin was prepared and equilibrated over 3 column volumes with buffer A (50 mM Tris, pH 8.0). The protein lysate was loaded onto the column followed by washing with buffer A until the baseline was reached. Elution of the protein was achieved by increasing the concentration of NaCl from 0 to 500 mM over 10 column volumes. The fractions collected (10 ml) were run on 12% SDS polyacrylamide gels (Figure 3.4). The fractions containing the protein were pooled and concentrated to 1 ml using a 10, 000 Da Vivaspin concentrator.

The second step of purification utilised Sephacryl 200(S200) gel filtration column. The gel filtration column was run on AKTA FPLC(Amersham) as described in chapter 2, section 2.3.3. Buffer A contained 50 mM Tris, pH 7.5 and 100 mM NaCl and was used for the gel filtration experiments. 1 ml fractions were collected and checked by SDS PAGE as before running on the Mono-Q anion exchange column.

Mono-Q column was equilibrated for three column volumes with buffer A (50 mM HEPES, pH 7.0). The protein was filtered with 0.45 μ M syringe filter and loaded onto the column. The column was washed with buffer A after loading until

the baseline was reached. Elution was started by increasing the NaCl concentration in buffer B (Buffer A + 0.5 M NaCl) from 0 to 0.5 M. 10ml fractions were collected and analysed by SDS-Page.

3.2.4. Denatured purification and refolding of the N-terminal Hsp90 of *C. elegans*

CeHsp90-6 was also purified under denaturing condition. In this method, the pellet was lysed in the lysis buffer containing 100 mM NaH₂PO₄, 10 mM Tris, 6M GuHCl pH 8.0. The pellets were stirred gently at 4⁰C for 30 min. The lysate was then centrifuged at 22000 rpm for 1 hour. The supernatant was taken and filtered with 0.45 μM syringe filter. The lysate was purified by using Ni-NTA column. The column was attached to AKTA Prime (Amersham). The column was first equilibrated with 3 column volumes of buffer 1 (100 mM NaH₂PO₄, 100 mM Tris, 8M urea); pH 8.0. The protein was loaded into the column at 1 ml min⁻¹. The column was washed with buffer 1; pH 8.0 until the stable baseline was reached. The column was washed with three column volumes of buffer A; pH 6.3 at 1ml min⁻¹ to remove unspecific bound proteins. The protein was eluted then by using 10 column volumes buffer 1; pH 5.9. 10 ml fractions were collected at this elution stage. The fractions were run on 12% SDS-PAGE to visualise the protein.

In order to refold the protein two methods were tried. The rapid dilution method was carried out by injecting the protein slowly into cold stirred buffer (100mM Hepes, 100 mM NaCl, 100 mM, 3-(1-Pyridinio)-1-propanesulfonate; pH 7.5) in the ratio of 1 protein volume to 10 volume of the refolding buffer. The protein

was then left in the cold stirred buffer for 2 hrs before centrifuged at 22000 rpm for 1 hour. The supernatant was then dialysed overnight in buffer containing 100 mM Tris and 50 mM NaCl ; pH 7.5. The next day, the protein was concentrated to 1 ml and run on Superdex 200 gel filtration column. The second method to refold the protein was by carrying out the refolding step on the Ni-NTA column. In this method, the protein was loaded onto the column at 1 ml min⁻¹. The column was then washed by using buffer A as in native Ni-NTA purification (section 3.2.2.1) until stable baseline was reached. The column was then washed with three column volumes of 10% buffer B to remove the unspecific proteins. The column was loaded with the refolding buffer at 0.5 ml min⁻¹ for 20 column volumes. The protein was then eluted by running 100% of buffer B. 10 ml fractions were collected upon elution. The fractions were run on 12 % SDS gel and the fractions containing the protein were pooled and later on concentrated to 1 ml. The concentrated protein was then analysed by running on Superdex 200 gel filtration column.

3.2.5. Protein verification and confirmation

All the proteins were verified to be the correct proteins by Western blot with anti-Hsp90 antibodies. The Western blot was carried out as described in Chapter 2 (section 2.2.8).

3.3. Results and discussion

3.3.1. Polymerase chain reaction of genes encoding the N and C-terminal domains of *C. elegans* Hsp90

All the DNA fragments needed for cloning were successfully amplified (Figure 3.2) from cDNA of *C. elegans* and showed roughly the correct fragment sizes based on the agarose gel. As mentioned before, C1F, C2F, C3F and the N-terminal domain were around 386, 545, 635 and 660 bp respectively. The sequences of the regions were as shown in figure 3.1

3.3.2. Cloning of the *C. elegans* genes into shuttle vectors

All the genes were successfully cloned into the shuttle vectors. The colonies were amenable to blue/white screening as the shuttle vector contained *LacZ* genes at the cloning site. The *LacZ* genes were interrupted and hence not expressed if the DNA fragments were inserted between the genes. As a result of the interruption of the *LacZ*

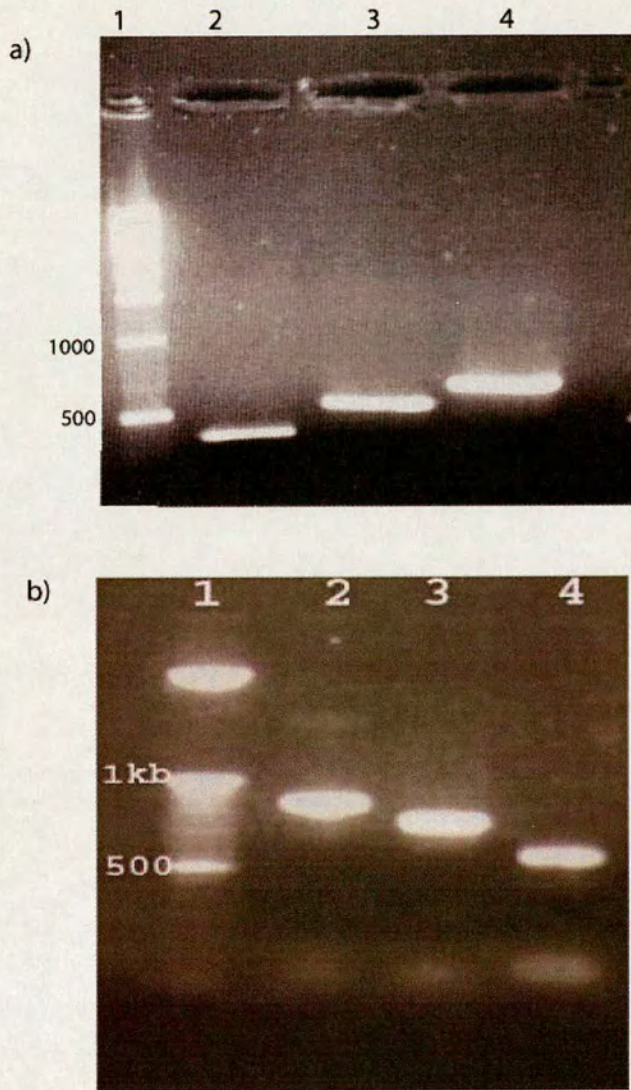


Figure 3.2. Agarose gel photos of the PCR products. a) PCR products of the DNA fragments that were used for cloning in the shuttle vectors. Lane 1: 1 kb DNA markers. Lane 2: C1F; Lane 3: C2F; and lane 3: C3F. The products were all of the expected size. b) PCR products obtained from the direct colony PCR screening. The primers used for screening were combinations of M13 forward primer and the genes reverse primer. The inserts were slightly bigger as the PCR products contained extra sequences of the vector. Lane 1:1 kb DNA marker. Lanes 2-4: C3F, C2F and C1F respectively. The inserts were confirmed by DNA sequencing.

expression, the cells were unable to utilize the X-gal on the LB plate; therefore the colonies appeared as white and not blue. The white colonies were picked and subjected to direct colony PCR screening (Figure 3.2). The positive transformants were grown up in 10ml LB broth containing the appropriate antibiotic. The next day, plasmid was extracted from the cells and sent for sequencing. Sequencing data confirmed the identity of the inserted fragment to be correct.

3.3.3. Cloning, expression and purification of the N and C-terminal domains of *C. elegans* Hsp90

DNA fragments encoding the C-terminal of *C. elegans* Hsp90 were cloned into three different vectors. However, the N-terminal genes were only cloned into the pET28a vector. The plasmid containing the genes was transformed into various expression hosts. The cells containing the plasmid were subjected to test expressions using 1 mM of IPTG in 10 ml of LB broth containing appropriate antibiotics as a standard screen. Table 3.3 summarises the successful cloning and over-expression of the *C. elegans* Hsp90 constructs.

All the C-terminal *C. elegans* Hsp90 DNA fragments were trialed in the three systems (pQE30, pET28a and Gateway), however only the successful experiments are listed in Table 3.3. All the trials using pQE30 as the cloning/expression vector were unsuccessful. All the DNA fragments were cloned into the Gateway system successfully. However, not all of the constructs could be over-expressed. For example, construct C1F (ceHsp90-525) may not have been expressed as this system has not been optimised for the expression of relatively small proteins. To try and overcome this problem, pDest15 with a GST tag of around 20 kDa was used to test if

Construct name	Protein name	Protein sequences	Vectors	Tag	Hosts	Notes
N-terminal C.elegans Hsp90	<i>CeHsp90-6</i>	6-219 of <i>C.elegans</i> Hsp90	pET28a	His	BL21(D E3) pLysS	Protein was expressed, good yield but tag not functional
C1F	<i>CeHsp90-575</i>	575-702 of <i>C.elegans</i> Hsp90	pDest17	His	BL21 (DE3) BL21 A1	No protein expressed
C2F	<i>CeHsp90-575</i>	575-702 of <i>C.elegans</i> Hsp90	pDest15	GST	BL21 A1	Protein is expressed but has non-cleavable tag
	<i>CeHsp90-525</i>	525-702 of <i>C.elegans</i> Hsp90	pDest17	His	BL21 (DE3)	Protein is expressed but in low yield. Does not purify well with Ni_NTA resin
C3F	<i>CeHsp90-492</i>	492-702 of <i>C.elegans</i> Hsp90	pDest 17	His	BL21 A1	Protein expressed in high yield but insoluble
	<i>CeHsp90-492</i>	492-702 of <i>C.elegans</i> Hsp90	pET 28a	His	BL21 (DE3) pLysS	Protein is produced in good yield and is soluble

Table 3.3. Summary of the cloning and expression of C-terminal *C. elegans* Hsp90. Only successful cloning experiments are listed in the table. The table also lists the various expression hosts used and also the quality of the protein yielded by these hosts.

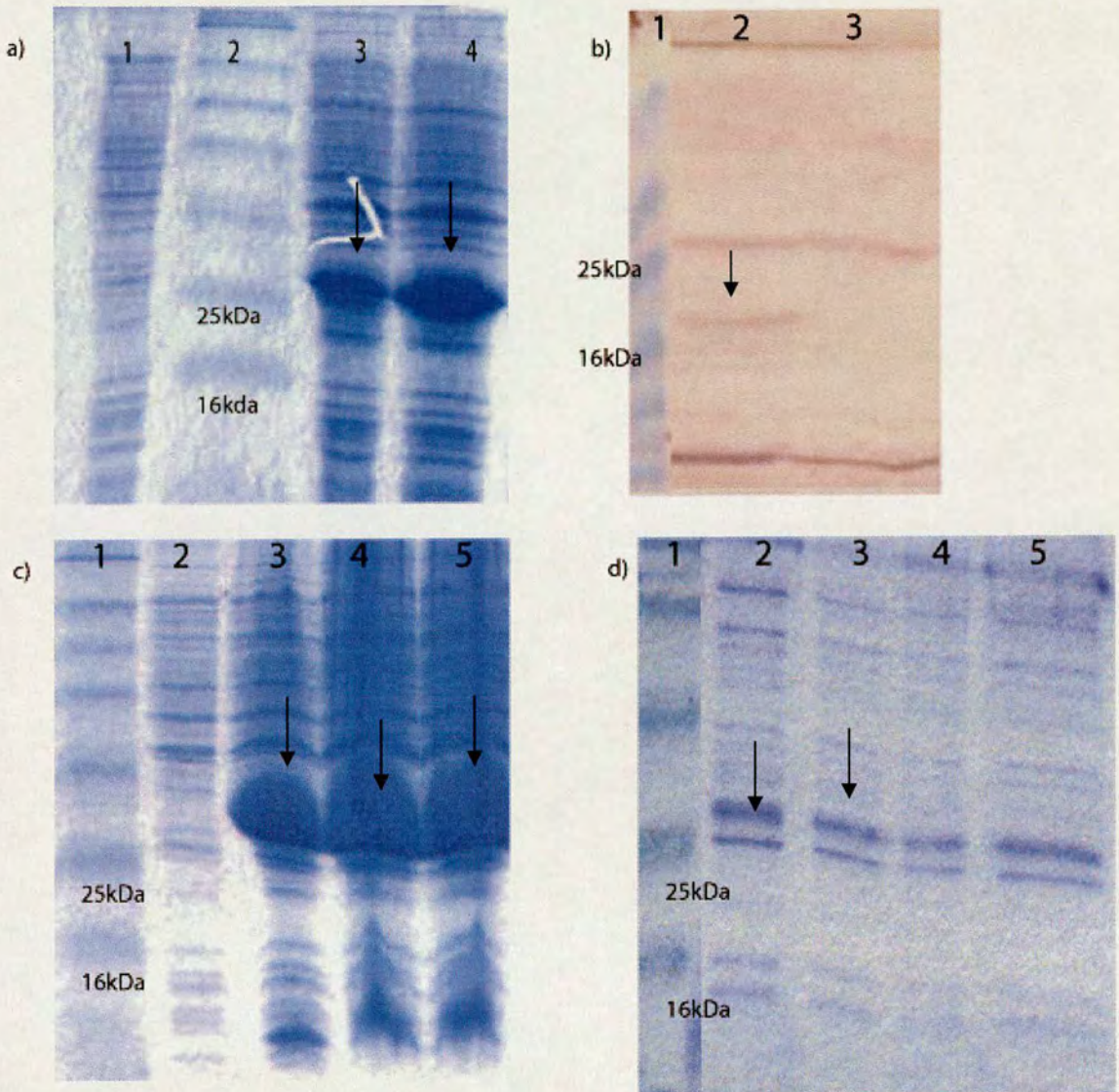


Figure 3.3. SDS polyacrylamide gels and a Western blot of the C-terminal *C. elegans* Hsp90 proteins. a) The expression of the C1F genes encoded for ceHsp90-575 in GST tag vector. Lane 1: Non-induced sample. Lane 2: Protein Markers. Lanes 3 and 4: ceHsp90-575. Arrows indicate the bands corresponding to the proteins. b) Western blot of C2F genes encoded for ceHsp90-525 using anti-Hsp90 antibodies. Lane 1: Protein markers. Lane 2: ceHsp90-525 Lane 3: Non induced sample. Arrow indicates the band corresponds to the protein. c) The over-expression of C3F genes encoding for ceHsp90-492 in pDest17 vector. Lane 1: Proteins marker. Lane 2: Non induced sample. Lane 3-5: CeHsp90-492. Arrows indicate the bands correspond to the protein of interest. d) SDS polyacrylamide gel of the ceHsp90-525 fractions collected over the course of the Ni-NTA purification. Arrows indicates the band of interest. The protein is neither hugely over-expressed.

the protein can be expressed with a larger protein acting like a carrier protein. The GST construct did express some protein, however the protein did not readily purify on a GST affinity column (Figure 3.3). Even if the protein had purified well, the construct did not contain a cleavage site to remove the GST therefore it would have been of limited use in crystallisation trials.

For C2F, the genes were successfully cloned into the pDest17 vector. The protein could also be expressed in BL21 DE3 competent cells (Novagen), but the yield from these cells was very low. The protein was further characterised by Western blot using anti-Hsp90 antibodies (refer Chapter 2; Section 2.2.8) (Figure 3.3). This protein also did not purify very well with the nickel column. The purity was only 40% (Figure 3.3). The attempt to clone the gene into pET28a was unsuccessful.

The gene product designated C3F encoding for the C-terminal region of *C. elegans* Hsp90 492-702 was successfully cloned into both pDest17 and pET 28a vectors. The C3F was first cloned into the pDest17 vector. The protein was over expressed to a very high level in this vector (Figure 3.3). Unfortunately, the protein was totally insoluble. In order to make it soluble, several approaches were tried. The first approach was to use different temperatures after induction. The cells were grown at 37⁰C until OD₆₀₀ ~0.6 was reached. The cells were induced with 1 mM IPTG at either 25/15⁰C and grown for 6 hrs post induction at these temperatures. The protein was once again highly over-expressed but still mostly insoluble if it was grown at 25⁰C. The protein yield was not very good when the cells were grown at 15⁰C and was still mostly in the insoluble fraction. The next approach tried was to add sorbitol and also betaine to the growth medium. The aggregation of protein in the

bacterial cells can be reduced by adding polyols such as sorbitol and betaine. It has been shown that addition of these agents during the expression phase can help stabilise the protein as it is expressed [3]. By adding these chemicals to the growth media, it is hoped that the protein will not form any aggregates and will therefore be both more stable and soluble. Therefore, LB broth containing 2.5 mM glycine betaine and 1 M *D*-sorbitol were used to grow the bacterial cells at 25⁰C [1]. The protein was expressed really well in this media but was still insoluble (Figure 3.4). The genes encoding the proteins were cloned into the pET28a vector. The protein over-expressed well and was soluble (Figure 3.4), the reasons why the protein become soluble in this vector are unknown. In order to purify a large quantity of the the ceHsp90-492 protein, a 4L culture of LB broth containing 50 µg/ml of kanamycin. The cells were harvested and lysed. The protein was purified using a Talon affinity column (refer Chapter 2; Section 2.3.2. The protein was approximately 80% pure after this first affinity step and could be further purified (>95% pure) on a S200 column.(Figure 3.4).

The N-terminal domain of ceHsp90-6 was successfully cloned into the pET28a vector. The genes can be expressed very well and the protein was soluble. However, the problem arises as the protein can not bind to Ni-NTA affinity column through its N-terminal His-tag under native conditions. The protein can be purified very well under denatured purification condition (Figure 3.5). However, attempts to refold the protein in solution and on the column were not successful as the protein was over 20kDa. So far most of the protein that successfully refolded was having size less than 20kDa. Furthermore, the protein also consist several flexible loops which make it not easy to refold due to instability of the loops.

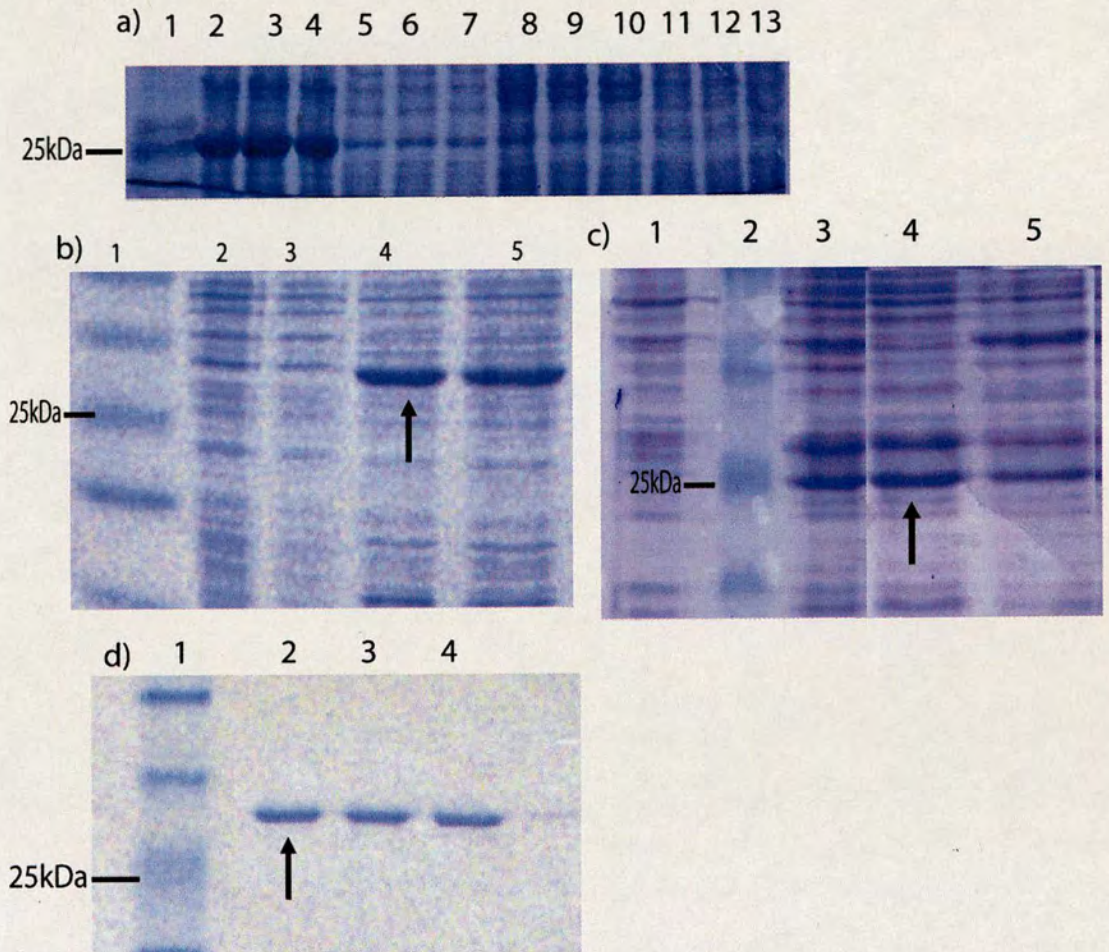


Figure 3.4. SDS polyacrylamide gel of ceHsp90-492. Arrows show the band corresponded to ceHsp90-492. a) Different temperatures were used to try and increase the solubility of the protein. Lane 1: Protein markers. Lanes 2-4 and 8-10: Insoluble fraction` at 25⁰C and 15⁰C respectively. Lanes 5-7 and 11-13: Soluble portions at 25⁰C respectively. The protein was not expressed very well at 15⁰C for 6 hrs. b) and c) show the expression at 37⁰C of ceHsp90-492 in pDest17(b) and pET28a (c). Lanes 2(b), 3 (b) and 4(c): Soluble portions of the lysate. Lanes 4(b), 5(b) and 5(c): Insoluble portions of the lysate. Lane 1(c): Non-induced sample. Lane 3(c): Induced sample. d) Fractions collected from S200 purification. Lane 1: Protein markers. Lanes 2-4: *ceHsp90-492*.

The probable reason for the non functional tag is that the His-tag was buried and therefore was not accessible to bind to the Ni²⁺. Therefore, the protein was natively purified using a three step purification protocol. This involved two ion exchange columns and a gel filtration step between them. The first step of the purification used Q-sepharose anion exchange column (refer Chapter 2: Section 2.3.4). The fractions containing the protein were pooled. At this step the protein was only 50% pure (Figure 3.5). The second step of the purification was by using S200 gel filtration. At this time, the protein was only 70% pure (Figure 3.5). The fractions containing the “cleanest” protein were pooled and loaded onto the Mono-Q column as the final purification step. The fractions containing the protein were pooled and concentrated again. The purity at this stage was about 80% (Figure 3.5). There are still several bands present in the purified sample. No further purification steps were tried to purify the proteins, as the total proteins especially the protein of interest were lost throughout the purification and the three purification steps was already time consuming and make the protein become degraded.

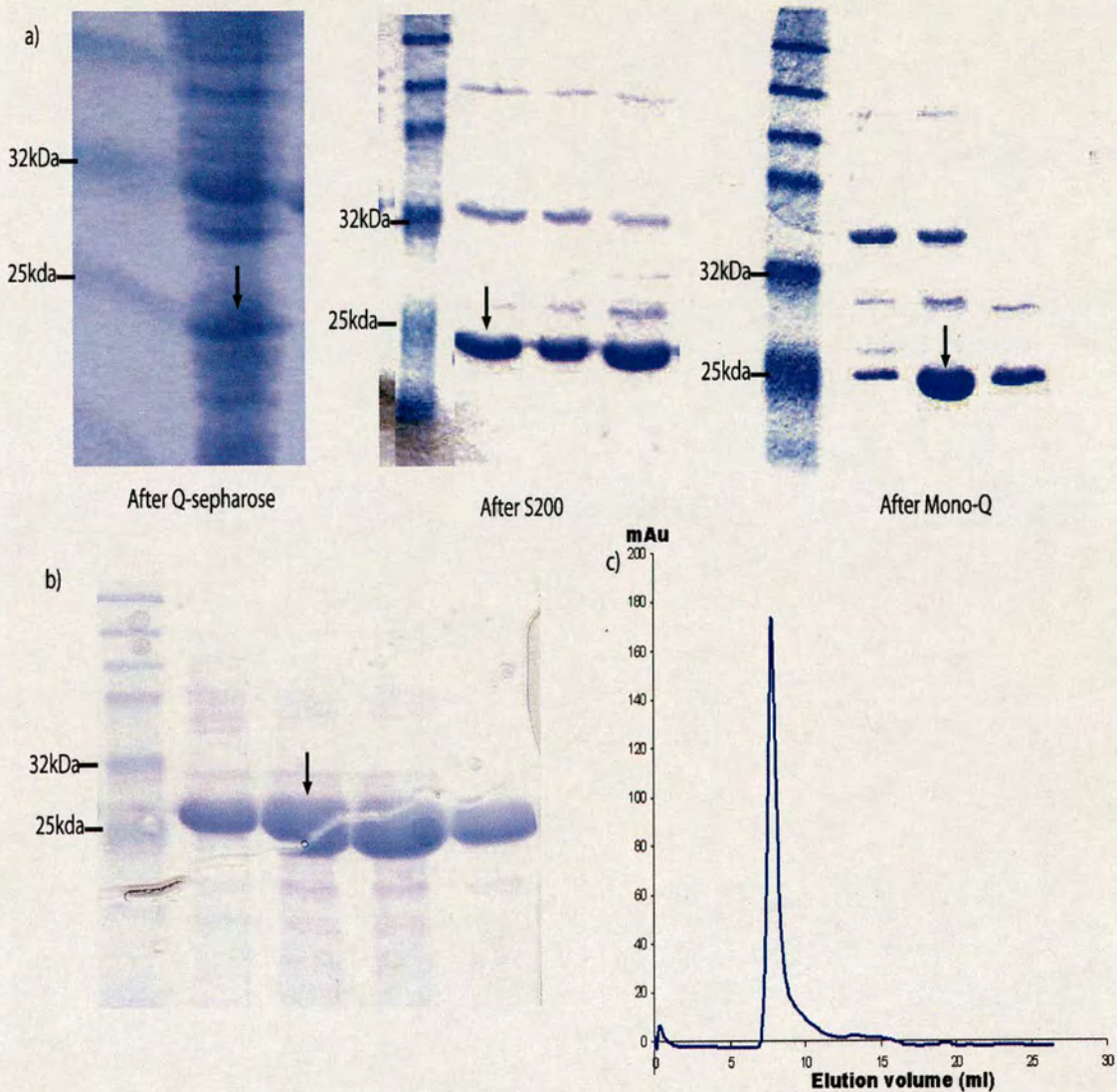


Figure 3.5. Purification of ceHsp90-6 under native and denatured conditions. a) CeHsp90-6 was natively purified by three steps purification that utilised Q-sepharose resin, S200 gel filtration and mono-Q resin. The fractions after mono-Q still contained unwanted proteins. Arrows showed the protein of interest. b) The purification of ceHsp90-6 under denatured condition by using Ni-NTA column. The protein was very pure after the purification. However, the protein can not be refolded. c) Elution profile of the protein on Superdex 200 after refolding step. The protein was eluted at the void volume indicated that the protein formed aggregates and was not refolded.

3.3.4. Expression and Purification of the C-terminal domain of human Hsp90

The plasmid encoding the C-terminal of human Hsp90 was transformed into appropriate competent cells. All the proteins involved in the expression and purification were listed in Table 3.4. Figure 3.7 shows the location of the C-terminal domains of human Hsp90 α purified in this chapter. The All the proteins were successfully expressed (Figure 3.6) by growing them in LB broth containing 50 $\mu\text{g/ml}$ of kanamycin. The cells were induced at $\text{OD}_{600}\sim 0.6$ and incubated for another 4 hrs. 1 mM IPTG was used to induced the cells. The proteins were confirmed by Western blot with anti-His (Sigma) or anti Hsp90 (Stressgen). The proteins were showed to be the proteins of interest by using anti-Hsp90. However, hHsp90- $\alpha 604$ was not recognised by the anti-His reagent.

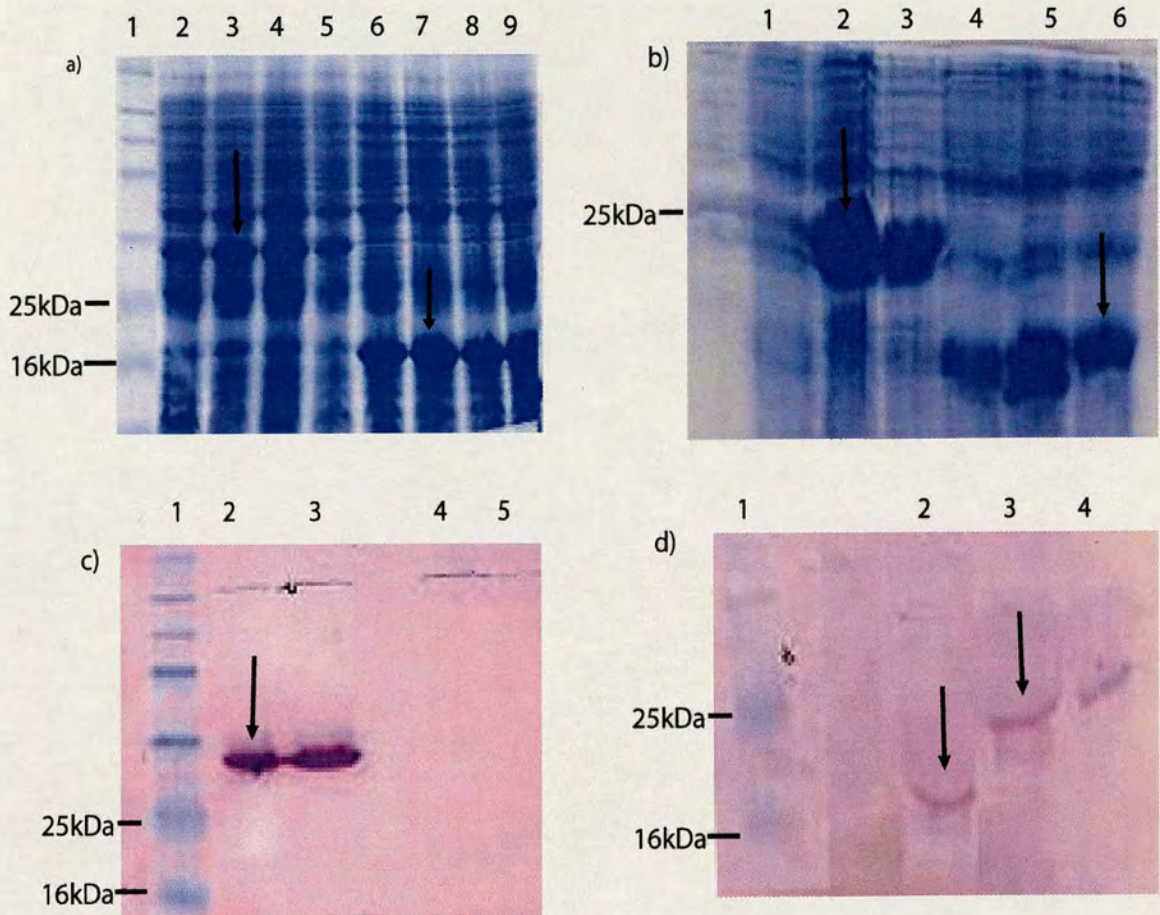


Figure 3.6. Sds polyacrylamide gel and Western blot of the expression of the C-terminal domain of human Hsp90 α . Arrows show the protein bands mentioned in the legends at each of the panel. a) SDS gel showed the expression of hHsp90- α 521 and hHsp90- α 604. Lane 1: Prestained broad range protein marker. Lanes 2- 5: hHsp90- α 521 with size around 28kDa. Lanes 6-9: hHsp90- α 604 with the size around 18kDa. b) SDS gel of the expression of hHsp90- α 596 and hHsp90- α 631. Lane 1: Prestained broad range protein marker. Lanes 2 and 3: hHsp90- α 596 with size around 24 kDa. Lanes 4-6: hHsp90- α 631 with the size around 12 kDa. c) Western blot with anti-His antibodies of hHsp90- α 521 and hHsp90- α 604. Lane 1: Prestained broad range protein marker. Lanes 2 and 3: hHsp90- α 521. Lanes 4 and 5: hHsp90- α 604 but no bands correspond to the expected size were observed. d) Western blot of hHsp90- α 631 and hHsp90- α 596 with anti-His antibodies. Lane 1 Prestained broad range protein marker. Lane 2: hHsp90- α 631. Lanes 3 and 4: hHsp90- α 596.

Protein names	Sequences	Vector	Expression host
hHsp90- α 521	Residues 521-732	pET28a	BL21 DE3
hHsp90- α 596	Residues 596-73	pET 28a	BL21 DE3
hHsp90- α 604	Residues 604-732	pET28a	BL21 DE3
hHsp90- α 631	Residues 631-732	pET28a	BL21 DE3

Table 3.4. Lists of the constructs of the C-terminal of human Hsp90 α . The lists showed the vector used to clone the genes and the expression cells used to express the proteins. The constructs were supplied by Thomas Rataczak.

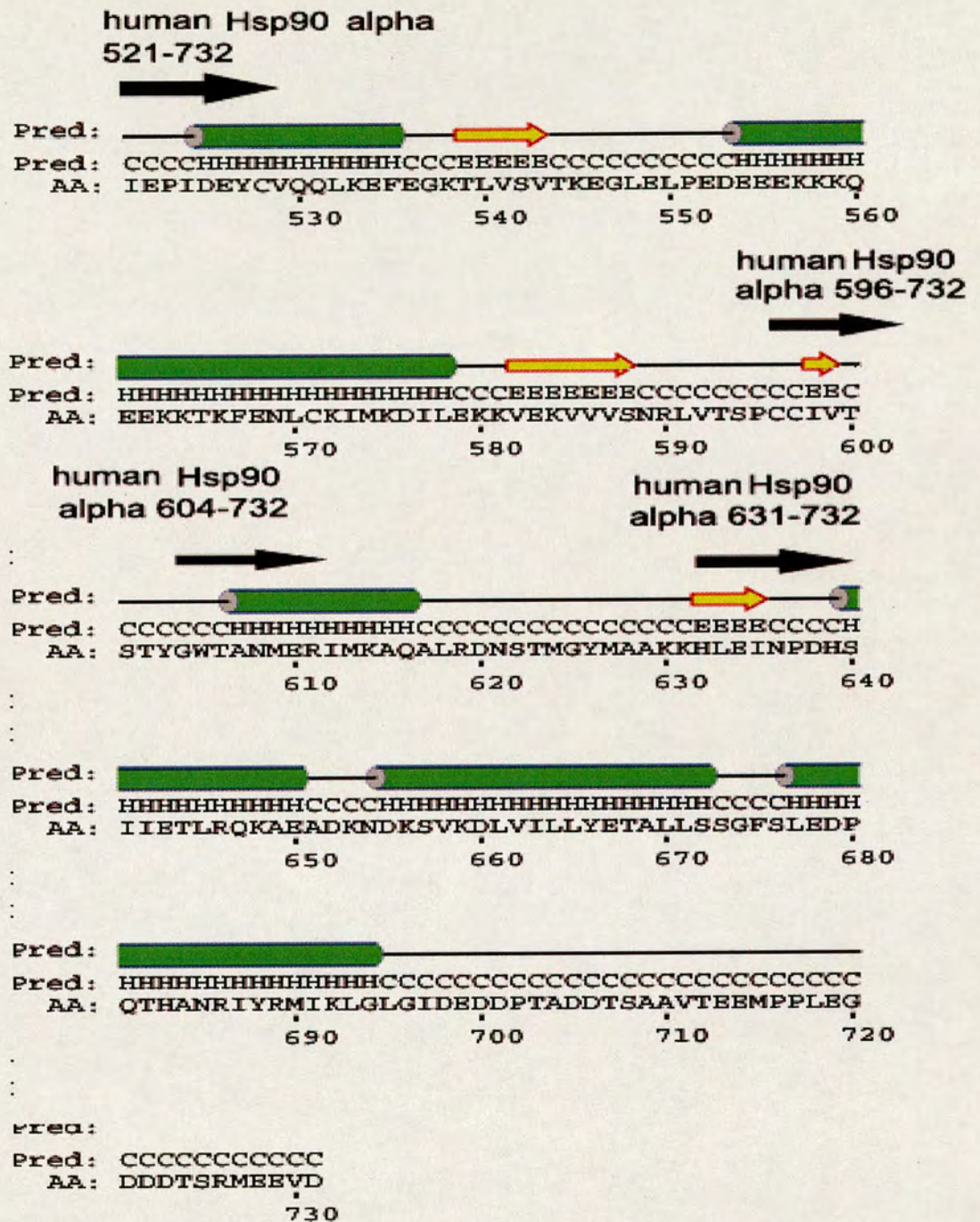


Figure 3.7. Amino acid sequences of human Hsp90 α show the location of protein constructs. Arrows mark the beginning of each of the C-terminal Hsp90 human α constructs overexpressed and purified in this chapter.

The cells were grown in 4L of LB broth containing 50 μ g/ml kanamycin. The cells were harvested and lysed by adding 1 mg/ml of lysozyme and sonication. The proteins were purified using an affinity column. hHsp90- α 521, hHsp90- α 596 and hHsp90- α 631 were purified using a column of Ni-NTA. hHsp90- α 604 did not bind to the nickel affinity column. No further investigations were carried out to determine the reason the protein did not bind to the nickel column. Even though the other proteins bound to the nickel affinity column, they were not really pure following this step (Figure 3.6). The purification was optimized by adding 20 mM β -mercaptoethanol and 1mM of PMSF. Only hHsp90- α 521 gave 80% pure proteins using these conditions (Figure 3.8). The other two protein constructs were still not very pure. In order to overcome the problem, Talon resin (BD Biosciences) was used to try and purify both hHsp90- α 596 and hHsp90- α 631. The resin was working very well to purify hHsp90- α 631 but not hHsp90- α 596. Mono-Q resin (Pharmacia) which is an anion-exchange resin was used as the second step in the purification of hHsp90- α 596, however this was not very successful. For hHsp90- α 521 and hHsp90- α 631, an S200 gel filtration column was used as the second purification step to get rid off the other contaminating proteins and to get the proteins as homogenous as possible prior to crystallisation and characterisation experiments.

In the purification steps with the nickel affinity column, a reducing agent was added to the buffer to get purer proteins. The reducing agent was needed to break any non-specific interactions between the proteins of interest as well as any potential disulphide bonds formed between the protein of interest and any contaminating proteins [2]. PMSF was used to inhibit protease activity that could degrade the

protein quickly. The addition of the reducing agent was successful in helping in the purification of hHsp90- α 521. However, hHsp90- α 631 needs to be purified by using

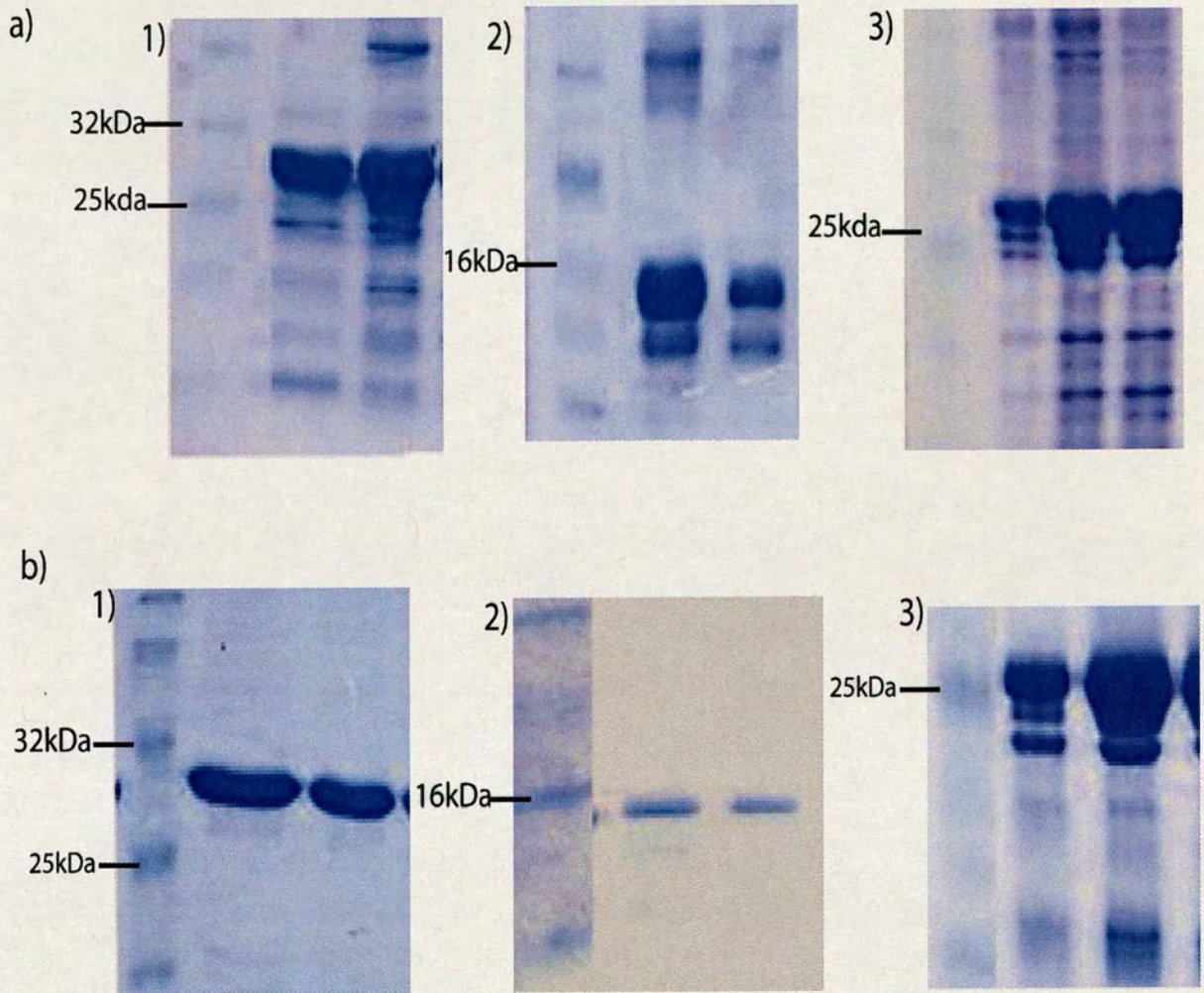


Figure 3.8. SDS polyacrylamide gel of the C-terminal domain of human Hsp90 α after purification. a) After purification with Ni-NTA affinity column following basic purification protocols. Most of the proteins still are not very pure. b) The same proteins after optimization and gel filtration column. 1) Final purity of hHsp90- α 521 after optimization of Ni-NTA column and S200 gel filtration. 2) Final purity of hHsp90- α 631 after Talon and S200 gel filtration column. 3) Final purity of hHsp90- α 596 after Talon and Mono-Q. The proteins were still not pure as the other two proteins.

Talon affinity column (BD sciences). Talon resin is a cobalt charged resin with a higher affinity for hexa-histidine tagged proteins than that seen with the nickel resin [4]. Therefore it binds more specifically to hHsp90- α 631 rather than other protein in the preparation that contains one or two nearby histidine residues. By using these optimisation steps, two of the proteins (hHsp90- α 521 and hHsp90- α 631) were 80% pure. The use of a gel filtration column after this step was to get the proteins to a purity of 90% and to make sure the protein were homogenous (Figure 3.8).

3.4. Conclusion

A number of C-terminal human Hsp90 α constructs have been successfully over-expressed. However, the purification of these proteins demands multiple conditions and techniques. Based on the purity, the proteins were chosen and further used for crystallization trials and other biophysical assays. The ability of these pure proteins provided the basis for analysing the results obtained later in a systematic way. The cloning, expression and purification of the *C. elegans* proteins gave a protein construct to explore and reveal more about the unique properties of the C-terminal Hsp90. In summary, the proteins that were purified well are hHsp90- α 521, hHsp90- α 631 and ceHsp90-492. Most of the work described in this thesis was focused on these three proteins.

References

1. Gonzalez, C.F., Ackerley, D.F., Park, H. C, MATIN, A. (2003) A Soluble Flavoprotein Contributes to Chromate Reduction and Tolerance by *Pseudomonas putida*. *Acta Biotechnol.* 23 (2003) 2–3, 233–239 23: 233-239
2. Qiagen (2003) *The QIAexpressionist*, 5th edn. Qiagen
3. Schumann, Wolfgang, and, Ferreira, S. LC (2004) Production of recombinant proteins in *Escherichia coli*. *Genetics and Molecular Biology* 27: 442-453
4. Tchaga, S. G, Hopp, J., Nelson, P. (1998) Rapid One-Step IMAC Purification using TALON™ Superflow CLONTECHniques. Nucleic Acid Chemistry Group CLONTECH Laboratories, Inc.

Chapter 4: Characterisation of the C-terminal domain of human Hsp90 alpha

4.1. Introduction

In this chapter, the results of the biochemical and biophysical characterization of the C-terminal domain of human Hsp90 α are reported. Several constructs of different lengths were made and expressed in *E. coli*, the purification was discussed in Chapter 3. Only two of the constructs gave very pure protein, hHsp90- α 521 and hHsp90- α 631. Both of the proteins contain the MEEVD sequence that is essential for binding to the TPR client proteins. The proteins were characterized using several different techniques such as fluorescence, gel filtration, and surface plasmon resonance. The characterization was carried out to study the proteins alone as well as their interactions with other compounds/partner proteins.

As mentioned earlier, the residues at the C-terminal end of the protein (MEEVD) are important in interactions with partner proteins (Figure 4.1). This sequence motif is able to bind to the TPR client proteins such as Hop, PP5 [33] and Cyp40 [5]. Interaction of the C-terminal domain of human Hsp90 β with Cyp40 was shown by conventional pull-down assays between the two proteins [33], site directed mutagenesis to the Cyp40 TPR domain allowed identification of residues key to the interaction to be determined.

In this study, a number of constructs of the C-terminal domain of human Hsp90 α (an isoform of human Hsp90 β) were provided by Thomas Rataczak, Department of Pharmacology, University of Western Australia. The proteins were used to further characterize the interaction with Cyp40 with the techniques available in house.

Hsp90 has also been shown to bind to drugs such as geldanamycin (GA) [3, 16, 18, 24, 26]. GA was shown to bind to the ATP binding site on the N-terminus of Hsp90. The binding inhibits the hydrolyzation of ATP which is important for in vivo function of Hsp90 [21, 22] and without Hsp90 function, the cell will be dead. GA is a very potent inhibitor; however it is unsuitable for clinical use due to its marked hepatotoxicity and narrow therapeutic window [28]. The C-terminal domain of Hsp90 contains the binding site for novobiocin [15, 35, 36]. Interestingly, the same site also recognizes ATP. Therefore, it is of interest to study the binding of the C-terminus of human Hsp90 α to novobiocin and ATP as they can provide more understanding towards Hsp90 function as well as structure.

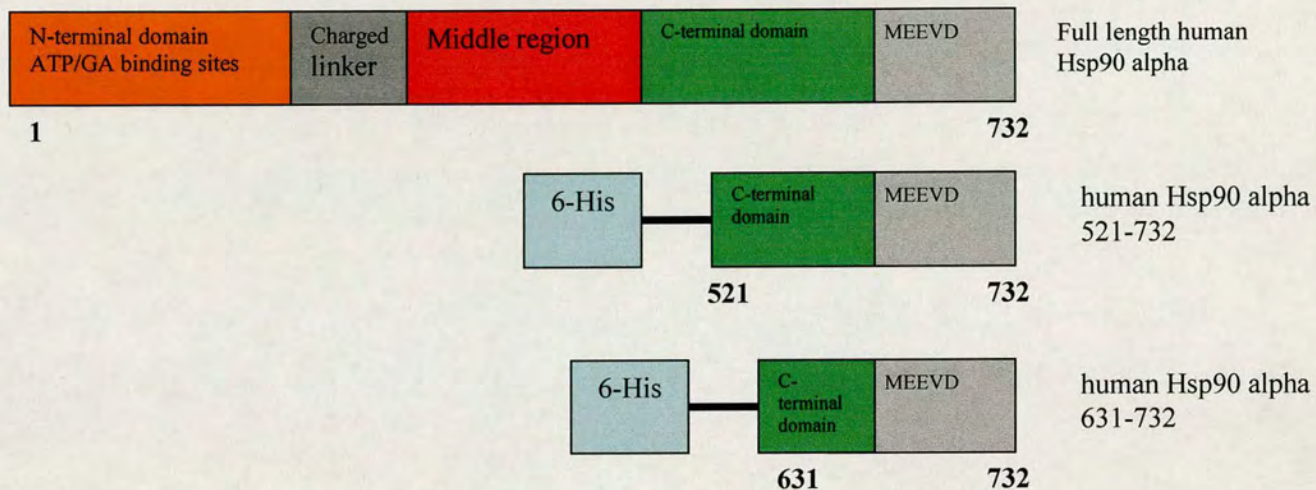


Figure 4.1. A cartoon representation of the C-terminal domains of the human Hsp90 α constructs used in this study. Full length human Hsp90 α is also shown for comparison. Both of the constructs contained a histidine tag at the N-terminus. The MEEVD motif was also present in all of the constructs. The MEEVD motif is essential for the protein to bind to the TPR client proteins.

4.2. Materials and methods

4.2.1. Determination of the oligomeric forms of human Hsp90 α C-terminal domain

4.2.1.1. Gel filtration

The experiment was carried out using a Superdex S200 column. First, the column was calibrated using an Amersham calibration kit. The experimental protocol

was from the kit manual and was described in chapter 2. In order to determine the protein molecular mass, 100 μM (250 μL) of the sample was load onto the Superdex 200 column attached to an AKTA FPLC (Amersham Bioscience). The V_e was noted and the K_{av} was calculated. The molecular size was estimated from calibration curve.

4.2.1.2. Mass spectroscopy

The experiment was carried out by Andrew Cronshaw as part of the Edinburgh Protein Interaction Centre (EPIC). Basically, the protein was run on a polyacrylamide gel. The gel was stained by using Gelcode (Pierce) for an hour. The band of interest was cut out from the gel and the sample was sent to EPIC. The band was subjected to trypsin digest. Basically, the slice gel was incubated in solution containing 300 μl of Buffer 1 (200 mM NH_4HCO_3 and 50% acetonitrile) at RT for 30 min to remove SDS. The step was repeated twice. Then, the gel sliced was incubated with the Buffer 1 but with the addition of 20 mM DTT. The incubation was carried at 32⁰C for 1 hour. The mixture was then washed three times with Buffer 1. The mixture was incubated with alkylate cysteines made up with iodoacetamide and Buffer 1 at RT in dark for 20 min. After the incubation the mixture was washed twice with 500 μl of buffer 1. The band was cut to small pieces and spun down at 13000 rpm for 2 min. The gel slices were then covered with 200 μl of 50% acetonitrile in a microcentrifuge tube for 2 min. The supernatant was decanted and the gel was left to dry. Trypsin stock was prepared in 50 mM NH_4HCO_3 at 4⁰C. The gel pieces were swelled by adding the trypsin stock. The mixture was kept at

4⁰C until the gel pieces were swollen and incubated at 32⁰C for 16-24hrs. The sample was then analysed using a Maldi –Tof spectrometer.

4.2.2. Determination of the dimerisation constant of protein

The dimerisation constant of the proteins were determined by gel filtration. A series of protein concentrations were prepared in buffer containing 50 mM Tris, 100 mM NaCl, pH 7.7. The proteins were run through a Superdex 200 column as above. The elution volumes of the peaks were recorded and dissociation curves based on the elution volume plotted. The analysis of the curve was based on the assumption that at any given time the monomeric and dimeric species were in equilibrium [27]. Data were fitted by using Kaleidagraph based on the equation 1

$$EV=EV_{\text{mono}}-(EV_{\text{mono}}-EV_{\text{dimer}})\times\left(\frac{[\text{Protein}]}{([\text{protein}]+K_{\text{d(app)}})}\right) \text{ (eq.1)}$$

where EV represent the elution time, EV_{mono} is the elution volume of the monomeric species, and EV_{dimer} is the elution volume of the dimeric species. The dissociation constant (K_{d}) obtained is an apparent K_{d} since the proteins were diluted several fold during the course of the experiment. Therefore, the real K_{dimer} was obtained by dividing the $K_{\text{d(app)}}$ by the dilution factor.

4.2.3. Study of the interaction of the C-terminal domain of human Hsp90 α with Cyclophilin 40 (Cyp40)

4.2.3.1. Gel filtration

This method was used to investigate the binding interaction between Hsp90 C-terminal domains and a TPR containing protein Cyp40. Firstly the proteins were analysed individually using an Superdex 200 (Amersham) column attached to an AKTA FPLC (Amersham Biosciences) run as described in Section 2.3.3 in Chapter 2. This allowed the elution volume of the individual components of the complex to be determined. The protein concentrations used were 100 μM and 50 μM for Hsp90 and Cyp40 respectively. Secondly, the Hsp90 C-terminal domain proteins and Cyp40 were mixed together in the same concentration as their individual protein gel filtration (50 μM Hsp90: 100 μM Cyp40) assuming that the stoichiometry of the interactions will be one dimer of Hsp90 that binds to two monomeric Cyp40 molecule. The mixture in a total volume of 250 μL was incubated at 10°C for 30 min and run through the Superdex 200 gel filtration column. 0.5 ml fractions were collected throughout the run. A difference in the elution volume of the peaks between that of the proteins alone and the complex mixture indicates that a complex had indeed formed. In order to visualise the complexes formed, 30 μl samples of the fractions collected over the peaks from all the experiments were analysed by SDS-PAGE.

4.2.3.2. Intrinsic Tryptophan fluorescence

4.2.3.2.1. *Human Hsp90 α 521-732 (hHsp90- α 521)*

A number of reaction mixtures with a final volume of 200 μ l were set up in 1.5 ml eppendorf tubes as described in Chapter 2; section 2.4.1. Each reaction consisted of a fixed concentration (1 μ M) of hHsp90- α 521. However, the final concentration of Cyp40 was varied in each tube and ranged from 1 to 50 μ M. Measurements were also carried out for the same concentrations of Cyp40 alone. The reaction was incubated at 20 $^{\circ}$ C for 30 minutes before the measurement was taken using a Fluoromax-3 (Jobin Yvon, Hariba). The Trp fluorescence measurement was obtained by excitation at 295 nm and emission at 350 nm, data was acquired using time base data acquisition over 60 seconds. The slits were set at 2.5 mm for both excitation and emission. The emission values for each of the concentrations were averaged.

4.2.3.2.2. *Human Hsp90 α 631-73(hHsp90- α 631)*

Several reaction mixtures of 200 μ l were set up as before. However, in this series of experiments the concentration of Cyp40 was kept constant while that of hHsp90- α 631 was varied. The rationale behind this approach was to use hHsp90- α 631 (which has no Trp residues) to monitor changes in the environment of the Cyp 40 Trp residues by changing the concentration of the Hsp90. The concentration of hHsp90- α 631 used in this experiment ranged from 1 to 150 μ M. The reaction was incubated at 20 $^{\circ}$ C for 30 minutes before measurements were taken as above. The same concentrations of the

proteins alone were also measured for Trp fluorescence using excitation at 295 nm, emission at 350 nm and time base acquisition of data over 60 seconds. The slits were 2.0 mm for excitation and 5.0 mm for emission. The emission values for each concentration were averaged.

For both of the proteins, F_{obs} is the observed emission at 350 nm minus both the buffer signal and the emission of the individual proteins at the same concentrations. The F_{obs} was corrected against the inner filter effect using equation 2

$$F_{corr} = F_{obs} / e^a \text{ (with } a = -2.303 \times \epsilon \times L \times c \text{) - equation 2}$$

where F_{corr} is the corrected emission in the experiment. ϵ is the extinction coefficient in $M^{-1} cm^{-1}$. L is the path length of the cuvette used for measurement. c is the molarity concentration of the various proteins used. F_{corr} was then added to the emission values of the proteins alone. The values obtained were plotted against the different concentrations of the proteins used in the experiment, the data was fitted to equation 4 using Kaleidagraph 3.5 (Synergy).

The corrected fluorescence signal, F_{corr} can be defined as

$$F_{corr} = F_f + (F_f - F_b) \text{ - Equation 3}$$

where F_f is the fluorescence of free protein and F_b is the fluorescence of the protein A : protein B complex at infinite concentration of protein B. At any total concentration of

protein A [A], F depends on the total protein B [B] concentration and on the equilibrium constant for the complex (K_d) according to equation 4.

$$F_{\text{corr}} = F_f + (F_b - F_f) \times \left\{ \frac{(K_d + [A] + [B]) - \sqrt{((K_d + [A] + [B])^2 - (4 \times [A] \times [B]))}}{2 \times [B]} \right\} - \text{equation 4}$$

4.2.3.3. Surface Plasmon Resonance (SPR)

SPR measurements were performed on a Biacore 3000 instrument (Biacore Instruments Limited). hHsp90- α 521 was immobilized on the NTA sensor chip as described in Chapter 2: section 2.4.2. The sensor was loaded with Ni^{2+} . His-tagged hHsp90- α 521 at concentration of 200 nM in running buffer (10 mM HEPES pH 7.4; 150 mM NaCl; 0.005% surfactant P20) was passed over the sensor surface for 60s at a flow rate of $5 \mu\text{L min}^{-1}$ to get a saturation of response units of approximately 550 RU. The injection of the protein was stopped followed by a wash with running buffer for 100 seconds. Various concentrations of Cyp40 (2 to 300 μM) were passed over the immobilized protein at a flow rate of $30 \mu\text{l min}^{-1}$ for 180s. The complex dissociated when running buffer was passed over the surface for 300s at $30 \mu\text{l min}^{-1}$. The surface was regenerated with 5 mM EDTA in running buffer between applications of different concentrations of Cyp40. The NTA-chip recharged with Ni^{2+} and the cycle repeated as before. The data was analyzed with the software supplied by Biacore.

4.2.4. Study of the interaction of the C-terminal domain of human Hsp90 α with small ligands

This part of the study aimed to investigate potential interactions of the C-terminal domain of human Hsp90 α with both ATP and novobiocin. Interaction of the protein with the ligands was interesting in a number of ways, including as a tool to further characterise the protein biochemically and biophysically and also to help with crystallisation trials as the protein could be more stable with a ligand bound. The techniques used to study the interactions were Hummel-Dreyer gel filtration, Isothermal Titration Calorimetry (ITC), Tryptophan fluorescence and ATPase assay.

4.2.4.1. Hummel-Dreyer gel filtration

The experiment follows the method established by Hummel and Dreyer in the 1960's [4]. This experiment utilizes the principles of a gel filtration experiment to study interactions between the C-terminal human Hsp90 α and ATP by monitoring the peak/trough that is formed by ATP. The appropriate gel filtration column was equilibrated with buffer containing ATP. A stable and straight baseline should be observed. Then, a sample containing fixed concentration of protein and the same concentration of ATP was run on the column. A trough should be observed if there is a complex as some of the ATP in the sample involved in the complex formation and the concentration of free ATP eluted was less than the equilibrated buffer. The area under the trough was calculated. The same concentration of ATP was used to form the complex every time because the concentration of the protein is constant. Therefore, as

the ATP concentration was increased in the sample, more free ATP was available and eluted at the same elution volume. A peak will then form if the concentration of free ATP in the sample is more than the concentration in the equilibrated buffer. The areas under the peaks were calculated as well. The graph of areas under the peak/trough were plotted against ATP concentrations in the samples. When there is no peak or trough observed, the free ATP concentration is the same concentration as that of ATP in the buffer. Therefore, the concentration of the complex and also free protein can be calculated.

The experiment used a Superdex 75 gel filtration column, equilibrated with running buffer (50 mM Tris; pH 7.5, 100 mM NaCl) containing 75 μ M ATP. A sample containing 75 μ M ATP (no protein) was loaded onto the column and run with the same running buffer. A straight and stable baseline was observed during the run. A sample containing 80 μ M protein with 75 μ M ATP was run onto the column. Samples containing a constant 80 μ M of protein mixed with increasing concentrations of ATP (75 to 200 μ M) were applied to the column. The areas under the trough/peak were calculated. A graph of the areas under the troughs/peaks against the ATP concentration was plotted. The concentration of ATP when the area is zero was determined. The K_d was calculated. The graph of bound ATP over free ATP against bound ATP was also plotted. From this graph both the K_d and the stoichiometry of the interaction were obtained and explained further in the results section.

4.2.4.2. Trp fluorescence

The binding of increasing concentration of ATP (0-1200 μ M) or Novobiocin (0-50 μ M) to C-terminal domain of human Hsp90 α (1 μ M) or N-acetyl tryptophan was monitored by fluorescence spectroscopy, with excitation at 295 nm and emission at 355 nm in a 0.5 cm path length cuvette. The final titration volume was only 1% of the initial volume. The fluorescence values observed were corrected against dilution factors and inner filter effects using the equation below.

$$F_{\text{corr}} = \text{dilution factor} \times F_{\text{obs}} / e^{-2.303 \times \epsilon \times L \times c} \text{—equation 5}$$

where F_{obs} is the observed fluorescence. ϵ is the extinction coefficient in $\text{M}^{-1}\text{cm}^{-1}$. L is the path length of the cuvette used for measurement. c is the variable concentrations of the proteins in moles L^{-1} . The corrected fluorescence was fitted with the equation below and plotted using Kaleidagraph.

$$F = F_f + [(F_b - F_f) \times \{ (K_d + [A] + [ATP]) - \sqrt{((K_d + [A] + [ATP])^2 - (4 \times [A] \times [ATP]))} / 2 \times [A] \}] \text{—equation 6a}$$

where F_f is the fluorescence of free un-complexed protein and F_b is the fluorescence of compound A:ATP complex at infinite concentration of ATP. At any total concentration of compound A $[A]$ concentration, F depends on the total ATP $[ATP]$ concentrations and the equilibrium constant for the complex (K_d).

For the novobiocin experiment, a “two binding sites equation” (equation 6b) was used instead of equation 6a above.

$$F_{\text{obs}} = F_f - \left[\frac{(F_c/2) \times \left(\{ (K_{d1st} + [A/2] + [\text{novobiocin}]) - \sqrt{((K_{d1st} + [A/2] + [\text{novobiocin})]^2 - (4 \times [A/2] \times [\text{novobiocin}))} \right)}{2 \times [A/2]} \right) + \left\{ \frac{(F_b \times [\text{novobiocin}])}{K_{d2nd} + [\text{novobiocin}]} \right\} \right] \text{---equation 6b}$$

where F_f is the fluorescence of free un-complexed protein and F_c is the fluorescence of protein A:novobiocin complex at certain concentration of novobiocin on the first binding site. F_b is the fluorescence of compound A:novobiocin complex at infinite concentration of novobiocin on the second binding site. At any total concentration of compound A $[A]$ concentration, F_{obs} depends on the total novobiocin $[\text{novobiocin}]$ concentrations and the equilibrium constants of both the binding sites (K_{d1st} and K_{d2nd}) for the complex.

4.2.4.3. Malachite green ATPase assays

The assays were performed in Eppendorf tubes incubated at 37°C in a temperature controlled heat block. 5 μM of either the C-terminal domain of human Hsp90 α, human CypA or 1 nM Phosphofructokinase (PFK) was mixed with a series of ATP concentrations (0.15, 0.25, 0.5, 0.6, 0.7, 1, 1.25, 1.5, 2 mM) for 90 minutes for C-terminal human Hsp90 α and CypA, 3 minutes for PFK). The reactions were stopped by adding 320 μL of Malachite green solution at RT (Upstate, UK) and mixing well. 50 μL of a 34% (w/v) of sodium citrate was added to the mixture, which was left for 15 min at RT. All samples were transferred to a 1 ml cuvette and the absorbance at 620 nm

measured using a spectrophotometer. A standard curve of the absorbance of phosphate alone was also made following the protocol supplied by the manufacturer as described in Chapter 2 section 2.4.4. Based on the standard phosphate curve, the amount of phosphate release was obtained and used to calculate the rates of ATP hydrolysis.

4.2.4.4. ATPase inhibition assays

C-terminal human Hsp90 α or PFK were mixed with a series of concentrations of novobiocin and incubated at 37⁰C for 30 min. ATP was added to the mixture and incubated for an additional 60 minutes or 3 minutes for PFK. The final concentrations of protein and ATP are 5 μ M and 1 mM respectively. The final concentrations of novobiocin used ranged from 1-100 μ M. The reactions were stopped by adding 320 μ L of Malachite green solution (Upstate, UK) and mixing well at RT. 50 μ L of 34% (w/v) of sodium citrate was added to the mixture left for 15 min at RT. The absorbances of the samples at 620 nm were then measured. The experiment was repeated with PFK although different protein and ATP concentrations were used (1 nM and 5 mM respectively). The final concentrations of novobiocin were from 1- 300 μ M.

4.2.4.5. Isothermal Titration Calorimetry (ITC)

ITC was carried out to study the interaction of novobiocin and hHsp90- α 521. Preliminary trials with ITC show that novobiocin precipitated in the ITC syringe at high concentrations. Therefore, as a solution to this problem, novobiocin was placed in the

sample cell. 100 μM novobiocin dissolved in 100 mM Tris, 50 mM NaCl pH 7.5 was degassed and 1.4ml of the solution was put inside the sample cell. The reference cell was filled up with 1.4 ml of buffer only. The ITC syringe was filled with 280 μl of hHsp90- α 521 (460 μM). The jacket temperature of both cells was set up to 20⁰C. The syringe was placed inside the sample cells. The sample was stirred at 300 rpm. The injection profile (injecting protein into the ligand solution in the sample cell) was programmed as follows:- The initial injection volume was 5 μl , with 3 minutes between injections. Subsequent injection volumes were either held at 5 μl or increased to 10 μl , dependent upon the signal of the heat change between injections. The number of injections per experiment was either 50 or 25 and was dependent upon the volume used per injection as the total volume that can be taken up by the syringe is 280 μl . The reaction was left to run and later on the data was analysed by using the Origin software supplied with the machine.

4.3. Results

4.3.1. Native forms of the C-terminal domains of human Hsp90 α

The native form of the C-terminal domain was studied by using gel filtration. The study aimed to obtain the approximate size of the C-terminal proteins and the

Standard proteins	Size(kDa)	Elution volume (Ve)(ml)	Kav
Ferritin	440	10.51	0.16
Catalase	232	12.1	0.26
Aldolase	158	13.1	0.32
Albumin	67	13.53	0.35
Ovalbumin	43	14.65	0.42
chymotrypsinogen	25	16.52	0.53
Ribonuclease A	13.7	17.21	0.58

Table 4.1. Proteins standards used to calibrate the Superdex 200 gel filtration column. The elution volumes were taken and the Kav calculated from them. Based on the Kav values , a standard curve was plotted.

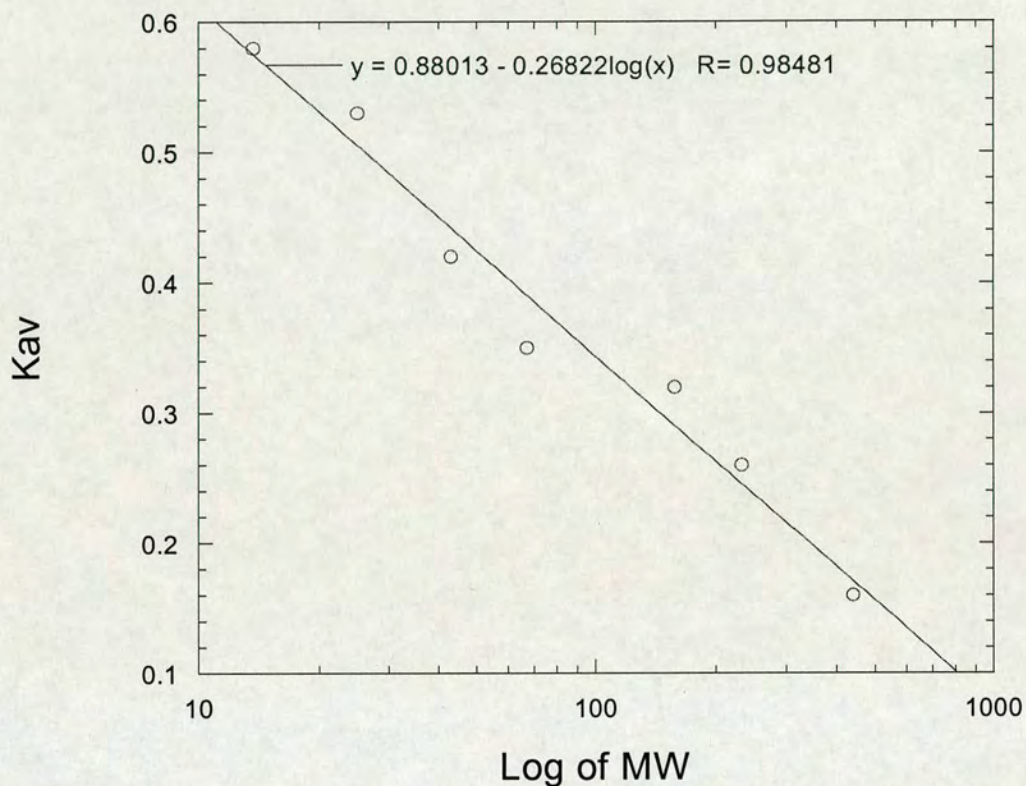


Figure 4.2. Calibration curve of Superdex 200 plotted based on the Kav of the standard proteins. The data was obtained by running standard proteins through the column according to Amersham manual. The elution volume of each protein was noted and the Kav calculated. The graph can be used to estimate the molecular weight of unknown proteins applied to the column.

oligomeric state of the proteins in solution. The aim can only be achieved by monitoring the size and profile of the protein eluted from the gel filtration column. In order to get the information needed, the column has to be calibrated with known or standard proteins. The column used was Superdex 200 (Amersham). Based on the protocol from

the Amersham High and Low MWT gel filtration Calibration kits, the protein standards were loaded in two batches. The first run consisted of ribonuclease A, ovalbumin, aldolase and ferritin. The second run of the column consisted of chymotrypsinogen A, albumin and catalase. The elution volume of each of the proteins was noted, from the elution volume the K_{av} of each of the reference proteins was calculated (Table 4.1). A graph of the log of size against the K_{av} value was plotted (Figure 4.2). The graph was used to estimate the size of unknown individual proteins and also that of the complexes formed.

All the C-terminal domain proteins of human Hsp90 α were analysed by gel filtration on the S200 column. The V_e from each run was obtained and the K_{av} calculated (Table 4.2). Based upon the gel filtration results, hHsp90- α 521 contains two distinct peaks, A and B of approximately 148 and 296 kDa respectively (Figure 4.3). Peak A corresponding to 148 kDa, was the dominant peak, comprising approximately 90 % of the sample which correspond to the dimer form of hHsp90- α 521. Peak B which corresponds to 296 kDa, was shown to be reduced upon time and diminish in size over three days, suggesting some sort of aggregation which degraded to form dimer or small portion of the proteins.

hHsp90- α 631 produced a single peak when run on the Superdex 200 gel filtration column. The molecular mass of the protein as obtained from its elution volume was estimated at 135 kDa. However, the elution volume was dependent upon the protein concentration applied to the column (Figure 4.3). The apparent size of the protein reduced as the protein concentration decreased. It is believed that this illustrates the protein changing from a dimeric form present at higher concentrations to a monomer at

low concentrations. This will be explained in greater detail later in this chapter in section 4.3.2.

Proteins	Column	V _e (ml)	K _{av}	Molecular weight (kDa)
hHsp90-α521	Superdex 200	A:12.7; B : 11.4	A :0.31; B: 0.21	A :148; B: 296
hHsp90-α631	Superdex 200	13	0.31	135

Table 4.2. Lists of the information obtained by running 100 μM of each proteins through Superdex 200

As described above, using the elution volumes obtained from the gel filtration experiments, the sizes of the proteins were estimated and the oligomeric state of the native proteins predicted. However, the estimated sizes of the entire human Hsp90 C-terminal domains were very big compared to what was expected from the sequence. The

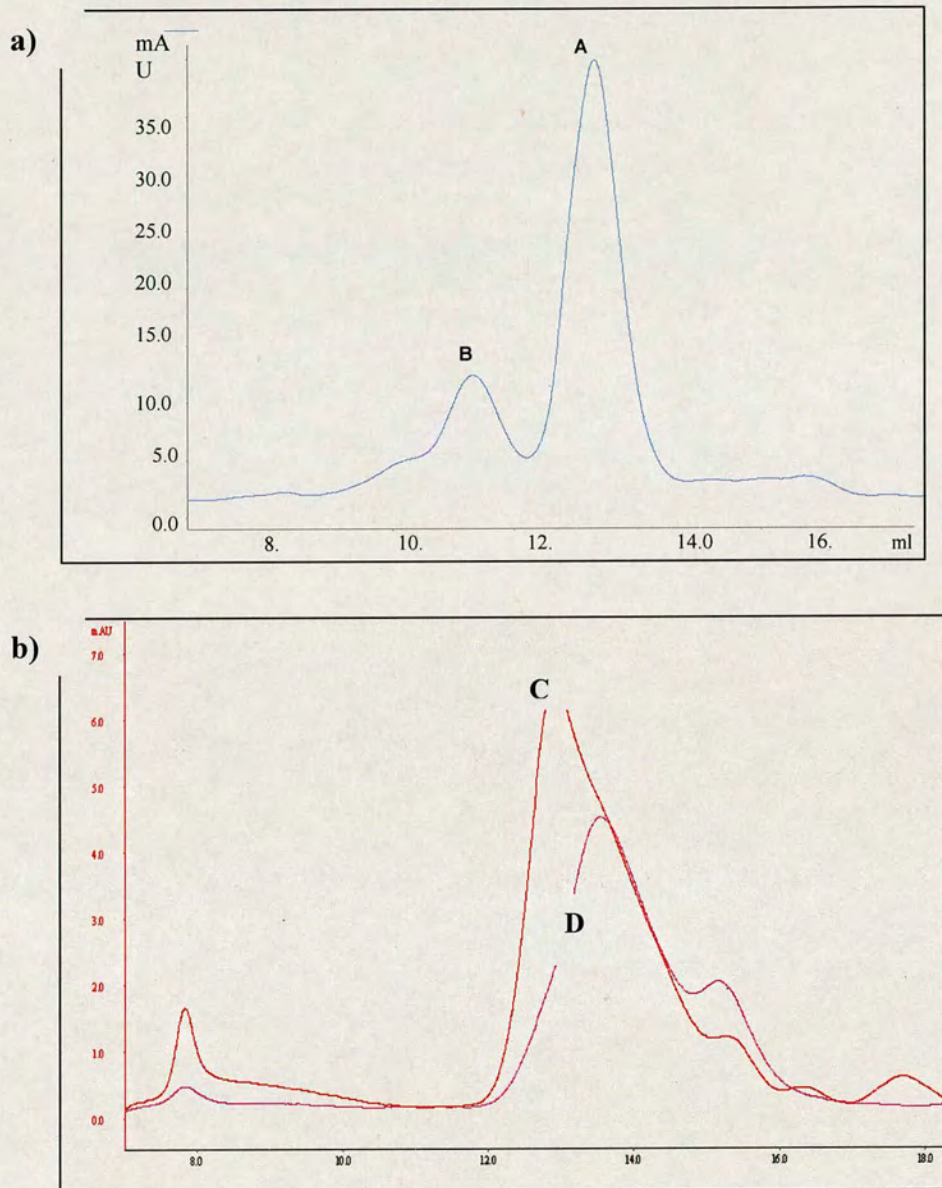


Figure 4.3. Chromatogram of the proteins eluted from Superdex 200 (Amersham Biosciences) gel filtration column. a) hHsp90- α 521 as eluted from the column consisted of two peaks (A, B), shown in blue. (b) HHsp90- α 631 eluted from the column. However the elution volume of peak C and D was dependent upon protein concentration. For example, the elution volume for C which is 100 μ M protein was different from that seen with peak D which is 50 μ M protein.

sizes of the proteins were bigger than those predicted from polyacrylamide gel electrophoresis results. The proteins were expected to be either monomer or dimer in their native forms, therefore the expected sizes were about 28 or 56 kDa for either monomer or dimer for hHsp90- α 521. HHsp90- α 631 was expected to be either monomeric or dimeric with an estimated size of 12 or 24 kDa respectively. However, the apparent molecular weights of the proteins are significantly larger than expected. The different sizes as obtained are likely to be due to the shape of the protein. As mentioned before, gel filtration is very useful in determining the molecular size of spherical symmetrical proteins [27], however it is likely that the Hsp90 proteins are not present in a compact, globular spherical form amenable to easy interpretation using gel filtration data.

4.3.2. Dimerisation constants of the C-terminal human Hsp90 α

A series of concentrations of hHsp90- α 631 (3, 5, 25, 50, 100, 150, 250 μ M) were run on Superdex 200 column. The elution volumes of the peak for each concentration were noted (Figure 4.4) and fitted using the equation 1. From the fit of the curve, the K_{dimer} obtained was an apparent dimerisation ($K_{\text{dimer}(\text{app})}$) constant. In order to obtain the real K_{dimer} , the $K_{\text{dimer}(\text{app})}$ has to be divided by the dilution factor. The dilution factor was obtained by dividing the elution volume of the peak with the volume of sample loaded onto the column. All the proteins were diluted 16 fold during the experiments. Therefore, the real K_{dimer} from the experiment is $4.98 \pm 2.12 \mu\text{M}$.

However, it was not possible to determine the K_{dimer} of hHsp90- α 521 because of technical limitations imposed by the available equipment. Protein concentrations lower

than $1\mu\text{M}$ were not detectable and the elution profiles seen at any concentration above that of $1\mu\text{M}$ showed no differences.

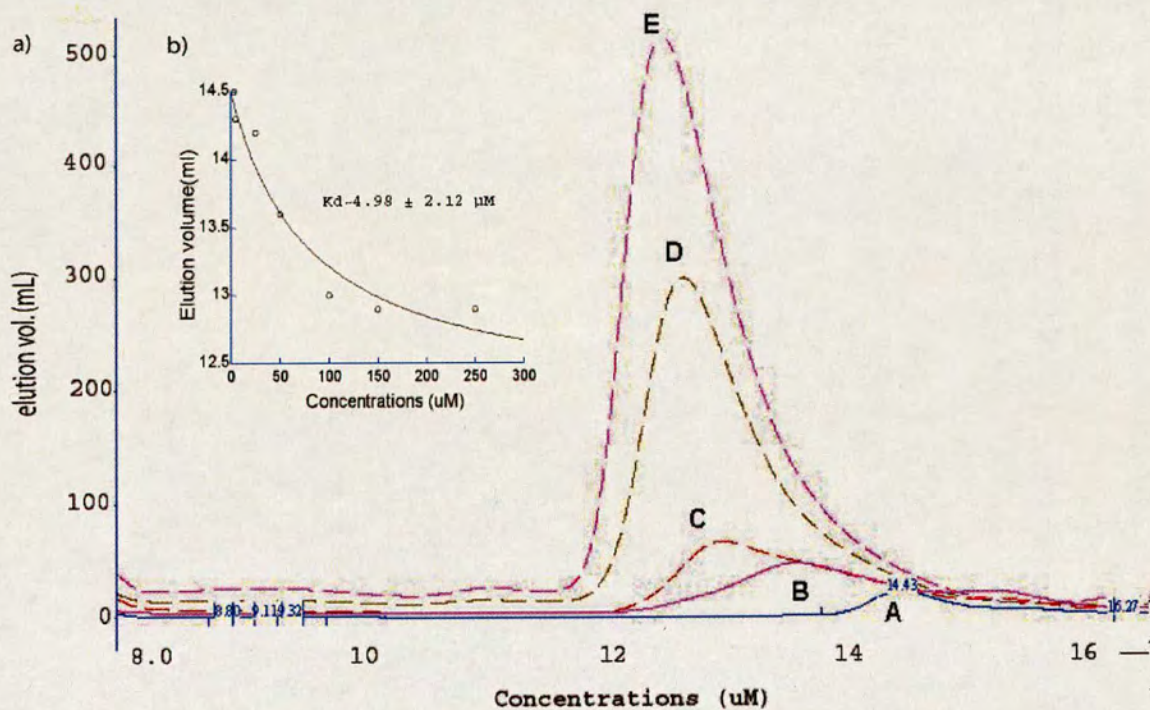


Figure 4.4. HHsp90- α 631 dimer formation. a) Graph of the various concentrations of protein run on the Superdex200. The elution peaks shifted from A to E as the concentration increased from 3 to 250 μM . The shift in the elution peaks was used to calculate a dimerisation constant. b) Plot of the elution volume of the peaks against the protein concentration. Based on this graph the apparent K_d was calculated by fitting equation 1. The k_d on the graph is the real K_d of dimerisation.

4.3.3. Interaction of the C-terminal domain of human Hsp90 α with Cyclophilin 40 (Cyp40)

Several methods were used to study the binding of the C-terminal domain of human Hsp90 α with Cyp40, including gel filtration, intrinsic tryptophan fluorescence, near UV circular dichroism and surface plasmon resonance. However not all the techniques a promising results. Therefore only convincing positive or negative results are presented here.

4.3.3.1. C-terminal human Hsp90 α binds to the bovine Cyp40 as shown by gel filtration

Gel filtration was used to investigate the interaction of the C-terminal domains of human Hsp90 α with Cyp40. The mixture of proteins was run through a Superdex S200. The elution peaks of the protein mixture were compared with those of the individual proteins applied to the same column. Any shift in elution volume was then analysed by SDS PAGE to determine the constituent proteins present in any given peak. The profile of the α 631-Cyp40 complex on Superdex S200 was shown to be different from that of the proteins alone (Figure 4.5). Peak A from the gel filtration of hHsp90- α 631 alone was shifted to peak C when the complex was run on the same column. Besides, most of peak B from gel filtration of Cyp40 alone disappeared. The total area under peak C was the same as that of peaks A and B combined. The size of the complex based upon the elution volume of peak C also showed an increase of 50 kDa (which corresponds well to the size of Cyp40 calculated from peak B). The fractions collected from gel filtration experiments were loaded on SDS PAGE gels (Figure 4.5). Based on the gel, bands

a)

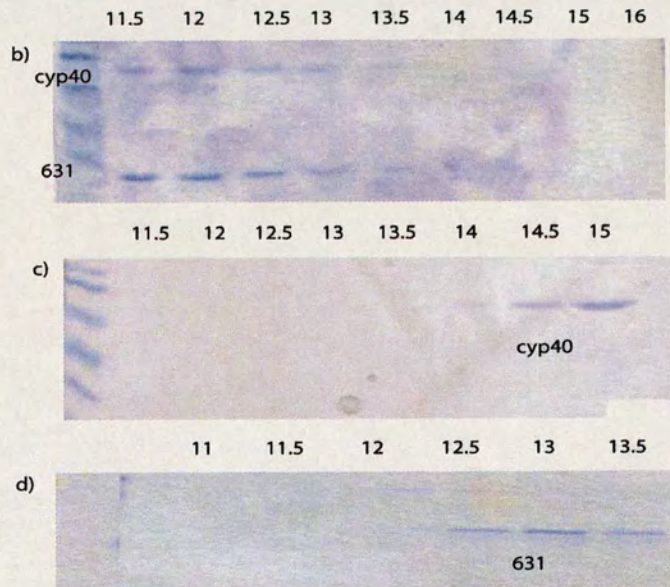
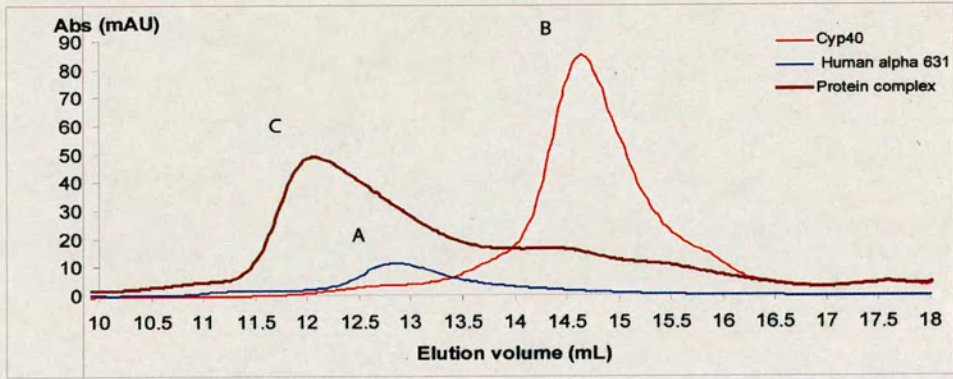


Figure 4.5. Gel filtration studies of complex formation using hHsp90- α 631 and bovine Cyp40. a) Plot of the gel filtration profiles from all Superdex 200 runs. A, B and C peaks were observed in each of the independent runs. Peak C was the peak that corresponded to the formation of a complex while A and B were observed when the proteins were analysed individually. A shift from peak A or B to peak C indicated complex formation. Panels b and c and d show the SDS polyacrylamide gel analysis of all the fractions obtained over the runs. The fractions were numbered based on their elution volume with 0.5 ml each. b) Fractions collected from the gel filtration run of the complex. c) and d) Fractions collected from the individual runs of Cyp40 and hHsp90- α 631 respectively.

corresponding to Cyp40 were shifted from fraction no.14.5 to fractions no.11.5 upon complex formation.

Similarly, the complex of hHsp90- α 521 and Cyp40 also showed a different elution profile from that of its individual protein components following gel filtration on a Superdex 200 column (Figure 4.6). Peak A from hHsp90- α 521 alone was shifted to peak C. Peak B from the individual Cyp40 gel filtration run almost disappeared. The area under peak C was corresponded to that of A and B together. SDS polyacrylamide gel (Figure 4.6) of the fractions collected showed that Cyp40 was detectable in earlier fractions. The band corresponding to hHsp90- α 521 was also detectable in earlier fractions. Break down products from the protein(s) can also be seen in the gel.

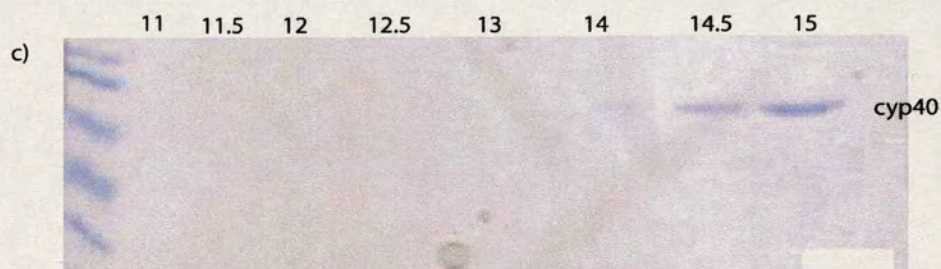
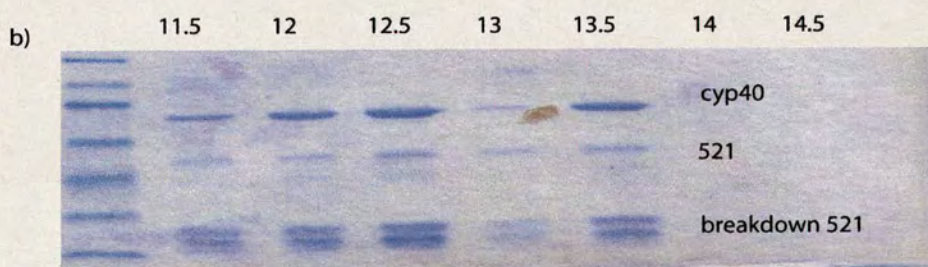
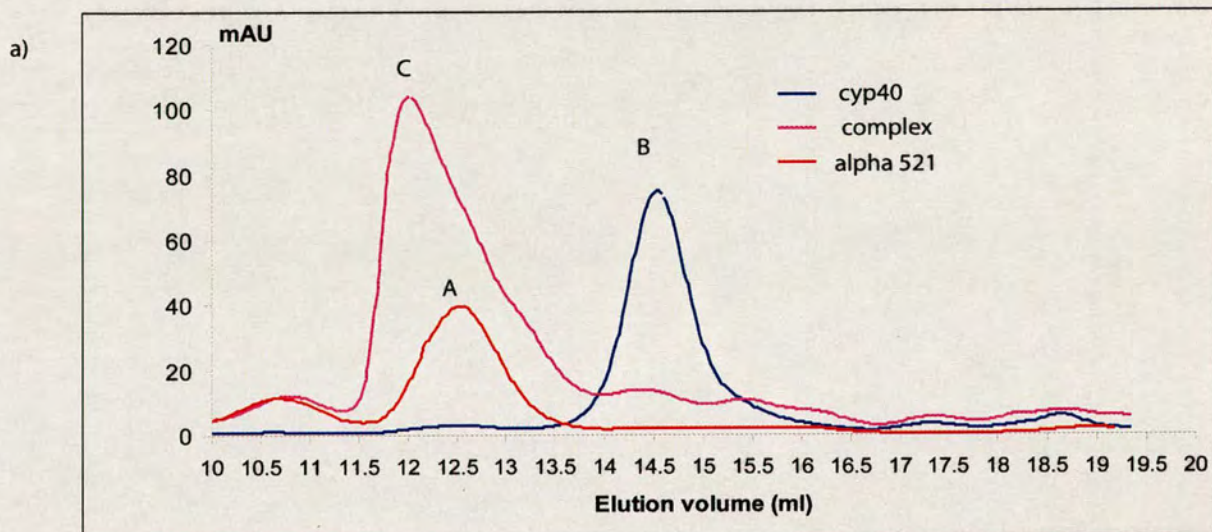


Figure 4.6. Gel filtration studies of the formation of complex between hHsp90- α 521 and bovine Cyp40. a) Graph showing the gel filtration profiles from each run on the Superdex 200. Peaks A and B (hHsp90- α 521 and Cyp 40 respectively) were shifted to peak C indicating the formation of a complex. b) and c) show the SDS polyacrylamide gel of the fractions collected from over the complex and Cyp40 peaks respectively. In gel b) breakdown products of hHsp90- α 521 can also be seen in addition to both of the target proteins.

4.3.3.2. The dissociation constant (Kd) of the interaction between Cyp40 and C-terminal human Hsp90 α obtained from Trp fluorescence

Trp fluorescence is one of the tools widely used to monitor the changes in protein. The technique monitors the changes that happen to the Trp residues or their environment when the protein makes a contact to other compounds or proteins. These changes can be monitored by looking at the fluorescence intensity, maximum wavelength, anisotropy, fluorescence lifetimes and energy transfer [32]. In this series of experiments, changes in Trp intensity were used to monitor the changes that occurred to the Trp residues of the proteins when complex was formed. The study was carried out to investigate the binding of the C-terminal domain of human Hsp90 α with Cyp40. From the study of the Trp fluorescence, the dissociation constant (Kd) can be calculated.

In the first experiment, various concentrations of hHsp90- α 631 (1 to 160 μ M) were added to a fixed amount of Cyp40 (1 μ M) and the changes in fluorescence were monitored. The excitation wavelength of the complex was 295 nm; the emission fluorescence was taken at 350 nm. The observed fluorescence was corrected against inner filter effects and background. The observed fluorescence from the experiment was subtracted with the fluorescence of Cyp40 alone at the same concentration used in the experiment. The background subtracted fluorescence was corrected against the inner filter effects. A graph of the corrected fluorescence against concentration (μ M) was plotted (Figure 4.7). Based upon the graph, equation 4 was fitted to get the Kd. The Kd of the interaction is $39 \pm 7.4 \mu$ M.

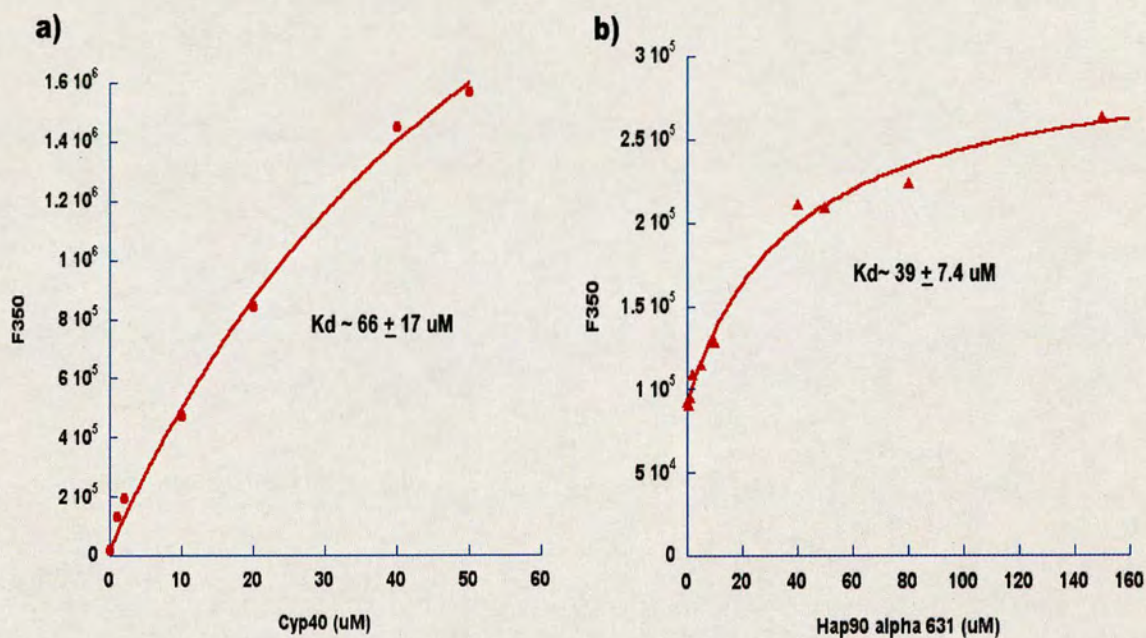


Figure 4.7. Graphs showing Trp fluorescence measurements of the interaction between the C-terminal domain of human Hsp90 α with bovine Cyp40. a) Various concentrations of bovine Cyp40 were added to 1 μ M of hHsp90- α 521. The emission at 350 nm at each concentration of Cyp40 was monitored. The K_d for the interaction is $66 \pm 17 \mu\text{M}$ and was obtained by fitting the curve with Equation 4. b) Increasing concentrations of hHsp90- α 631 were added to a solution of 1 μ M Cyp40. The emission was also monitored at 350 nm and the K_d was obtained by fitting the curve with equation 6. The K_d of the interaction is $39 \pm 7.4 \mu\text{M}$.

The same experiment was carried out to study the binding of hHsp90- α 521 to Cyp40. In this experiment, a fixed concentration of hHsp90- α 521 was used and mixed with various concentrations of Cyp40. The fluorescence values were corrected

against both the inner filter effects and the background. Based on the graph, the K_d for the interaction is $66 \pm 17 \mu\text{M}$ (Figure 4.7).

4.3.3.3. Surface Plasmon Resonance (SPR) also supports the binding of the C-terminal human Hsp90 α with bovine Cyp40

The SPR experiments were carried out with the assistance of Dr John Butler from BIACORE. The experiment used the NTA chip to study the interaction between hHsp90- α 521 and Cyp40. The NTA chip was charged with Ni^{2+} by following manufacturer's protocols. Figure 4.8 indicates one single cycle of SPR carried out to study the interaction of the proteins. The cycle of SPR was started by coupling the hHsp90- α 521 onto the surface of a Ni-NTA chip via the His-tag on the protein to nickel ions bound on the surface of the sensor. The on-rate for the binding of the protein to the sensor is $0.1 \mu\text{M}^{-1}\text{s}^{-1}$ which gives a K_d of $1 \mu\text{M}$ and the dissociation rate is 0.05s^{-1} . The respond signal was decreased around 0.2RU s^{-1} . Cyp 40 (at the concentration of $37.5 \mu\text{M}$ in the figure 4.8) was passed over the chip at a flow rate of $30 \mu\text{l min}^{-1}$. Cyp40 binds to the hHsp90- α 521 on the surface and dissociated by itself over 180s. Dissociation of hHsp90- α 521 from the surface was carried out by washing with running buffer. 5 mM EDTA was used to completely remove the protein and the Ni^{2+} from the surface as well as regenerating surface. The surface was recharged with the Ni^{2+} . The cycle was then repeated for other concentration of Cyp40. The binding of increasing concentrations of Cyp40 (2 to $300\mu\text{M}$) onto the hHsp90- α 521 was shown in figure 4.9. When a series of

concentrations of Cyp40 (2 to 300 μM) were passed over the immobilised Hsp90, the RU

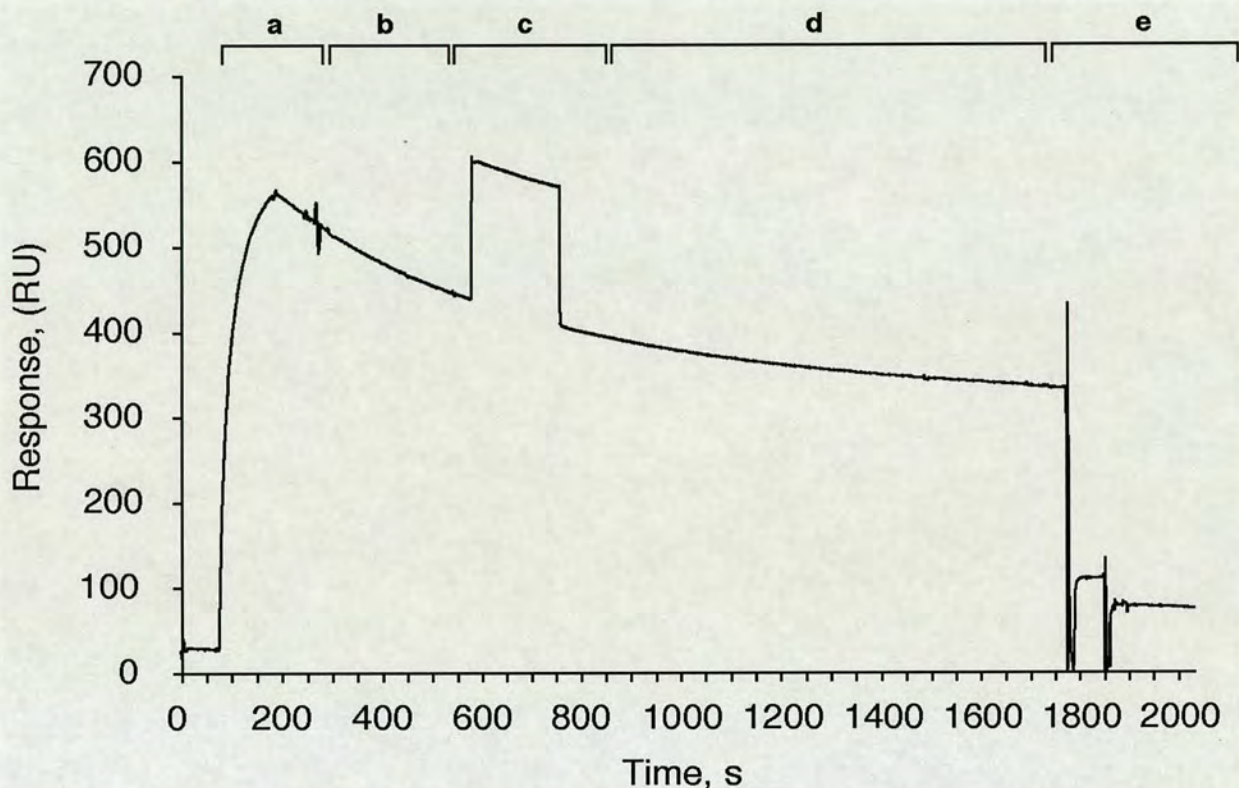


Figure 4.8. Generation of an NTA-hHsp90- α 521 sensor surface. The reference corrected SPR sensorgram from a Biacore3000 machine to the capture (phase **a**), of 200 nM Hexa- hHsp90- α 521, in *Running Buffer* (10 mM HEPES, pH 7.4; 150 mM NaCl; 0.005% surfactant P20), for 60 sec at $5 \mu\text{l}\cdot\text{min}^{-1}$, over an Ni^{2+} -NTA sensor surface. Following injection of hHsp90- α 521 (the capture signal response in this experiment ~ 550 RU. The mean value was 531 ± 28 RU; \pm SE, $n = 30$) the injection of protein was stopped and the lines washed with *Running Buffer* (phase **b**). The response signal drops steadily due to hHsp90- α 521 dissociating from the surface (phases **b - d**). The off-rate for this dissociation is $\sim 0.05 \text{ s}^{-1}$, corresponding to a baseline drift of $\sim 0.2 \text{ RU}\cdot\text{s}^{-1}$, as seen in the Cyp40 binding-phase (phase **c** and Figure 4.9). The on-rate for hHsp90- α 521 binding is $\sim 0.1 \mu\text{M}^{-1}\text{s}^{-1}$, giving a K_d of $\sim 1 \mu\text{M}$. Following washing of the injection lines, a 180 s injection at $30 \mu\text{l min}^{-1}$, of (in this case $37.5 \mu\text{M}$) Cyp40 in *Running Buffer* (phase **c**) was performed. Dissociation (phase **d**) was performed in *Running Buffer* for 300 s at $30 \mu\text{l min}^{-1}$.

Following this, the surface was regenerated with 5 mM EDTA in *Running Buffer*, the NTA-chip recharged with Ni^{2+} and the cycle repeated according to recommended Biacore protocols (phase e).

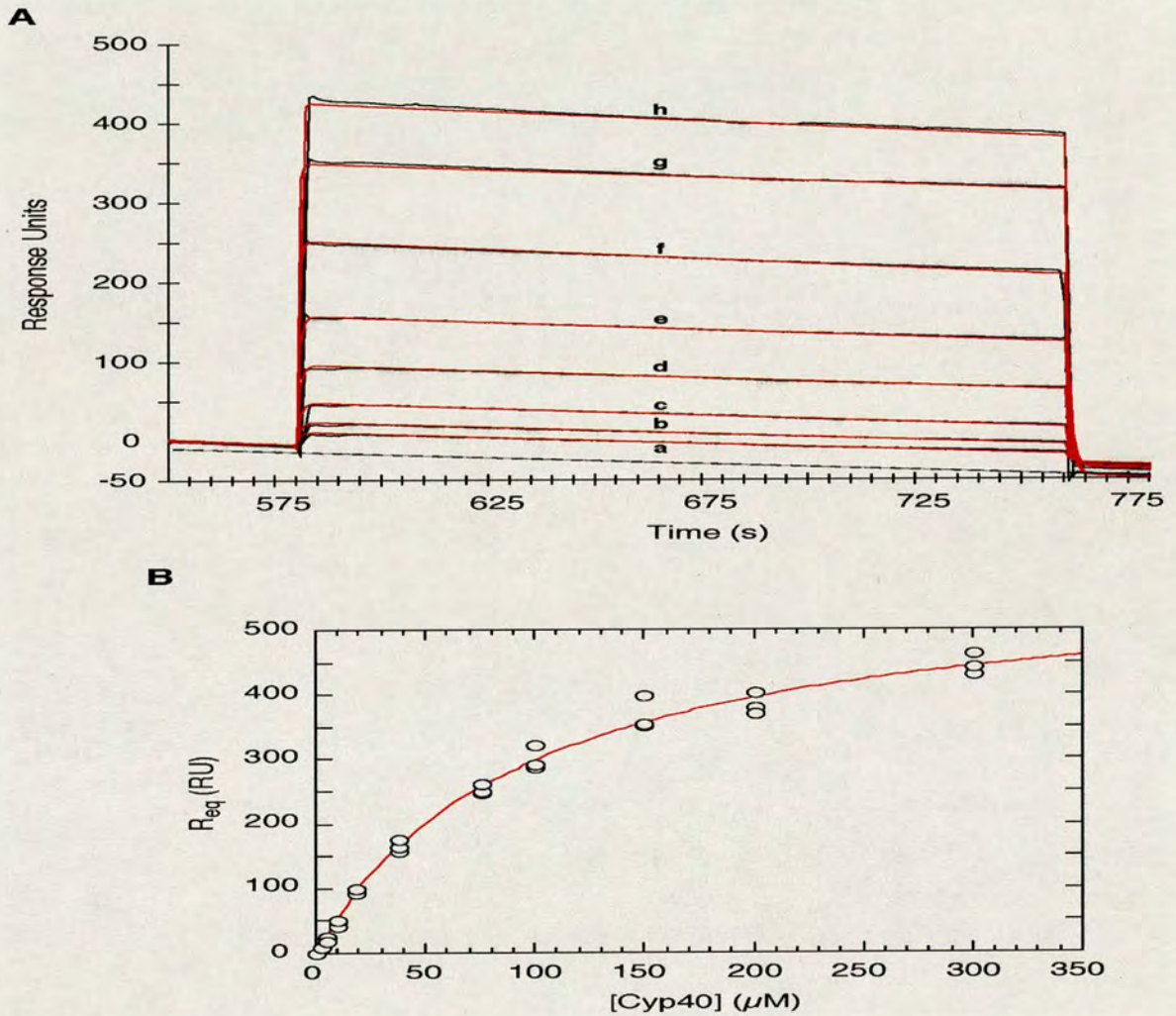


Figure 4.9. Binding of Cyp40 to Ni^{2+} -NTA immobilized hHsp90- α 521 . (A) Reference corrected SPR binding curves (black) for various concentrations of Cyp40 monitored on a surface of Ni^{2+} -NTA captured hHsp90- α 521 . The data was globally fitted (red) using a kinetic model (with a drifting baseline of -0.2 RU s^{-1}) where a 1:1 complex is formed between hHsp90- α 521 and Cyp40. From this experiment the apparent on-rate constant (k_+) is $0.018 \mu\text{M}^{-1}\text{s}^{-1}$, and the apparent off-rate constant (k_-) is 1.3 s^{-1} giving an equilibrium dissociation constant (K_d^{kin}) of $72.2 \mu\text{M}$, for Cyp40 binding to hHsp90- α 521 .Running buffer was 10 mM HEPES, pH 7.4; 150 mM NaCl; 0.005% surfactant P20. Curve **a**, $2.35 \mu\text{M}$ Cyp40; **b**, $4.7 \mu\text{M}$ Cyp40; **c**, $9.4 \mu\text{M}$ Cyp40; **d**, $18.8 \mu\text{M}$ Cyp40; **e**, $37.5 \mu\text{M}$ Cyp40; **f**, $75 \mu\text{M}$ Cyp40; **g**, $150 \mu\text{M}$ Cyp40; **h**,

300 μM Cyp40. **(B)** Plot of steady-state response units, R_{eq} , versus the concentration of Cyp40 in μM . A least squares fit of the equation $R_{\text{eq}} = (R_{\text{eqsat}} \times [\text{Cyp40}]) / ([\text{Cyp40}] + K_d^{\text{Eq}})$, to data from three repeat experiments is shown in red. R_{eq} is the equilibrium response (RU), R_{eqsat} is the saturated equilibrium response for the chip surface, $[\text{Cyp40}]$ is the total Cyp40 concentration in μM and K_d^{Eq} is the equilibrium dissociation constant. The mean K_d^{Eq} value = $95.7 \pm 19.5 \mu\text{M}$ (\pm SE).

seen were plotted against the concentration of Cyp40 (Figure 4.9). The graph was fitted with equation below.

$$R_{\text{eq}} = (R_{\text{eqsat}} \times [\text{Cyp40}]) / ([\text{Cyp40}] + K_d^{\text{Eq}}) \text{ -equation 7}$$

The experiments were repeated three times. R_{eq} is the equilibrium response of the interaction in RU units, R_{eqsat} is the saturated equilibrium response for the chip surface which is 500 RU, $[\text{Cyp40}]$ is the total Cyp40 concentration in μM and K_d^{Eq} is the equilibrium dissociation constant. The mean K_d^{Eq} value = $95.7 \pm 19.5 \mu\text{M}$ (\pm SE; $n=3$). From the experiment, the equilibrium dissociation constant (K_d^{Kin}) is 76 ± 19.5 (\pm SE; $n=3$) with apparent on-rate constants, K_+ ($\mu\text{M}^{-1}\text{s}^{-1}$) and off-rate constants of, K_- (s^{-1}) 0.018 ± 0.002 and 1.3 ± 0.3 respectively.

4.3.4. Interaction of the C-terminal domain of human Hsp90 α with ATP and novobiocin

Besides studying the interactions of C-terminal human Hsp90 α with bovine Cyp40, another area of interest of the project was to study the interaction of the proteins with ligands. The ligands that were studied were ATP and novobiocin. The interest in

both of these ligands arose mainly because they were shown to bind to the C-terminal domain of the Hsp90 proteins [8, 30]. However, these interactions are not particularly well documented, few groups have investigated the binding of the C-terminal domain Hsp90 with ATP (in contrast to the situation of the N-terminal ATP binding which has been well characterised). Therefore, the availability of relatively large quantities of these proteins presents an opportunity to study the interactions of the C-terminal domain with both ATP and novobiocin. Novobiocin has previously been shown to bind to the C-terminus of Hsp90 [14, 15, 36]. Novobiocin also inhibits the binding of ATP to C-terminal Hsp90 [14].

4.3.4.1. Trp fluorescence showed that ATP bind to hHsp90- α 521

Intrinsic Trp fluorescence was used to investigate the binding of ATP to hHsp90- α 521. The experiments were carried out by titrating ATP into a solution of the proteins. The fluorescence signal of individual concentrations of ATP was also determined. ATP does not give any significant absorbance at 295 nm, it also does not fluoresce significantly under the experimental conditions used, therefore the background fluorescence was negligible and has been ignored when analysing the data from this series of experiments. The observed fluorescence was corrected against the dilution factor resulting from the titrations only. The final volume added was only a maximum of 1% of the total initial volume. The values for the corrected fluorescence were plotted and the curve was fitted with the equation (equation 6b) mentioned before in section

4.4.2 using Kaleidagraph 3.5 (Figure 4.10). The K_d obtained for the interaction of hHsp90- α 521 is $101 \pm 15 \mu\text{M}$.

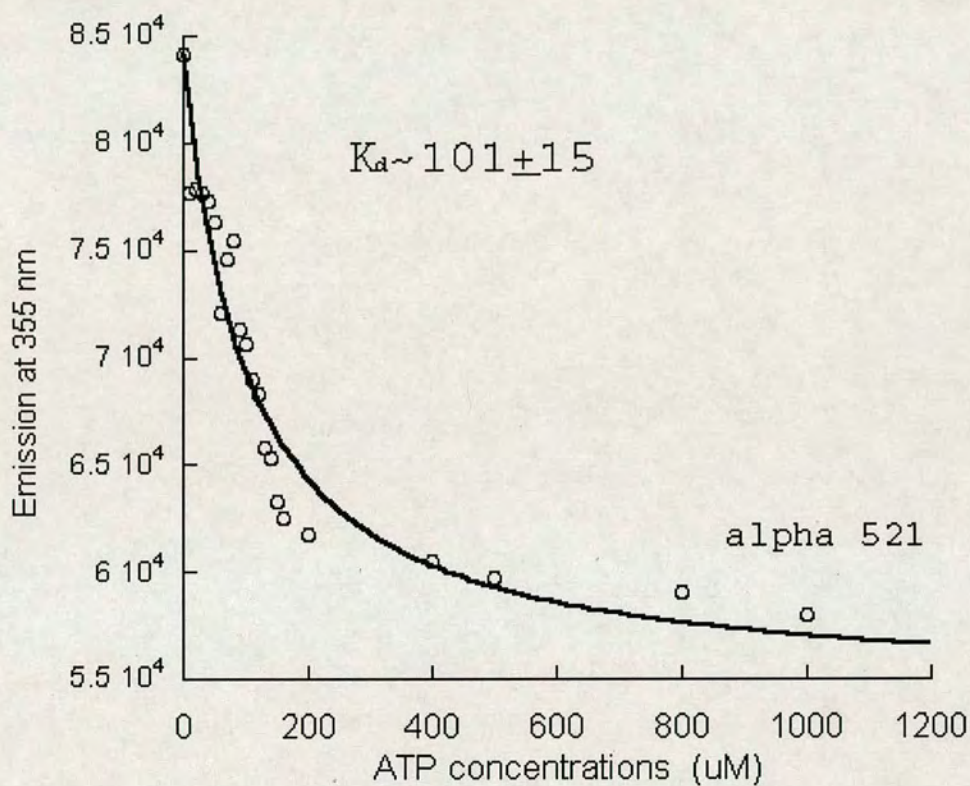


Figure 4.10. Intrinsic Trp fluorescence of hHsp90- α 521 titrated with an increasing concentration of ATP. The fluorescence experiment was carried out with excitation at 295 nm, emissions were measured at 355 nm. The observed emissions were corrected against the inner filter effects as well as the background. The curve was fitted using Kaleidagraph 3.5. Based from the fit, the K_d observed is $101 \pm 15 \mu\text{M}$

As a control, the experiment was also carried out with cyclophilin A that does not bind to ATP. The results of this experiment showed that the graph is linear with a negative slope. The result indicated that, as predicted, there is no interaction between ATP and cyclophilin A.

4.3.4.2. Hummel-Dreyer gel filtration showed ATP binds to hHsp90- α 521 but not hHsp90- α 631

The interaction of hHsp90- α 521 with ATP was also shown by the Hummel-Dreyer experiment (Figure 4.11). In this experiment, 75 μ M ATP was added to the running buffer used to equilibrate the gel filtration column. Samples containing hHsp90- α 521 with various concentrations of ATP were applied to the column. The initial concentration of ATP in the sample was the same as in the running buffer. The change from trough to peak as the ATP concentration increased indicates interaction between protein and ATP. The trough to peak changes was caused by the differences in concentration of ATP eluted from the sample with the concentration of ATP in buffer that equilibrated the column as mentioned in section 4.2.4.1. In these experiments, the concentrations of ATP used varied from 75 to 200 μ M, the concentration of protein was fixed at 80 μ M. The change from trough to peak was observed when the concentration of ATP was increased (Figure 4.11). The areas under the trough or peak were calculated and the graph of the area versus ATP concentration was plotted. From the graph, the value of the ATP concentration when neither peak nor trough was determined. The concentration of ATP at this point indicated that the free ATP concentration was the same as that in the running buffer. The ATP concentration in the sample is

approximately 100 μ M when neither a trough nor a peak were observed. From this value, free hHsp90- α 521 can be calculated as well as the concentration of complex. These values were then used to calculate the K_d based on the equation below.

$$K_d = \frac{[\alpha 521_{\text{free}}][\text{ATP}_{\text{free}}]}{[\alpha 521:\text{ATP}]} \text{- equation 8}$$

The K_d of the interaction of ATP and hHsp90- α 521 from the Hummel-Dryer experiment is $300 \pm 90 \mu\text{M}$ (mean \pm S.E, $n = 3$) (Fig 4.11). The stoichiometry of the interaction is 1: 0.75 (hHsp90- α 521: ATP). The stoichiometry was obtained by plotting a Scatchard graph of $[\text{ATP}_{\text{bound}}]/[\text{ATP}_{\text{free}}]$ against $[\text{ATP}_{\text{bound}}]$ (Figure 4.11). The slope of the graph is equal to $-1/K_d$ and the intersection of the plot with the abscissa give the potential concentration of protein occupy the binding site (in this case $60 \mu\text{M}$). The K_d obtained from this graph is $277 \mu\text{M}$ which is very similar to the K_d obtain from other experiments. The experiment was repeated with hHsp90- α 631 but showed that the protein did not bind to ATP

4.3.4.3. ATPase activity of hHsp90- α 521 detected by malachite green assay

The ATPase activity of the proteins was measured using an assay system based on malachite green. The assay was performed using $5 \mu\text{M}$ hHsp90- α 521-732. The linear phase of the ATPase activity against time was determined first prior to any experiments using different amount of ATP (Figure 4.12b (insert)). The experiments were then carried out to determine the rate of ATPase activity by measuring the concentration of

phosphate release caused by a fixed concentration of protein over a fixed time with a series of ATP concentrations.

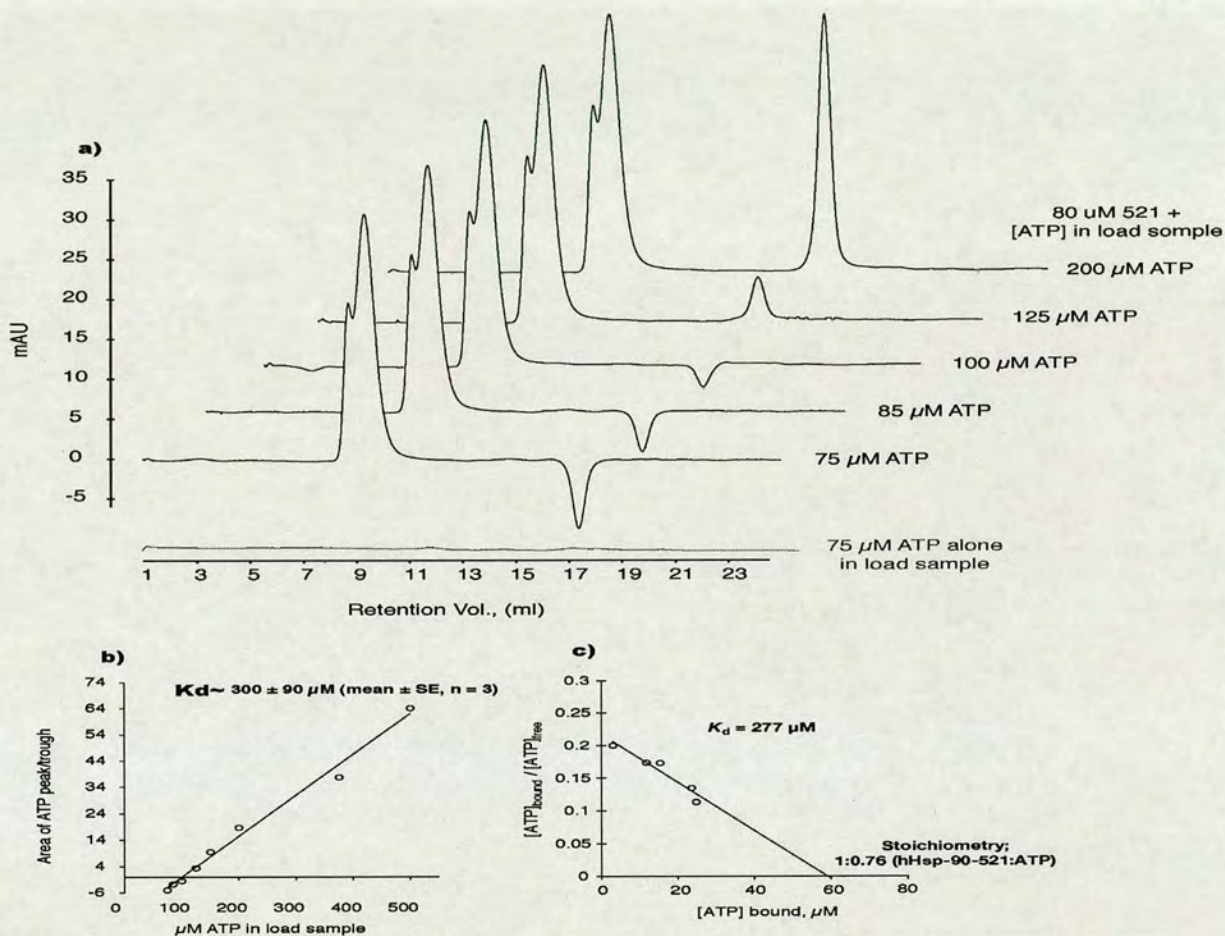


Figure 4.11. Hummel- dryer experiment of hHsp90- α 521 and ATP. a) The graph of the change from trough to peak as the ATP concentration in the sample loaded was increased from 75 μM to 200 μM . b) The graph of the areas under the peak/ trough againsts the concentration of ATP. The value of the ATP concentration when the area is zero was determined to be approximately 100 μM .The value indicates the concentration of free ATP was equal to that in the running buffer. From this value all other parameters were determined and fitted to equation 8 to obtain the K_d . The K_d shown above was obtained from 3 experiments. c) The graph of ATP bound over free ATP against bound ATP was plotted. The K_d is determined by the negative inversion of the slope. The stoichiometry of the interaction was determined by

dividing the concentration of ATP at abscissa with the amount of protein in the sample loaded. The K_d s determined by both of these plots were very similar, the stoichiometry of the interaction is 1: 0.76 which is close to 1:1.

The background amount of phosphate released due to self hydrolyzing ATP was also measured and subtracted from the results obtained. The concentration of phosphate released ($M \text{ min}^{-1}$) was plotted against the concentration of ATP using Kaleidagraph 3.5. The graph was fitted with equation below.

$$\text{Rates (M min}^{-1}\text{)} = (K_{\text{cat}} \times [\alpha 521]) \left(\frac{[\text{ATP}]}{K_m + [\text{ATP}]} \right) \text{- equation 9}$$

From the graph (Figure 4.12), the k_{cat} is $0.021 \pm 0.002 \text{ min}^{-1}$ and the K_m is $377 \pm 101 \mu\text{M}$. The malachite green ATPase assay experiment showed that hHsp90- $\alpha 631$ has no significant activity above that of the background (Figure 4.12). The assay was also carried out using Phosphofructokinase (PFK) (a well characterised protein that has well known ATPase activity) as a positive control. The results (Figure 4.12) show the K_{cat} of the reaction is $116 \pm 25 \text{ s}^{-1}$ with a K_m of $770 \pm 5 \mu\text{M}$. The assay was also carried out using CypA as a negative control, as anticipated no ATPase activity was detectable from this molecule.

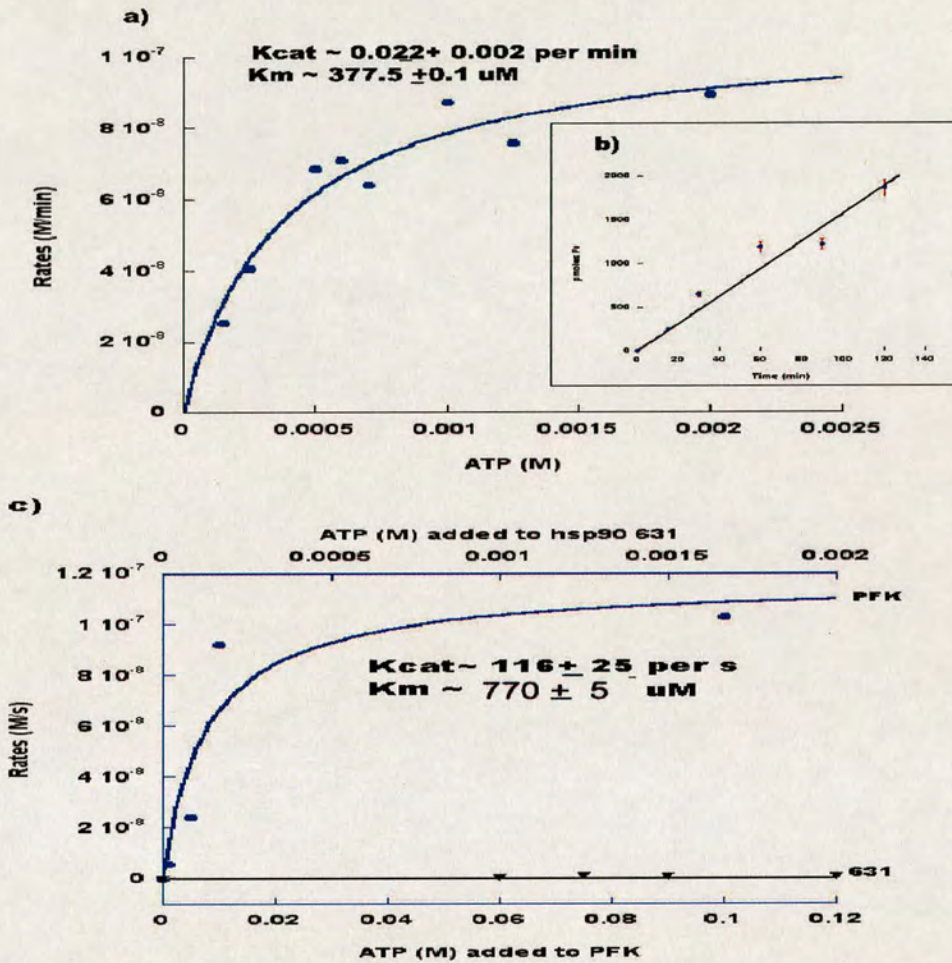


Figure 4.12. ATPase activity of C-terminal human Hsp90 α using the malachite green assay system. a) ATPase activity of hHsp90- α 521 with increasing concentrations of ATP. The rate of the phosphate release was monitored over 60 min by measuring the absorbance of the phosphomolybdate compound at 620 nm. b) Rate of phosphate release from the initial substrate 2mM ATP against time from 0 to 120 min. Based on this graph the time required to measure the ATPase activity was determined to be 60 minutes. c) Graph of ATPase activity of the control protein PFK and hHsp90- α 631, plotted on two different x-axes scales for clarity. The ATPase activity of hHsp90- α 631 is negligible and is considered as a background suggesting as no ATPase activity.

4.3.4.4. Novobiocin binds to the C-terminal human Hsp90 α determined by Trp fluorescence and ITC

The interaction of novobiocin with the C-terminal domain of human Hsp90 α was also investigated using Tryptophan fluorescence studies. The binding of novobiocin to the C-terminal Hsp90 was not well documented in literature compared to geldanamycin. Therefore, it will be useful if more information can be obtained from this study. However, only hHsp90- α 521 was amenable to studies with this technique as hHsp90- α 631 does not contain any Trp residues. Attempts to study the interactions by Hummel-Dreyer were unsuccessful as novobiocin itself stuck to the gel filtration column. The novobiocin was also found to be sticky and stacked to each other especially at high concentrations. In the fluorescence experiments, increasing concentration of novobiocin were titrated into 1 μ M protein in a 3 ml cuvette. The protein was excited at 295 nm and the emission collected at a wavelength of 355 nm over a 60 second time period. The data from increasing concentrations of novobiocin without the protein were also measured to determine the background fluorescence. Novobiocin itself exhibits background fluorescence, the fluorescence emission of the complexes were corrected againsts both background and the inner filter effects using equation 5. The corrected emission data were plotted and fitted with two binding sites equation 6b. The K_d obtained from the experiment is $1.26 \pm 0.46 \mu$ M (Figure 4.13). However, the second K_d was large and with huge error showed that the second binding was unspecific and due to the novobiocin which is sticky. In order to determine if the binding of novobiocin to hHsp90- α 521 is genuine, the experiment was repeated using N-acetyl tryptophan as a

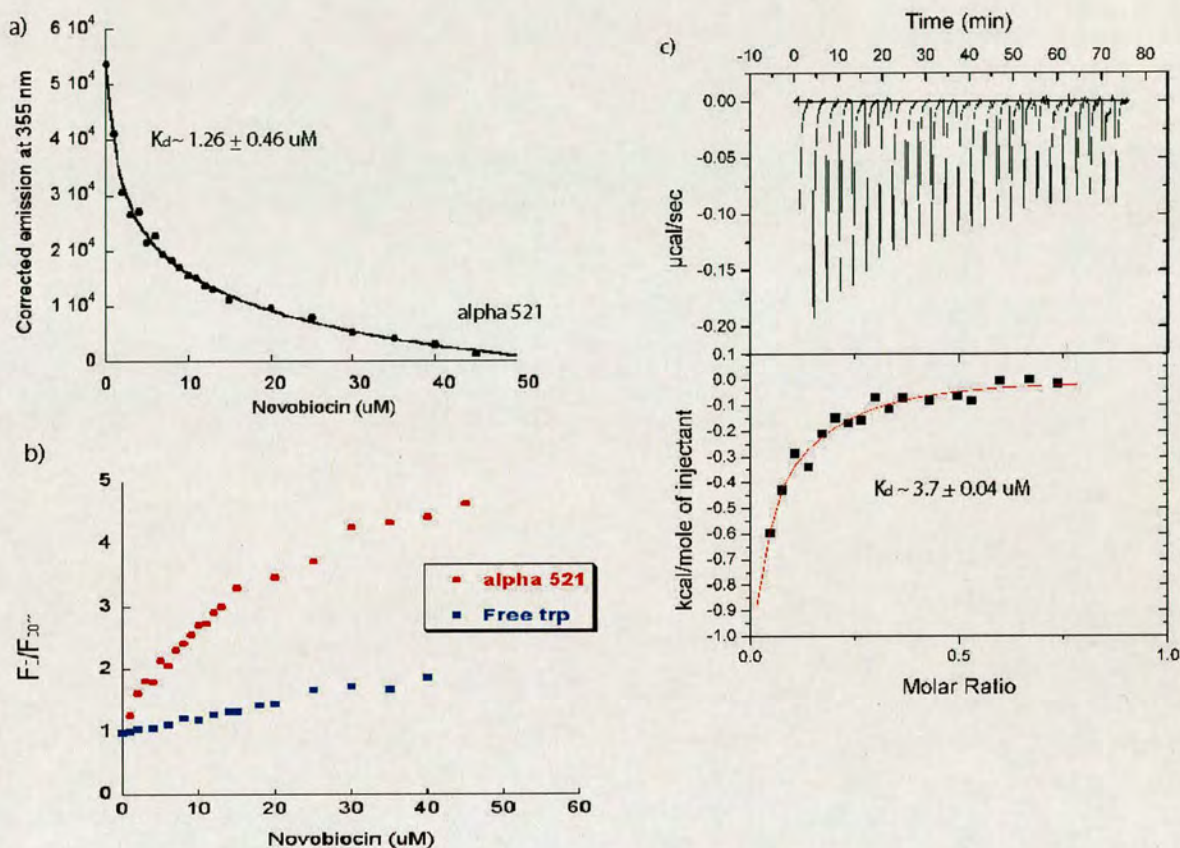


Figure 4.13. Study of the interactions of hHsp90- α 521 and N-acetyl tryptophan with novobiocin. The study was done by using intrinsic Trp fluorescence and isothermal titration calorimetry (ITC). a) The graph shows the changes in emission caused by the titration of an increasing concentration of novobiocin into a fixed amount of hHsp90- α 521. The graph was then fitted with equation 6b to obtain the K_d which is $1.26 \pm 0.46 \mu\text{M}$. b) A Stern-Volmer plot of the fluorescence data from both of the experiments. From the Stern-Volmer plot, the bimolecular quenching constant of free Trp and novobiocin was determined to be $900 \mu\text{M}$. The Stern-Volmer plot of hHp90 α 521 was also displayed. The plot shows the interaction deviated from linearity and indicates specific interaction. The facts were explained further in discussion. c) ITC data of the interaction between hHsp90- α 521 with novobiocin. The K_d determined from the experiments was $3.7 \pm 0.04 \mu\text{M}$.

control. The emission fluorescence were corrected and plotted using the Stern –Volmer equation , $F_0/F = 1+K_D[\text{Novobiocin}]$. From the K_D , the bimolecular quenching constants can be calculated by using $K_D= k_q t_0 [\text{Novobiocin}]$ where k_q is the bimolecular quenching constants and the t_0 is the half life of Trp which is 3.6 s.

From available data the bimolecular quenching constants for the N-acetyl- Trp is about $900\mu\text{M}$, which indicates the binding is non-specific. The interaction of the protein with novobiocin was also determined by using ITC. The ITC data was fitted by using two binding sites equation provided by manufacturer. From the fitted curved, the K_d for the specific interaction was $3.7 \pm 0.04 \mu\text{M}$ whereas the unspecific K_d was about $150 \mu\text{M}$. The reaction was entropically favourable with a $\Delta G = -6.6.\text{kcal mol}^{-1}$, $\Delta H= -2.14 \times 10^{-1} \text{kcal mol}$ and $\Delta S= 2.41 \times 10^{-2} \text{kcal mol}^{-1}\text{K}^{-1}$.

4.3.4.5. The inhibition of ATPase activity by novobiocin

The next experiment is to investigate if novobiocin was able to inhibit the ATPase activity of hHsp90- α 521as novobiocin was showed [14, 15] to compete with ATP at the C-terminal. The experiment was carried out as described. Absorbance at 620 nm was converted to the amount of phosphate released against time (pmoles min^{-1}) and the graph of rate versus concentration of novobiocin was plotted. The IC_{50} was obtained by fitting the curve with equation 10 as below.

$$\text{Rates (pmoles min}^{-1}\text{)} = (\text{rates}_{\infty} + (\text{rates}_{\text{mit}} - \text{rates}_{\infty})) (1 + ([\text{novobiocin}]/\text{IC}_{50})^1) \text{ -equation 10}$$

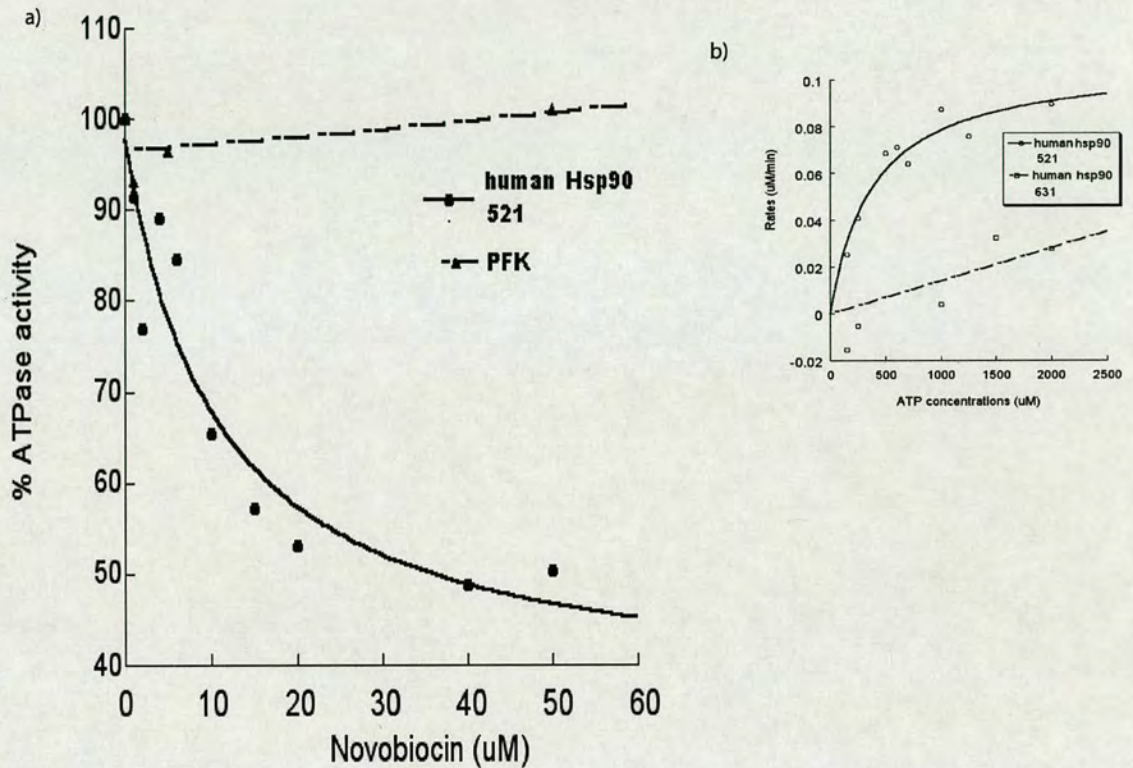


Figure 4.14. Inhibition of ATPase activity by novobiocin using the Malachite green assay. a) The inhibition graph of hHsp90- α 521 and PFK. The assay was carried out using either 5 μ M of hHsp90- α 521 or 1 nM PFK. Increasing concentrations of novobiocin were incubated with the proteins at 37°C for 30 min. The ATPase assay was carried out as described in chapter 5, section 4.2.4.4. The IC_{50} of hHsp90- α 521 inhibition was obtained by fitting equation 10. The IC_{50} (10.8 μ M) and the K_m (377 μ M) were fitted to equation 11 to get the K_i which is $2.79 \pm 2.02 \mu$ M. The inhibition of ATPase assay was also carried out using PFK. Even though up to 300 μ M of novobiocin was added to the 1 nM protein, no inhibition of the ATPase activity was detectable. b) ATPase activity of both of the C-terminal human Hsp90 α just as a comparison to the inhibition.

where $rates_{\infty}$ is the rate of ATPase activity at infinite concentration of novobocin. $Rates_{init}$ is the initial rate of ATPase activity in the absence of novobiocin. From the graph, the IC_{50} is $10.8 \pm 6.8 \mu M$. The inhibition constant (K_i) was calculated using equation 11.

$$K_i = IC_{50} / (1 + ([ATP]/K_m)) \text{ --equation 11}$$

Where the IC_{50} was obtained from the previous ATPase experiment. $[ATP]$ is the concentration of ATP used ($1000 \mu M$) and the K_m ($377 \mu M$) was obtained from the ATPase assay, resulting in a calculated K_i of $2.79 \pm 2.02 \mu M$. The inhibition of ATPase activity was also carried out using PFK at $1nM$ concentration as a control (Figure 4.14). No inhibition of the ATPase activity was observed even at a concentration of $300 \mu M$.

4.4. Crystallization trials

Crystallisation trials have been setup using various kits and precipitants. The commercial kits which have been tried are Structure screens 1 and 2 (MDL Ltd), Peg/Ion screen (MDL Ltd), Crystal screens 1 and 2 (Hampton Research) and the Sodium malonate screen. Besides the kits, precipitants such as ammonium sulphate and various types of PEG were also tried. The proteins were also used in co-crystallization experiments with Cyp40, ATP and novobiocin, unfortunately to date no useful crystals have been obtained. The best lead so far was obtained from hHsp90- α 521 from condition no. 4 of Structure Screen 1. The solution consists $3.4 M$ 1,6-hexanediol, $0.2M$

MgCl₂.6H₂O and 0.1M Tris pH 8.5. However the crystals obtained were very small and did not grow (Figure 4.15). Seeding was used in an attempt to encourage the crystals to grow but was unsuccessful. The crystals were screened but did not diffract.



Figure 4.15. Crystals of hHsp90- α 521. The crystals were tiny and formed a single needle-like shape (inset). The crystals were obtained from solution 4 of the Structure Screen 1 kit (MDL). Optimization experiments in an attempt to obtain better crystals were unsuccessful. The crystal did not diffract when screened on beamline 14.1 at CCLRC Daresbury.

4.5. Discussion

4.5.1. The dimerisation of the C-terminal human Hsp90 α

The study on hHsp90- α 521 and hHsp90- α 631 showed that both of the proteins exist in solution as a dimer. The K_{dimer} of hHsp90- α 631 can be measured using gel filtration. However, the dimerisation constant of hHsp90- α 521 K_{dimer} could not be determined as it was likely to be in the μM range and therefore below the available limits of detection for the in house system. A previous study had mapped the sites involved in the dimerisation of human Hsp90 β to residues 548-567, 661-667 and 679-728 [19, 27]. All of the sites or parts of them were present in the C-terminal of human Hsp90 α proteins. Therefore, it was likely that the proteins would exist as dimer. In the previous studies [34] showed that the site most important for dimer formation is 650-732. However, the dimer only exists if the region is paired with another human Hsp90 α region containing the middle and the C-terminal domain (human Hsp90 α 400-732) [34]. Our hHsp90- α 631 consists of only part of the sequences needed for dimer formation hence dimer formation was observed between the same proteins region (631-732) with a weaker K_{dimer} . In agreement with [13], the dimer can still exist but a stronger dimer can be formed if the other monomer is longer. Therefore, the dimer of hHsp90- α 631 is weaker with a K_{dimer} of approximately 5 μM and dependent on concentration. Furthermore, in the HtpG structure, the dimerisation motif was formed by two long helices (H4 and H5) comprised of residues 587-624. These helices interact with their equivalent counterparts from the second molecule and forming four helical bundles [12].

The motif was also similar in the recently published yeast Hsp90 full-length crystal structure. In addition to this motif, a helix segment residues 587-610 is also involved in the dimer formation [2]. The residues 587-624 of htpG were equivalent with residues 652-693 of human Hsp90 α whereas residues 587-610 of yeast Hsp90 were equivalent with 607 to 630 of human Hsp90 α . The lack of residues 607-630 in hHsp90- α 631 was probably another reason for its weak dimer formation. hHsp90- α 521 contains all of the residues important for dimer formation in addition to a number of residues from the middle domain. Therefore, it can be assumed that hHsp90- α 521 forms a tight dimer and has a K_{dimer} in the nM range. The assumption was made as the K_{dimer} of the full length of yeast Hsp90 is 60nM [27] and if the dimerisation is only caused by the C-terminal, therefore the K_{dimer} of hHsp90- α 521 must also be in the nM range.

4.5.2. Cyp40 bind to the C-terminal human Hsp90 α via MEEVD motif

Based on all the experiments studying the binding of Cyp40 to C-terminal Hsp90, an interaction between these two molecules can clearly be established. The interaction was showed by gel filtration using Superdex 200. Cyp40 was also shown to interact with human Hsp90 β , the interaction being mediated through the MEEVD motif of Hsp90 [33]. In that experiment, 24 amino acids of the TPR domain were mutated by site directed mutagenesis. The mutants were then used in interaction studies with the C-terminal domain of human Hsp90 β , using the yeast two hybrid β -galactosidase filter assay. The interactions of the TPR domain mutants with Hsp90 was as shown by GST pull down experiments and an ELISA of the mutants of certain amino acid of Cyp40 to

the C-terminal of human Hsp90 β . Even though, the binding of Cyp40 to Hsp90 had been shown previously [5, 6, 23, 31], however little was known as to the specific affinity of the interaction. In this study, the dissociation constants of the interaction between the C-terminal of Hsp90 with Cyp40 were investigated. The K_d of the interactions between the C-terminal constructs of human Hsp90 α that we have, were between 39 to 95 μM . The K_d was determined by intrinsic Trp fluorescence or SPR. Cyp40 was also shown to bind to the MEEVD peptide with a K_d of $34 \pm 20 \mu\text{M}$ which is very similar to the K_d of the interaction of Cyp40 with the larger C-terminal region of Hsp90. Based on the SPR results, it is also noteworthy that the dissociation of the complex was very rapid with an off-rate (k_{off}) of 1.3 s^{-1} when compared to the on-rate of $0.018 \pm 0.002 \mu\text{M}$. There is also agreement between the K_d^{Eq} and the K_d^{Kin} which can be calculated from the apparent the off- and on-rate. Due to the rapid equilibrium of the complex, some of the techniques used in an attempt to characterize the interactions were unsuitable for this particular experimental system. Near UV Circular Dichroism (Near CD) is an example of such a technique, where the binding of the two proteins was very rapid that the change in the protein structure can not be detected (data not shown).

From my experiments, it was also shown there is a difference in the dissociation constants between the C-terminal human Hsp90 α proteins analysed. The dissociation constant was lower for the hHsp90- α 631 construct which indicated tighter binding than that seen with the hHsp90- α 521 construct. As described earlier, the constructs differ in length, hHsp90- α 631 lacks 110 amino acids from the N-terminus, secondary structure predictions show hHsp90- α 631 to be missing 4 helices. In other Hsp90, TPR binding proteins such as Hop (Hsp90 Organiser Protein), the mammalian homolog of Sti1,

partial deletion of the N-terminal domain of Hsp90 resulted in decreased binding affinity with Sti1 [33]. However, no similar effect was seen to occur with immunophilin binding when the N-terminal of Hsp90 was deleted [7, 25]. It has also been shown that the binding of the C-terminal domain of human Hsp90 β to Cyp40 was similar to that seen with full length human Hsp90 β , indicating that this binding interaction is not influenced by the N-terminal domain [33]. Our results suggest that the shorter Hsp90 hHsp90- α 631 construct when compared with the hHsp90- α 521 construct is more accessible for immunophilin binding and also shows a lower dissociation constant but is still not hugely different. Similarly, the binding of the MEEVD peptide to Cyp40 also a roughly the same dissociation constant. In contrast, ITC experiments using full length human Hsp90 and human Cyp40 exhibited dissociation constants of about 226 ± 61 nM [23], which is lower than the K_d of our truncated Hsp90 constructs providing evidence in support of the argument that binding interactions are influenced by not just the C-terminal of Hsp90. Thus, even though the binding of the C-terminal of human Hsp90 was different between them, the K_d of the interaction between the full length human Hsp90 α and Cyp40 was probably lower than their C-terminal proteins. However, it is difficult to determine the effect of the deletion of the N-terminal and the middle domains upon the interactions with partner proteins as we do not have the full length human Hsp90 protein

Further support of the requirement for other Hsp90 domains has also been shown by ITC. Hsp90 binds both Sti1 and Cpr6, the dissociation constants (K_d) from these experiments are 330 nM and 240 nM respectively [25]. In this experiment, the binding of Sti1 was influenced by the N-terminal domain of Hsp90 [25]. Direct comparison of

the binding interactions between these TPR containing proteins and those described in this thesis is not possible as different Hsp90 constructs were used, however a previous ITC study suggests the interaction needs the presence of other Hsp90 domains for the interactions with the TPR domain. However, there was still a difference in their affinity to bind to Hsp90. The difference in affinity was probably because they function at different times in the cell as illustrated in figure 1.18, Chapter 1. In the intermediate folding complex, Sti1/Hop was present and the inherent ATPase activity inhibited. The inhibition was later relieved when Sti1 /Hop is replaced by other co-chaperones in the mature complex. In this complex, the C-terminal domain of Hsp90 was bound by an immunophilin co-chaperone such as Cyp40.

4.5.3. The C-terminal domain contains a second ATP binding site and has low ATPase activity

Apart from binding to TPR containing proteins, Hsp90 also binds to ATP. Binding to ATP/ADP is mediated through the N-terminal domain. The N-terminus of Hsp90 was shown by structural and biochemical studies to contain ADP/ATP binding sites [10, 24, 29]. It was also shown that Hsp90 can hydrolyse ATP [20, 22, 27] and that ATP hydrolysis is vital for its chaperone function in vitro [22]. An ATP binding site has also been suggested in the C-terminal region of Hsp90 [8, 14]. ATP binds to the C-terminus of Hsp90 in the presence of Mg^{2+} as shown by using ITC [8]. Several truncated C-terminal constructs of chicken Hsp90 were shown to bind to ATP Sepharose [14]. Based on our Trp fluorescence results, hHsp90- α 521 binds to ATP with a K_d of

101 ± 15 μM. Our result from the Hummel-Dreyer gel filtration experiment using running buffer containing ATP also showed ATP binding to the protein, with a higher K_d of approximately 250 to 300 μM. Both of the assays were carried out without Mg^{2+} in the buffer. Trp fluorescence studies cannot be used with hHsp90-α631 as this region of the protein does not contain a tryptophan. Attempts to carry out Hummel-Dreyer experiment with this protein also failed as the breakdown products of the protein interfere with the ATP elution peak/ trough analysis. Therefore, it is uncertain whether the deletion of amino acid acids 521-630 has any effect on the capability of the C-terminus to bind ATP.

As a result of the ability of hHsp90-α521 to bind to ATP, it is of interest to investigate if the C-terminal region itself can hydrolyse ATP. In order to do this, the malachite green assay described earlier was used. The assay was utilised as it is rapid and easy to use compared to the PFK enzyme coupled reactions. Malachite green has been used to detect ATPase activity in a number of proteins including Hsp90 [1, 9, 11, 28]. In this assay, phosphate ions released are captured by free molybdate ions. The resulting phosphomolybdate compound reacts with the malachite green dye, the absorbance resulting from this reaction can be measured at 620 nm [28]. Based on the results, ATPase activity was observed in the hHsp90- α521 construct. However, the activity was only 30% of that for full length human Hsp90 α (0.092 min⁻¹ [16, 17]). The most active Hsp90 ATPase yet characterized is that of yeast hsp82 that has an ATPase activity of 0.47 min⁻¹ [16, 17, 28].

4.5.4. Novobiocin binds to the C-terminal domain and inhibits ATPase activity

The C-terminal domain of Hsp90 was also shown to bind to novobiocin [14, 15, 36]. Novobiocin (Chapter 1; figure 1.16), is an antibiotic known to bind adjacent to the ATP binding site of bacterial gyrase B. There is evidence showed that native chicken Hsp90 and a number of its truncated C-terminal constructs were able to bind to novobiocin sepharose [14]. The binding of novobiocin at that site interferes with nucleotide binding where the truncated C-terminal constructs was inhibited to bind to ATP sepharose [14]. In agreement with these results, we showed novobiocin binds to hHsp90- α 521 with a range of K_d of 1.26 to 3.77 μ M. A further study carried out by [14, 15] has also shown that a motif corresponding to region 657-677 of chicken Hsp90 was able to compete with the Hsp90 mutants for novobiocin binding to the novobiocin sepharose resin. Furthermore, deletion of this region reduced the binding of chicken Hsp90 mutants to novobiocin sepharose [14]. This region is conserved in human Hsp90 α (residues 659 to 680). Therefore, this suggested that the same motif is also involved in the binding of novobiocin to our C-terminal constructs.

In order to make sure the interaction of novobiocin to Hsp90 is specific, the experiment was repeated using N-acetyl- tryptophan as a control for Trp fluorescence experiment. From the Stern-Volmer plot (Figure 4.13), a linear relationship was observed when the concentration of novobiocin increased. This relationship is expected as novobiocin can bind to free Trp without any restriction. Both molecules can bind and disassociate rapidly, therefore a linear relationship was observed. The same plot was

used to analyse the binding of novobiocin to hHsp90- α 521 (Figure 4.13). The graph shows a linear relationship at the beginning of the experiment which then plateaus as the novobiocin concentration is increased. This pattern would have been expected in the case where one Trp residue in the protein is inaccessible to the “quencher” and therefore the resulting fluorescence signal from this residue cannot be quenched. However, hHsp90- α 521 contains a single Trp residue which can be “seen” by fluorescence studies in the early stages of the experiment. Therefore, the plateauing of the curve seen was caused by novobiocin binding specifically to the protein. Additionally, the bimolecular quenching constants (k_q) of the free Trp bound to novobiocin can be inverted to become the dissociation constants of the interaction. The K_d for this interaction is $900\mu\text{M}$. The K_d of the interaction between novobiocin and the protein is 900-fold more than that of the K_d of the interaction between novobiocin and free Trp indicating that binding of novobiocin to protein was more specific than to that of the free Trp. Further support for the suggestion that novobiocin binds to Hsp90. HHsp90- α 521 came from ITC data which show the binding and give a K_d about $3.7\mu\text{M}$. All the K_d s obtained were almost similar therefore suggesting genuine binding.

As mentioned before, novobiocin was shown to inhibit binding between ATP and the C-terminal domain of Hsp90 [14, 15]. In this series of experiments, Hsp90 was inhibited from binding to novobiocin Sepharose by ATP and vice-versa. Based on our results, the ATPase activity of hHsp90- α 521 can be inhibited by novobiocin. The IC_{50} of the inhibition is $10.8 \pm 6.8\mu\text{M}$ and the K_i is approximately $2.8\mu\text{M}$. The K_i is in agreement with the K_d from the fluorescence experiments. As a control, the same experiment was carried out using PFK. The ATPase activity of PFK was not inhibited by

novobiocin even though the concentration of novobiocin used was 300 μM to a 1 nM solution of PFK. This indicates that the inhibition seen with Hsp90 is specific to the protein. The fact that the ATPase activity of hHsp90- α 521 can be inhibited by novobiocin also provides support for the results presented earlier that the ATPase activity and binding seen in the C-terminal domain is genuine.

4.6. Conclusion

Chapter 4 described the interactions of the C-terminal domain of human Hsp90 α with Cyp40 and also with small ligands such as ATP and novobiocin. The chapter also support the dimer formation of Hsp90 and identifies possible region for the dimer formation. The experiments also provide greater information on the binding strength between the proteins with the use of several biophysical techniques. In addition, more knowledge about the binding of C-terminal to ATP and novobiocin were revealed. Even though, some of the results are new and controversial, it does not mark the end of it. In future more study are needed to investigate the findings. Table 4.3 summarises the results obtained in this chapter.

Protein	<i>T</i> (°C)	Ligand or inhibitor	Methods	<i>K_d</i> (μM)	<i>IC50/Ki</i> (μM)	<i>K_m</i> (μM)	<i>k_{on}</i> (M ⁻¹ s ⁻¹)	<i>k_{off}</i> (s ⁻¹)	<i>K_{d kin}</i> (μM)	<i>k_{cat}</i> (min ⁻¹)	<i>K_{dimer}</i> (μM)	Figure
hHsp90-α521	4	ATP	Hummel-Dreyer	300 ± 90								4.11
	25	ATP	Trp fluorescence	101 ± 15								4.10
	37	ATP	Malachite green ATPase assay			377 ± 101				0.021 ± 0.002		4.12
	25	Novobiocin	Trp fluorescence	1.26 ± 0.46								4.13
	20	Novobiocin	ITC	3.7 ± 0.04								4.13
	37	Novobiocin	Malachite green ATPase assay		10.8 ± 6.8/ 2.79 ± 2.02							4.14
	25	Cyp40	Trp fluorescence	66 ± 17								4.7
	25	Cyp40	SPR	95.7 ± 19.5			0.018 ± 0.002	1.3 ± 0.3	76 ± 19.5			4.9
	4	Cyp40	Gel filtration									4.6
hHsp90-α631	4	ATP	Hummel-Dryer	No binding observed								
	37	ATP	Malachite green ATPase assay							No ATPase activity		
	25	Cyp40	Trp fluorescence	39 ± 7.4								4.7
	4	Cyp40	Gel filtration									4.5
	4		Gel filtration								4.98 ± 2.12	4.4

Table 4. 3. List of results obtained from all the human Hsp90 α experiments that were carried out in Chapter 4

References

1. Aherne, W., Maloney, A., Prodromou, C., Rowlands, G. M., Hardcastle, A., Boxall, K., Clarke, P., Walton, I. M., Pearl, L., Workman, P. (2003) Assays for HSP90 and inhibitors. *Methods Mol Med* 85: 149-61
2. Ali, M. M., Roe, M. S., Vaughan, K. C., Meyer, P., Panaretou, B., Piper, W. P., Prodromou, C., Pearl, H. L. (2006) Crystal structure of an Hsp90-nucleotide-p23/Sba1 closed chaperone complex. *Nature* 440: 1013-7
3. Bedin, M., Gaben, M. A., Saucier, C., Mester, J. (2004) Geldanamycin, an inhibitor of the chaperone activity of HSP90, induces MAPK-independent cell cycle arrest. *Int J Cancer* 109: 643-52
4. Beeckmans, S. (1999) Chromatographic methods to study protein-protein interactions. *Methods* 19: 278-305
5. Carrello, A., Ingley, E., Minchin, F. R., Tsai, S., Ratajczak, T. (1999) The common tetratricopeptide repeat acceptor site for steroid receptor-associated immunophilins and hop is located in the dimerization domain of Hsp90. *J Biol Chem* 274: 2682-9
6. Carrello, A., Allan, K. R., Morgan, L. S., Owen, A. B., Mok, D., Ward, K. B., Minchin, F. R., Toft, O. D., Ratajczak, T. (2004) Interaction of the Hsp90 cochaperone cyclophilin 40 with Hsc70. *Cell Stress Chaperones* 9: 167-81
7. Chen, S., Sullivan, P. W., Toft, O. D., Smith, F. D. (1998) Differential interactions of p23 and the TPR-containing proteins Hop, Cyp40, FKBP52 and FKBP51 with Hsp90 mutants. *Cell Stress Chaperones* 3: 118-29
8. Garnier, C., Lafitte, D., Tsvetkov, O. P., Barbier, P., Leclerc-Devin, J., Millot, M. J., Briand, C., Makarov, A. A., Catelli, G. M., Peyrot, V. (2002) Binding of ATP to heat shock protein 90: evidence for an ATP-binding site in the C-terminal domain. *J Biol Chem* 277: 12208-14
9. Ghildyal, P., Manchanda, R. (2004) Effects of cooling and ARL 67156 on synaptic ecto-ATPase activity in guinea pig and mouse vas deferens. *Auton Neurosci* 115: 28-34
10. Grenert, P. J., Sullivan, P. W., Fadden, P., Haystead, A. T., Clark, J., Mimnaugh, E., Krutzsch, H., Ochel, J. H., Schulte, W. T., Sausville, E., Neckers, M. L., Toft, O. D. (1997) The amino-terminal domain of heat shock protein 90 (hsp90) that binds geldanamycin is an ATP/ADP switch domain that regulates hsp90 conformation. *J Biol Chem* 272: 23843-50
11. Hackney, D. D., Jiang, W. (2001) Assays for kinesin microtubule-stimulated ATPase activity. *Methods Mol Biol* 164: 65-71
12. Harris, F. S., Shiau, K. A., Agard, A. D. (2004) The crystal structure of the carboxy-terminal dimerization domain of htpG, the *Escherichia coli* Hsp90, reveals a potential substrate binding site. *Structure* 12: 1087-97
13. Ishiwatari-Hayasaka, H., Maruya, M., Sreedhar, S. A., Nemoto, K. T., Csermely, P., Yahara, I. (2003) Interaction of neuropeptide Y and Hsp90 through a novel peptide binding region. *Biochemistry* 42: 12972-80
14. Marcu, G. M., Chadli, A., Bouhouche, I., Catelli, M., Neckers, M. L. (2000) The heat shock protein 90 antagonist novobiocin interacts with a previously unrecognized ATP-binding domain in the carboxyl terminus of the chaperone. *J Biol Chem* 275: 37181-6
15. Marcu, G. M., Schulte, W. T., Neckers, L. (2000) Novobiocin and related coumarins and depletion of heat shock protein 90-dependent signaling proteins. *J Natl Cancer Inst* 92: 242-8
16. McLaughlin, H. S., Smith, W. H., Jackson, E. S. (2002) Stimulation of the weak ATPase activity of human hsp90 by a client protein. *J Mol Biol* 315: 787-98
17. McLaughlin, H. S., Ventouras, A. L., Lobbezoo, B., Jackson, E. S. (2004) Independent ATPase activity of Hsp90 subunits creates a flexible assembly platform. *J Mol Biol* 344: 813-26
18. Miyata, Y. (2005) Hsp90 inhibitor geldanamycin and its derivatives as novel cancer chemotherapeutic agents. *Curr Pharm Des* 11: 1131-8
19. N J, X M, P L, K R, D F, G S-G, MG C, EE B, F. C. (1999) Delimitation of Two Regions in the 90-kDa Heat Shock Protein (Hsp90) Able to Interact with the Glucocorticosteroid Receptor (GR). *Experimental Cell Research* 247: 461-474

20. Nadeau, K., Das, A., Walsh, T. C (1993) Hsp90 chaperonins possess ATPase activity and bind heat shock transcription factors and peptidyl prolyl isomerases. *J Biol Chem* 268: 1479-87
21. Obermann, M. W, Sondermann, H., Russo, A. A, Pavletich, P. N, Hartl, U. F (1998) In vivo function of Hsp90 is dependent on ATP binding and ATP hydrolysis. *J Cell Biol* 143: 901-10
22. Panaretou, B., Prodromou, C., Roe, M. S, O'Brien, R., Ladbury, E. J, Piper, W. P, Pearl, H. L (1998) ATP binding and hydrolysis are essential to the function of the Hsp90 molecular chaperone in vivo. *Embo J* 17: 4829-36
23. Pirkel, F., Buchner, J. (2001) Functional analysis of the Hsp90-associated human peptidyl prolyl cis/trans isomerases FKBP51, FKBP52 and Cyp40. *J Mol Biol* 308: 795-806
24. Prodromou, C., Roe, M. S, O'Brien, R., Ladbury, E. J, Piper, W. P, Pearl, H. L (1997) Identification and structural characterization of the ATP/ADP-binding site in the Hsp90 molecular chaperone. *Cell* 90: 65-75
25. Prodromou, C., Siligardi, G., O'Brien, R., Woolfson, N. D, Regan, L., Panaretou, B., Ladbury, E. J, Piper, W. P, Pearl, H. L (1999) Regulation of Hsp90 ATPase activity by tetratricopeptide repeat (TPR)-domain co-chaperones. *Embo J* 18: 754-62
26. Prodromou, C., Pearl, H. L (2003) Structure and functional relationships of Hsp90. *Curr Cancer Drug Targets* 3: 301-23
27. Richter, K., Muschler, P., Hainzl, O., Buchner, J. (2001) Coordinated ATP hydrolysis by the Hsp90 dimer. *J Biol Chem* 276: 33689-96
28. Rowlands, G. M, Newbatt, M. Y, Prodromou, C., Pearl, H. L, Workman, P., Aherne, W. (2004) High-throughput screening assay for inhibitors of heat-shock protein 90 ATPase activity. *Anal Biochem* 327: 176-83
29. Scheibel, T., Neuhofen, S., Weikl, T., Mayr, C., Reinstein, J., Vogel, D. P, Buchner, J. (1997) ATP-binding properties of human Hsp90. *J Biol Chem* 272: 18608-13
30. Soti, C., Vermes, A., Haystead, A. T, Csermely, P. (2003) Comparative analysis of the ATP-binding sites of Hsp90 by nucleotide affinity cleavage: a distinct nucleotide specificity of the C-terminal ATP-binding site. *Eur J Biochem* 270: 2421-8
31. Taylor, P., Dornan, J., Carrello, A., Minchin, F. R, Ratajczak, T., Walkinshaw, D. M (2001) Two structures of cyclophilin 40: folding and fidelity in the TPR domains. *Structure* 9: 431-8
32. Vivian, JT., Callis a, R. (2001) Mechanisms of Tryptophan Fluorescence Shifts in Proteins. *Biophysical Journal* 80: 2093-2109
33. Ward, K. B, Allan, K. R, Mok, D., Temple, E. S, Taylor, P., Dornan, J., Mark, J. P, Shaw, J. D, Kumar, P., Walkinshaw, D. M, Ratajczak, T. (2002) A structure-based mutational analysis of cyclophilin 40 identifies key residues in the core tetratricopeptide repeat domain that mediate binding to Hsp90. *J Biol Chem* 277: 40799-809
34. Yamada, S., Ono, T., Mizuno, A., Nemoto, K. T (2003) A hydrophobic segment within the C-terminal domain is essential for both client-binding and dimer formation of the HSP90-family molecular chaperone. *Eur J Biochem* 270: 146-54
35. Yu, M. X, Shen, G., Neckers, L., Blake, H., Holzbeierlein, J., Cronk, B., Blagg, S. B (2005) Hsp90 inhibitors identified from a library of novobiocin analogues. *J Am Chem Soc* 127: 12778-9
36. Yun, G. B, Huang, W., Leach, N., Hartson, D. S, Matts, L. R (2004) Novobiocin induces a distinct conformation of Hsp90 and alters Hsp90-cochaperone-client interactions. *Biochemistry* 43: 8217-29

Chapter 5: Characterization of *C. elegans* Hsp90

5.1. Introduction

All the work relating to the *C. elegans* Hsp90 part of the project is described in this chapter. In the series of experiments outlined, two different protein constructs were used in an attempt to compare and contrast the roles of the N and C-terminal domains in their interactions with potential partner proteins or ligands. The constructs were full length *C. elegans* Hsp90 (ceHsp90) and C-terminal Hsp90 (ceHsp90-492). The aims of the study were to explore the interaction of the proteins with immunophilins such as Cyp40 and also with a number of small ligands, including ATP, geldanamycin and novobiocin. One of the aims of this part of the project was to mirror some of the experiments described in Chapter 4, utilising full-length protein from a different species in an attempt to shed more light onto the nature of the interaction between Hsp90 molecules and their partner proteins/ligands. The results of this study could potentially be very interesting and could help to unravel the properties of Hsp90. Such information could be useful in many ways including crystallization trials of the protein both free and with bound ligand.

The *C. elegans* Hsp90 constructs were either made in-house or with the help of Dr Tony Page from Wellcome Centre for Molecular Parasitology, The Anderson

College, University of Glasgow who also kindly supplied the *C. elegans* cDNA. The constructs chosen are shown in Figure 3.1 and Table 3.1 displayed in Chapter 3. The full length was purified and supplied by Sandra Bruce which is in the same laboratory as the author. The cloning, expression and purification protocols for the C-terminal proteins were described in Chapter 3, section 3.2.1 and 3.2.2. *C. elegans* has provided many genetic insights into the highly conserved signalling pathways. The Hsp90 ortholog in *C. elegans* has been identified as *daf-21*. The protein is approximately 74% identical to human Hsp90 α [8]. As mentioned earlier, this chapter is focused on the results obtained from two different constructs of the *C. elegans* Hsp90, the C-terminal domains individually as well as full length *C. elegans daf-21*.

5.2. Material and methods

5.2.1. Gel filtration and mass spectroscopy to confirm the identities and oligomeric properties of the *C.elegans* Hsp90 proteins

5.2.1.1. Gel filtration

The oligomeric form of the proteins was investigated by running 50 μ M of the proteins through a Superdex 200 column (Amersham) using an AKTA FPLC. The elution volumes of the proteins were measured and the predicted size of the molecule was calculated from the calibration curve as outlined in Chapter 4.

5.2.1.2. Mass spectroscopy

The proteins were also sent to EPIC for mass spectroscopy analysis to confirm the identity and the mass of the proteins. The method employed was the same as that described in Chapter 4

5.2.2. Study of the interaction of *C.elegans* Hsp90 with bovine Cyp40 by intrinsic Trp fluorescence and Surface Plasmon Resonance (SPR)

5.2.2.1. Trp fluorescence

1 μ M of ceHsp90 or ceHsp90-492 was mixed with an increasing concentration of Cyp40 to a total volume of 200 μ l. The mixtures were incubated at room temperature for 30 min prior to the fluorescence measurements being taken. The measurements were carried out with excitation at 295 nm and emission at 350 nm. The emissions from individual concentrations of Cyp40 alone were also measured. The emissions of the complex were corrected for both inner filter effects and the background fluorescence of Cyp40. The corrected emission data was plotted against the concentration of Cyp40. The curve was fitted with equations 1 and 2 and the Kd was estimated from the fitted curve.

The emission, F_{corr} , was corrected as below,

$$F_{\text{corr}} = F_{350} / e^{-2.303 \times L \times \epsilon \times [\text{Cyp40}] \times [\text{protein}]} - \text{equation 1}$$

where L is the path length of the cuvette which is 0.1 cm. ϵ is the extension coefficient at 295 nm for Cyp40 which is $6675 \text{ M}^{-1} \text{ cm}^{-1}$. $[\text{Cyp40}]$ is the concentration of Cyp40 added during the measurement and $[\text{protein}]$ is the concentration of *C. elegans* protein used in moles per litre. The curve was then fitted with equation 2 to estimate the K_d .

$$F_{\text{corr}} = F_f + (F_b - F_f) \times \left\{ \frac{(K_d + [A] + [\text{Cyp40/ligand}]) - \sqrt{((K_d + [A] + [\text{Cyp40/ligand}])^2 - (4 \times [A] \times [\text{Cyp40/ligand}]))}}{2 \times [\text{Cyp40/ligand}]} \right\} - \text{equation 2}$$

where F_f is the fluorescence of free uncomplexed protein and F_b is the fluorescence of the protein A: Cyp40/ligand complex at infinite concentration of Cyp40/ligand. At any total concentration of protein A $[A]$, F depends on the total Cyp40/ligand $[\text{Cyp40/ligand}]$ concentration and the equilibrium constant for the complex (K_d) according to equation 2.

5.2.2.2. Surface plasmon resonance (SPR)

SPR measurements were performed on a Biacore T100 instrument (Biacore Instruments Limited). ceHsp90-492 was immobilized on the CM5 sensor chip as described in Chapter 2: section 2.4.2. The sensor was loaded with the protein through the binding with primary amine. Various concentrations of Cyp40 (2 to 600 μM) were passed over the immobilized protein at a flow rate of $30 \mu\text{l min}^{-1}$ for 180s. The complex dissociated when running buffer (10 mM HEPES pH 7.4; 150 mM NaCl; 0.005% surfactant P20) was passed over the surface for 300s at $30 \mu\text{l min}^{-1}$. The surface was washed with running buffer between applications of different concentrations of Cyp40. The data was analyzed with the software supplied by Biacore.

5.2.3. The study of the interaction of *C. elegans* Hsp90 with small ligands.

It is also of great interest to study the interactions of the *C. elegans* Hsp90 with small ligands, to shed more light onto the nature of the interaction between the protein and some potentially inhibitory small molecules. The ligands that were involved are novobiocin, ATP and geldanamycin (GA). GA is known to bind and inhibit the function of Hsp90 in yeast and human [15, 16, 20, 21]. However, *C. elegans* is resistant to the drug, indicating that the *C. elegans* Hsp90 differs in some way from those species susceptible to GA[8]. Therefore, it is of great interest to investigate this property of the *C. elegans* Hsp90 using full-length *C. elegans* Hsp90 (ceHsp90) and also to further investigate the interaction with GA. Besides GA, novobiocin binds to the C-terminal Hsp90 and it is also of interest to characterize the binding of this drug to ceHsp90 and also to the ceHsp90-492. Interactions of ATP with a number of Hsp90 constructs have been reported in the literature, similar studies have been undertaken in this series of experiments using *C. elegans* Hsp90. The availability of a number of different lengths of constructs covering both the full length and C-terminal domains of the proteins has allowed further characterisation of the site of interaction of ATP with the ceHsp90. It is to be hoped that the results of such studies will provide an understanding of the interaction and may prove useful in attempts to crystallize the protein. The techniques used for these studies were intrinsic Trp fluorescence as well as ATPase activity assays using the malachite green method.

5.2.3.1. Intrinsic Trp fluorescence

Increasing concentrations of the ligands were titrated into a 1 μM solution of protein. The buffers for the experiments were dependent on the ligands used. Basically, the buffer consists of 100 mM Tris pH 7.5 and 50 mM NaCl. 0.1% DMSO was added to the buffer to increase the solubility of GA. The experiment was carried out using a 3 ml cuvette. The fluorescence was measured by using Fluoromax-3 (Jobin Yvon, Hariba). The measurement was carried out by excitation at 295 nm and emission at 355 nm. The emission produced by the increasing ligand concentration alone was also measured. The emission fluorescence was corrected against the following: the dilution factor, inner filter effects and background fluorescence using equation 1 in section 5.2.2, with a few amendments. The amendments were as follows: L is 0.5 cm; ϵ is the extinction coefficients of GA. For the ATP titration experiment; negligible background and no inner filter effect was observed, therefore no correction except for the dilution factor was required for the data. The graph was plotted and the curve was fitted with equation 2 in section 5.2.2. However, for the Trp fluorescence using Novobiocin, two binding sites equation (equation 3) was used instead of equation 2 above.

$$F_{\text{obs}} = F_f - \left[\frac{(F_c)}{2} \times \left(\left\{ (K_{d1st} + [A/2] + [\text{novobiocin}]) - \sqrt{((K_{d1st} + [A/2] + [\text{novobiocin}])^2 - (4 \times [A/2] \times [\text{novobiocin}]))} \right\} / 2 \times [A/2] \right) + \left\{ (F_b \times [\text{novobiocin}] / (K_{d2nd} + [\text{novobiocin}])) \right\} \right] \text{---equation 3}$$

where F_f is the fluorescence of free un-complexed protein and F_c is the fluorescence of protein A:novobiocin complex at certain concentration of novobiocin on the first binding site. F_b is the fluorescence of compound A:novobiocin complex at infinite concentration of novobiocin on the second binding site. At any total concentration of compound A $[A]$ concentration, F_{obs} depends on the total novobiocin[novobiocin] concentrations and the equilibrium constants of both the binding sites (K_{d1st} and K_{d2nd}) for the complex

5.2.3.2. Malachite green ATPase activity assay

The assays were performed in Eppendorf tubes at 37°C. 5 to 10 μ M of the protein was mixed with a series of ATP concentrations (0.15 to 2mM) for 30min for ceHsp90 or 60 min for ceHsp90-492. The reaction was also carried out using the same ATP concentrations in the absence of any protein to check for ATP self hydrolysis. The reaction time (30 or 60 min) was determined from previous assays that measured the activity of a single concentration of ATP against a fixed concentration of protein over 15 to 120 min. The reactions were stopped by the addition of 320 μ l of malachite green solution (Upstate, UK), mixed well and left at room temperature. 50 μ l of 34% (w/v) of sodium citrate was added to the mixture which was left for an additional 15 minutes. The absorbance of each of the samples at 620 nm were then measured. The amount of the phosphate released was obtained by using the phosphate standard curve derived earlier. The amount of phosphate released was subtracted from the amount of phosphate released by self hydrolysis of ATP (background). The rates of ATPase activity (in

Mmin⁻¹) of the protein at individual ATP concentrations were calculated and a curve was plotted. The curve was fitted using equation 4.

$$\text{Rates (M min}^{-1}\text{)} = (K_{\text{cat}} \times [\alpha 521]) \left(\frac{[\text{ATP}]}{K_m + [\text{ATP}]} \right) \text{ - equation 4}$$

5.2.3.3. ATPase inhibition assays

The *C. elegans* Hsp90 protein was mixed with a series of concentrations of novobiocin or geldanamycin followed by incubation at 37°C for 30 min. The ATPase assay was carried out using the mixtures after the incubation period. The final concentrations of protein and ATP used were 5 μM and 1 mM respectively. The final concentrations of novobiocin used varied from 1-100 μM. GA concentrations used in the assay was only up to 200 μM. The data was treated as in section 5.2.3.2 although the rates were expressed in relative percentage ATPase activity, assuming the rates of activity in the absence of the inhibitors as 100%. The graph of the relative percentage rates obtained against novobiocin/ geldanamycin concentrations was plotted. This graph was fitted with equation 5 to give the IC₅₀. Based on the IC₅₀, the inhibitor dissociation constant was calculated using equation 6.

$$\text{Rates (\% ATPase activity)} = (\text{rates}_{\infty} + (\text{rates}_{\text{mit}} - \text{rates}_{\infty})) \left(1 + \left(\frac{[\text{novobiocin}]}{\text{IC}_{50}} \right)^1 \right) \text{ - equation 5}$$

$$K_i = \text{IC}_{50} / \left(1 + \left(\frac{[\text{ATP}]}{K_m} \right) \right) \text{ - equation 6}$$

5.2.3.4. Surface plasmon resonance (SPR)

SPR measurements were performed on a Biacore T100 instrument (Biacore Instruments Limited). CeHsp90-492 was immobilized on the CM5 sensor chip as described in Chapter 2: section 2.4.2. The sensor was loaded with the protein through the binding with primary amine. Various concentrations of Cyp40 (50 to 800 μM) were passed over the immobilized protein at a flow rate of 30 $\mu\text{l min}^{-1}$ for 180s. The complex dissociated when running buffer (10 mM HEPES pH 7.4; 150 mM NaCl; 0.005% surfactant P20) was passed over the surface for 300s at 30 $\mu\text{l min}^{-1}$. The surface was washed with running buffer between applications of different concentrations of Cyp40. The data was analyzed with the software supplied by Biacore.

5.3. Results

5.3.1. *CeHsp90-492 forms a dimer*

CeHsp90-492 was run through a Superdex 200 column. The protein was present as one major peak that eluted at 12.9 ml, which corresponded to 133 kDa (Figure 5.1). As shown with the C-terminal domain of Hsp90 human α , the apparent molecular weight of the protein is larger than might be expected from the sequence. This is likely to be due to the protein being elongated rather than globular in shape, therefore the apparent MWT is larger. The identity of the protein was confirmed with mass spectroscopy to be

ceHsp90- 492 by carried out the trypsin digest and the profile of the digestion confirmed the identity of the protein.

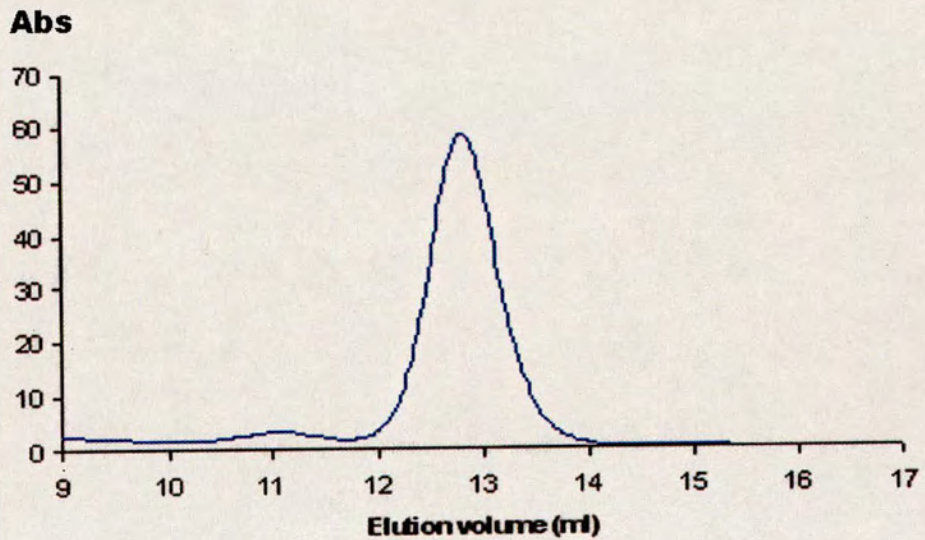


Figure 5.1. Chromatogram of the gel filtration experiment of ceHsp90 492 applied to a Superdex 200 column (Amersham). The protein has one major peak which elutes at 12.9 ml.

5.3.2. The interaction of *C. elegans* Hsp90 with bovine Cyp40

The study of the interaction involved the use of a number of techniques that have been described previously in Chapter 4. The techniques used were Trp fluorescence and Surface Plasmon Resonance (SPR).

5.3.2.1. The dissociation constants (K_d s) of the interaction between ceHsp90 and ceHsp90-492 with bovine Cyp40 determined by Trp fluorescence

Similar to the previous experiments, the Trp fluorescence was used to obtain quantitative results of the interaction such as the dissociation constant (K_d). In the experiment, increasing concentrations of Cyp40 were mixed with a fixed concentration of either ceHsp90 or ceHsp90-492. The mixtures were incubated at 25⁰C for 30 minutes. The measurements were taken by exciting the samples at 295 nm, the emissions at 350 nm were monitored. The experimental data were corrected and fitted using the equation as above in section 5.2.2. Based on the fitted data, the K_d for the interaction of the ceHsp90 with Cyp40 is $79.3 \pm 7.4 \mu\text{M}$ (Figure 5.2). The K_d of ceHsp90-492 interaction with Cyp40 was also obtained using the same protocols and the K_d is $140.3 \pm 7.9 \mu\text{M}$ (Figure 5.1).

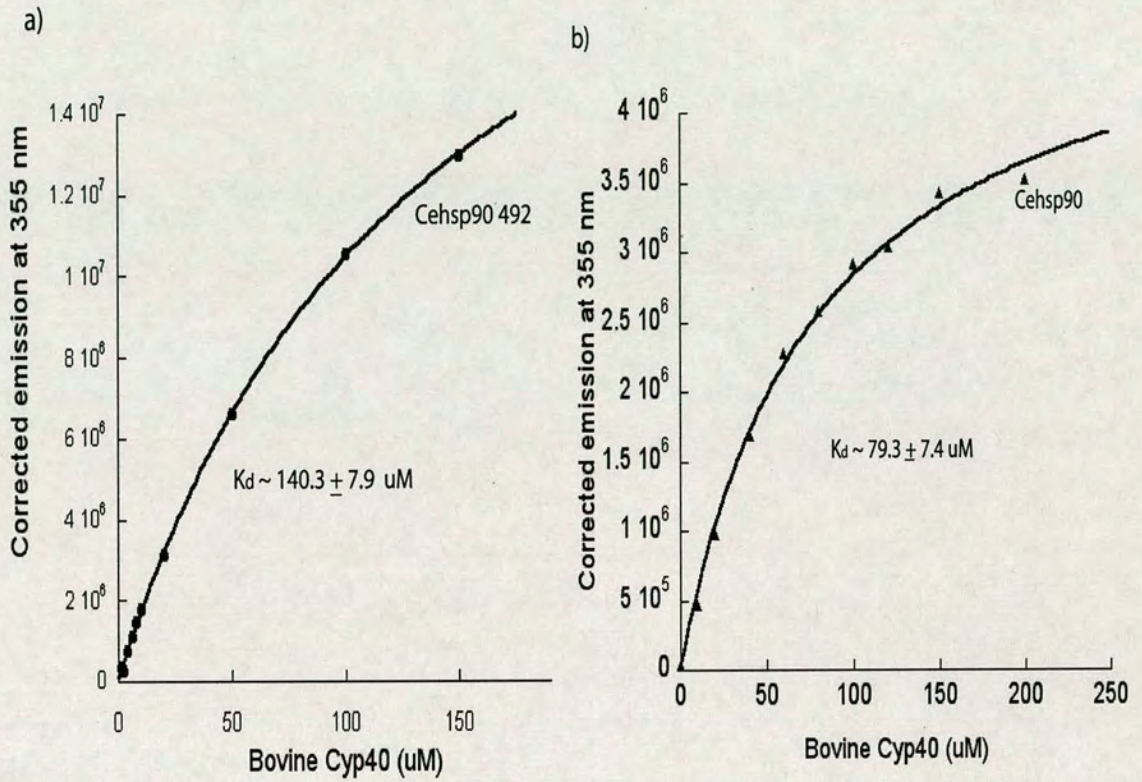


Figure 5.2. Interactions of *C. elegans* Hsp90 with bovine Cyp40. a) Trp fluorescence of CeHsp90-492 with bovine Cyp40. The curve was fitted using equation 2. The K_d obtained is $140.3 \pm 7.9 \mu\text{M}$ b) Trp fluorescence of full-length *C. elegans*. The data was treated in the same way as that above, the K_d of the interaction is $79.3 \pm 7.4 \mu\text{M}$.

5.3.2.2. The dissociation constants (K_d) of the interaction between bovine Cyp40 with ceHsp90-492 determined by SPR

SPR was also utilised to obtain the affinity of the interaction between ceHsp90-492 with bovine Cyp40. In the experiment, ceHsp90-492 protein was immobilised onto the CM5 sensor chip. The immobilisation was described in Chapter 2 section 2.4.2. Increasing concentrations of Cyp40 (50 to 800 μ M) were passed over the sensor chip containing the proteins as described in section 5.2.3.4. Each cycle was started by washing the surface of the sensor with running buffer. Then, Cyp40 was flowed over the surface and the binding was monitored through the response units (RU) and displayed as a sensorgram (Figure 5.3). The dissociation of Cyp40 was carried out by flowing the running buffer over the surface until the RU return to previous baseline (Figure 5.3). The cycle was then repeated with other concentrations of Cyp40. The graph of the RUs at steady state against concentrations of Cyp40 was plotted (Figure 5.3). The graph was then fitted with equation 7.

$$R_{eq} = (R_{eqsat} \times [Cyp40]) / ([Cyp40] + K_d^{Eq}) - \text{equation 7}$$

where R_{eq} is the equilibrium response of the interaction in RU units, R_{eqsat} is the saturated equilibrium response for the chip surface which is 3100 RU, $[Cyp40]$ is the total Cyp40 concentration in μ M and K_d^{Eq} is the equilibrium dissociation constant. The K_d^{Eq} obtained from the experiment is $107.1 \pm 18.8 \mu$ M. The on and off rates of the

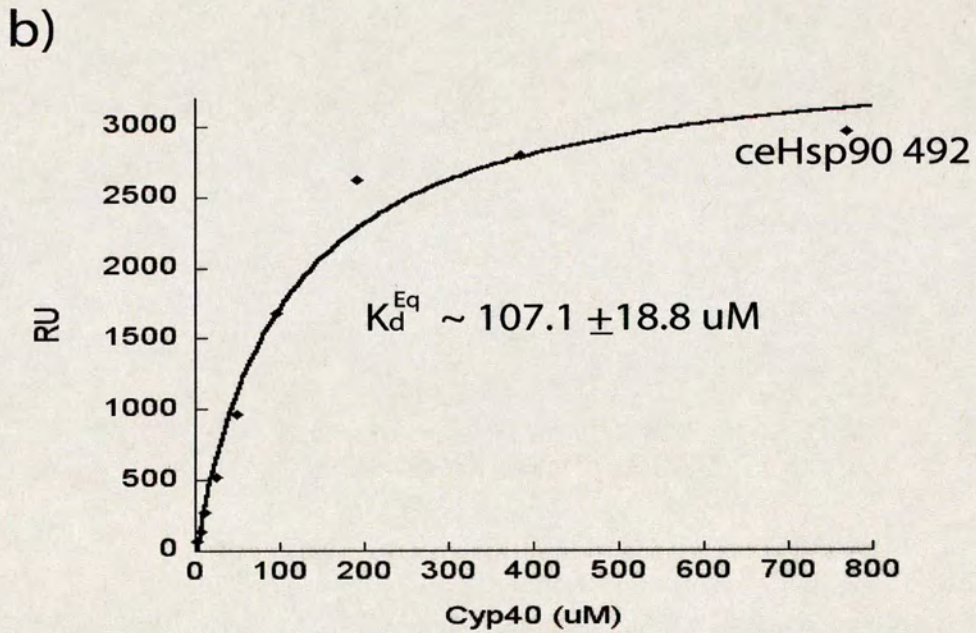
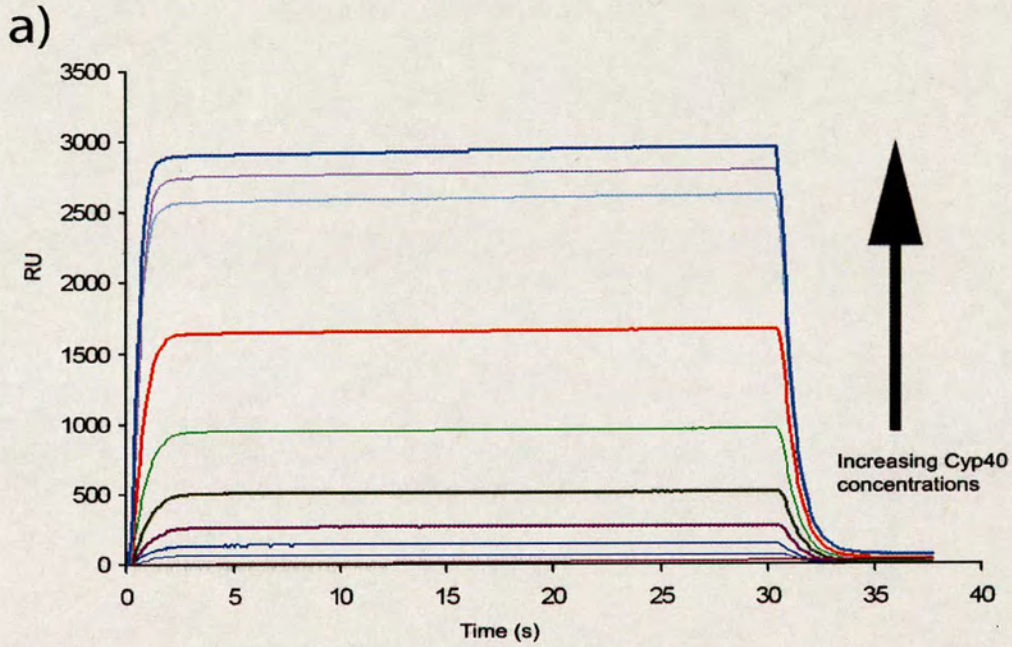


Figure 5.3. SPR of the interaction between ceHsp90-492 with Cyp40. a) Sensorgram shows the binding of increasing concentrations of Cyp40 to the surface of the sensor containing immobilised ceHsp90-492. b) The steady state plot of the RUs against the concentrations of Cyp40. The graph was fitted with equation 7 to obtain the K_d^{Eq} of $107.1 \pm 18.8 \mu\text{M}$

reaction were not available as the binding and dissociation of the complex were very rapid and can not be analysed.

5.3.3. The interaction of *C.elegans* Hsp90 with small ligands

The ligands used in the experiments were geldanamycin, novobiocin and ATP. In order to characterize the interaction of these ligands with *C. elegans* Hsp90, several techniques such as Trp fluorescence, Isothermal Titration Calorimetry (ITC) and ATPase assays were used.

5.3.3.1. Trp fluorescence showed GA bind weakly to ceHsp90

Geldanamycin (GA) is a well known ansamycin drug (Chapter 1, figure 1.16) that inhibits the N-terminal ATPase activity of Hsp90[15, 16, 20, 22]. However, *C.elegans* Hsp90 has been found to be resistant to GA following exposure of the whole nematode to the drug [8]. Affinity precipitation studies using chimeric worm-vertebrate fusion proteins or worm C-terminal truncations expressed in reticulocyte lysate revealed that the conserved nucleotide-binding fold of worm Hsp90 exhibits the novel ability to bind ATP but not GA [8]. In this study, the direct interaction between GA and the *C. elegans* Hsp90 was investigated. The study was carried out by titrating GA into a 1 μ M solution of ceHsp90. The changes in the emission at 355 nm were measured by excitation of the sample at 295 nm. The data was corrected against the inner filter effect, background and for the dilution effect. Both of the slits used throughout the experiments were set at 2.5 mm. The corrected emissions were plotted against the concentration of GA using Kaleidagraph and the curve was fitted with equation 2 as before (section

5.5.2). The K_d of the interaction of ceHsp90 to GA is very weak, $298.0 \pm 88.5 \mu\text{M}$ (Figure 5.4).

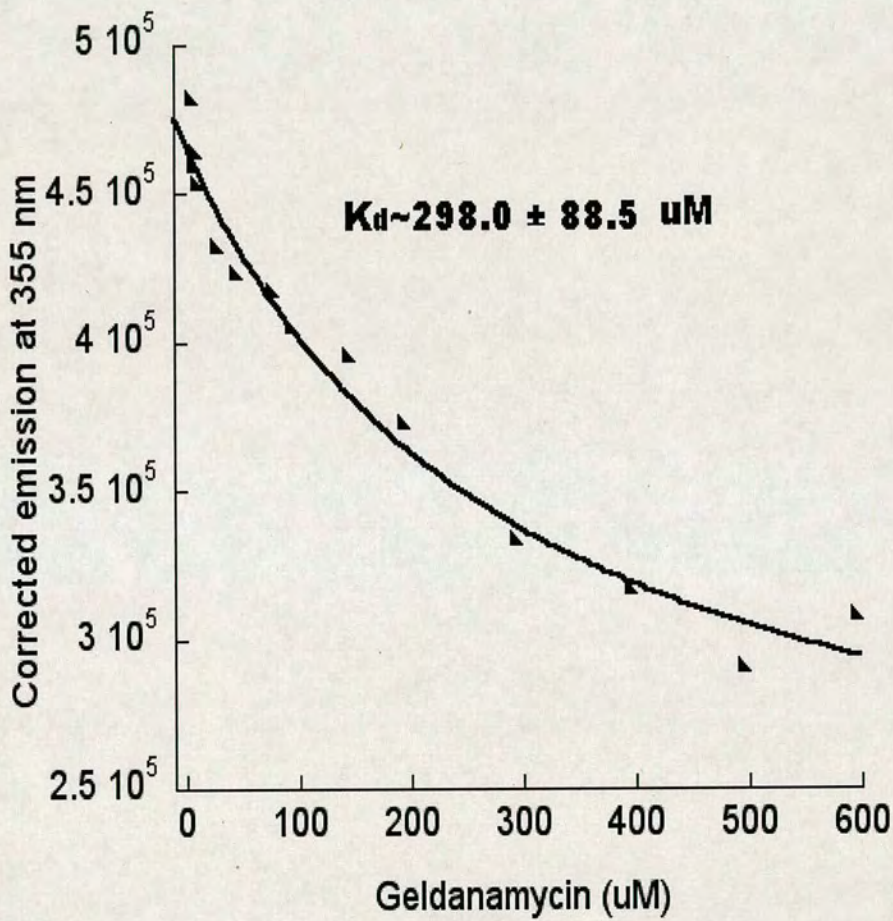


Figure 5.4. Trp fluorescence experiment of GA binding to full length *C. elegans* Hsp90. The emission data was corrected with equation 1 and fitted with equation 2. The binding was very weak with a K_d of $298.0 \pm 88.5 \mu\text{M}$

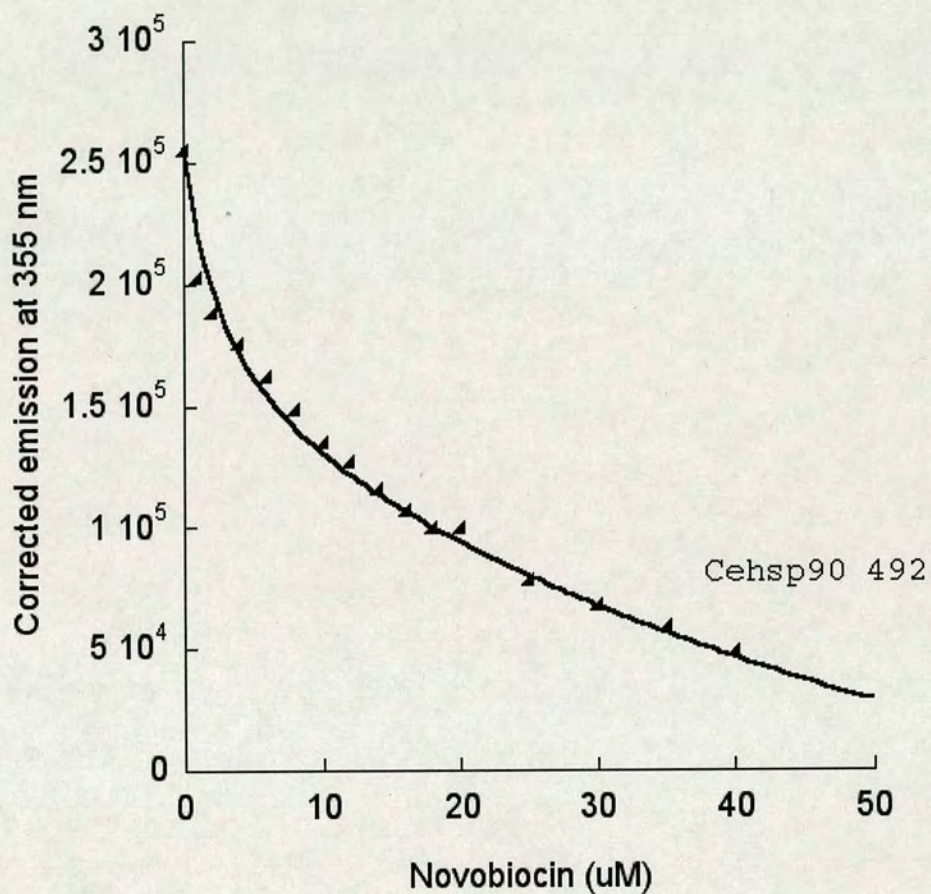


Figure 5.5. Graph of the Trp fluorescence observed upon binding between CeHsp90-492 and novobiocin. The emissions data were corrected against dilution effects, the inner filter effect and the background fluorescence of novobiocin. The data was fitted to a two site binding model using equation 3. The fitted curve gives two K_d 's indicating both specific and non specific binding of novobiocin. The specific K_d of the interaction is $2.48 \pm 1.8 \mu\text{M}$

5.3.3.2. Trp fluorescence showed novobiocin bind to ceHsp90-492

The next ligand used in the study was novobiocin. Novobiocin has been shown to bind to the C-terminal domain of Hsp90 [11, 12]. In this study, Trp fluorescence was used to monitor the interactions of ceHsp90-492. Fluorescence was carried out by exciting the samples at 295 nm and measuring the emission at 355 nm. The slits for the experiments were both set at 2.5 mm. The emission data were corrected against the inner filter effect and the background. The corrected emissions were plotted against the concentration of novobiocin and then fitted using equation 3. From the graph, the K_d of the interaction of ceHsp90-492 with novobiocin is $2.48 \pm 1.8 \mu\text{M}$ (Figure 5.5)

5.3.3.3. The interaction of ATP with both of the *C.elegans* protein constructs

In addition to the ligands discussed above, determining the nature of the interaction between *C. elegans* Hsp90 and ATP was also of great interest. The interactions of ATP with various species of Hsp90 including human and yeast are well studied and documented, however little is known as to the nature of the potential interactions with the *C. elegans* Hsp90 homolog. The data obtained from such studies could be very useful in shedding light onto the differences between species. The interaction between ceHsp90 and ATP was investigated using fluorescence as described previously. The experimental method involved exciting the samples at 295 nm and measuring the resultant emission at 355 nm. Increasing concentrations of ATP were

titrated into a 1 μ M solution of protein. The emission data were corrected only for the dilution factor as ATP did not have a

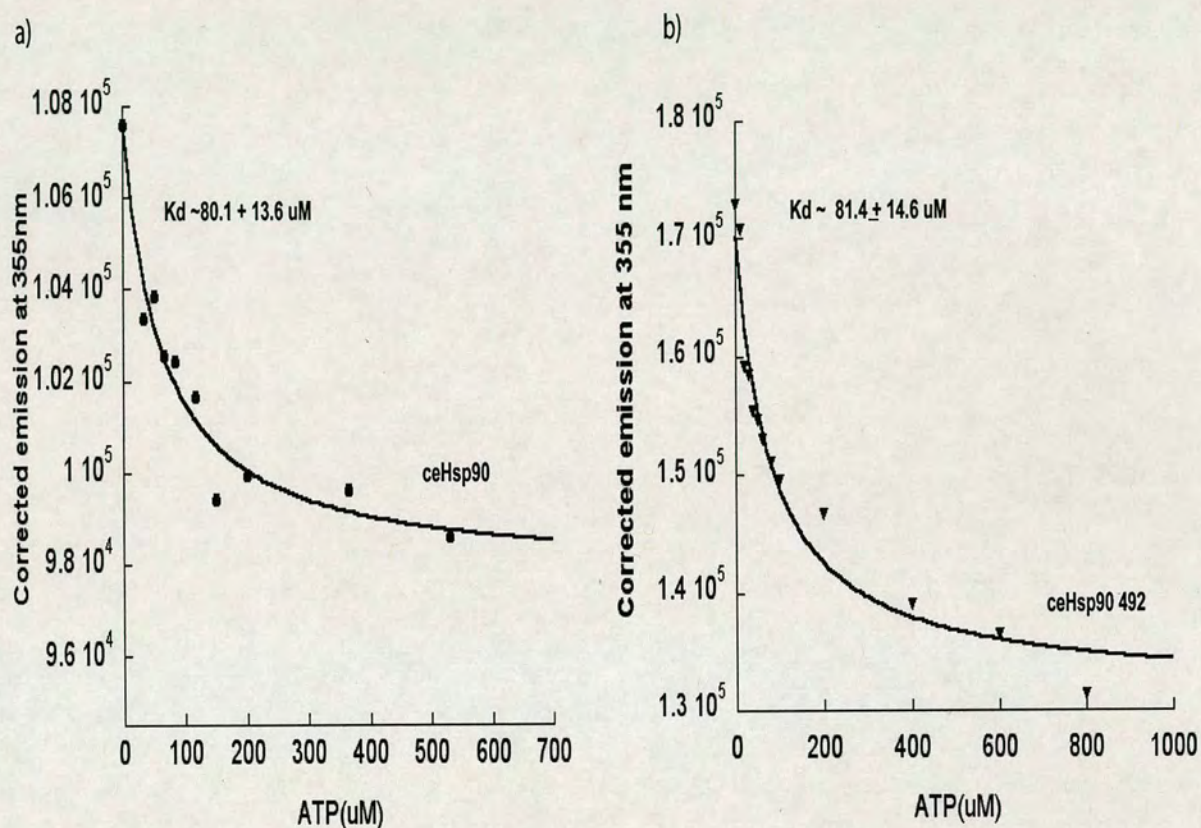


Figure 5.6. Graph of the Trp fluorescence observed upon binding of CeHsp90 with ATP. ATP was titrated into a 1 μ M solution of protein. The emissions at 355 nm were measured and corrected against the dilution factor. The data was plotted and fitted using equation 2. a) Graph of the interaction of ceHsp90 with ATP. The K_d obtained was $80.1 \pm 13.6 \mu\text{M}$. b) The graph of the interaction of ceHsp90-492 with ATP. The K_d obtained was $81.4 \pm 14.6 \mu\text{M}$.

background fluorescence and the inner filter effect was consequently negligible. The corrected emissions were plotted against the concentration of ATP and the data fitted using equation 2. From the graph, the K_d of the interaction between ceHsp90 and ATP is $80.1 \pm 13.6 \mu\text{M}$. The K_d for the interaction between the ceHsp90-492 and ATP is $81.4 \pm 14.6 \mu\text{M}$ (Figure 5.6).

5.3.3.4. ATPase activities showed in both of the *C.elegans* protein constructs

ATPase activity assays of these proteins were also carried out using the malachite green assay. The experiments were carried out at 37°C . The incubation periods were 30 min for ceHsp90 and 60 min for ceHsp90-492. Malachite green was added after the incubation period and the absorbance of each of the samples at 620 nm was measured. The absorbance at 620 nm for each concentration was subtracted from the absorbance of ATP alone without the protein. The corrected data were plotted and fitted using equation 4. The experiments were repeated three times. From the ATPase assays, the K_{cat} for ceHsp90 is $0.354 \pm 0.05 \text{ min}^{-1}$. The K_m for the reaction is $288 \pm 11.6 \mu\text{M}$ (Figure 5.6). No ATPase activity was detectable when the experiment was repeated in the absence of Mg^{2+} in the buffer suggesting that Mg^{2+} was needed to coordinate the hydrolysis of ATP. The ATPase assay was also used to characterise the activity of ceHsp90-492, the K_{cat} of this reaction was $0.010 \pm 0.00013 \text{ min}^{-1}$ and the K_m is $327 \pm 0.12 \mu\text{M}$ (Figure 5.7).

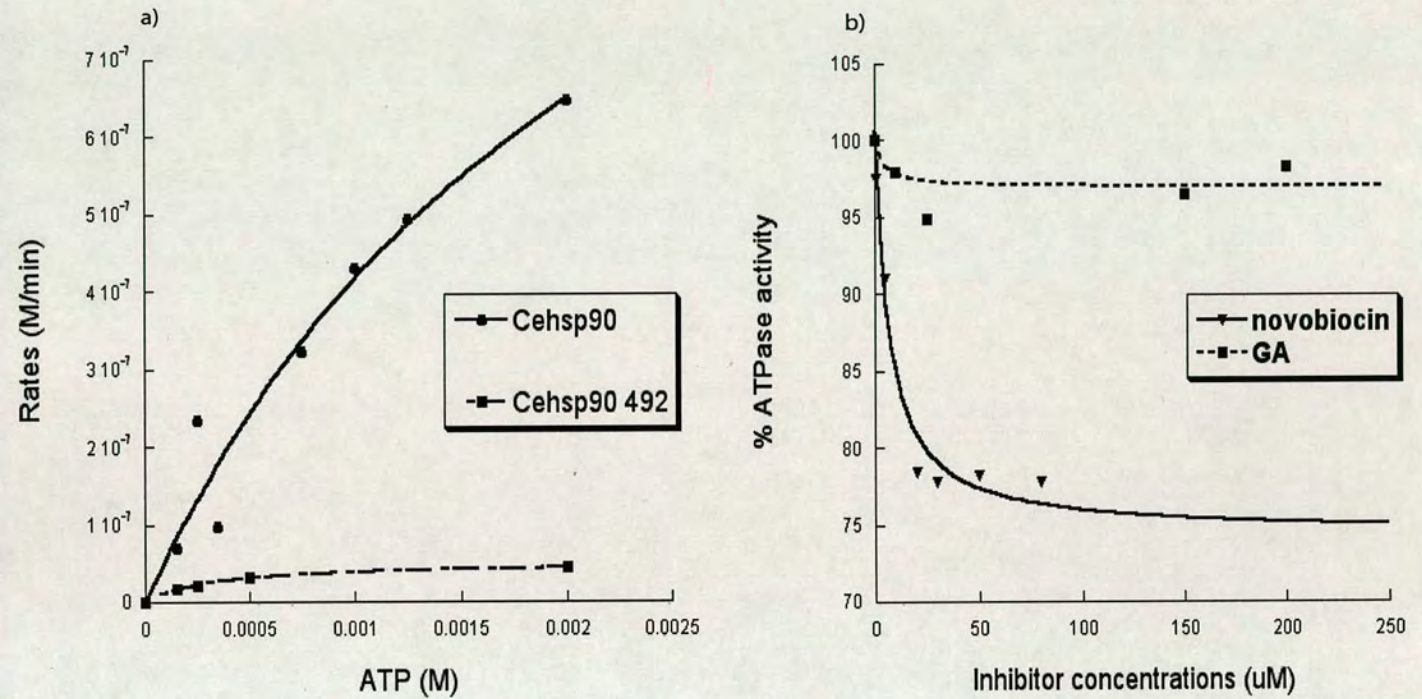


Figure 5.7. The ATPase activity of *C. elegans* protein and its inhibition of by novobiocin and geldanamycin. a) The ATPase activity of ceHsp90 and ceHsp90-492 was determined using the malachite green assay. The K_{cat} for ceHsp90 is $0.354 \pm 0.05 \text{ min}^{-1}$. The K_m for the reaction is $288 \pm 11.6 \mu\text{M}$. The K_{cat} for ceHsp90-492 was $0.010 \pm 0.00013 \text{ min}^{-1}$ and the K_m is $327 \pm 0.12 \mu\text{M}$. b) The inhibition of ceHsp90 ATPase activity by novobiocin and GA. No significant inhibition was observed when GA was used. Inhibition of the ATPase activity was observed when novobiocin was used. The IC_{50} determined from the inhibition data gives a value of $6.61 \pm 2.48 \mu\text{M}$, the K_i of the reaction was $1.48 \pm 0.55 \mu\text{M}$.

5.3.3.5. The inhibition of ATPase activities of both of the *C. elegans* protein constructs

Novobiocin was also used in ATPase inhibition experiments with both of the available constructs. In addition to the experiments with novobiocin, GA was also used to investigate inhibition of ceHsp90 ATPase activity despite a recent report [8] that this protein was resistant to the drug. Approximately 25 % of the ceHsp90 ATPase activity was inhibited by novobiocin (Figure 5.7). The IC_{50} determined from such an inhibition gives a value of $6.61 \pm 2.48 \mu\text{M}$. The IC_{50} was obtained by fitting the curve of the relative percentage rates of ATPase activity with equation 5. Using equation 6, the K_i of the reaction was determined to be $1.48 \pm 0.55 \mu\text{M}$. ATPase activity of ceHsp90-492 was 80% inhibited by novobiocin (Figure 5.8) at maximum concentration of $50 \mu\text{M}$. The IC_{50} of the inhibition was $15.1 \pm 4.9 \mu\text{M}$. Based on the IC_{50} , the calculated K_i was $3.7 \pm 1.2 \mu\text{M}$. No such inhibition of ATPase activity was observed when GA was tested in the same assay system (Figure 5.7). The concentration of GA used ranged from 1 to a maximum of $200 \mu\text{M}$.

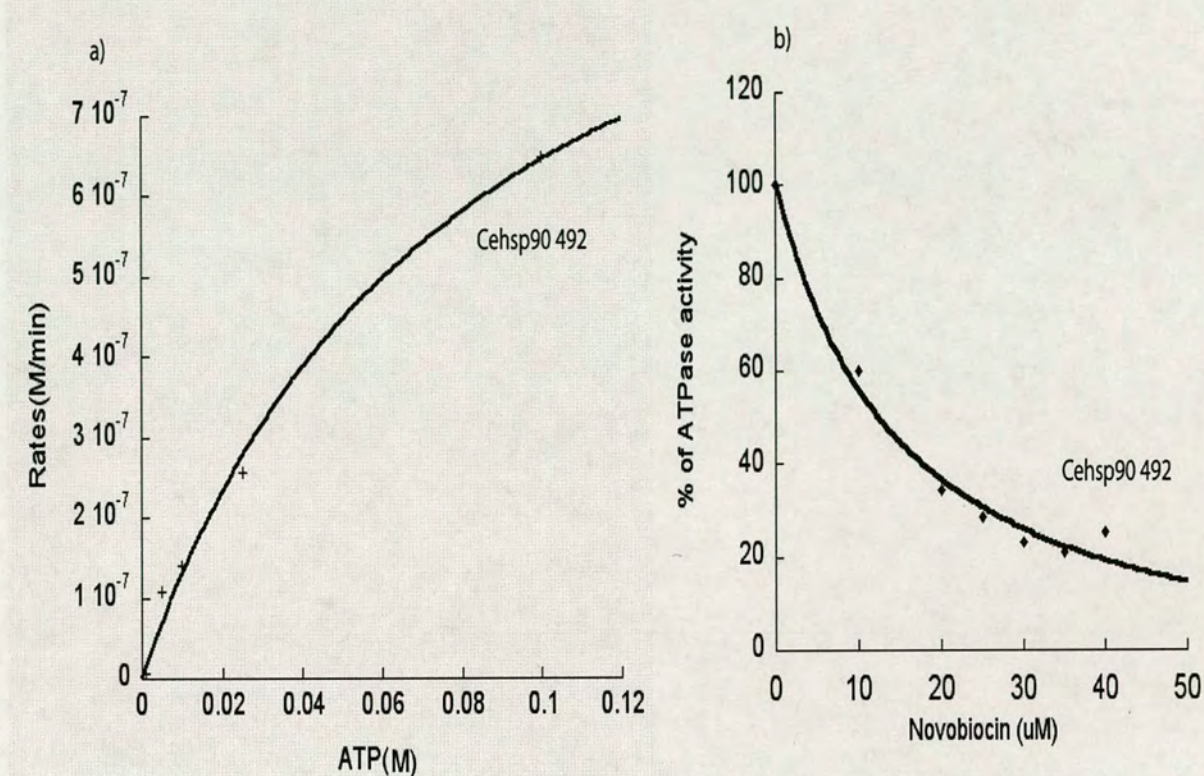


Figure 5.8. ATPase activity and inhibition of ceHsp90-492. a) The ATPase activity of ceHsp90-492 was determined using the malachite green assay method. The K_{cat} for ceHsp90-492 was $0.010 \pm 0.00013 \text{ min}^{-1}$ and the K_m is $327 \pm 0.12 \mu\text{M}$. b) Inhibition of the ATPase activity of ceHsp90-492 with novobiocin. The IC_{50} of the inhibition was $15.1 \pm 4.9 \mu\text{M}$. Based on the IC_{50} , the calculated K_i was $3.7 \pm 1.2 \mu\text{M}$.

5.3.4. Crystallization trials of *C.elegans* Hsp90 proteins

All the proteins were subjected to crystallization trials using the hanging drop vapour diffusion method as outlined in Chapter 2, section 2.5.1. The plates initially set up explored a range of possible precipitants including AS, various PolyEthyleneGlycols

(PEGs) and a number of commercially available screening kit such as Structure screens 1 and 2 (MDL), Premier, Classic and PEGS from (Nextal). The crystallization trials, unfortunately did not produce any crystals. Crystalline precipitate was observed in a number of drops, however optimization of the conditions around those producing crystalline precipitate still did not yield any crystals.

5.4. Discussion

5.4.1. CeHsp90-492 exists as a dimer

As mentioned before, this chapter outlines the series of experiments used to investigate and characterise *C. elegans* Hsp90. The experimental design was similar to that used in Chapter 4 section 4.2.3 when characterising the C-terminal domain of Hsp90 human α . There were however a number of significant differences in the approach taken between the two series of experiments, these will be discussed in greater detail later in this chapter. The purified proteins were produced as described in Chapter 3, section 3.2.4. Gel filtration experiments of the ceHsp90-492 using a Superdex 200 column showed that the protein was running with an estimated molecular weight much larger than the sequence alone would have suggested (Figure 5.1), likely indicative of the protein having a more elongated shape rather than a compact globular shape, similar to the situation seen with human hHsp90- α 521. It has been suggested that Hsp90 is an

asymmetrical and oblong molecule [23] Recent structural studies have shown that the structure of the C-terminal of yeast Hsp90 was almost identical with the structure of htpG [1, 10]. In both structures, the dimerisation domain is contributed by two helices in the region from 584 to 624 in htpG and region 632 to 677 in yeast Hsp90. In addition, residues 587-610 of yeast Hsp90 are also involved in the formation of dimer. Sequence alignments between the yeast Hsp90 and ceHsp90 showed that the dimerisation motif was conserved, thus suggesting ceHsp90-492 exists as a dimer.

5.4.2. *C. elegans* Hsp90 binds to Cyp40

C. elegans Hsp90 or *daf-21* shares with the human protein the presence of the MEEVD motif at the extreme C-terminus of the protein. These residues have been shown to be important in the binding of Hsp90 to the TPR containing proteins [3, 6, 7] including Cyp40 [4, 24], Sti1 [9, 18], PP5 [7] and many others. Cehsp90 and ceHsp90-492 were shown to bind to Cyp40 based upon the results of the Trp fluorescence experiments. CeHsp90 interacts with Cyp40 with a K_d of $79.3 \pm 7.4 \mu\text{M}$ whereas ceHsp90-492 interacts with Cyp40 with a K_d of $140.3 \pm 7.9 \mu\text{M}$.(Table 5.1). The binding of ceHsp90- 492 with Cyp40 was also shown by the SPR. The K_d^{Eq} of the reaction was $107.1 \pm 18.8 \mu\text{M}$. The K_d^{Eq} from SPR was in agreement with the K_d from Trp fluorescence. However, the on and off rate of as well as the kinetic dissociation constant of the binding were unavailable. This is due to the rapid association and dissociation of the complex where it is not possible to monitor them. It is shown from the experiments above; that binding of full length *daf-21* to Cyp40 was tighter than the

binding seen with the C-terminal domain alone. These results showed that the interaction was not only caused by the C-terminal alone but it can be enhanced by the wild type protein thus, suggesting there is cooperation between other regions in the N and middle domains of *C. elegans* Hsp90 that are involved in the promotion of the interaction between Hsp90 and its partner proteins. Inter domain co-operation could result in an altered conformation of the full length protein having greater affinity to Cyp40. The effect of conformational flexibility was observed in the binding of p23 to Hsp90 where the proteins can only interact when Hsp90 has ATP bound [1, 5, 26]. ATP binding to Hsp90 is also affected by the conformation changes seen when Hsp90 converts from dimer to monomer [14].

5.4.3. *C. elegans* Hsp90 binds ATP and exhibits ATPase activity

As expected, ceHsp90 exhibited binding to ATP similar to that seen in other species such as yeast Hsp90 [14, 16] and human Hsp90 α [13 17, 18] The K_d of the interaction of ceHsp90 with ATP is $80.1 \pm 13.6 \mu\text{M}$.(Table 5.1) The K_d was obtained by fitting the curve with an equation using a single binding site model. The curve was also fitted using a two binding sites model equation which gave a very similar K_d but with a large error. There is also evidence that shows the second binding site at the C-terminal was hidden and only open when the N-terminal site was occupied [21]. Thus, suggested that, sequential binding occurs in the interaction. Observations from the data obtained in this series of experiments comparing the interactions of the ceHsp90 and ceHsp90-492 suggested that the binding of ATP could occur sequentially between N and C-terminal

domains. However, Trp fluorescence measurement were of limited value in detecting sequential binding events, by simply fitting the curve with a two sites binding model equation did not provide strong evidence to support the model. Further experiments with the aim of confirming the sequential binding events were carried out by using isothermal titration calorimetry (ITC). However, the energy difference between the titrations was too small to be used for analysing the interaction.

5.4.4. Inhibition of the ATPase activity

The K_d obtained here was lower than that observed for Hsp90 human α , which is $240 \pm 14 \mu\text{M}$ (from stop flow fluorescence experiments) [13, 14] and also for yeast ($132 \pm 47 \mu\text{M}$) [14] which suggested that the interaction was slightly tighter with ceHsp90. The ATPase activity of ceHsp90 by malachite green assay showed a K_{cat} of $0.354 \pm 0.05 \text{ min}^{-1}$ which is slower than yeast Hsp90 that has a K_{cat} of 0.4 min^{-1} [15, 16] but faster than human Hsp90 which is 0.092 min^{-1} [14]. In the yeast Hsp90 ATPase cycle, it has been proposed that the binding or the resultant conformational change of Hsp90 is the rate limiting step [25]. However, there is also a finding suggesting that the cleavage of ATP is the rate limiting step in the Hsp90 ATPase cycle [14]. Our results show that ATPase activity was increased from human Hsp90 to ceHsp90/yeast and their binding affinity to ATP also increased suggesting that the binding of ATP probably helps to facilitate the ATPase cycle to become faster than the full length human Hsp90 α .

ATPase activity was also detected in the ceHsp90-492 construct but at a very low level. The ATPase activity at the C-terminus is only 5% of that seen with the whole protein. Indirectly, this is also supported by the facts that the C-terminal Hsp90 also binds to ATP [11, 12]. Our results also showed that 25% of the ATPase activity of the full length protein can be inhibited by novobiocin. Further experiments showed that novobiocin inhibited 80% of the ceHsp90-492 ATPase activity. Previous studies showed that novobiocin can disrupt the Hsp90 dimer formation [2]. Therefore it is likely that the 25% inhibition observed was probably as a result of the disruption of the dimer of Hsp90. However, the inhibitor constants (K_i) obtained from 25% of the inhibition is $1.48 \pm 0.55 \mu\text{M}$ and is very similar to the K_d of novobiocin binding to ceHsp90-492 (as determined by fluorescence) which is $2.48 \pm 1.8 \mu\text{M}$ (Table 5.1). In agreement with this, the K_i obtained from the C-terminal of *daf21* (ceHsp90-492) ATPase inhibition was $3.7 \pm 1.2 \mu\text{M}$ (Table 5.1) which is once again very similar to the other dissociation constants derived from this series of experiments. Only 20% of the C-terminal Hsp90 dimer was disrupted at $100 \mu\text{M}$ of novobiocin [2], but from our results 80% of the ATPase activity was inhibited when $50 \mu\text{M}$ of novobiocin is used. This suggested that the ATPase inhibition of the full length or the C-terminal Hsp90 was mainly caused by the binding of novobiocin to the same site for ATP. However, the disruption of dimer formation can also contribute to the ATPase inhibition especially if a high concentration of novobiocin was used.

The effect of GA on the ceHsp90 ATPase activity was also investigated, but no effect was seen at the concentrations tested. Previous studies [8] indicated that the *C.elegans* Hsp90 was resistant to GA. This study showed that immobilized GA did not

bind to *daf-21*. In order to further investigate the interaction of ceHsp90 and GA, Trp fluorescence was used to examine the effect of titrating the drug into ceHsp90. Surprisingly, GA binds to ceHsp90 with K_d of $298.0 \pm 88.5 \mu\text{M}$ (Table 5.1). The binding was very weak and the ATPase inhibition was only tested up to $200 \mu\text{M}$ of GA which not enough to inhibit the ATPase activity. GA binds to yeast Hsp90 with a K_d of $1.2 \mu\text{M}$ [19]. Yeast Hsp90 ATPase activity was also 50% inhibited by GA with IC_{50} of $4.8 \pm 0.8 \mu\text{M}$ [20].

5.5. Conclusion

In this chapter the results of the biochemical and biophysical characterisation of both full length *cehsp90* and its C-terminal domain are presented. The interaction with immunophilins showed that the full length protein binds more tightly to its partner protein than the C-terminal domain alone suggesting there is cooperation between domains. In addition, full length protein was also properly folded which contributes to the better interaction with immunophilins compare to the C-terminal domain alone. The ATPase activity of the wild type was reduced by novobiocin which disrupts the dimer formation and inhibits the C-terminal domain ATPase activity. GA was shown to bind weakly to the *C. elegans* Hsp90 and did not inhibit the ATPase activity at concentration of GA up to $200 \mu\text{M}$, this is consistent with inhibitor not working very well to inhibit *C. elegans* Hsp90. The findings will help provide in understanding of the structural and

functional properties of *C. elegans* Hsp90. Table 5.1 summarises the results obtain in Chapter 5.

Protein	T (°C)	Ligand or inhibitor	Methods	K _d (μM)	IC50/Ki(μM)	K _m (μM)	k _{cat} (min ⁻¹)	Figure
ceHsp90-492	25	ATP	Trp fluorescence	81.4 ± 14.6				5.6
	37	ATP	Malachite green ATPase assay			327 ± 0.12	0.010 ± 0.00013	5.7 & 5.8
	25	Novobiocin	Trp fluorescence	2.48 ± 1.8				5.5
	37	Novobiocin	Malachite green ATPase assay		15.1 ± 4.9/ 3.7 ± 1.2			5.8
	25	Cyp40	Trp fluorescence	140.3 ± 7.9				5.2
	25	Cyp40	SPR	107.1 ± 18.8				5.3
ceHsp90	25	ATP	Trp fluorescence	80.1 ± 13.6				5.6
	37	ATP	Malachite green ATPase assay			288 ± 11.6	0.354 ± 0.05	5.7
	25	Novobiocin	Trp fluorescence					
	37	Novobiocin	Malachite green ATPase assay		6.61 ± 2.48/ 1.48 ± 0.55			5.7
	25	Geldanamycin	Trp fluorescence	298 ± 88.5				5.4
	37	Geldanamycin	Malachite green ATPase assay		No inhibition			5.7
	25	Cyp40	Trp fluorescence	79.3 ± 7.4				5.2

Table 5.1. List of the results obtained from all the experiments carried out to the *C. elegans* Hsp90 in chapter 4

References:

1. Ali, M. M, Roe, M. S, Vaughan, K. C, Meyer, P., Panaretou, B., Piper, W. P, Prodromou, C., Pearl, H. L (2006) Crystal structure of an Hsp90-nucleotide-p23/Sba1 closed chaperone complex. *Nature* 440: 1013-7
2. Allan, K. R, Mok, D., Ward, K. B, Ratajczak, T. (2006) The carboxy-terminal domain Of Hsp90: Modulation of chaperone function and cochaperone interaction by novobiocin. Evidence that coumarin antibiotics disrupt Hsp90 dimerization. *J Biol Chem*
3. Brinker, A., Scheufler, C., Mulbe VD, F., Fleckenstein, B., Herrmann, C., Jung, G., Moarefi, I., Hartl, U. F (2002) Ligand discrimination by TPR domains. Relevance and selectivity of EEVD-recognition in Hsp70 x Hop x Hsp90 complexes. *J Biol Chem* 277: 19265-75
4. Carrello, A., Allan, K. R, Morgan, L. S, Owen, A. B, Mok, D., Ward, K. B, Minchin, F. R, Toft, O. D, Ratajczak, T. (2004) Interaction of the Hsp90 cochaperone cyclophilin 40 with Hsc70. *Cell Stress Chaperones* 9: 167-81
5. Chen, S., Sullivan, P. W, Toft, O. D, Smith, F. D (1998) Differential interactions of p23 and the TPR-containing proteins Hop, Cyp40, FKBP52 and FKBP51 with Hsp90 mutants. *Cell Stress Chaperones* 3: 118-29
6. Cheung-Flynn, J., Roberts, J. P, Riggs, L. D, Smith, F. D (2003) C-terminal sequences outside the tetratricopeptide repeat domain of FKBP51 and FKBP52 cause differential binding to Hsp90. *J Biol Chem* 278: 17388-94
7. Cliff, J. M, Williams, A. M, Brooke-Smith, J., Barford, D., Ladbury, E. J (2005) Molecular recognition via coupled folding and binding in a TPR domain. *J Mol Biol* 346: 717-32
8. David, L. C, Smith, E. H, Raynes, A. D, Pulcini, J. E, Whitesell, L. (2003) Expression of a unique drug-resistant Hsp90 ortholog by the nematode *Caenorhabditis elegans*. *Cell Stress Chaperones* 8: 93-104
9. Flom, G., Weekes, J., Williams, J. J, Johnson, L. J (2005) Effect of mutation of the TPR and DP2 domains of Sti1 on Hsp90 signaling and interaction in *Saccharomyces cerevisiae*. *Genetics*
10. Harris, F. S, Shiau, K. A, Agard, A. D (2004) The crystal structure of the carboxy-terminal dimerization domain of htpG, the *Escherichia coli* Hsp90, reveals a potential substrate binding site. *Structure* 12: 1087-97
11. Marcu, G. M, Chadli, A., Bouhouche, I., Catelli, M., Neckers, M. L (2000) The heat shock protein 90 antagonist novobiocin interacts with a previously unrecognized ATP-binding domain in the carboxyl terminus of the chaperone. *J Biol Chem* 275: 37181-6
12. Marcu, G. M, Schulte, W. T, Neckers, L. (2000) Novobiocin and related coumarins and depletion of heat shock protein 90-dependent signaling proteins. *J Natl Cancer Inst* 92: 242-8
13. McLaughlin, H. S, Smith, W. H, Jackson, E. S (2002) Stimulation of the weak ATPase activity of human hsp90 by a client protein. *J Mol Biol* 315: 787-98
14. McLaughlin, H. S, Ventouras, A. L, Lobbezoo, B., Jackson, E. S (2004) Independent ATPase activity of Hsp90 subunits creates a flexible assembly platform. *J Mol Biol* 344: 813-26
15. Panaretou, B., Prodromou, C., Roe, M. S, O'Brien, R., Ladbury, E. J, Piper, W. P, Pearl, H. L (1998) ATP binding and hydrolysis are essential to the function of the Hsp90 molecular chaperone in vivo. *Embo J* 17: 4829-36
16. Prodromou, C., Roe, M. S, O'Brien, R., Ladbury, E. J, Piper, W. P, Pearl, H. L (1997) Identification and structural characterization of the ATP/ADP-binding site in the Hsp90 molecular chaperone. *Cell* 90: 65-75
17. Prodromou, C., Panaretou, B., Chohan, S., Siligardi, G., O'Brien, R., Ladbury, E. J, Roe, M. S, Piper, W. P, Pearl, H. L (2000) The ATPase cycle of Hsp90 drives a molecular 'clamp' via transient dimerization of the N-terminal domains. *Embo J* 19: 4383-92

18. Prodromou, C., Pearl, H. L (2003) Structure and functional relationships of Hsp90. *Curr Cancer Drug Targets* 3: 301-23
19. Roe, M. S, Prodromou, C., O'Brien, R., Ladbury, E. J, Piper, W. P, Pearl, H. L (1999) Structural basis for inhibition of the Hsp90 molecular chaperone by the antitumor antibiotics radicicol and geldanamycin. *J Med Chem* 42: 260-6
20. Rowlands, G. M, Newbatt, M. Y, Prodromou, C., Pearl, H. L, Workman, P., Aherne, W. (2004) High-throughput screening assay for inhibitors of heat-shock protein 90 ATPase activity. *Anal Biochem* 327: 176-83
21. Soti, C., Vermes, A., Haystead, A. T, Csermely, P. (2003) Comparative analysis of the ATP-binding sites of Hsp90 by nucleotide affinity cleavage: a distinct nucleotide specificity of the C-terminal ATP-binding site. *Eur J Biochem* 270: 2421-8
22. Stebbins, E. C, Russo, A. A, Schneider, C., Rosen, N., Hartl, U. F, Pavletich, P. N (1997) Crystal structure of an Hsp90-geldanamycin complex: targeting of a protein chaperone by an antitumor agent. *Cell* 89: 239-50
23. Toft, D. (1998) Recent Advances in the Study of hsp90 Structure and Mechanism of Action. *Trends in Endocrinology and Metabolism*, Issue 6, 9: 238-243
24. Ward, K. B, Allan, K. R, Mok, D., Temple, E. S, Taylor, P., Dornan, J., Mark, J. P, Shaw, J. D, Kumar, P., Walkinshaw, D. M, Ratajczak, T. (2002) A structure-based mutational analysis of cyclophilin 40 identifies key residues in the core tetratricopeptide repeat domain that mediate binding to Hsp90. *J Biol Chem* 277: 40799-809
25. Weikl, T., Muschler, P., Richter, K., Veit, T., Reinstein, J., Buchner, J. (2000) C-terminal regions of Hsp90 are important for trapping the nucleotide during the ATPase cycle. *J Mol Biol* 303: 583-92
26. Yun, G. B, Huang, W., Leach, N., Hartson, D. S, Matts, L. R (2004) Novobiocin induces a distinct conformation of Hsp90 and alters Hsp90-cochaperone-client interactions. *Biochemistry* 43: 8217-29

Chapter 6: General conclusions and future work

6.1. Summary

The thesis described the study of the Hsp90 proteins from *homo sapiens* (Hsp90 human α) and *Caenorhabditis elegans*. The study involved the characterisation of the function of Hsp90. The aims of the study were

- To characterise the interactions of the C-terminal and full length Hsp90 with TPR containing proteins including Cyp40 by biochemical and biophysical methods.
- To characterise the interactions of C-terminal and full length Hsp90 with small ligands such as novobiocin, ATP and geldanamycin by biochemical and biophysical methods.

Table 6.2 at the end of the chapter, summarises the main results of experiments described in the thesis.

6.2. Sequence alignment of Hsp90 C-terminal domains

From sequence alignment of Hsp90, the identities between species are about 60 to 70% except with htpG which is significantly lower at 30%. The alignment of the C-

terminal sequence of ceHsp90-492, yeast Hsp90 and htpG to hHsp90- α 521 give a identity of 74%, 50% and 25% respectively (Figure 6.1). From the alignment of the sequence, hHsp90 α 521 and ceHsp90-492 are very similar and are expected to have similar functions.

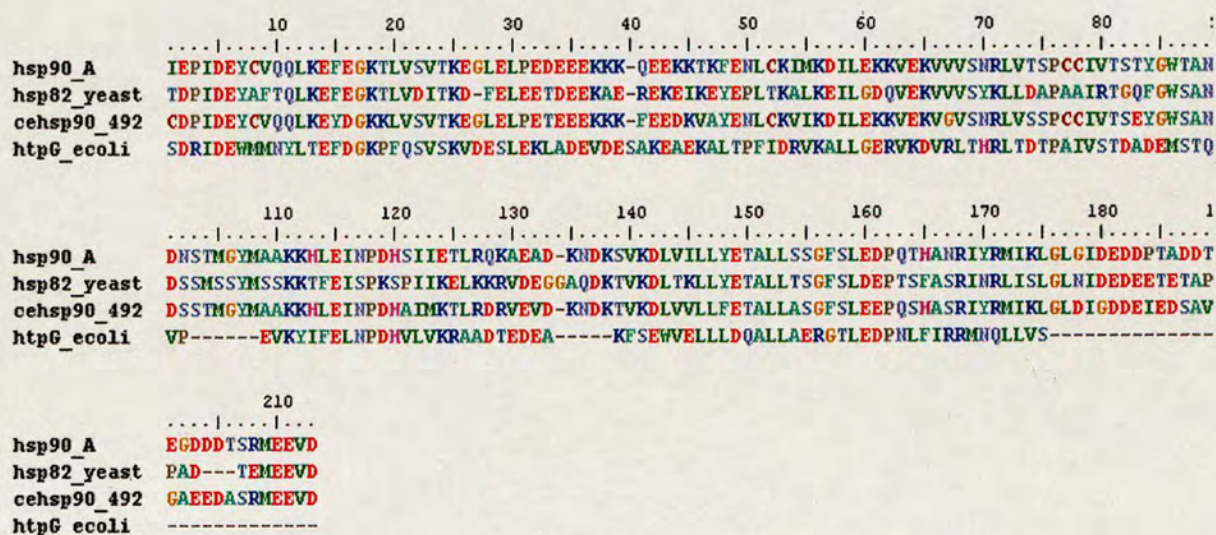


Figure 6.1. The sequence alignment of C-terminal human Hsp90 α (hHsp90- α 521), yeast hsp82, daf21(*C. elegans*) and htpG

The secondary structure prediction of the hHsp90- α 521 and ceHsp90-492 indicates that both of the sequences comprise six α helices and either three or four β strands. However, the location of the helices and the β -sheets were slightly different. Both of the proteins contain the C-terminal MEEVD motif and were shown to bind to the TPR containing protein Cyp40.

6.4. C-terminal domains bind to Cyp40

Both of the proteins were shown to bind to Cyp40 and biophysical analyses have been carried out to study the interactions by using SPR, Trp fluorescence and gel filtration. Based on these experiments, figure 6.3 illustrates the mechanism of interaction starting from the ATPase cycle. The illustration was adapted and modified from [17] with the addition of the Cyp40 cycle based on our study.

The study described in chapter 4 (section 4.2.3) and chapter 5 (section 5.2.2) showed that Cyp40 binds to Hsp90 through its C-terminal with a stoichiometry of one monomer of Hsp90 to one monomer of Cyp40. The dissociation constants of the interactions obtained from our study were in the micromolar concentration range. The following sequence of events is suggested: ATP and Cyp40 binds to Hsp90. ATP also induces a conformational change. Later on, Cyp40 is released when ATP is hydrolysed to ADP. Evidence to support this scheme was obtained from a study of Sti1 and Cpr6 binding to yeast Hsp90 [15]. However, Hsp90 can still bind to Cyp40 without its N and middle domains. The affinity of the binding can be enhanced with the use of full length protein as was shown with *C.elegans* Hsp90. There is also an evidence from the study of Hop where the N and the C-terminal domains of Hsp90 are needed to maintain its conformation when Hsp90 binds to Hop [5].

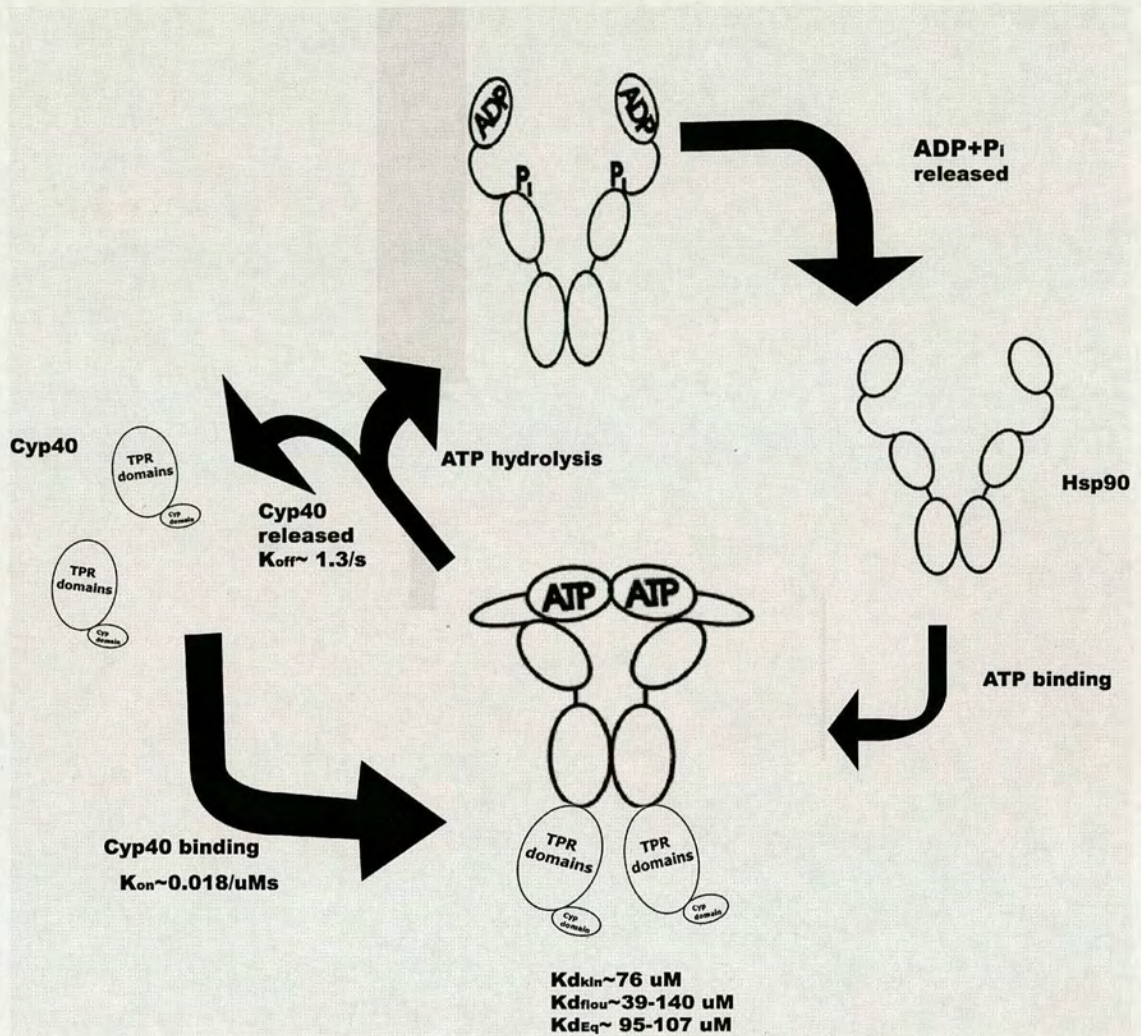


Figure 6.3. Illustration of the binding of Cyp40 to the Hsp90. The kinetic and binding data were obtained from our study using SPR and tryptophan fluorescence. The illustration was adapted and modified from Richter and Buchner [17]. The illustration did not consider the binding of p23 to the N-terminal domain during ATP bound form.

6.5. Sequence alignment predicted possible binding site for ATP and novobiocin

From our results, hHsp90 α 521 and ceHsp90 492 bind to ATP and novobiocin. Both of the proteins also have low ATPase activity and can be inhibited by low concentrations of novobiocin. However, we do not yet have information on how ATP binding and ATPase activity of the C-terminal Hsp90 influences the function or mechanism of Hsp90. In order to obtain more information on ATP binding and hydrolysis, the sequences of the C-terminal Hsp90 of four of the Hsp90 species which are yeast, human α , *C. elegans daf-21* and htpG *E. Coli* were aligned and analysed.

The sequences were compared to ABC transporters that are known to bind and hydrolyse ATP.[3, 7, 9] ABC transporters have two nucleotide binding subunits (NBDs) which power the transport and hydrolysis of ATP. Several conserved sequence motifs such as Walker A and Walker B motifs can be found in the proteins [6]. In the NBD domains, the Walker A motif consists of the GXXGXGKS/T sequences. This Walker A motif or also known as the P loop, binds to the α and β phosphate of ATP or ADP. The Walker B motif consists of XXXXDE sequences where the X amino acids were usually aliphatic residues. The Walker B motif coordinates the binding of Mg^{2+} via its Asp residue, which follows the motif binds to the attacking water and Mg^{2+} and may act as the catalytic base for the hydrolysis. There is also a Q loop which is made of by Gln followed by Glu which acts as the lid that bind to γ -phosphate as well as bind to the attacking water and Mg^{2+} . In ABC transporters the linker motif LSGGQ binds to the γ -

Motif	Consensus sequence	Function
Walker A or P loop	GXXGKST	ATP binding via α and β phosphate
Q loop or lid	Q	<ul style="list-style-type: none"> • Q-E bond to Mg • Bind to attacking water
LSGGQ	LSGGQ	ATP binding via γ phosphate
Walker B	hhhhD h: aliphatic amino acids	D makes a water bridged contact with Mg^{2+}
	E following Walker B	<ul style="list-style-type: none"> • Binds to attacking water • Binds to Mg through a water

Table 6.1. Function of conserved motifs in the nucleotide binding domain of ABC transporter. The table was adapted and modified from [6]

phosphate of ATP but only in the dimer forms. Dimerisation is needed for the ABC transporters to become catalytically active as the LSGGQ motif binds to the γ phosphate of ATP. However, ATP needs to bind to each of the monomers before the LSGGQ motif can bind to the ATP. The conserved motifs in ABC's NBD were listed in Table 6.1 which was modified from [6].

From alignment of the C-terminal Hsp90 sequences, only three residues (GKT/K) at the end of the Walker A motif were identified in the C-terminal Hsp90 (Figure 6.4). The Walker B sequence was also identified in the C-terminal domains of the four species of Hsp90 that were used in the alignment, however the amino acid residues before Asp-698 is a glycine residue (Gly) whereas in ABC transporters it is either leucine (Leu) or isoleucine (Ile). The Walker B motif in the C-terminal sequence was followed with Glu-699, which is also present in ABC transporters. The putative Q-loop is only found in human Hsp90 α and not in other species from the alignment. The LSGGQ motif was also found in the C-terminal of Hsp90 but in the sequence of LXSGF and overlaps with the novobiocin binding site. The motif was most similar to human Hsp90 α compared with Hsp90 from other species human Hsp90 α contains the sequence LSSGF instead of LSGGQ.

The presence of the ATP-binding motifs identified in the C-terminal sequences, suggest the presence of an ATP binding pocket. Novobiocin probably binds to the LXSGF motif and inhibits the ATPase activity of the C-terminal. All the motifs mentioned in ABC transporters were more similar in human Hsp90 α rather than Hsp90 *C.elegans* or other Hsp90 species. We suggest that this is the reason for higher ATPase activity of hHsp90 α 521 compared to ceHsp90 492. In summary, we suggest that, based

on the sequence comparison of Hsp90 with ABC transporter that ATP binds to the C-terminal domain of Hsp90 proteins.

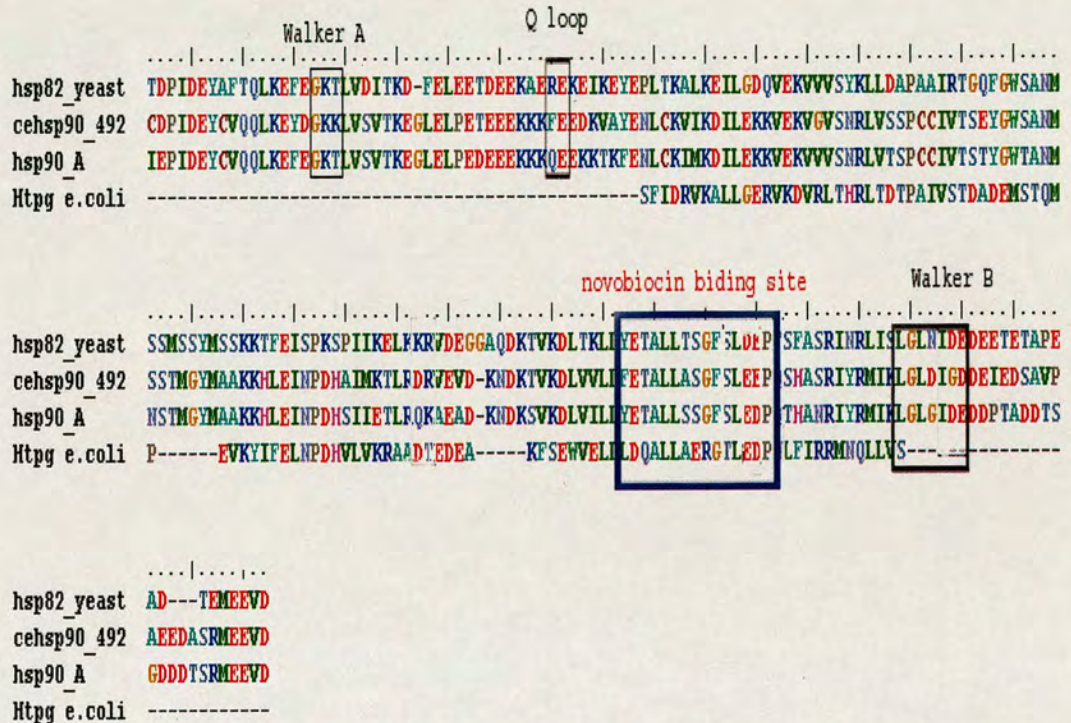


Figure 6.5. Sequence alignments of yeast, *daf21*, human α and *htpG* C-terminal Hsp90 to show the motifs involved in ATP binding and hydrolysis. The motifs are boxed and labelled on top for clarity.

6.6. Possible mechanism for ATP binding and novobiocin inhibition.

Recently, the crystal structure of the full length yeast Hsp90 has been solved and published [1]. By using the solved structure as the template, the C-terminal domain of

human Hsp90 α was submitted to Swiss-Model to obtain the structural model. The C-terminal of *C.elegans* should be very similar to the human as their sequence is 75% identical. This modelling part was done by Mr. Liam Worrall. The template for modelling utilised the closed (PDB Id 2CG9) and open (PDB Id 2CGE) yeast crystal structures recently deposited. The closed structure refers to the ATP bound state of the N-terminal domain. From the modelled structure, the binding site for ATP and novobiocin were predicted by using MEdock software [4].

Novobiocin has the preference to bind to the YETALLSSGF motif (Figure 6.7.). Biologically, the site was predicted to bind to novobiocin [10, 11] and later on, novobiocin was shown to disrupt the dimer formation of C-terminal Hsp90 [2]. From the htpG structure, the novobiocin binding site is also located in the helices that form the dimerisation motifs. In addition, our modelling structure also showed that novobiocin binds to the YETALLSSGF motif. Therefore, it seems likely that novobiocin binds to the YETALLSSGF motif and can cause the disruption of the dimer.

Our results showed that ATPase activity can be inhibited with novobiocin and from the sequence alignment the novobiocin binding site consists of the LSSGF residues that resembles the LSGGQ motif needed for ATP binding and hydrolysis in ABC transporter. Therefore, by considering all of the information the YETALLSSGF motif is probably the site that binds to ATP. Therefore ATP was docked into the structural model

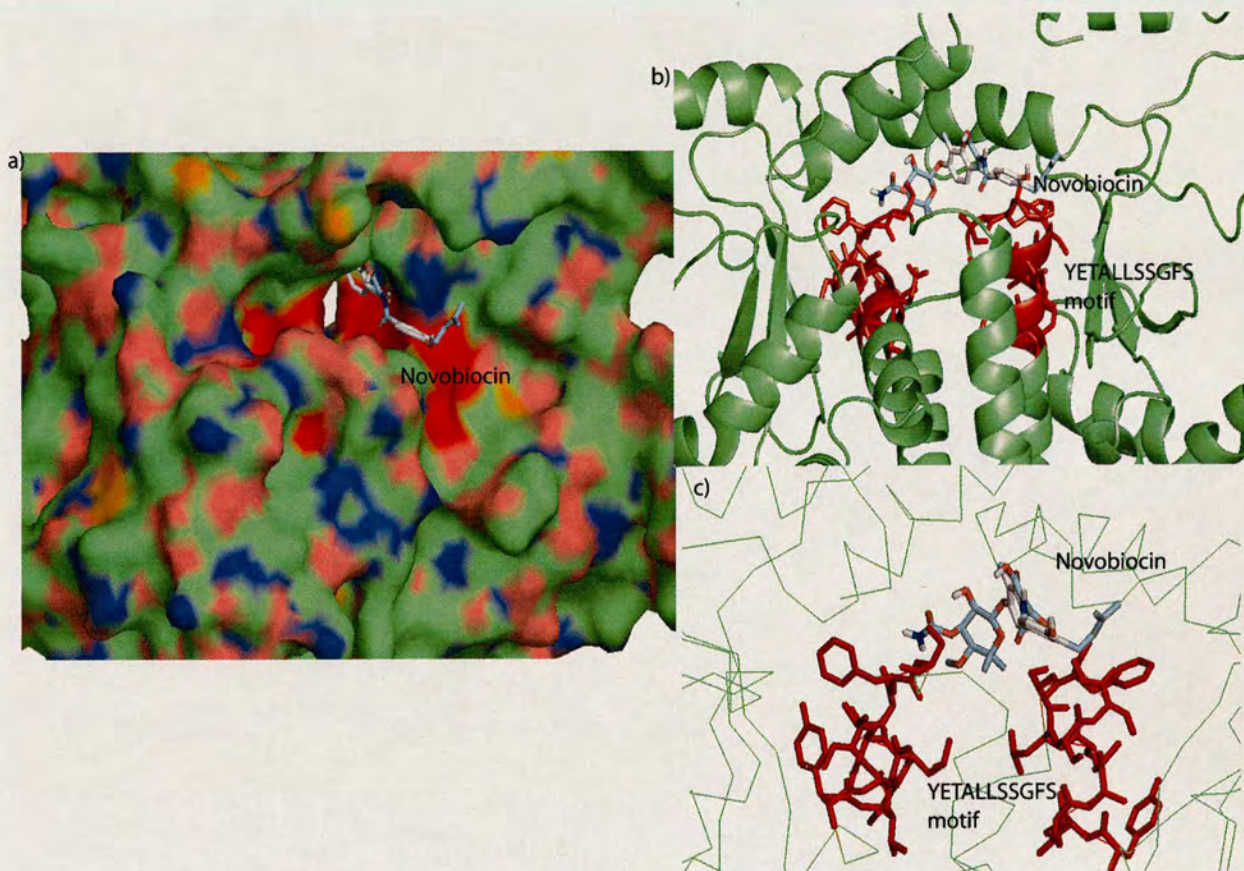
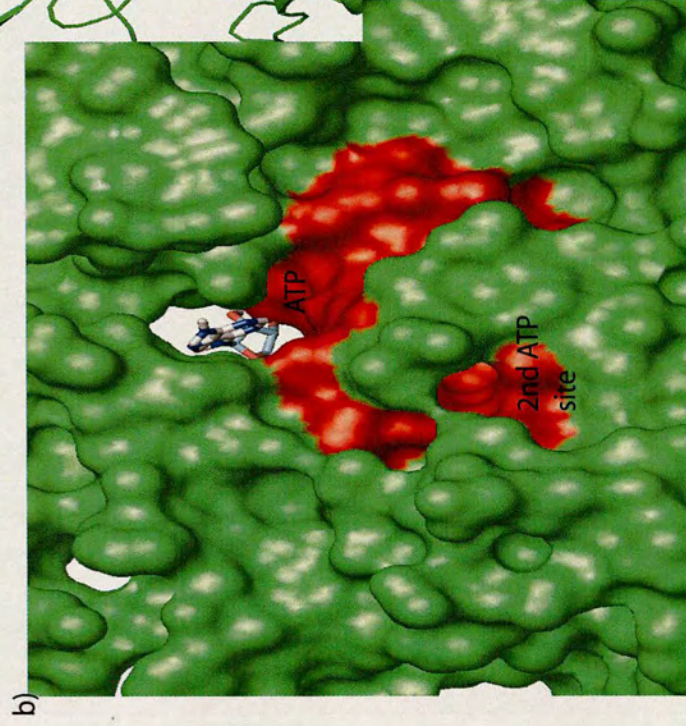
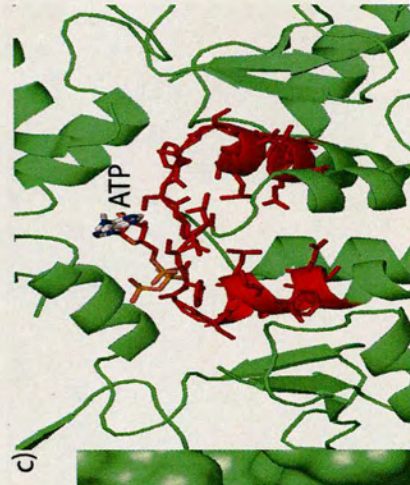
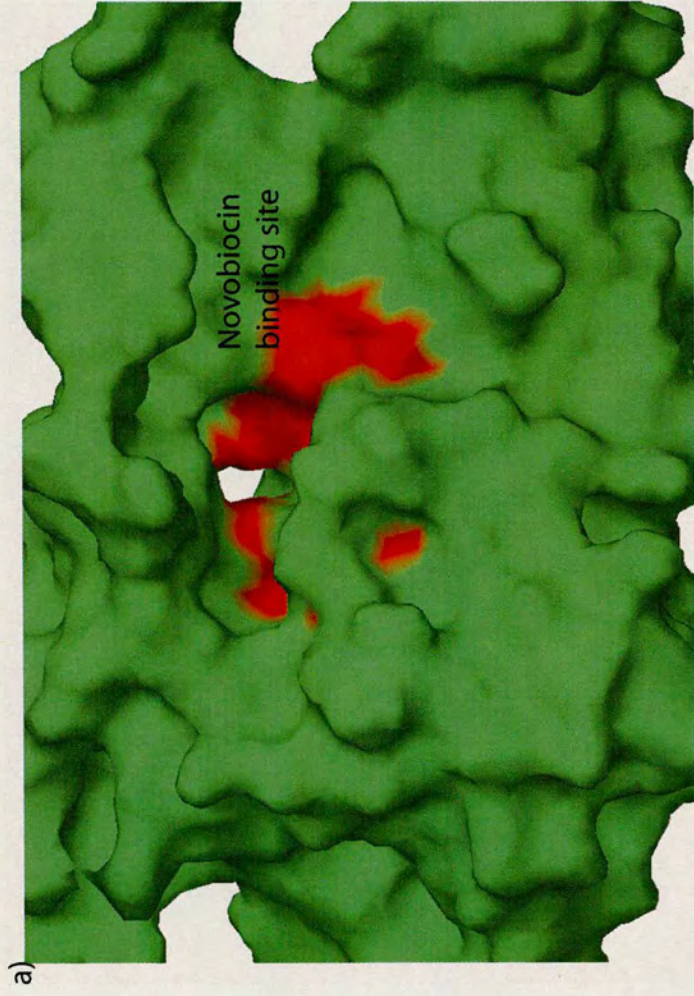


Figure 6.7. Novobiocin binds to the C-terminal human Hsp90 α model structure. a) Surface view of the model structure with novobiocin binds to the binding pocket. The red colour shows the YETALLSSGF motif. b) Ribbon view of the model structure with novobiocin binds at the binding site. c) Cartoon view shows novobiocin binding to the binding pocket.

to identify the possible binding site for ATP. The closed structure was used as the template because it is thought that the binding to the C-terminal will resemble the closed conformation of the yeast crystal structure. Interestingly, two ATP molecules were found to dock on the dimer molecule (Figure 6.8). One of the ATP molecules occupied

the same binding site for novobiocin which is at the YETALLSSGF motif. The other binding site for ATP was also near the same motif (Figure 6.8). Therefore, ATP did bind to the same binding site as novobiocin. In addition there is also another binding site for a second ATP. The possible reason for this is that when the first ATP binds to the same site as novobiocin, it makes the second site available to bind to another ATP molecule, thus suggesting that second ATP binds to the dimer sequentially. After that, both of the ATP molecules become hydrolysed.



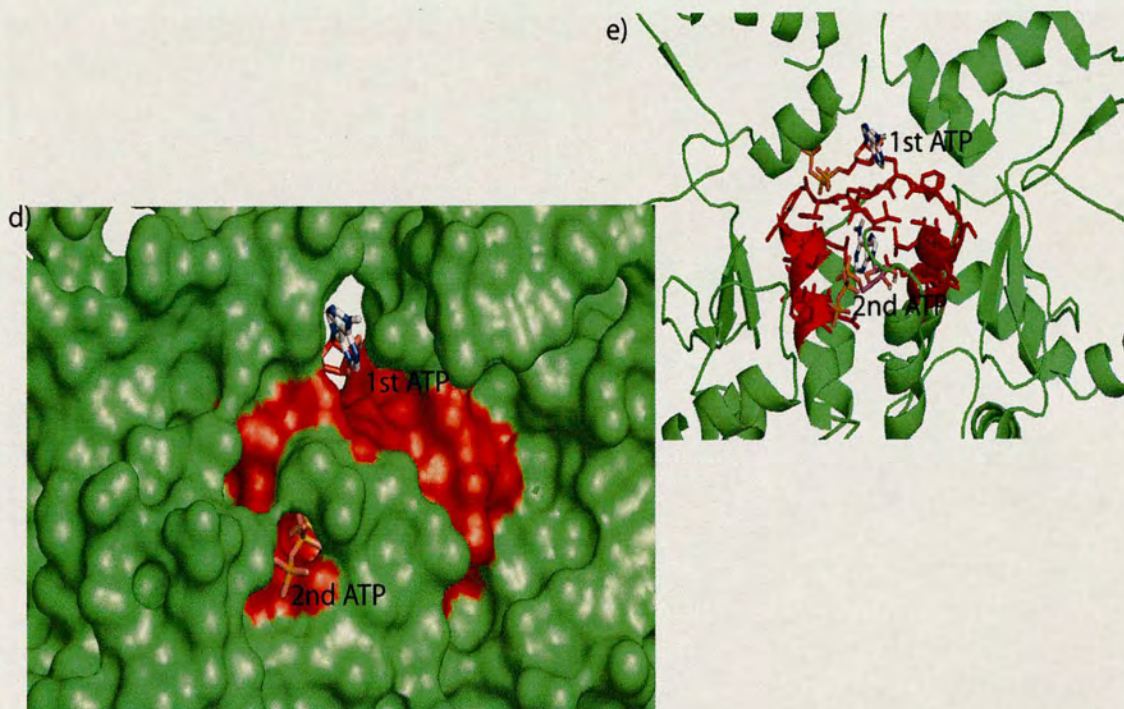


Figure 6.8 .Two molecules of ATP bind to the C-terminal binding pocket.of human Hsp90 a) Surface view of novobiocin binding pocket without novobiocin molecule. b)Surface view of 1st ATP binds to the binding pocket. The second binding pocket becomes available. c) Cartoon view of the 1st ATP in the binding pocket. d) Surface view shows both ATP molecules in the binding pocket. e) Cartoon view shows the binding of both ATP to their binding pocket. Red colour in all the panels show the position of the YETALLSSGF motif.

Further increase in the novobiocin concentrations will disrupt the dimer. The proposed mechanism for ATP binding to the C-terminal Hsp90 dimer was illustrated in figure 6.9.

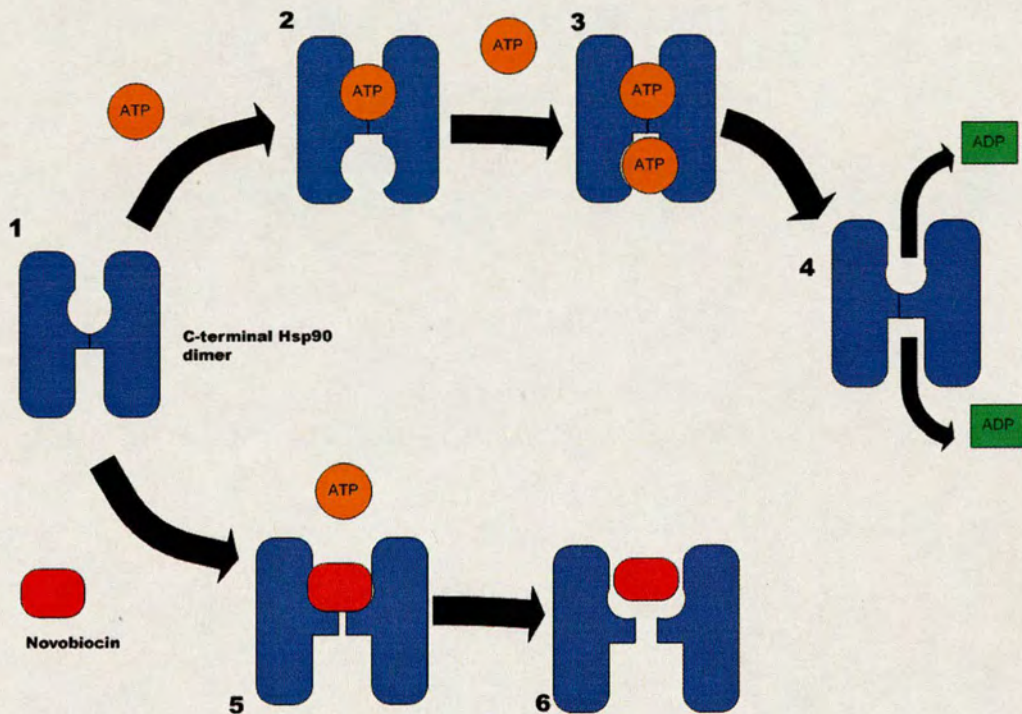


Figure 6.9. Illustration of the mechanism of ATP binding to the C-terminal of Hsp90. 1) C-terminal dimer formation at its free state without novobiocin or ATP bound (see figure 6.8a). Only one binding pocket available 2) In the presence of ATP, the dimer binds to 1st ATP (see figure 6.8b and c) and makes the second binding pocket available. 3) Both of the binding pockets occupied by ATP molecules (see figure 6.8d and e). 4) ATP hydrolysis occurs and ADP are released. In the presence of novobiocin, the dimer moves from 1 to 5 by binding to novobiocin (see figure 6.7). ATP is inhibited from binding to the C-terminal as the binding pocket is occupied by novobiocin. 6) Novobiocin disrupts the dimer formation as previously suggested [2].

In earlier discussion in this chapter, we predicted several motifs involve in the binding and hydrolysis of ATP such as Walker A and Walker B, and from the structure

modelling it is almost convinced only LSGGQ was involved and not the other motifs mentioned above. However, it is still unsure if the other motifs were totally secluded in the binding of ATP and novobiocin. There is no other proof available yet to verify this. In future, more experiments are planned to go deeper to prove this.

6.7. Future work

The binding of Cyp40 to the C-terminal Hsp90 was confirmed in these studies. Furthermore, ATP binding and hydrolysis were also shown by various methods. Further study will be to verify the significance of the binding sites of ATP in the C-terminal Hsp90. This can be done by site directed mutagenesis on the residues that may be important for the binding or by producing protein constructs that have the residues deleted. More information can also be obtained if the full length human Hsp90 is available and utilised in the mutagenesis study to investigate the roles of ATP binding site on the C-terminal to overall structure and function of Hsp90.

It is also of interest to investigate the relationship of the ATP binding site at the C-terminal domain with the binding of co-chaperones at the MEEVD motif. This can be done by using SPR to study the mode of binding of both components to the C-terminal of Hsp90 as well as ATPase activity assay. Novobiocin was shown to bind to C-terminal Hsp90 and compete with ATP binding. It will also be of interest to investigate if novobiocin can inhibit the binding of co chaperones at the C-terminal and get more

information on the kinetic of the interaction. This can be done by using the SPR and also ITC. Furthermore, the effect to the structure of C-terminal during the binding or inhibition can also be monitored by using circular dichroism.

GA was shown to bind weakly to the full length of *daf21* and our attempt to produce the N-terminal of Hsp90 of *C.elegans daf21* was not successful since the protein was very difficult to purify. Further future experiments should also include recloning the protein with C-terminal histidine tag using other vectors. Hopefully, the protein can be purified and can be used in crystallisation to see the difference in its structure compare to the other N-terminal structure that have been solved. The protein could also be used for further characterisation in finding other ligands more potent than GA but less toxic.

Since the structure of htpG and yeast Hsp90 were solved, reliable models of the C-terminal domains of other species of Hsp90 can be generated. The models should provide suggestions for site-point mutations that could lead to the design of more stable Hsp90 C-terminal domains as well as mutants that lack of the unstable loop can be made to produce proteins that suitable for crystallisation.

Protein	<i>T</i> (°C)	Ligand or inhibitor	Methods	<i>K_d</i> (μM)	<i>IC50/Ki</i> (μM)	<i>K_m</i> (μM)	<i>k_{on}</i> (M ⁻¹ s ⁻¹)	<i>k_{off}</i> (s ⁻¹)	<i>K_{d kin}</i> (μM)	<i>k_{cat}</i> (min ⁻¹)	<i>K_{dimer}</i> (μM)	Figure/ ref
hHsp90 α521	4	ATP	Hummel-Dreyer	300 ± 90								4.11
	25	ATP	Trp fluorescence	101 ± 15								4.10
	37	ATP	Malachite green ATPase assay			377 ± 101				0.021 ± 0.002		4.12
	25	Novobiocin	Trp fluorescence	1.26 ± 0.46								4.13
	20	Novobiocin	ITC	3.7 ± 0.04								4.13
	37	Novobiocin	Malachite green ATPase assay		10.8 ± 6.8/ 2.79 ± 2.02							4.14
	25	Cyp40	Trp fluorescence	66 ± 17								4.7
	25	Cyp40	SPR	95.7 ± 19.5			0.018 ± 0.002	1.3 ± 0.3	76 ± 19.5			4.9
	4	Cyp40	Gel filtration									4.6
hHsp90 α631	4	ATP	Hummel-Dryer	No binding observed								
	37	ATP	Malachite green ATPase assay							No ATPase activity		
	25	Cyp40	Trp fluorescence	39 ± 7.4								4.7
	4	Cyp40	Gel filtration									4.5
	4		Gel filtration								4.98 ± 2.12	4.4
	25	ATP	Trp fluorescence	81.4 ± 14.6								5.6
	37	ATP	Malachite green ATPase assay			327 ± 0.12				0.010 ± 0.00013		5.7 & 5.8
	25	Novobiocin	Trp fluorescence	2.48 ± 1.8								5.5

ceHsp90 492	37	Novobiocin	Malachite green ATPase assay		15.1 ± 4.9/ 3.7 ± 1.2							5.8
	25	Cyp40	Trp fluorescence	140.3 ± 7.9								5.2
	25	Cyp40	SPR	107.1 ± 18.8								5.3
ceHsp90	25	ATP	Trp fluorescence	80.1 ± 13.6								5.6
	37	ATP	Malachite green ATPase assay			288 ± 11.6				0.354 ± 0.05		5.7
	25	Novobiocin	Trp fluorescence									
	37	Novobiocin	Malachite green ATPase assay		6.61 ± 2.48/ 1.48 ± 0.55							5.7
	25	Geldanamycin	Trp fluorescence	298 ± 88.5								5.4
	37	Geldanamycin	Malachite green ATPase assay		No inhibition							5.7
	25	Cyp40	Trp fluorescence	79.3 ± 7.4								5.2
Human Hsp90	10	AMP-PNP	Stopped flow fluorescence	106 ± 7			$5.6(\pm 0.1) \times 10^4$	4.5 ± 0.7	80 ± 13			[13]
	10	ATP	Stopped flow fluorescence	284 ± 26			$1.0(\pm 0.1) \times 10^5$	16.3 ± 2.3	161 ± 24			
	25	AMP-PNP	ITC	148 ± 12								
	25	ATP	Stopped flow fluorescence	240 ± 14		190 ± 20	$2.3(\pm 0.1) \times 10^5$	9.0 ± 3.0	39 ± 13			
	25	ADP	Stopped flow fluorescence	7.2 ± 0.3								
	37	ATP	Stopped flow fluorescence			840 ± 60 ^a				0.09 ± 0.006		[12]
	37	AMP-PNP	ITC	790 ± 45								

	37	ADP	ITC	41±4									
	25	ADP	Stopped flow fluorescence	11±2			$3.7(\pm 0.1) \times 10^5$	2.7±1.6	7.2±1.6				[13]
Human Hsp90+GR	25	AMP-PNP	ITC	7.4±0.9									
	25	ATP	ITC	15±1									
	25	ADP	ITC	41±6									
Human Hsp90ΔC	25	AMP-PNP	ITC	80±40									
	37	ATP	Stopped flow fluorescence			230±10					0.0072 ± 0.003.		
Pig Brain Hsp90		ATP	ITC	100									[8]
		ATP	Trp fluorescence	40									
Yeast Hsp90	37	ATP									0.78		[16]
	25	ATP		132±47		100			500 ^ε				[14]
	25	ADP		9±3					150 ^ε				
	25	MABA-ATP					$1.6(\pm 0.3) \times 10^5 \xi$	2.9±0.2 ^ε	18.0±0.7 ^ε				[19]
	25	17-AAG					8.7 ± 2.3						[18]
	25	Radicicol					0.9 ± 0.4						
	25	Geldanamycin					4.8 ± 0.8						

Table 6.2. List of the results obtained from the experiments that were carried out throughout the thesis. The results of the data that already been published were also listed

References

1. Ali, M. M, Roe, M. S, Vaughan, K. C, Meyer, P., Panaretou, B., Piper, W. P, Prodromou, C., Pearl, H. L (2006) Crystal structure of an Hsp90-nucleotide-p23/Sba1 closed chaperone complex. *Nature* 440: 1013-7
2. Allan, K. R, Mok, D., Ward, K. B, Ratajczak, T. (2006) The carboxy-terminal domain Of Hsp90: Modulation of chaperone function and cochaperone interaction by novobiocin. Evidence that coumarin antibiotics disrupt Hsp90 dimerization. *J Biol Chem*
3. Biswas-Fiss, E. E (2006) Interaction of the Nucleotide Binding Domains and Regulation of the ATPase Activity of the Human Retina Specific ABC Transporter, ABCR. *Biochemistry* 45: 3813-23
4. Chang, T. D, Oyang, J. Y, Lin, H. J (2005) MEdDock: a web server for efficient prediction of ligand binding sites based on a novel optimization algorithm. *Nucleic Acids Res* 33: W233-8
5. Chen, S., Sullivan, P. W, Toft, O. D, Smith, F. D (1998) Differential interactions of p23 and the TPR-containing proteins Hop, Cyp40, FKBP52 and FKBP51 with Hsp90 mutants. *Cell Stress Chaperones* 3: 118-29
6. Davidson, L. A, Chen, J (2004) ATP-BINDING CASSETTE TRANSPORTERS IN BACTERIA. *Annual Review of Biochemistry*. 73: 241-268
7. Furukawa, T., Akiyama, S. (2006) [Mechanisms of substrate transport by ABC transporter, MRP1/ABCC1]. *Seikagaku* 78: 110-21
8. Garnier, C., Lafitte, D., Tsvetkov, O. P, Barbier, P., Leclerc-Devin, J., Millot, M. J, Briand, C., Makarov, A. A, Catelli, G. M, Peyrot, V. (2002) Binding of ATP to heat shock protein 90: evidence for an ATP-binding site in the C-terminal domain. *J Biol Chem* 277: 12208-14
9. Gross, H. C, Abdul-Manan, N., Fulghum, J., Lippke, J., Liu, X., Prabhakar, P., Brennan, D., Willis, S. M, Faerman, C., Connelly, P., Raybuck, S., Moore, J. (2006) Nucleotide-binding domains of cystic fibrosis transmembrane conductance regulator, an ABC transporter, catalyze adenylate kinase activity but not ATP hydrolysis. *J Biol Chem* 281: 4058-68
10. Marcu, G. M, Chadli, A., Bouhouche, I., Catelli, M., Neckers, M. L (2000) The heat shock protein 90 antagonist novobiocin interacts with a previously unrecognized ATP-binding domain in the carboxyl terminus of the chaperone. *J Biol Chem* 275: 37181-6
11. Marcu, G. M, Schulte, W. T, Neckers, L. (2000) Novobiocin and related coumarins and depletion of heat shock protein 90-dependent signaling proteins. *J Natl Cancer Inst* 92: 242-8
12. McLaughlin, H. S, Smith, W. H, Jackson, E. S (2002) Stimulation of the weak ATPase activity of human hsp90 by a client protein. *J Mol Biol* 315: 787-98
13. McLaughlin, H. S, Ventouras, A. L, Lobbezoo, B., Jackson, E. S (2004) Independent ATPase activity of Hsp90 subunits creates a flexible assembly platform. *J Mol Biol* 344: 813-26
14. Prodromou, C., Roe, M. S, O'Brien, R., Ladbury, E. J, Piper, W. P, Pearl, H. L (1997) Identification and structural characterization of the ATP/ADP-binding site in the Hsp90 molecular chaperone. *Cell* 90: 65-75
15. Prodromou, C., Siligardi, G., O'Brien, R., Woolfson, N. D, Regan, L., Panaretou, B., Ladbury, E. J, Piper, W. P, Pearl, H. L (1999) Regulation of Hsp90 ATPase activity by tetratricopeptide repeat (TPR)-domain co-chaperones. *Embo J* 18: 754-62
16. Prodromou, C., Panaretou, B., Chohan, S., Siligardi, G., O'Brien, R., Ladbury, E. J, Roe, M. S, Piper, W. P, Pearl, H. L (2000) The ATPase cycle of Hsp90 drives a molecular 'clamp' via transient dimerization of the N-terminal domains. *Embo J* 19: 4383-92
17. Richter, K., Buchner, J. (2001) Hsp90: chaperoning signal transduction. *J Cell Physiol* 188: 281-90

18. Rowlands, G. M, Newbatt, M. Y, Prodromou, C., Pearl, H. L, Workman, P., Aherne, W. (2004) High-throughput screening assay for inhibitors of heat-shock protein 90 ATPase activity. *Anal Biochem* 327: 176-83
19. Weikl, T., Muschler, P., Richter, K., Veit, T., Reinstein, J., Buchner, J. (2000) C-terminal regions of Hsp90 are important for trapping the nucleotide during the ATPase cycle. *J Mol Biol* 303: 583-92

Appendix A. Crystallographic study of cyclophilin-ligand interactions

A.1. Introduction

One major aim of the work carried out in this thesis was to structurally characterise Hsp90 and its protein partners. Structural information from such studies will provide an excellent starting point for structure-based drug discovery. There are already some interesting published studies of small molecule Hsp90 ligands of potential medical relevance [1, 3, 7, 9]. One of the binding partners for Hsp90 human is cyclophilin40 and it is of biological and possibly medical interest to study the role of cyclophilin inhibitors on the interaction of the large immunophilins with Hsp90.

A second general theme of this thesis is to explore different approaches of studying protein ligand interactions using different biophysical techniques. The work described in this section outlines a novel method of studying ligand-protein interactions by using X-ray protein crystallography. In this study cyclophilin 3 (Cyp3) protein crystals were used. The ligand in this study is a dipeptide (Gly-Pro). This work is a continuation of the study that has been done with Cyp3 and Ala-Pro [6]. The aim of the study is to obtain the ligand binding constants of the interaction. The study also aims to compare the detailed binding differences between the two dipeptide ligands, namely Gly-Pro and Ala-Pro.

A.2. *C.elegans* cyclophilin 3 (Cyp3)

Cyclophilin 3 is the most abundant cyclophilin isoform that is expressed in the free living nematode *Caenorhabditis elegans* (*C. elegans*) [2]. All cyclophilins show peptidyl-prolyl isomerase (PPIase) activity. PPIases help the folding of the protein by catalyzing the *cis-trans* isomerization of Xaa-Pro peptide bonds (where Xaa is the preceding amino acid) in oligopeptides, thus accelerating the slow rate-limiting steps in the refolding of several proteins *in vitro* [4, 5, 8]. *In vitro*, cyclophilin accelerates the *cis/trans* prolyl isomerisation step in the folding pathway of proline rich proteins [2]. It has also been suggested that cyclophilin affects the dynamics of protein-protein interaction by preventing aggregation of early folding intermediates of protein substrates, possibly by acting as a chaperone.

Cyp3 used in this study was produced in house. The crystal structure of the protein has already been solved and published [2]. Basically, two crystal forms were obtained, both as tetragonal plates. The native structure of Cyp3 is shown in figure A.1.



Figure A.1. Cyclophilin 3 crystal structure. The Arg62 residue was labelled as it is the key focus on the study of this appendix. The structure was modified from PDB file id 1DYW by using pymol.

A.3. X-ray crystallographic ligand binding studies using Cyp3

Cyclophilin is a very good template to study protein and ligand interactions as they show a conserved backbone conformation on binding. The protein was selected as the template for this binding study because of the availability of high symmetry, well-diffracting crystals which were suitable for ligand soaking experiments [2, 6]. Previous

studies showed that the PPIase activity can be inhibited weakly by Ala-Pro that exhibited a K_d of about 23.3 mM.

These studies [6] also showed for the first time that protein crystallography could be used in a novel way to determine so called K_{dc} values – the dissociation constant of the ligand in the crystal. This technique involves soaking the protein crystal in a given concentration of ligand solution. The refined X-ray structure provides an ‘occupancy’ of the ligand in the crystal. A series of crystal structures in which the crystals have been soaked at different ligand concentrations can then be used to calculate the apparent dissociation constant by relating the refined crystallographic occupancy of the ligand with the ligand concentration in the soaking solution. The K_{dc} for Ala-Pro which was obtained from the ligand soaking experiment was 26.8 mM, showing close agreement with the value obtained from its biochemical assay [6].

The study described in this appendix is aimed to explore further this X-ray crystallographic technique and extend the series of Xaa-Pro dipeptides ligands (Gly-Pro, Ala-Pro and Ser-Pro) in attempt to dissect the individual contribution of the components to the binding interaction. Figure A.2 shows the ligands involved in the study. The other aim of the study is to investigate the side-chain of the Xaa moiety. The Xaa-Pro dipeptide ligand in this series increases in a modular fashion – H to CH_3 to $\text{CH}_2\text{-OH}$ – with the proline moiety and the peptide bond to the Xaa amino acid common to all three. Therefore, any differences in binding affinities, assuming the energetic contribution of proline in all cases is equivalent and that the microscopic water structure around the binding site is also equivalent, can be attributed to the addition of a CH_3 or an OH group. In general, the study can be used as a starting point for rational drug-design and protein

engineering. However, only the ligand soaking study contributed by Gly-Pro is discussed as this is the only work done by the author

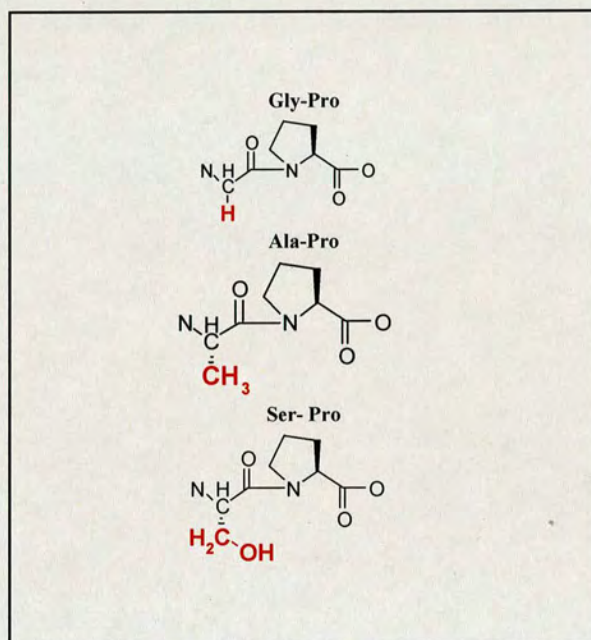


Figure A.2. The Xaa-Pro dipeptide utilised in the study. The inhibitors utilised were Gly-, Ala- and Ser-Pro. The dipeptide ligands were different in the side chain which changes in modular fashion from H to CH₃ to CH₂-OH.

A.4. Materials and methods

A.4.1. Expression, purification and crystallization of *C. elegans* Cyp3

The expression, purification and crystallization of *C. elegans* Cyp3 was carried out based on Dornan *et. al.*, [2]. Basically, the plasmid containing Cyp3 genes were

transformed into BL21 (DE3 pLysS) cells (Novagen). Cyp3 was expressed following a 4 h induction with 0.4 mM isopropyl-1-thio- β -D-galactopyranoside. The cell pellets were solubilized in lysis buffer containing 50 mM HEPES, 5 mM benzamidine, 5 mM EDTA, 5 mM 2-mercaptoethanol, pH 7.5. Lysozyme (Sigma) was added to 0.1% w/v and incubated on ice for 1 h. The cell was lysed and the supernatant was obtained by centrifuging at 22,000 rpm for 1 hr and the pH of the supernatant was adjusted to 6.8. Protein extract was purified to homogeneity using two purification steps: SP-Sephacrose cation exchange chromatography with the following buffers: Buffer A, 50 mM HEPES, 5 mM EDTA, 5 mM 2-mercaptoethanol, pH 6.8, and Buffer B, Buffer A + 0.5 M NaCl (pH 6.8). Column fractions were tested on 15% SDS-polyacrylamide electrophoresis gels and fractions containing the protein of interest were dialyzed overnight against Buffer A. Protein solution was filtered through a 0.2 μ m filter and applied to Resource S resin (Amersham Pharmacia Biotech). Cyp3 was eluted from this resin with the following buffers: Buffer A, 20 mM HEPES, pH 6.8, Buffer B, Buffer A + 0.5 M NaCl.

A.4.2. Crystallization and Gly-Pro soaking experiment

Cyp3 was crystallized at 18°C by the hanging drop vapour-diffusion method using 29 - 31 % poly(ethylene glycol) methyl ether 5000 (MPEG 5000) as precipitant [Dornan, 1999 #14]. Native Cyp3 crystals were soaked in 10 μ l drops of well solution containing increasing concentrations of Gly-Pro. Crystals were soaked for between 1

and 3 hours. The composition of the cryoprotectant was glycerol (0.2 mL), MPEG 5000 (0.7 mL), 1.0 M sodium citrate/citric acid (0.1 mL, pH 5.6). Crystals were mounted in a 0.2 - 0.3 mm cryoloop (Hampton Research, Inc.), dipped in cryoprotectant for a few seconds, and frozen by plunging into liquid nitrogen. The frozen crystal was then transferred to a magnetic goniometer head in a stream of nitrogen at 100 K. All diffraction data were collected on a 300-mm MarResearch imaging plate system mounted on an ENRAF Nonius FR571 rotating anode generator operating at 40 kV, 80 mA, and producing Cu_K radiation from a graphite crystal monochromator.

A.4.3. Crystal data refinement

The Cyp3 native structure was used as a starting model. Positional and B-factor refinement were performed using SHELX97 and the methodology described [Wu Sy, 2001 #37]. The coordinates of Arg62_n, Arg62₁, Xaa-Pro dipeptide, W_a, W_b, W_c, and W_d were fixed during occupancy refinement. Arg62_n represents the Arg62 conformation in the native (free) form of Cyp3 and Arg62₁ represents the Arg62 conformation with Xaa-Pro dipeptide bound to Cyp3. The B-factors of Arg62_n, W_a, W_b, W_c, and W_d were fixed to the same B-factor values as those of the native structure. Individual atomic B-factors for Arg62₁ and Xaa-Pro were refined together with occupancy. The restraints applied in the occupancy refinement are summarized below:

$$Q_{\text{Arg62n}} + Q_{\text{Arg621}} = 1$$

$$Q_{\text{Arg621}} = Q_1$$

$$Q_{\text{Arg62n}} = Q_{\text{Wa}} = Q_{\text{Wb}} = Q_{\text{Wc}} = Q_{\text{Wd}}$$

Where Q_{Arg62n} is the occupancy of the Arg62 conformation in the native (free) protein, Q_{Arg62l} is the occupancy of the Arg62 conformation with Xaa-Pro bound, and Q_l is the occupancy of Xaa-Pro. By regarding the crystal soaking experiment as a simple equilibrium in which each protein molecule in the crystal lattice can be bound or free, the ligand occupancy (Q_l) is related to the dissociation constant by equation 4;

$$Q_l = (Q_{\text{max}} \times [L]) / ([L] + K_{\text{dc}}) \quad - \quad \text{equation . 4}$$

where Q_l is the occupancy of ligand (fraction of the protein sites in the crystal occupied by ligand), K_{dc} is the crystal dissociation constant, $[L]$ is the concentration of the ligand (it is assumed that the concentration of ligand in the 10 μl drop is constant throughout the soaking experiment and Q_{max} is the maximal fractional occupancy of the ligand at saturation (fixed at 1).

A.5. Results and discussion

Native crystals of Cyp3 were obtained after at least three days incubation at 18⁰C. At least two crystals were picked and soaked with series of concentrations of the Gly-Pro ligand. The concentrations of Gly-Pro used were 0, 6, 12, 100 and 150 mM. The crystal was soaked between 30 min to 2 hrs. The soaking time was dependent on the survival of the crystal inside the soaking solution. The crystal was observed every 30

	GlyPro			
	150mM	100mM	12mM	6mM
Space group P4 ₁ 2 ₁ 2 Cell (Å)	a=b= 62.7 c=122.8	a=b= 61.6 c=123.1	a=b= 60.9 c= 123.3	a=b= 61.5 c=123.1
Resolution range (Å)	35.9 – 1.78	35.56 – 1.72	43.44 – 1.60	43.44 – 1.60
Number of observations	103431 (13246)	117343 (14723)	185734 (12950)	191993 (13360)
Number of unique reflections	22426	24133	29409	28256
Completeness (%)	92.6	93.1	93.6	88.5
I/σ(I)	11.2	13.08	19.5	22.84
Multiplicity	4.3 (4.2)	4.6 (4.2)	6.0 (3.2)	6.4 (4.4)
R-factor (F>4SIG(F))	0.22 (0.20)	0.21 (0.19)	0.21 (0.20)	0.26 (0.26)
R _{free} (F>4SIG(F))	0.24 (0.22)	0.25 (0.23)	0.23 (0.22)	0.29 (0.29)
RMS bond lengths (Å)	0.007	0.008	0.09	0.007
RMS angle distances (Å)	0.023	0.024	0.025	0.030
Cyclophilin 3	31.895	23.377	19.887	15.358
Dipeptide	30.043	29.387	26.995	20.052

Table A.1. Crystallographic statistics of the four Cyp3 structures

min and was taken out from the soaking solution if the crystal looked damaged. If the crystal remained stable and not damaged, it was left in the solution for 2 hrs before being removed. The observation was made by observing the crystal under microscope. The crystal was handled as in section A.2.2. The diffraction data was processed by using Mosflm and further refined to obtain the occupancy. Table A.1 showed the

crystallographic statistics of the Gly-Pro complexes. The graph of occupancy over the ligand concentrations was plotted by using Kaleidagraph 3.5. The graph was then fitted with equation 4 (Figure A.3). The crystal dissociation constants (K_{dc}) of the interaction of Cyp3 to Gly-Pro dipeptide based from crystal soaking was 37.6 ± 22.8 mM.

The $2F_0-F_c$ density maps around the binding sites of Cyp3 complexes show the position of Arg62 at the lowest concentrations of Gly-Pro (6mM) and the highest concentration of the ligand used (150 mM) (Figure A.4). At 6 mM of gly- pro, the Arg62 exhibited a mixture of native Cyp3 and also the ligand bound form of the complex. At the highest concentrations of Gly-Pro (150 mM), Arg62 was observed to exhibit the fully bound form (Figure A.4).

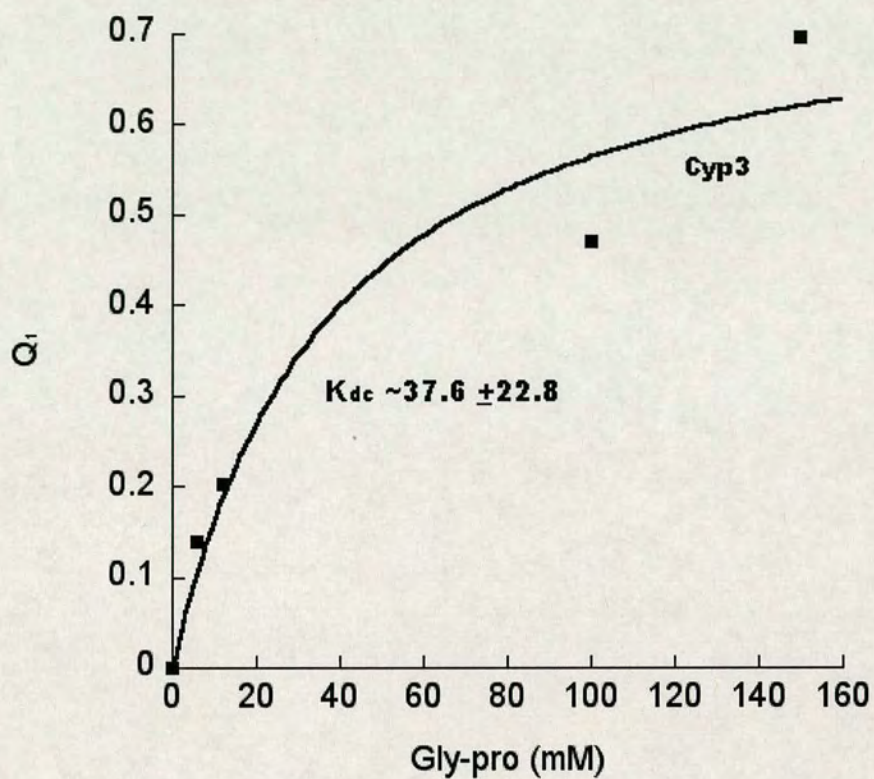


Figure A.3. Refined occupancy of different crystal soaked in the series of Gly-Pro concentrations. Each of the points represents each of the occupancy of the ligands. The crystals were soaked in 0, 6, 12, 100 and 150 mM of ligand concentrations. The crystal dissociation constant (K_{dc}) obtained from the graph was 37.6 ± 22.8 mM.

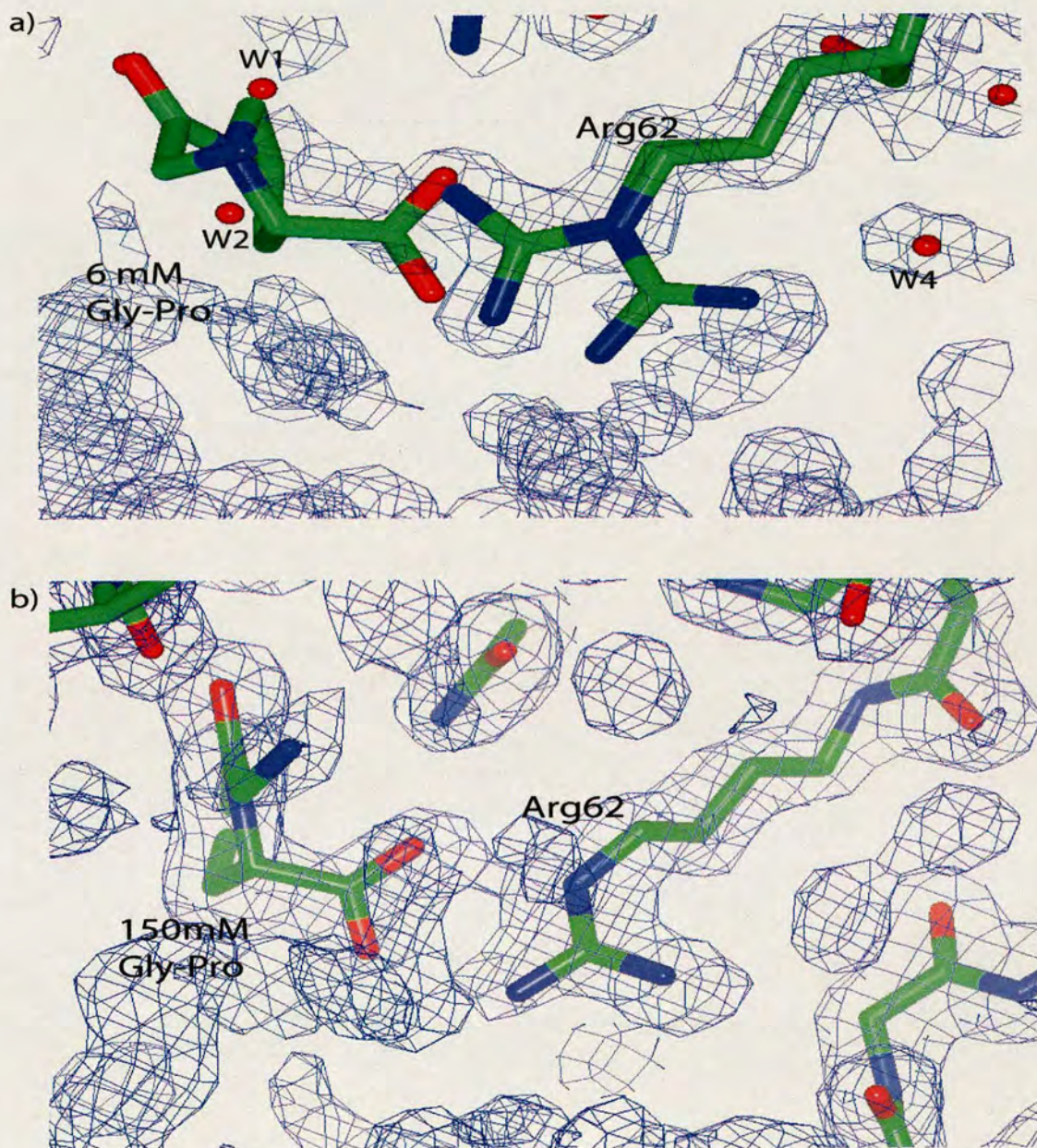


Figure A.4. Two density maps of Cyp3 soaked with Gly-Pro a) and b) The $(2F_0 - F_c)$ density maps show the position of Arg62 when the crystals were soaked with 6 and 150 mM Gly-Pro. The Gly-Pro peptide totally displaced the water molecules when the Gly-Pro concentration was 150 mM. At 6mM Gly-Pro, the Arg62 position was a mixture between the native form and the bound form. Three of the water molecules (W1, W2 and W4) were still available. The pictures were generated by using ccp4mg.

Based on the crystal soaking data of the Gly-Pro and Ala-Pro X-ray structures, a decrease in the K_{dc} from 37.6 mM to 26.8 mM is observed. A recent soaking of Ser-Pro (D. Kan, unpublished results), gives a K_{dc} of 6.1 mM. As the Xaa-Pro dipeptide ligands move from glycine to serine, there is an increase in a modular fashion – H to CH₃ to CH₂-OH (Figure A.5). Therefore any changes in the interaction between these ligands must be contributed by the side chain of the peptide. The interaction of the three dipeptide ligands used also show a tighter binding as the side chain becomes bulkier. Cyp3 catalyses the PPIase activity through this site and by considering the effect on the side chain of the dipeptide on the activity suggested that the bulkier the side chain, the more efficiently the Xaa-Pro dipeptide acts as a PPIase inhibitor. However, this conclusion is based on the results of only three dipeptides used and must be confirmed further with the same experiments by utilising Xaa-Pro dipeptides with bulkier side chains.

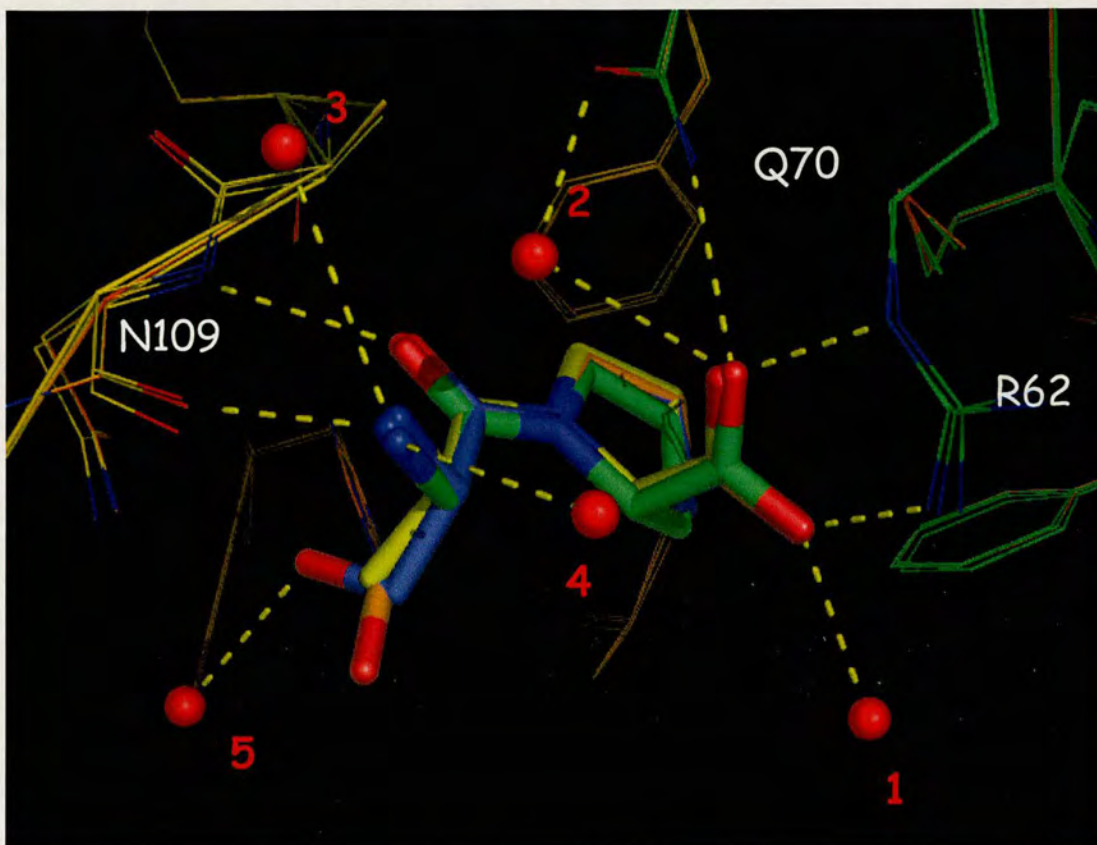


Figure A.5. Superposition of Xaa-Pro dipeptide:Cyp3 structures. The position of 5 composite waters are shown as red spheres. Arg 62 (R62) positions in all structure was in the ligand bounded formations. The three dipeptide also did not exhibit any different except for the side chain.

A.6. Conclusion

Based on the Gly-,Ala-, and Ser-Pro dipeptide utilised in the experiments, the involvement of the side chain in the ability to bind to Cyp3 can be investigated. The

increases from – H to CH₃ to CH₂-OH were enough to cause the interaction become tighter. A summary of the K_{dc} and K_{ds} values for the available Xaa-Pro /Cyp3 complexes is given in Table A.2). It is remarkable that the solution binding constants are so similar to the K_{dc} values in the crystal. These results show that protein crystal structures do indeed provide biologically relevant models for the study of protein ligand interactions.

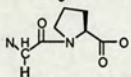
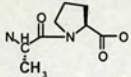
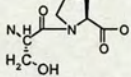
Dipeptide / Structure	K_{ds}^{cis} mM (solution data)	K_{dc}^{cis} mM (crystal data)
Gly-Pro 	49	36
Ala-Pro 	23.3	26.8
Ser-Pro 	5.9	6.1

Table A.2. A summary of the K_{dc} and the K_{ds} values of the the Xaa-Pro interaction with Cyp3. The K_{dc} values were obtained from the crystal soaking experiments. The K_{ds} values were obtained from the PPIase assay.

References

1. Chiosis, G., Rodina, A., Moulick, K. (2006) Emerging Hsp90 inhibitors: from discovery to clinic. *Anticancer Agents Med Chem* 6: 1-8
2. Dornan, J., Page, P. A, Taylor, P., Wu, S., Winter, D. A, Husi, H., Walkinshaw, D. M (1999) Biochemical and structural characterization of a divergent loop cyclophilin from *Caenorhabditis elegans*. *J Biol Chem* 274: 34877-83
3. Howes, R., Barril, X., Dymock, W. B, Grant, K., Northfield, J. C, Robertson, G. A, Surgenor, A., Wayne, J., Wright, L., James, K., Matthews, T., Cheung, M. K, McDonald, E., Workman, P., Drysdale, J. M (2006) A fluorescence polarization assay for inhibitors of Hsp90. *Anal Biochem* 350: 202-13
4. Li, J., Chen, J., Gui, C., Zhang, L., Qin, Y., Xu, Q., Zhang, J., Liu, H., Shen, X., Jiang, H. (2005) Discovering novel chemical inhibitors of human cyclophilin A: Virtual screening, synthesis, and bioassay. *Bioorg Med Chem*
5. Pemberton, J. T, Rulten, L. S, Kay, E. J (2003) Identification and characterisation of *Schizosaccharomyces pombe* cyclophilin 3, a cyclosporin A insensitive orthologue of human USA-CyP. *J Chromatogr B Analyt Technol Biomed Life Sci* 786: 81-91
6. Sy W, S., S., Dornan, J., Kontopidis, G., Taylor, P., Walkinshaw, D. M (2001) The First Direct Determination of a Ligand Binding Constant in Protein Crystals. *Angew Chem Int Ed Engl* 40: 582-586
7. Terry, J., Lubieniecka, M. J, Kwan, W., Liu, S., Nielsen, O. T (2005) Hsp90 inhibitor 17-allylamino-17-demethoxygeldanamycin prevents synovial sarcoma proliferation via apoptosis in in vitro models. *Clin Cancer Res* 11: 5631-8
8. Yang, HP, Zhong, HN, Zhou, HM (1997) Catalysis of the refolding of urea denatured creatine kinase by peptidyl-prolyl cis-trans isomerase. *Biochim Biophys Acta*. 1338: 147-150
9. Yu, M. X, Shen, G., Neckers, L., Blake, H., Holzbeierlein, J., Cronk, B., Blagg, S. B (2005) Hsp90 inhibitors identified from a library of novobiocin analogues. *J Am Chem Soc* 127: 12778-9